Draft FINAL REPORT

U.F. Project No: 49104504031
Contract No: BD 545
RPWO#: 13

Evaluation of Feasibility of Using Composite Pavements in Florida By Means of HVS Testing

Mang Tia
Chung-Lung Wu
Patricio Tapia
Wasantha Kumara

February 2007

Department of Civil & Coastal Engineering
College of Engineering
University of Florida
Gainesville, FL

1. Report No.	2. Government Accession No.	3. Recipient's Catalog No.
Final Report		

4. Title and Subtitle

EVALUATION OF FEASIBILITY OF USING COMPOSITE PAVEMENTS IN FLORIDA BY MEANS OF HVS TESTING

5. Report Date: February 2007

6. Performing Organization Code:

8. Performing Organization Report No.: 4910-4504-031

7. Author(s)

Mang Tia, Chung-Lung Wu, Patricio Tapia and Wasantha Kumara

9. Performing Organization Name and Address

University of Florida
Department of Civil and Coastal Engineering
365 Weil Hall / P.O. Box 116580
Gainesville, FL 32611-6580

10. Work Unit No. (TRAIS):

11. Contract or Grant No.: BD545 – RPWO #13

13. Type of Report and Period Covered: Final Report

August, 2003 – February, 2007

12. Sponsoring Agency Name and Address

Florida Department of Transportation
Research Management Center
605 Suwannee Street, MS 30
Tallahassee, FL 32399 Phone: (804) 414-4615

14. Sponsoring Agency Code:

15. Supplementary Notes

Prepared in cooperation with the U.S. Department of Transportation and the Federal Highway Administration

16. Abstract

The main objectives of this research are (1) to develop analytical models for analysis of the behavior of WT pavements, (2) to evaluate the potential performance of the WT pavement test sections for use under Florida conditions, and (3) To assess the applicability of WT techniques for rehabilitation of asphalt pavements in Florida.

A total of nine full-scale and instrumented WT test sections were constructed and tested using a Heavy Vehicle Simulator (HVS). A 3-D finite element model was developed to analyze the behavior of the WT pavement test sections. The model was verified and calibrated using the measured FWD deflections and HVS load-induced strains from the test sections. The model was then used to evaluate the potential performance of these test sections under a typical critical temperature-load condition in Florida.

Maximum stresses in the pavement were computed for the critical condition when a 24-kip single axle load (which is higher than the legal limit of 22 kips in Florida) was placed at the mid-edge of the slab (which is the most critical loading position) and when the temperature differential in the concrete slab was +20 °F (which is a typical severe temperature condition in the summer time in Florida.) Based on the computed maximum stresses in the concrete, the expected numbers of repetitions of the 24-kip single axle loads at the critical thermal condition were computed for the nine test sections.

The results show that with a relatively thin AC layer of 4.5 inches as typical for Florida conditions, a WT pavement with a 4-inch concrete layer can be used for low volume roads with heavy (24-kip single axle) loads. The allowable traffic volume increases as the concrete slab thickness increases. In order to be able to withstand the critical load without fear of fatigue failure (for an infinite number of critical load repetitions), a minimum slab thickness of 6 inches would be needed for a joint spacing of 4 ft, and a minimum slab thickness of 8 inches would be needed for a joint spacing of 6 ft.

17. Key Words	18. Distribution Statement
Whitetopping, Composite Pavement, Concrete-asphalt Interface, Critical Loading Condition, Temperature Differential, 3-D Finite Element Model, Bonded Slab, Partially Bonded Slab, Elastic Modulus, Shear Strength.	No restrictions. This document is available to the public through the National Technical Information Service, Springfield, VA, 22161

19. Security Classif. (of this report)	20. Security Classif. (of this page)	21. No. of Pages	22. Price
Unclassified	Unclassified	177	

DISCLAIMER

"The opinions, findings and conclusions expressed in this publication are those of the authors and not necessarily those of the Florida Department of Transportation or the U.S. Department of Transportation.

Prepared in cooperation with the State of Florida Department of Transportation and the U.S. Department of Transportation."

SI* (MODERN METRIC) CONVERSION FACTORS

APPROXIMATE CONVERSIONS TO SI UNITS

Symbol	When You Know	Multiply By	To Find	Symbol
		LENGTH		
in	inches	25.4	millimeters	mm
ft	feet	0.305	meters	m
yd	yards	0.914	meters	m
mi	miles	1.61	kilometers	km
		AREA		
in^2	square inches	645.2	square millimeters	mm^2
ft^2	square feet	0.093	square meters	m^2
yd^2	square yards	0.836	square meters	m^2
ac	acres	0.405	hectares	ha
mi^2	square miles	2.59	square kilometres	km^2
		VOLUME		
fl oz	fluid ounces	29.57	milliliters	ml
gal	gallons	3.785	liters	l
ft^3	cubic feet	0.028	cubic meters	m^3
yd^3	cubic yards	0.765	cubic meters	m^3
NOTE: Volumes greater than 1000 l shall be shown in m^3.				
		MASS		
oz	ounces	28.35	grams	g
lb	pounds	0.454	kilograms	kg
T	short tons (2000 lb)	0.907	megagrams	Mg
		Temperature (exact)		
°F	Fahrenheit temperature	5(F-32)/9 or (F-32)/1.8	Celcius temperature	°C
		ILLUMINATION		
fc	foot-candles	10.76	lux	lx
fl	foot-Lamberts	3.426	candela/m^2	cd/m^2
		FORCE and PRESSURE or STRESS		
lbf	poundforce	4.45	newtons	N
psi	poundforce per square inch	6.89	kilopascals	kPa

APPROXIMATE CONVERSIONS FROM SI UNITS

Symbol	When You Know	Multiply By	To Find	Symbol
		LENGTH		
mm	millimeters	0.039	inches	in
m	meters	3.28	feet	ft
m	meters	1.09	yards	yd
km	kilometers	0.621	miles	mi
		AREA		
mm^2	square millimeters	0.0016	square inches	in^2
m^2	square meters	10.764	square feet	ft^2
m^2	square meters	1.195	square yards	yd^2
ha	hectares	2.47	acres	ac
km^2	square kilometers	0.386	square miles	mi^2
		VOLUME		
ml	milliliters	0.034	fluid ounces	fl oz
l	liters	0.264	gallons	gal
m^3	cubic meters	35.71	cubic feet	ft^3
m^3	cubic meters	1.307	cubic yards	yd^3
		MASS		
g	grams	0.035	ounces	oz
kg	kilograms	2.202	pounds	lb
Mg	megagrams	1.103	short tons (2000 lb)	T
		Temperature (exact)		
°C	Celcius temperature	1.8C + 32	Fahrenheit temperature	°F
		ILLUMINATION		
lx	lux	0.0929	foot-candles	fc
cd/m^2	candela/m^2	0.2919	foot-Lamberts	fl
		FORCE and PRESSURE or STRESS		
N	newtons	0.225	poundforce	lbf
kPa	kilopascals	0.145	poundforce per square inch	psi

* SI is the symbol for the International System of Units. Appropriate rounding should be made to comply with Section 4 of ASTM E380. (Revised August 1992)

ACKNOWLEDGMENTS

The Florida Department of Transportation (FDOT) is gratefully acknowledged for providing the financial support for this study. The FDOT Materials Office provided the additional testing equipment, materials and personnel needed for this investigation. Sincere thanks go to the project manager, Dr. Bouzid Choubane, for providing the technical coordination and advices throughout the project. Sincere gratitude is extended to the FDOT Materials Office personnel, particularly to Messrs. Tom Byron, Steve Ross, Charles Ishee, Richard Delorenzo, Greg Sholar, Abdenour Nazef and Vidal Francis, and the staff at the FDOT APT facility. Sincere thanks also go to George Lopp for his guidance with the IDT tests and to Irene Scarso for her expert editing of this report.

Table of Contents

List of Tables

List of Figures

CHAPTER 1
INTRODUCTION

1.1 Background

The increasing truck weights and tire pressures on our pavements in recent years have pushed the demand on the performance of our pavements to a higher level. Many asphalt pavements have experienced rutting while many others have experienced longitudinal cracking. One of the possible solutions to this problem is the use of whitetopping, which is placing a concrete layer over an existing asphalt pavement. Whitetopping has an advantage over an asphalt overlay in that the concrete surface is stronger and thus is more resistant to rutting and surface-initiated cracking. The better durability and long-term performance characteristics of concrete pavement surfaces can significantly reduce traffic delays associated with the frequent maintenance of asphalt pavements. In addition, when concrete surfaces are used, skid resistance and safety can be substantially improved, especially under wet conditions. In recent years, with the skyrocketing price of asphalt, concrete is becoming more competitive in cost with that of asphalt. This makes the use of whitetopping a more economically viable alternative for rehabilitation of asphalt pavements.

There are three type of whitetopping based on the thickness of the concrete slab. Ultra-Thin Whitetopping (UTW) is a relatively new technique for resurfacing deteriorated asphalt pavements. It involves placing very thin concrete slabs, 2 to 4 inches thick, on an old asphalt pavement to create a bonded (or partially bonded) composite pavement. The reduction of thickness is justified by the use of a high quality concrete, shorter joint spacing, and good bond between the concrete and the existing asphalt pavement.

Thin Whitetopping (TWT) involves placing relatively thicker concrete slabs, normally 5 to 8 inches thick, bonded (or partially bonded) over an existing asphalt pavement. Similar to UTW pavements, TWT pavements use short joint spacing and good bond between the concrete and the asphalt layer.

Conventional whitetopping (CWT) involves placing concrete slabs which are typically greater than 8 inches in thickness. The concrete slabs are typically not bonded to the underlying asphalt layer.

Experimental UTW pavements have been constructed in many states, including Colorado, Georgia, Iowa, Kansas, Kentucky, Missouri, New Jersey, North Carolina, Pennsylvania and Tennessee. Preliminary evaluations of these recently constructed UTW projects have shown that UTW is a viable rehabilitation method for asphalt pavements. The Florida Department of Transportation (FDOT) has also experimented with UTW in recent years. Three UTW test tracks were constructed behind the FDOT State Materials Office in Gainesville in 1996. An experimental UTW project was also constructed at the Ellaville Truck Weigh Station on I-10 in northwest Florida in 1997. However, the performance of these test sections were less than ideal, with the observation of some early cracking on the concrete surface. These problems were attributed mainly to the fact that all of the UTW test sections were inadequately designed for the traffic at the Ellaville Weigh Station (Tia et al, 2002). While the UTW technique may provide durable wearing surface for normal traffic loads on residential and city streets, low-volume roads, street intersections, general aviation airports, and parking areas, the UTW technique was probably not an appropriate rehabilitation alternative for weigh stations subjected to frequent applications of heavy truck traffic. The use of TWT or CWT might have been a more appropriate choice in such an application.

With the potential economical and technical benefits of whitetopping pavements, there was a need to effectively evaluate the feasibility and proper application of UTW, TWT and CWT pavements in Florida, so that the whitetopping techniques can be properly and effectively utilized to achieve the maximum benefits to the traveling public.

1.2 Objectives of Research

The main objectives of this research are as follows:

(1) To develop analytical models for analysis of the behavior of UTW, TWT and CWT pavements. These models were to be verified by and fine-tuned by full-scale experimental results.

(2) To evaluate the potential performance of the WT pavement test sections for use under Florida conditions.

(3) To assess the applicability of UTW, TWT and CWT techniques for rehabilitation of asphalt pavements in Florida.

1.3 Approach and Scope of Research

The objectives of this research study were to be achieved through the following main tasks:

(1) A literature review on the state-of-the-art of whitetopping pavements.

(2) Development of an experimental design and instrumentation plan for evaluation of several UTW, TWT and CTW pavement test sections by means of accelerated pavement testing using the HVS.

(3) Construction of the UTW, TWT and CWT test sections located at the Florida DOT Research Park and testing them by means of the HVS.

(4) Characterization of the test sections by laboratory testing of cored samples and FWD testing to obtain pavement parameters of the test sections.

(5) Development of analytical models for analysis of UTW, TWT and CWT pavements, and fine-tuning of analytical models by comparing the analytical results with experimental results from the test sections.

(6) Evaluation of the potential performance of the WT pavement test sections for use under Florida conditions.

The FDOT Materials Office has a Heavy Vehicle Simulator (HVS) and an Accelerated Pavement Testing (APT) facility for the operation of this HVS. The HVS can apply realistic full-size wheel loads to full-size pavements to assess their behavior and performance directly. The HVS has the capability to simulate 20 years of interstate traffic on a pavement test section within a period of 1 to 4 months. This accelerated pavement testing facility was used in this study to evaluate the behavior and performance of Whitetopping pavements in Florida in a direct and effective manner.

1.4 Significance of Research

In the past, there have been many studies where whitetopping pavements were constructed and their performance observed. There have also been some studies where whitetopping pavements were modeled and analyzed with respect to the various factors which may affect their performance. However, there has been little work done where the whitetopping pavements were instrumented and the measured responses were compared to the analytical results to validate the models used.

The significance of this research work is that the analytical model developed was validated and fine-tuned by measured responses from full-scale and instrumented WT pave-

ments, which had not been done before. The 3-D finite element model used also had further refinements from previous work in this area. In the past research work, 2-D models using 4-node elements and 3-D models using 8-node elements had been used to analyze this type of pavements. In this research, a 3-D finite element model with 20-node 3D solid elements was used to model the pavement structure. Previous models had used a 4-slab system to model the WT pavements. In this research, a 12-slab system was used. Using a 12-slab system can give better modeling of the effects of the adjacent slabs. The bond interface between the concrete slab and the AC layer was also modeled with special elements to cover the range from a fully bonded to fully un-bonded condition. How well this can model the actual behavior of the WT pavements was validated by measured responses from the full-scale test sections.

1.5 Scope of Report

This report presents all the work performed in this project. It includes (1) a literature review, (2) design of experiment, (3) construction and instrumentation of the test sections, (4) HVS testing of the test sections and collection of data, (5) laboratory testing of cored specimens and FWD testing of the test sections, (6) development of analytical models for analysis of WT pavements and fine-tuning of these models, and (7) evaluation of the potential performance of the WT pavement test sections for use under Florida conditions.

CHAPTER 2
LITERATURE REVIEW ON WHITETOPPING

2.1 General Concepts

The concept of resurfacing existing asphalt pavement using Portland cement concrete (whitetopping) is not new. In fact, the first reported use of whitetopping dates back to 1918 (Hutchinson, 1982). However, this technology has improved over the years as the concrete paving technology has improved. Plain concrete, reinforced concrete and fibrous (fiber reinforced) concrete have been used to resurface flexible pavements (Hutchinson, 1982 and McGhee, 1994). In the 1940's and 1950's, plain concrete was mainly used at civil and military airports. Concrete thickness used in these projects ranged from 8 to 18 in. (200 to 460 mm). Since 1960, plain concrete has been extensively used to resurface existing highway pavements in states such as California, Utah, and Iowa. Concrete thickness of these resurfacing projects ranged from 7 to 10 in. (175-250 mm). Continuously reinforced concrete and fiber-reinforced concrete were also used on a limited number of projects. NCHRP synthesis 204 listed 189 whitetopping projects constructed in the United States between 1918 and 1992. This list included streets, highways, and airfield projects.

There are several advantages of using whitetopping for rehabilitating asphalt pavements. Whitetopping provides long-term benefits to the traveling public, and to roadway or airport agencies. Concrete durability and long-term performance characteristics decrease the maintenance required and life cycle costs of pavements. As a result, concrete surfaces significantly reduce traffic delays associated with the frequent maintenance of asphalt pavements. In addition, when concrete surfaces are used, skid resistance and safety are substantially improved, especially

under wet conditions. These advantages promote and contribute to the use of concrete pavements over asphalt surfaces.

Ultra-Thin Whitetopping

Ultra-thin whitetopping (UTW) is a relatively new technique for resurfacing deteriorated asphalt pavements. It involves placing very thin concrete slabs (2 to 4 in. thick) on top of an asphalt pavement to form a bonded (or partially bonded) composite pavement. The reduction of thickness is justified by the use of high quality concrete with relatively high strength, shorter joint spacing, and bond between the concrete and the existing asphalt pavement.

The first UTW experimental project was constructed on the access road to a waste disposal landfill in Louisville, Kentucky in September 1991(Cole and Mohsen, 1993, Brown, 1995, and Risser et al. 1993). The concrete mixture was designed to provide relatively high early compressive strength, 3,500 psi at 24 hours. A low water-cement ratio of 0.33 was selected to achieve higher strength and reduce drying shrinkage. Two concrete slab thicknesses, 2 in. and 3.5 in., and two joint spacings, 2 ft and 6 ft were used. The Louisville UTW pavement has performed well, carrying many more traffic loads than predicted by design procedures available at that time.

Following the success of the Louisville UTW project, many other states, including Tennessee, Georgia, North Carolina, Kansas, Iowa, Pennsylvania, New Jersey, Colorado, Missouri, Mississippi, Virginia and Florida, have constructed and are currently evaluating UTW projects. Over 200 UTW pavements have been built in the last decade. The development of a mechanistic design procedure for UTW pavements in 1997 represented another major step in advancing this promising technique (Wu et al, 1997, Mack et al, 1997, and ACPA, 1997).

Thin Whitetopping (TWT)

Thin Whitetopping is a variation of the UTW where thicker concrete slabs are used. Slab thicknesses in the range of 5 to 7 inches are normal for this type of pavements. TWT may have a bonded or an unbonded interface between the concrete slab and the AC layer. While more attention has been paid to investigate the behavior of UTW pavements, few studies have focused in the alternative of using TWT when the conditions for the thinner slabs cannot be met. Among the states that have undertaking projects involving TWT are Colorado (Tarr et al, 1997), Minnesota (Vandenbossche et al, 2002), and Mississippi.

Conventional Whitetopping (CWT)

Whitetopping pavements with a slab thicknesss greater than 8 inches are commonly known as Conventional Whitetopping (CWT). CWT pavements are generally used for pavements subjected to heavier traffic loads, and have been designed based on the assumption that the existing asphalt concrete (AC) layer does not contribute directly to the load-carrying capacity of the pavement structure. Rather, the AC layer is considered to serve as a base layer for the new concrete overlay, and no bond is considered to exist between the overlay and the existing asphalt. Longer joint spacing (comparable to those of conventional jointed concrete pavements (JCP)) is generally incorporated in CWT.

2.2 Concrete Mixture Proportions and Properties

The concrete mix for a particular UTW and TWT project is often selected based on the requirements for early opening to traffic. A normal mix design includes cement, coarse and fine aggregates, air-entraining agent, admixtures, and a lower water-cement ratio. Fibers have been used in many UTW projects; however, the effects of fiber have not been well documented. Compared to aggregate used for thicker concrete pavements, the top-size of coarse aggregate for

UTW and TWT is reduced. Materials and mix proportions selected for the first experimental project in Louisville, Kentucky are shown in Table 2.1.

Table 2.1. Concrete Mix Proportions Used in Louisville Experimental Project (Riser et al. 1993).

Constituents	Quantity
Cement (ASTM C 150 Type I)	800 lb/cy
Coarse Aggregate	1800 lb/cy
Fine Aggregate	1150 lb/cy
Water	260 lb/cy
Polypropylene Fibers	3 lb/cy
High Range Water Reducer	14 oz/100 lb cement

The concrete mixture was designed to provide relatively high strength at early ages (3500 psi or 24.2 MPa at 36 hours). A low water-to-cement ratio (0.33) was selected to achieve higher strength and reduce drying shrinkage. Polypropylene fibers were used to enhance the flexural strength, increase impact and freeze-thaw resistance, and further reduce drying and plastic shrinkage cracking.

Similar mix proportions were used in the Tennessee (Speakman et al. 1996) and Georgia (Cown, 1993) projects. In the Leawood, Kansas site, the mixture proportions were slightly different; cement content was less (611 lb/yd^4), but a setting-accelerating admixture was used (Dumitru et al, 2002). Compressive strength of 3000 psi (20.7 MPa) at 24 hours was achieved. Three pounds of polypropylene fibers were also used in this mixture. The mix design used in the Kansas UTW project is presented in Table 2.2.

In April 2000, an old asphalt runway was rehabilitated using the UTW technique at the Savannah-Hardin County Airport (SNH) in Tennessee (Saeed et al. 2001). The runway was original constructed in 1962 and was subsequently overlaid and extended in 1975. The original

pavement consisted of an AC surface of 3.5 in. and a crushed aggregate base of 6.5 in. A 3-in. AC overlay was added during the 1975 rehabilitation.

At the time of UTW construction, the AC surface had exhibited significant fatigue and thermo cracking. Design UTW thickness was 4 in. with a joint spacing of 48 in. Design concrete flexural strength was 700 psi. The concrete mix design is shown in Table 2.3.

Table 2.2. Concrete Mix Proportions Used in Leawood, Kansas (Wu et al. 1997).

Constituents	Quantity
Cement (ASTM C 150 Type I)	611 lb/cy
Coarse Aggregate SSD (Crushed Limestone)	1730 lb/cy
Fine Aggregate SSD (Natural Sand)	1345 lb/cy
Total Water	225 lb/cy
Pave Air	5 oz/cy
Pozzutec	65 oz/cy
Rheobuild	43 oz/cy

Table 2.3. Concrete Mix Proportions Used in SNH, Tennessee (Saeed et al. 2002).

Constituents	Attributes
Cement	Type I, 573 lb/cy
Fly Ash	Maximum 15% by weight of cementitious materials
Strength	700 psi flexural
Slump	Between 1/2 and 2 in.
Water/Cement Ratio	0.35
Air Content	6% by volume
Synthetic Fiber	3 lb/cy

In 1997, the Illinois Department of Transportation (IDOT) began investigating the use of whitetopping as an intersection repair method (Winkelman, 2003). Eight projects, including main lines and intersections, were selected to be analyzed in this research. The projects are identified in Table 2.4 along with the mixture design used in each case. All of the mixture designs

contained an air entraining admixture. The mixture designs also included a water reducer except for the project on Clay County Highway 3. The project listed in Decatur contained a super-plasticizer. The water to cement ratios for all of these projects ranged from 0.34 to 0.36 except for the Clay County project, which was 0.46.

Table 2.4. Mix Proportions for Eight Whitetopping Projects in Illinois.

Project-Location	Coarse Aggregate (lb)	Fine Aggregate (lb)	Cement (lb)	Water (lb)	Polipropylene Fibers (lb)
Decatur - Intersection of US-36 and Oakland Avenue	1713	1210	705	239	N/A
Carbondale - Intersection of US-51 and Pleasant Hill Road	1805	1008	755	273	3.0
Harrisburg - Intersection of US-45 and Illinois Rt. 13	1811	975	755	302	3.0
Anna - Illinois Rt. 146 (Intersection of Vienna and Main Streets)	1811	975	755	302	3.0
Tuscola - US-36	1704	1035	755	255	N/A
Clay County Highway 3	1814	1286	534	244	N/A
Piatt County Highway 4	1957	1220	534	179	N/A
Cumberland County Highway 2	1836	1256	575	197	N/A

The performances of the thin whitetopping on the four mainline pavements and the ultrathin whitetopping sections on the intersections have been reported as excellent.

Middleton et al. 2005, investigated the impact of different cement materials, synthetic fiber types, and curing procedures on compressive strength, flexural strength, shrinkage and scaling durability of concrete. According to the results, high early strength concrete containing ordinary or rapid-hardening cement along with a low water-cement ratio gave excellent compressive and flexural strength at the age of one day. It was also noted that it provided high resistance to scaling from de-icing agent. The use of Class C fly ash gave acceptable final

strength, but the early strength was lower than the one obtained in mixes without fly ash. On the other hand the fly ash concrete showed poor scaling resistance.

2.3 Construction Procedures

UTW pavements are constructed with slipform or fixed form pavers in essentially the same way as conventional concrete pavements, with some special provisions. The construction procedures consist of the following steps: preparing asphalt surface, placing the concrete, finishing, surface texturing, curing, and sawing the joints.

Asphalt pavement surface preparation prior to concrete placement is a very important procedure to achieve better bond and good performance of UTW. Milling, followed by cleaning with compressed air to remove all laitance, dust, grit and all foreign materials, is the best way to prepare the asphalt surface. It is recommended that an adequate asphalt thickness of a minimum of 3 in. (75 mm) after milling, be used, if possible (Mack et al. 1997).

Concrete used in UTW can be produced at a ready-mix plant and delivered to the site by ready-mix trucks. Normal slipform pavers can be used to spread, screed, and consolidate the concrete in an efficient manner. After the surface is finished and textured, a curing compound is immediately sprayed on the entire surface to achieve adequate curing. The curing compound is generally applied at a rate twice the normal application rate for thicker concrete pavements because thin concrete slabs can lose water rapidly (ACPA, 1998). Joint sawing must be performed as soon as surface conditions permit, or when the concrete is able to support the equipment and the operator. Usually joints are not sealed because joint openings are generally narrow due to the short joint spacing.

2.4 UTW and TWT Design Considerations

A parametric investigation of the variables affecting the performance of whitetopping pavements was performed in Gainesville, Florida. Confirming the results from previous studies, Tia el al. 2003, concluded that the main factors affecting the behavior of UTW and TWT are the thickness of the concrete slab, the joint spacing, the bond in the interface and the thickness of the asphalt layer.

2.4.1 Slab Thickness

A major benefit of UTW is the reduction in concrete thickness. As defined above, the recommended thickness for ultra-thin whitetopping is not more than 4 in. (100 mm). For most of the experimental projects, thickness ranges from 2 in. (50 mm) to 4 in. (100 mm). The reduction in thickness is justified by the use of high quality concrete with relatively high compressive and flexural strength, closely-spaced joints, and good bonding between UTW and the existing asphalt base.

2.4.2 Joint Spacing

Spacing between joints is an important factor controlling the performance of UTW. In the Louisville experimental project, 6-ft transverse and longitudinal joint spacings (6-ft panels) were compared with 2-ft panels. Although the 6-ft panels exhibited cracking, no signs of distress were observed on the 2-ft panels. This performance was attributed to the smaller panels (2-ft) transferring the load completely to the flexible base and the concrete being mostly under compression. Comparatively, when larger panels are used, some of the load is absorbed by slab bending. The contribution of the existing asphalt is based on the assumption that the overlay is bonded to the flexible base. The American Concrete Pavement Association (ACPA) has recommended that joint spacing be about 12 to 15 times of the slab thickness. For example,

spacing for UTW of 2 in. (50 mm) of thickness should be between 2 and 3 ft (0.6 and 0.9 m). Spacing at a Georgia site was 2-ft (0.6 m) and in Kansas 3-ft (0.9 m) in one section, and 4-ft (1.2 m) in the other.

It is not practical to install dowel bars, tie bars, or keyway in UTW pavements because of the very thin slabs. Field evaluation has indicated that load transfer provided by aggregate interlock is generally high because of the short joint spacing and the support provided by the asphalt layer. For UTW pavements, field performance demonstrated the need for thicker slabs at the transition areas between the UTW and the asphalt roadways. Figure 2.1 shows transition details for UTW pavements, as recommended by ACPA.

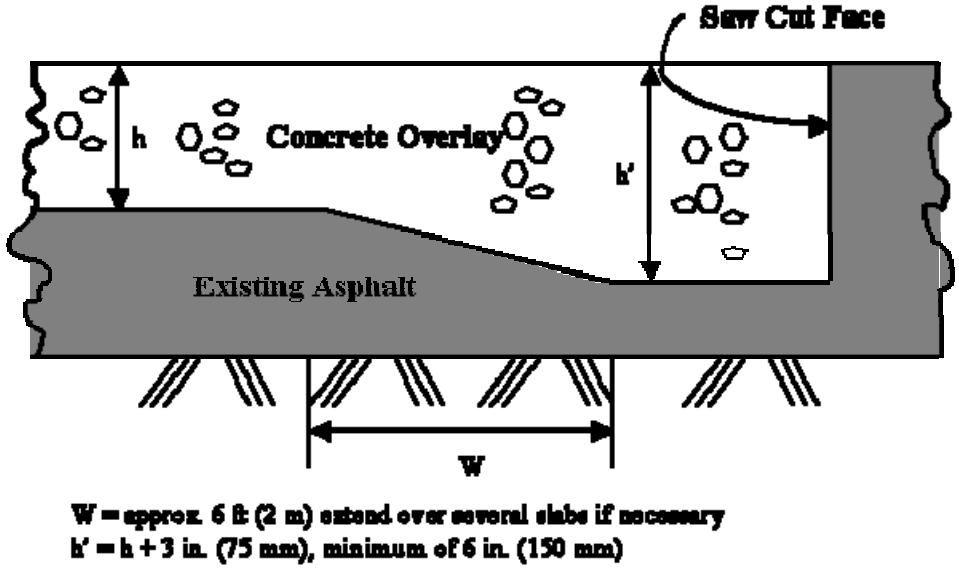

Figure 2.1. Transition Between UTW and Adjoining Asphalt Pavement (ACPA, 1998).

2.4.3 Interface Bonding Strength

Bond between UTW and existing asphalt pavement is a key factor controlling the performance of the UTW composite pavement. The existence of bond strength not only significantly reduces the stresses in the concrete section, but also allows the section to perform and be analyzed as a composite section. A wide range of bond strength (shear strength between the two

layers) was measured at some of the experimental sites; from the average strength of 50 psi (0.34 MPa) measured at the Swedish site to the over 200 psi (1.38 MPa) measured at some Florida UTW test sections. Bond strength can be improved by milling the old asphalt pavement; the roughness in the surface and the exposed aggregates lock the layers together thus increasing the bond.

An experiment intended to evaluate the bonded condition in the interface of concrete overlay was performed in Iowa by Nishiyama et al. 2005. This experiment included field and laboratory testing to evaluate the bond at different times after concrete placement. The project concluded that bond strength between an overlay and the existing pavement gradually increases over the time regardless of the initial bond strength.

To evaluate the interface condition, other authors have proposed the use of the vertical tensile strength in the interface as an indicator of the bond, in addition to the shear strength. By performing pull-off test on the composite samples, it is also possible to characterize the vertical interaction between layers.

Rasmussen et al. 2001, presented a method to characterize the axial slab support restraint by running full-scale push-off test to obtain the stiffness and strength of the interface bond. These parameters can be used in analytical models to better represent the interface condition in whitetopping pavements.

2.5 Design Procedure for UTW and TWT Pavements

Because of the thin slabs, the Portland Cement Association's (PCA) thickness design procedure (PCA, 1984) does not completely apply to UTW. Furthermore, the AASHTO thickness design method (AASHTO, 1993) does not account for the bond between the two layers. As the development of the UTW technique continued, it became apparent that a design procedure for

selecting the optimum UTW thickness and joint spacing subjected to anticipated traffic and environmental loading was needed.

In 1994 the PCA sponsored a comprehensive research effort aimed at developing a mechanistic based design procedure for UTW (Wu et al. 1997 and Mack et al. 1997). The PCA's UTW pavement design procedure was developed in 1997. Work conducted in developing the design procedure included a thorough literature review of past and current work; condition surveys of UTW sites in Georgia and Tennessee; instrumentation and load testing of several test sections; development of a 3-dimensional finite element model for UTW analysis; and development of a design procedure and construction guidelines.

Development of this design procedure included the following elements:

1. Verification of the 3-dimensional finite element model. Strain (stress) data collected from the Spirit of St. Louis Airport UTW test sections were used to calibrate and verify the three-dimensional model that was developed in this study and was used as an analytical tool to analyze the UTW pavement behavior and to develop the design procedure. To calibrate and verify the model, stresses were computed under each loading and temperature condition, and were compared with the load testing results obtained from the test pavements.
2. Identification of degree of bonding existed in the field. It has been established from the results of field testing that UTW pavements behaved as partially bonded composite pavements. Using field data and the 3-D model, an effort was made to quantify the additional structural capacity (or load carrying capacity) that could be offered by the asphalt layer to the UTW pavements.

3. Correlation between stresses calculated from ILSL2 and the 3-dimensional model. Since many computer runs would be required to develop the design guidelines, the use of the 3-dimensional model was not feasible due to the time needed for each run. Instead, correlations were developed between stresses computed by these two models, and were used in the development of the design guidelines.
4. Development of design guidelines. Processes involved in the development of the UTW design guidelines are the following:
    - Stresses induced by loads and temperature were separately computed for fully bonded UTW pavements using the 2-dimensional model, ILSL2. A wide range of pavement parameters and material properties were covered.
    - The 2-D model stresses were converted to 3-D model stresses using the conversion equations derived in the previous step.
    - The converted 3-D model stresses were increased by 36% to account for the partially bonded condition, as observed in the field testing.
    - Equations were developed to correlate the converted and adjusted stresses to different pavement parameters. Stresses and strains were then calculated for typical parameters for UTW pavements under different loading and temperature conditions, and were tabulated.
    - UTW pavement thickness design was accomplished by limiting both the concrete and asphalt strains within safe limits under anticipated traffic and environmental loadings in the pavement's design life.

A mechanistic design procedure for TWT was developed by the state of Colorado (Tarr et al. 1998). The procedure followed to develop this design method was very similar to the one

used in the PCA method. Experiments using slab thicknesses between 5 and 7 inches were performed and the measured strain values were used to calibrate and verify the computer model. Theoretical design equations to predict critical stresses and strain were identified. Correction factors for stresses due to load position and differences between the calculated and the measured stresses were included in the model. Also correction factors for the strains at the interface between the concrete slab and the asphalt layer were evaluated to account for the bond condition. An additional factor to consider the effect of temperature was added to the model, which modifies the stress in the concrete. The prediction equations were developed for load varying from 20 kips to 40 kips single-axle load. Failure criteria for both materials were assumed from fatigue relationships. As considered in the PCA design procedure, the number of load repetition for the concrete slab is a function of the flexural stress-to-strength ratio. The failure criterion for the asphalt concrete is based on the allowable number of repetitions, which was considered as a function of the asphalt elastic modulus and the volume of binder and voids. In this method the number of repetition that the asphalt concrete has already carried is also considered.

2.6 Performance of UTW and TWT Projects

Most of the experimental UTW and TWT project sites have performed very satisfactorily. At the Louisville site, two overlay thicknesses were evaluated (2 and 3.5 in.), and joint spacings of 6 ft and 2 ft. were used. UTW test sections with 2-ft joint spacing showed much less cracking than those 6-ft joint spacing for 2-in. thick slabs.

Evaluations in Georgia, conducted two years after construction, indicated good performance (Wu et al. 2001). The UTW test sections were located in a truck weigh station on I-85. The test sections had a design UTW thickness of 2.5 in. (64 mm) and the existing asphalt thickness was about 11 in. (279 mm). It was reported that the test sections had been subjected to

351,000 18-kip (80-kN) Equivalent Single Axle Loads (ESAL) in two years. Only 2% of the slabs had cracks for the test sections with fiber reinforced concrete and 5% of slabs had cracks for the non-fiber sections. A design evaluation using the PCA's design procedure also indicated that the UTW test sections were designed adequately.

A wealth of information on the behavior of UTW was generated from the Tennessee experience (Wu et al. 2001). After the first experimental project was constructed in Nashville in May of 1992, six more sites were built in Maryville, Chattanooga, McMinnville and Athens. Cracks observed on the first site (Nashville) were mainly attributed to the asphalt base. It was observed that during milling, the asphalt was completely removed and the concrete overlay was supported by a cobblestone base. A design evaluation also indicated that the test section was severely under-designed.

A UTW pavement project was constructed at the Spirit of St. Louis Airport to carry light-load aircraft (gross weight of 12,500 lb or 5,670 kg) traffic in 1995. The design thickness of the UTW pavements was 3 ½ in. (89 mm) with a joint spacing of 50 in. (1.3 m). The existing asphalt pavement was milled before concrete placement to create a rough surface. The asphalt thickness after milling was about 3.1 in. (79 mm). A visual condition survey of the UTW pavements was performed on July 2001 (Wu et al. 2002). It was observed that, after over six years of service, the UTW pavements performed extremely well, with very little distresses observed on the entire site. Out of the more than 7,200 panels, only 18 panels (0.25%) have exhibited distresses, with majority of them in the form of corner cracking.

The Iowa and Minnesota Departments of Transportation (DOT) have also been actively involved in the UTW technique development and evaluation. In 1994, Iowa constructed 7.2 miles (11.6 km) of UTW pavements on a segment of Highway 21 (Cable et al. 1997 and Cable et

al. 2001). The research was designed to evaluate the long-term performance of UTW pavements and their applicability in Iowa. Four major variables were included for evaluation, resulting in a total of 41 test sections. The four variables were overlay thickness, joint spacing, the use of fiber, and the asphalt surface preparation. The pavements were subjected to an estimated Average Daily Traffic (ADT) of 1,350 (or 40 ESAL's per day). Through continuous monitoring of the test sections, after seven years in service, the test sections have performed well and have exhibited minimal distresses.

In October 1997, the Minnesota DOT constructed several thin and ultra-thin whitetopping pavements on I-94 at the Minnesota Road Research (Mn/Road) (Vandenbossche et al. 2002). The existing asphalt pavement was in fairly good condition, with minor cracking and rutting. The asphalt pavements were milled to the depth of the overlay thickness to maintain the original pavement surface elevation. The UTW test sections had two different thicknesses, 3 in. and 4 in. (75 mm and 100 mm), with two different joint patterns, 4 ft by 4 ft and 5 ft by 6 ft (1.2 m by 1.2 m and 1.5 m by 1.8 m). After 3½ years and over 4.7 million ESALs, cracking (transverse and corner cracking) was observed in the UTW test sections. The majority of the cracking was in the truck lane. It was indicated in the research study that most of the corner cracking occurred along the inside longitudinal joint due to its location directly in the inside wheel path. Transverse cracking often occurred in the outside wheel path near a transverse joint. This indicated that using a joint layout that keeps the longitudinal joints outside the wheel paths could improve UTW pavement performance.

A forensic investigation of the UTW constructed in the Ellaville Weigh Station in Florida (Tia et al. 2002) showed that the poor performance of most of the six test sections was mainly due to an inadequate design of the overlay. The thickness of the test slabs were 3 to 4 inches,

with joint spacing of 4 and 6 feet. The premature cracking, the extensiveness and the severity of the cracking and the rapid progress of the cracking are also attributed to the lack of control on the layer thickness especially in the AC, which presented no thickness at all in some sections. The problem was aggravated by the loss of bond between the concrete slab and the asphalt layer, which had a great effect on the rapid progress of cracking and the large percentage of shattered slabs.

2.7 Accelerated Pavement Testing and Field Testing of UTW

In the spring of 1998, the Federal Highway Administration (FHWA), in partnership with concrete industry groups, undertook a study to evaluate the performance of ultra-thin white-topping under accelerated traffic load. Eight (8) sections of existing asphalt pavements were whitetopped and subjected to FHWA's accelerated loading facility (ALF) in McLean, Virginia. The experimental results indicate the bond between AC and concrete decreases the critical tensile stresses in the concrete overlay as the UTW section acts in a composite manner. Dynamic strain measurement of longitudinal strain indicates the concrete overlay experiences significant stress reversal as the wheel rolls over the pavements (Cole et al. 1999).

The Indiana Department of Transportation (INDOT) conducted an experimental study at the APT facility to investigate the performance of UTW pavement in Fall 1999 (Rajan et al. 2001). Four concrete mixtures were tested under slow moving loads. The results indicated the joint spacing of 1.2 m (4') in all the lanes was sufficient. The measured strains in the overlay were proportional to the applied load. The results showed that the pavement response was linear within the overlay. However the increase of the temperature in one of the lanes affected ~~to~~ the linearity of the pavement response. Strains at the asphalt surface increased considerably because of the temperature gradient. The researchers have found that the concrete overlay experienced

significant stress reversal as the wheel rolled over the pavement. It was also observed that the overlay thickness and the asphalt stiffness significantly affect the strains because of their influence on the location of the neutral axis (Rajan et al. 2001).

An UTW pavement with 3-inch thick concrete on 6 inch asphalt was constructed in the APT facility in Lancaster, Ohio for the purpose of measuring response under controlled loading and environmental conditions (Edwards et al. 1999). The measured strain was relatively proportional to the magnitude of the applied load over the range of 6 to10 kips at 50 °F and 5 mph. The measured tensile strains were higher on the AC surface than would be expected by projecting strains measured in the PCC layer down to the AC/PCC interface. The placement of the 3-inch thick PCC layer on 6-inch thick layer of AC lowered the neutral axis of this UTW pavement structure to the lower portion of the PCC where tensile strains were minimal.

The researchers at Purdue University and INDOT conducted an UTW pavement experiment to investigate the applicability of PCA design guidelines for UTW designs (Galal et al. 2004). Preliminary results indicate that the PCA design equations may be able to be used if the concept of an equivalent thickness is employed. Equivalent section was hypothesized to take into account the additional layer in the existing composite pavement structure. There was a good agreement between the measured strain in the composite UTW section and the computed strains from the ESLYM5 program.

Nishizama et al. 2003 performed full-scale experiments to evaluate the mechanical behavior of UTW pavements in Japan. The experiment included the appropriate instrumentation with strain gages embedded in the concrete slabs and thermocouples to monitor strain and temperature respectively. Two joint spacings were investigated (4’ and 6’). The loading periods included summer and winter time. The load was applied in two ways: stationary and moving. In

the stationary load test, a load was applied on the edge of the slab through a 30 cm diameter plate by a jack and a crane truck. The load was applied at increments of 9.8 kN up to 49 kN and strains were measured at each load increment. In the moving load test, the crane truck traveled on the test pavement at a low speed and dynamic strains were measured every 0.1 sec. A single thickness of 4 inches for both the concrete slab and AC layer was used in the test. The concrete slab was placed bonded to the AC layer. The measured strains were compared with the calculated ones obtained from a 3D FE model and the comparison showed a good match.

2.8 Analytical Models

Many efforts have been done to model whitetopping pavements. Most of them have focused on modeling the interface interaction between the concrete slab and the AC layer. In addition to the bond interface evaluation, the analytical models have to consider also the load transfer at joints. The general approach to these two types of interaction is the use of springs to represent the stiffness in different directions.

A 2D finite element model, NSLIP (Nelson et al, 2002) was developed to model the interface condition in composite pavements to study the delamination. In this model a 4-node slip finite element with displacement in the normal and shear direction was used. The stiffness in the normal direction was considered as infinitely large when the interface was in compression. It was hypothesized that when the interfacial strength is exceeded, delamination occurs in the interface.

The concept of friction factor was used in combination with the ISLAB2000 FE program (Khazanovich at al. 2002) to characterize the bond in the interface of composite pavements. The ISLAB2000 program contains two models to analyze the interface: the modified Coulomb friction model and the simplified friction model. For the analysis, Khazanovich utilized the

simplified friction approach in conjunction with the transformed section concept. The simplified friction model allowed for modeling of intermediate degrees of interaction between the fully bonded and un-bonded and the friction factor was shown to be a good indicator of level of bond.

Nishizawa et al. 2003, developed PAVED3D, a 3D FE model using 3D solid elements with 8 nodes per element. This model has the capability to model several slabs with the respective joints. The interaction between concrete slabs is modeled through spring elements that represent the stiffness in the plane of the joint (K_s and K_t), and in the normal direction (K_n). Springs were also used to model the interface interaction between the concrete slab and the AC layer. Similar to the joint case, three springs were utilized. The findings of this research were that by varying the stiffness of the springs used in the interface it is possible to model different levels of bond.

CHAPTER 3
INSTRUMENTATION AND CONSTRUCTION OF TEST SECTIONS

3.1 Description of the Testing Phases

The HVS testing of the test sections in this study were divided into two main phases, namely Phase I using bonded composite pavements, and Phase II using un-bonded composite pavements. Phase I was divided in two sub phases by using two different joint spacings. The description of the phases is as follows:

(1) Phase I-a - It involved three test sections on Lane 6 of the APT test area at the FDOT State Materials Research Park. The concrete slabs were placed bonded to the top of an asphalt concrete layer, and had a panel size of 6 feet by 6 feet. The three test sections had concrete slab thicknesses of 4, 5 and 6 inches. The thickness of the underlying AC varied from 4 to 5 inches.

(2) Phase I-b - It involved three test sections on Lane 7 of the APT test area. Similar to Lane 6 in Phase I-a, Lane 7 also had three test sections with concrete slab thickness of 4, 5 and 6 inches placed bonded to the top of a similar AC layer. The panel size in this case was 4 feet by 4 feet.

(3) Phase II - It involved three test sections on Lane 6 constructed after the test sections from Phase I-a were tested and removed. In this case, the concrete slabs were 6, 8 and 10 inches thick, placed un-bonded to the top of the asphalt layer. The concrete panel size was 6 feet by 6 feet.

Although there was some variation in the asphalt thickness in the test track, the thickness of the asphalt layer was not considered as a variable in this experiment and an average thickness of 4.5 inches was used in the analysis.

3.2 Layout of the Test Sections

3.2.1 Phase I

The test track in Phase I-a (on Lane 6) consisted of three test sections of 4, 5 and 6 inches of concrete placed bonded to the existing AC layer, with 6 ft by 6 ft joint spacing. The test track in Phase I-b (on Lane 7) consisted of three test sections with the same thicknesses as those used on Lane 6, but with 4 ft by 4 ft joint spacing. The concrete overlay in Lane 7 was also bonded to the existing AC layer. While the 4-inch concrete slabs are considered UTW, the 5- and 6-inch slabs fall in the category of TWT. Figure 3.1 shows the layout of the test sections in Lanes 6 and 7. The test sections are confined by two ends and transition concrete slabs constructed to support the HVS.

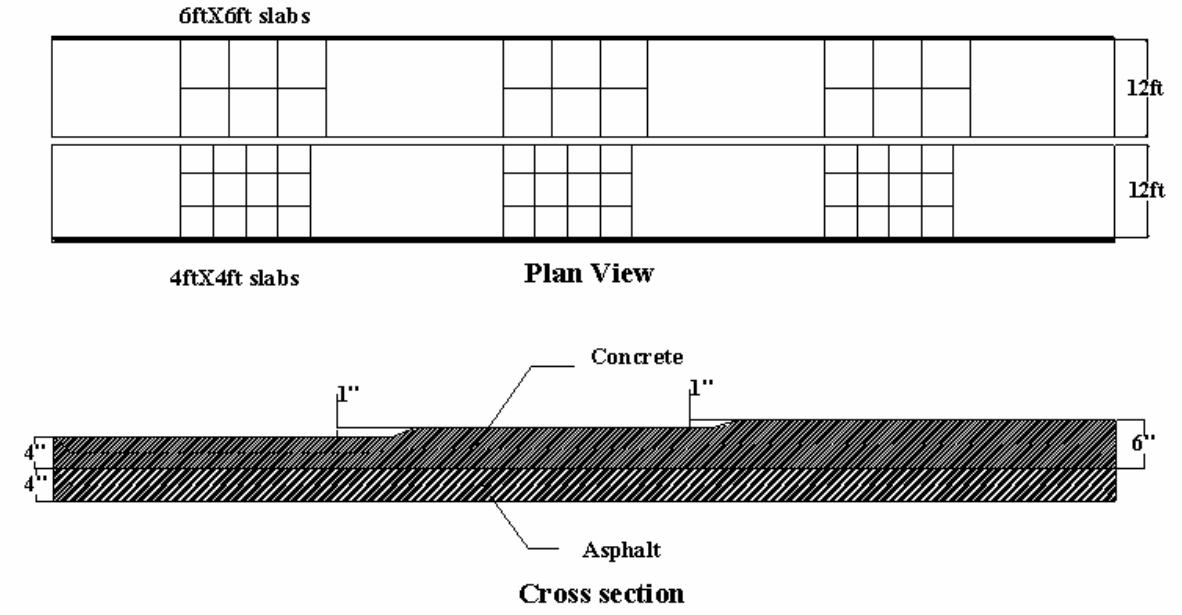

Figure 3.1. Layout of the Test Sections for Phase I.

3.2.2 Phase II

After the removal of the test sections for Phase I-a, Lane 6 was overlaid with 6, 8 and 10 inches of concrete placed un-bonded to the existing AC layer, with 6 ft by 6 ft joint spacing.

Because it was not possible to remove the concrete slab without damaging the AC layer (a very strong bond was observed), the existing asphalt layer was also removed and replaced with a new one with the same thickness and properties. To ensure an un-bonded condition in the interface in these test sections, a white pigmented curing compound was sprayed on the asphalt surface prior to the concrete placement. Figure 3.2 shows the test section layout for Phase II.

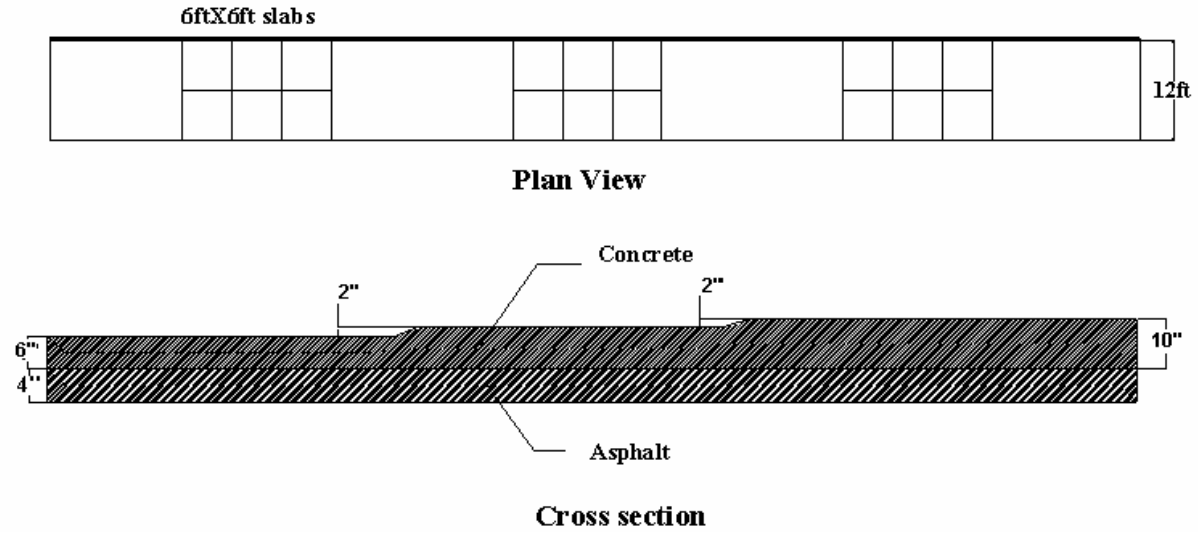

Figure 3.2. Layout of the Test Sections for Phase II.

3.3 Layout of the Instrumentation

3.3.1 Wheatstone Bridge Circuits

To monitor the strains in the test track, Wheatstone half-bridge circuits were used. In this configuration one strain gage was used as an active gage to monitor the load-induced strain, while another one was used as a dummy gage for temperature compensation. The Wheatstone half-bridge circuit used is shown in Figures 3.3 and 3.4. The active gage with a resistance of R_A is subjected to a temperature-induced strain (y) and a load-induced strain (x) simultaneously. The dummy gage with a resistance of R_D, is subjected only to a temperature-induced strain (y). The effect of the temperature-induced strain "(1+y)" is canceled out in this half bridge circuit, and only the load-induced strain is measured.

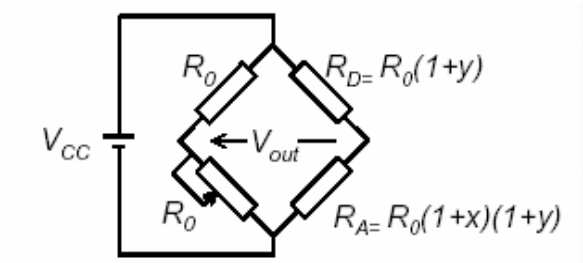

Figure 3.3. Strain Gage Arrangements in a Half Bridge Circuit.

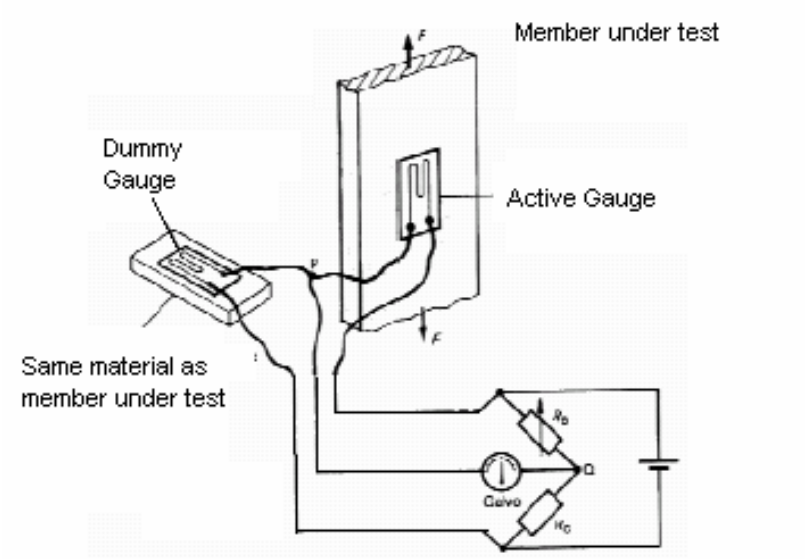

Figure 3.4. Connection of the Active and Dummy Strain Gages in the Half Bridge Circuit.

3.3.2 Preliminary Stress Analysis

To determine the instrumentation layout, a stress analysis was performed to estimate the maximum stresses. The capability of the ADINA program to consider a bonded condition between layers was used to model the composite pavement for the preliminary stress analysis in Phase I. A 3D model considering four slabs was built to evaluate the stresses under critical combinations of load and temperature. Two critical load conditions were considered in the stress

analysis: at the mid edge and at the corner of the slab. Also three cases of temperature differential were applied to the model: -10, 0, and 10 °C. The temperature differential is defined as the difference between the temperature at the top of the concrete slab and the temperature at the bottom.

The FEACONS IV (Finite Element Analysis of CONcrete Slabs version IV) program was used to calculate the anticipated stresses on the test slabs for the un-bonded condition in Phase II. The FEACONS program was developed at the University of Florida for the FDOT for analysis of concrete pavements subject to load and thermal effects. This program was chosen for use since both the University of Florida and FDOT have extensive experience with this program and its reliability has been demonstrated in previous studies.

The FEACONS program was used to analyze the stresses in the test slabs when subjected to a 12-kip (53-kN) single wheel load with a tire pressure of 120 psi (827 kPa) and a contact area of 100 in^2 (645 cm^2), and applied along the edge of the slab, which represents the most critical loading location. Similar to the case of bonded interface (Phase I), the analysis was performed for two different load positions, at the corner of the slab and at the middle of the edge, for the same temperature differentials in the concrete slabs. No load transfer at the joints was assumed in the analysis, which represents the worst condition.

3.3.3 Instrumentation Layout

With the results from the stress analysis, it was possible to identify the locations where the maximum stresses and strains in the test slab would occur so that strain gages could be placed to monitor these maximum induced strains. The following sections describe the instrumentation layout for Phases I and II.

Phase I

Figure 3.5 shows the instrumentation layout for the 6 ft by 6 ft test section (Phase I-a), which were placed on Lane 6 of the APT test area. Three locations (Location 1, 2 and 3) were identified to have the maximum anticipated strains due to the HVS load. Thus, strain gages were placed at these three locations. Figure 3.6 shows the vertical positions of the gages at these three locations along with the gage identification. While Location 1 had two gages, the other two locations had only one. At Location 1, one embedded strain gage was placed at a depth of 1 inch from the concrete surface, while the other embedded strain gage was placed 0.5 inch from the bottom of the concrete layer. Location 2 had a strain gage embedded 1 inch from the surface of the concrete slab. Location 3 had a strain gage embedded 0.5 inch from the bottom of the concrete slab. Two surface gages were also used to monitor any micro cracks that may occur in the concrete surface. These two gages were located next to the transversal joint at the middle of the slab, in the adjacent panels. These surface gages, located in the adjacent slabs, were also used to evaluate the load transfer at the joints.

Figure 3.5 also shows the locations of thermocouples to monitor the temperature in the slab. Two positions were considered for the thermocouples, one at the center of the slab and the other in the corner. Figure 3.7 depicts the vertical position of the thermocouples. They were placed 1" apart along the depth of the slab with the first starting at 1" from the surface. An additional thermocouple was placed on the surface of the AC layer to monitor daily variation of temperature in the asphalt layer.

Figure 3.8 shows the instrumentation layout for the 4 ft x 4 ft slabs in Phase I-b. In this case only two locations (namely Loc1 and Loc2) were identified as locations with maximum stresses and for placement of embedded gages. Four strain gages were placed on the surface of

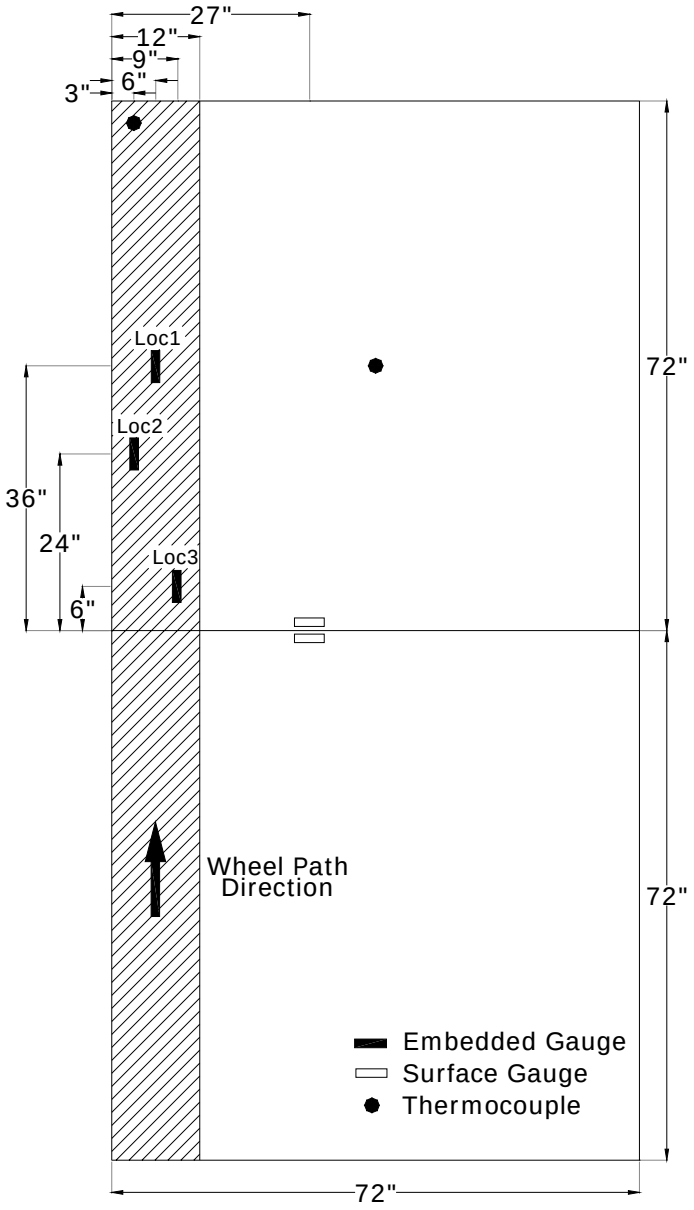

Figure 3.5. Instrumentation Layout for the Test Slabs in Phase I-a.

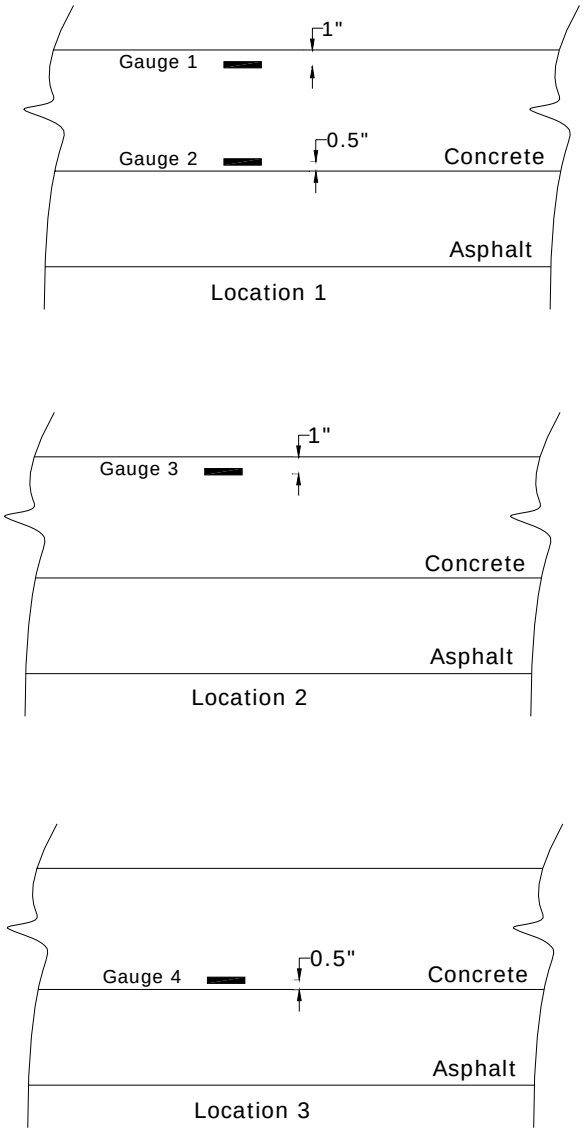

Figure 3.6. Vertical Positions of the Strain Gages in Phase I-a.

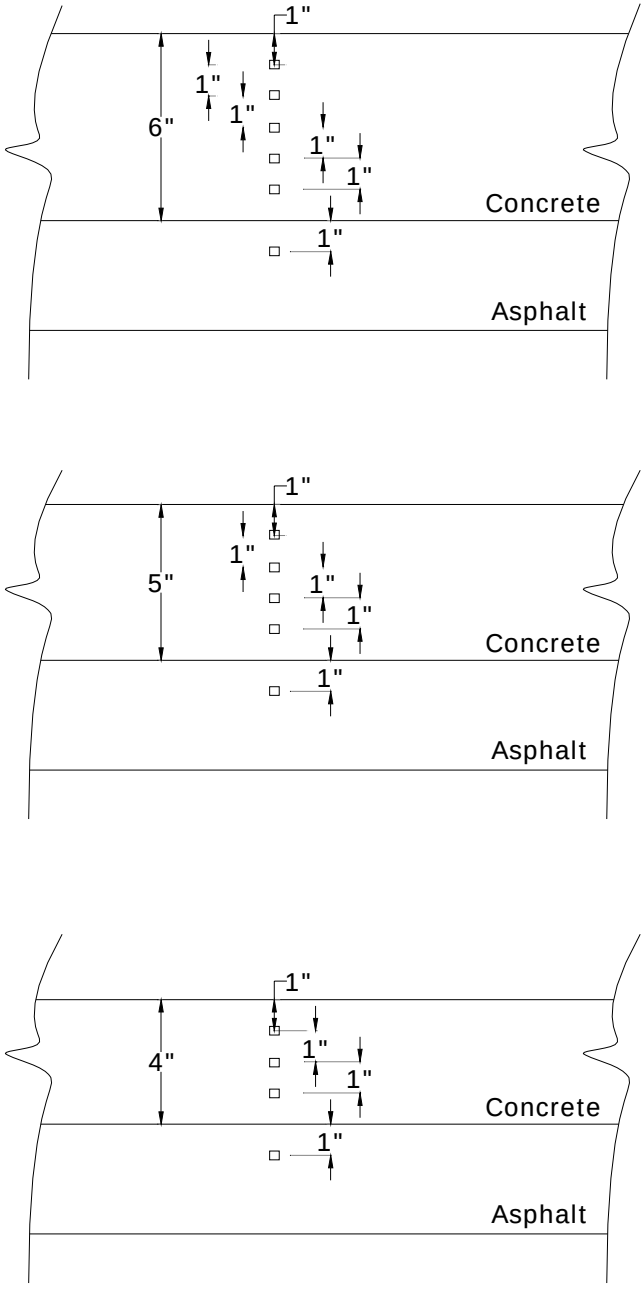

Figure 3.7. Vertical Positions of the Thermocouples for the 4", 5" and 6" Slabs in Phase I.

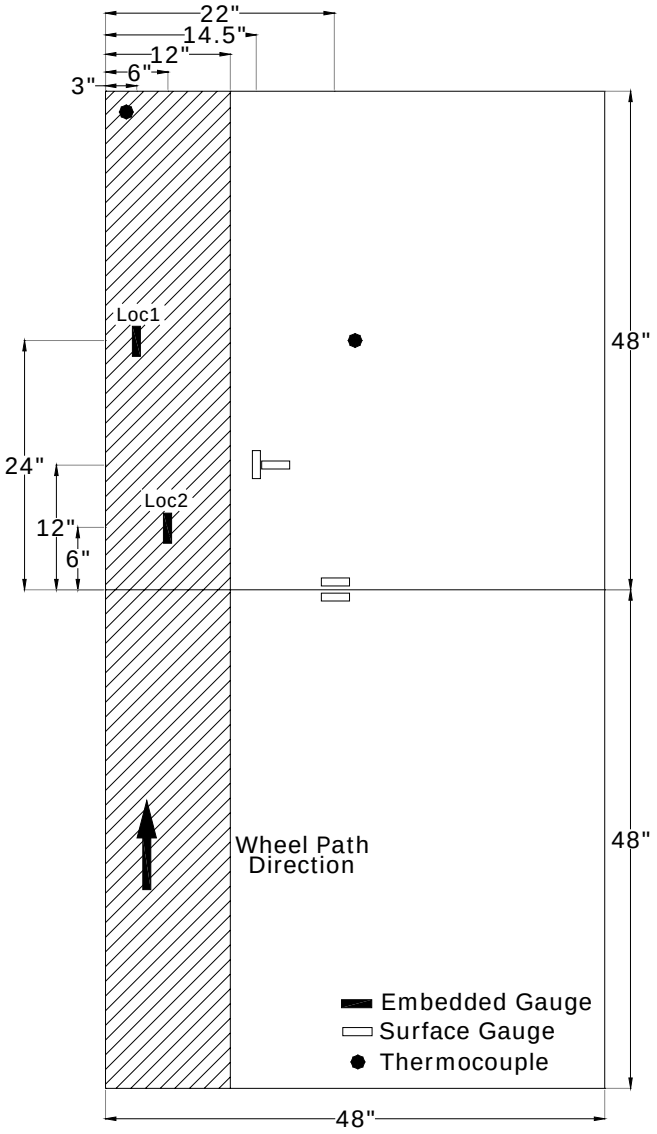

Figure 3.8. Instrumentation Layout for the Test Slabs in Phase I-b.

the concrete slab to monitor any micro cracks occurring in the slabs and load transfer at the joints. The vertical positions for the gages are indicated in Figure 3.9 along with the gage identification. At Location 1, three gages were used -- one at 1 inch from the surface of the concrete slab, the second at 0.5 inch from the bottom of the concrete slab, and the third one at 0.5 inch below the surface of the AC layer. The placement of these three gages allowed for not only the

monitoring of the maximum strain at the top and bottom of the concrete slab, but also for the comparison of the strain values near the interface of the layers. By comparing the strain values near the interface, it would be possible to know how well the bonding condition would be in the composite pavement.

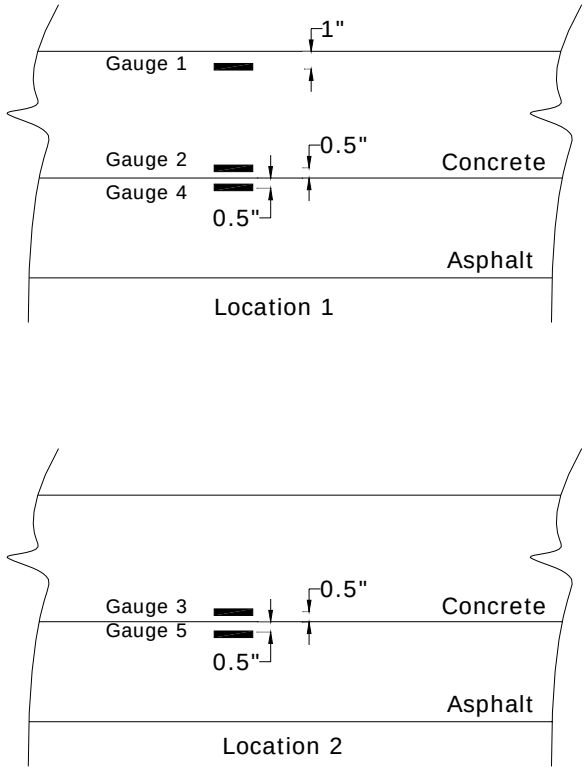

Figure 3.9. Vertical Positions of the Strain Gages in Phase I-b.

Location 2 had two gages -- one at 0.5 inch above the bottom of the concrete slab, and the other at 0.5 inch below the surface of the AC layer.

Figure 3.8 also shows the two locations for the thermocouples in Phase I-b. The vertical positions of the thermocouples in Phase I-b were the same as those used in Phase I-a, which are shown in Figure 3.7.

Phase II

Similar to Phase I, the strain gages were placed at the locations of maximum anticipated stresses due to the HVS loads. Figure 3.10 shows the instrumentation plan adopted. Taking advantage of the upgrade to the data collection equipment that allowed for more channels for data acquisition, five locations were selected for placement of strain gages. For each of these locations, a set of three strain gages were installed to monitor maximum strains in the concrete slab and the strain at the surface of the AC layer. One strain gage was placed at one inch under the surface of the concrete slab. A second strain gage was placed 1 inch from the bottom of the concrete slab. The third strain gage was located 1/2 inch below the top of the asphalt layer. The vertical positions of the strain gages are shown in Figure 3.11. Unlike the previous phase, surface gages were not used in Phase II.

The locations for the thermocouples are shown in Figure 3.10. In Phase II, three locations were used to monitor the temperature in the slabs. For each of the three thermocouple locations, a set of thermocouples were placed at depths of 1, 3, 5, 7 & 9 inches for the 10-inch slabs, at depths of 1, 3, 5 & 7 inches for the 8-inch slabs, and at depths of 1, 3 & 5 inches for the 6-inch slabs. At each of the locations, a thermocouple was also placed in the asphalt layer at a depth of 1/2 inch from the top of the asphalt layer. The vertical positions of the thermocouples are shown in Figure 3.12.

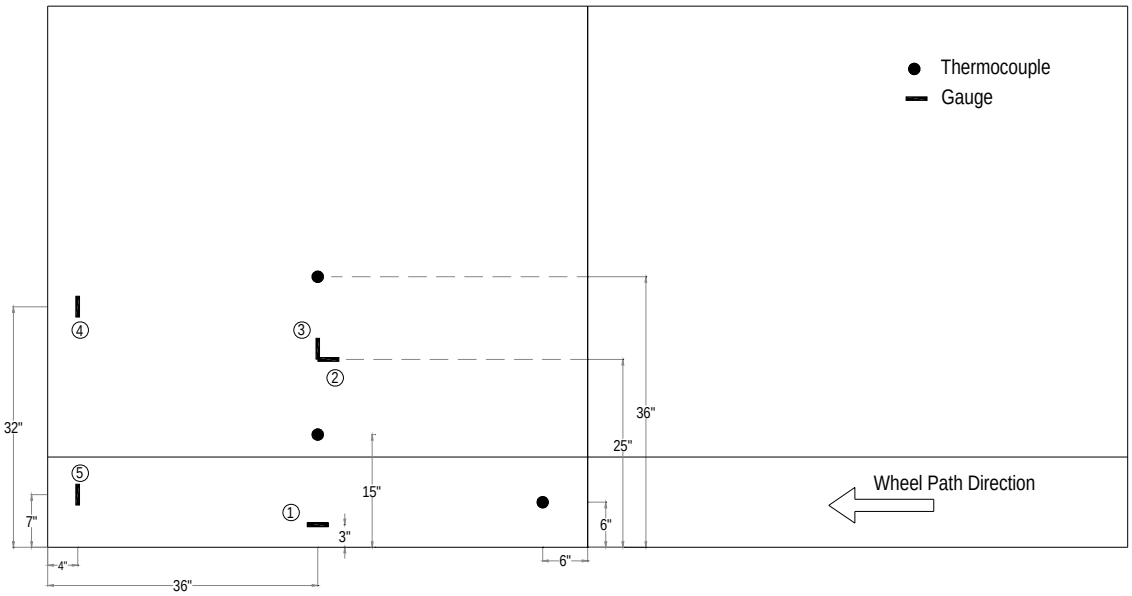

Figure 3.10. Instrumentation Layout for Phase II.

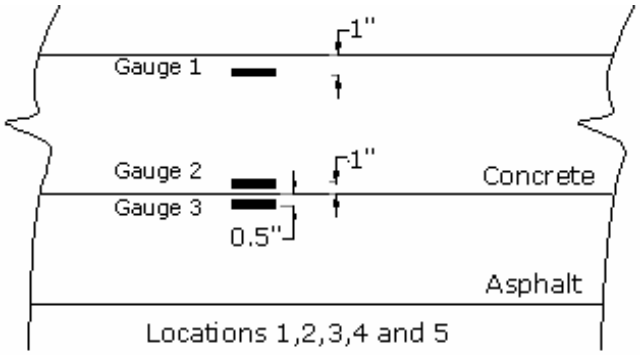

Figure 3.11. Vertical Positions of the Strain Gages in Phase II.

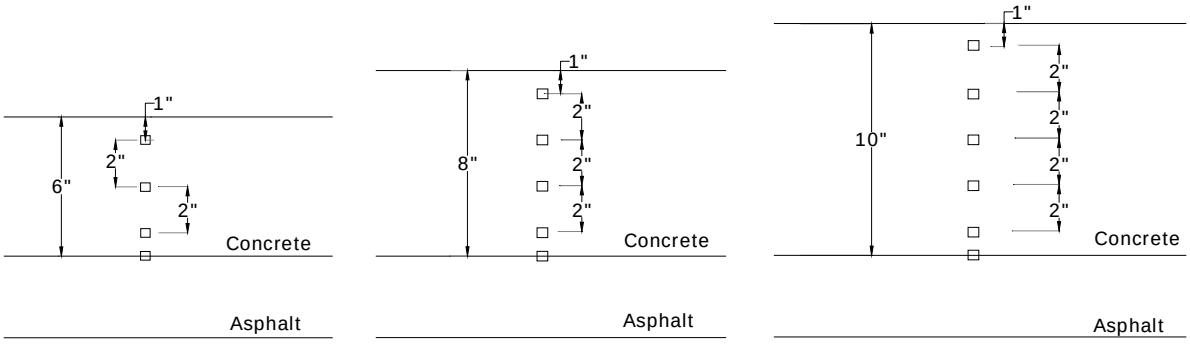

Figure 3.12. Vertical Positions of Thermocouples in Phase II.

3.4. HVS Loading Plan

Testing of the composite pavements was performed using a Heavy Vehicle Simulator (HVS), Mark IV model. HVS loading was scheduled to start 28 days after concrete placement with an initial load of 9,000 lb, super single tire, with a contact pressure of 120 psi. The wheel load traveled at a speed of 8 mph, in a uni-directional mode with no wander, and along the longitudinal edge of the test slab. Loading along the edge was chosen because it represents the most critical loading condition for a concrete slab.

If the composite pavement test sections could withstand the 9-kip load with no visible or detectable cracks for a certain period of time, the load would be increased to 12 kips, 15 kips, 18 kips, and 21 kips, to observe the behavior of the test sections under different loads, and the load at which cracking would occur.

3.5 Data Collection

For each test slab, the strain gages were connected to a strain indicator unit, Vishay System 6000 (Model 6100) for strain reading and data acquisition. This system has the ability to take individual strain readings at a very high frequency. This enabled the recording of dynamic strains as the wheel passed over the pavement. Data collection for load-induced strain was started immediately after the start of HVS loading. Strain data were collected for 30 seconds at one-hour intervals. The rate of data collection was 100 strain values per second. This rate allowed for the capture of the progression of the strain and to especially observe the strain reversal phenomenon. Strain gage readings due to a static wheel load were also taken for two wheel loading positions, namely corner (pt 1), and mid-edge (pt 2). Static readings were recorded while the wheel was traveling at slow speed towards the static loading position and while it stayed at the two load positions (pt 1 and pt 2) for 20 seconds each. Static strains were

measured only for Phase I-a for comparison purposes with the dynamic load application. Phase I-b and Phase II included only dynamic strain data collection. While in Phase I, strain data were collected only for the loading period, strain data collection in Phase II was started a few days after concrete placement to monitor strain due to temperature changes.

All the thermocouples were connected to the same data acquisition system. Temperature data were collected during the entire day at 5-minute intervals. In both phases, data collection for temperature was started before the loading period, especially in Phase II where strain due to temperature changes was monitored.

3.6 Construction of the Test Tracks

3.6.1 Construction of Concrete Test Tracks in Phase I

Asphalt surface preparation and formwork

The concrete test track for Phase I-a was constructed on Lane 6 on June 10, 2004, and that for Phase I-b was constructed on Lane 7 on August 10, 2004. These two concrete test tracks were constructed over an existing four-inch thick asphalt surface (two 2 in lifts of asphalt) at the APT test area at the FDOT State Materials Research Park. The asphalt surface was milled and cleaned prior to the placement of formworks for the test track. Figure 3.13 shows the milled asphalt surface in Lane 6. In the construction of Lane 7, a tapered formwork was used at the transition from one thickness to the other to make the placement of the concrete easier. Figure 3.14 shows the formwork used for Lane 7.

Figure 3.13. Milled Surface Before Concrete Placement on Lane 6 in Phase I-a.

Figure 3.14. Formwork Prepared for Lane 7 in Phase I-b.

Concrete Mix Proportions

A minimum 24-hour compressive strength of 2500 psi and minimum 28-day strength of 5800 psi were specified for the concrete for the test tracks. The mix designs used for Lanes 6 and 7 in Phases I-a and I-b are shown in Table 3.1.

Table 3.1. Mix Designs of Concrete Used in Phases I and II.

Lane No.	Material	Target	Actual	Moist, %	Remarks
Lane 6 PHASE I-a (06/08/2004)	Cement	508 lb	506 lb		
	D57 Stone	1801 lb	1798 lb	1.5	Pit # 08-012
	DOT Sand	1328 lb	1316 lb	5.0	Pit # 76-349
	Air entrainment, MBAE 90	1 oz	1.1 oz		
	Admixture, MBL 80	45 oz	40.2 oz		
	Water	15.6 Gal	17.2 Gal		
	W/C				
Lane 7 PHASE I-b (10/08/2004)	Cement	508 lb	504 lb		
	D57 Stone	1801 lb	1810 lb	1.8	Pit # 08-012
	DOT Sand	1328 lb	1346 lb	5.0	Pit # 76-349
	Air entrainment, MBAE 90	1 oz	1.1 oz		
	Admixture, MBL 80	45 oz	45 oz		
	Water	15.6 Gal	16.5 Gal		
	W/C				
Lane 6 PHASE II	Cement	508 lb			
	D57 Stone	1750 lb		6.99%	Pit # 08-004
	Silica Sand	1265 lb		5.84%	Pit # 76-349
	Air entrainment, MBAE 90	2 oz			
	Admixture, MBL 80	65.0 oz			
	Water	255 lb			
	W/C	0.502			

Placement of Concrete

Before placing the concrete on top of the asphalt layer, water was sprayed on the asphalt surface to promote a good bond between the concrete and the asphalt and to prevent the reduc-

tion of water from the concrete. Samples of concrete were taken from a selected truck during concrete placement. The slump, air content and temperature of the fresh concrete were measured. Samples were fabricated for compressive strength and elastic modulus, maturity test, and flexural strength tests. Figure 3.15 shows the concrete test track after placement of the concrete. After placement and finishing of the concrete on the test track, saw cuts were made to a one third (1/3) of the thickness to form the joints for the slabs. A diamond-bladed saw was used for these cuts to ensure a smooth, straight vertical surface.

Figure 3.15. After Placement of Concrete on Lane 6 in Phase I-a.

Placement of Strain Gages

Embedded strain gages were installed in the test slabs at the location described in Section 3.3.3. Each strain gage was fixed between two steel rods fixed to the base layer. At the locations

where both the top and bottom embedded gages needed to be placed, one gage was fixed at the top of two rods and the other gage was fixed at the bottom of the two rods using nuts and bolts. Figure 3.16 shows the placement of the top and bottom strain gages in a 4-inch test slab in Lane 7. The strain gages were placed in the concrete with a distance of 1 inch from the top and 0.5 inch from the bottom of the concrete. Surface gages were placed before loading was started on the test slab. The surface of the concrete where surface gages were placed was cleaned using a sand paper and applied with the recommended glue to bond the strain gages to the concrete. Figure 3.17 shows a picture of the surface gages at a joint on the 4-inch test slab in Lane 6.

Figure 3.16. Placement of Top and Bottom Strain Gages on Lane 7 in Phase I-b.

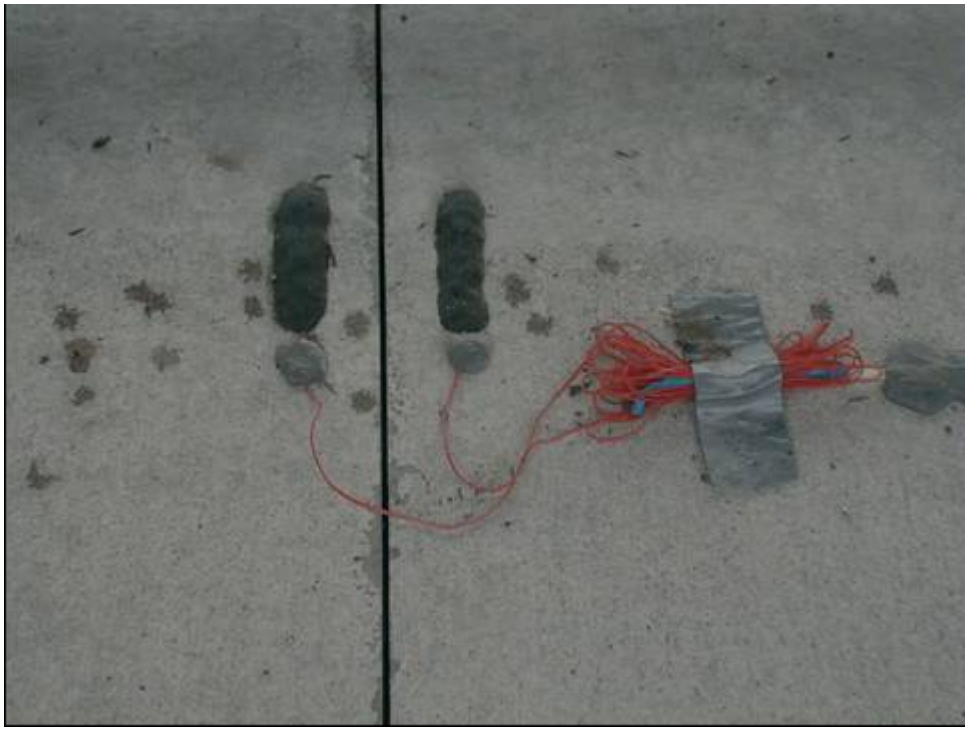

Figure 3.17. Placement of Surface Strain Gages at a Joint in Phase I-a.

Figure 3.18. Strain Gages in a Protective PVC Pipe Before Placing Concrete.

A PVC cylinder was placed around the embedded strain gages during placement of concrete, as shown in Figure 3.18. The concrete was placed in the cylinder manually to prevent disturbance from the concrete handling instruments. After the concrete was placed to the same thickness both inside and outside the PVC pipe, the PVC pipe was then removed by pulling it out vertically.

Placement of Thermocouples

Thermocouples were placed at various depths in the test slabs to monitor temperature variation. This was achieved by fixing the thermocouples to a PVC rod at different heights. The thermocouple-attached rods were fixed to the asphalt layer. Similar to the case of the strain gages, a PVC cylinder was placed around each of the rods to protect it from the concrete handling instruments during the concrete placement. The concrete was placed manually in the PVC pipe to prevent any disturbance from the concrete handling instrument. The PVC pipe was removed after the concrete was placed to the same thickness inside and outside of the PVC pipe. This procedure ensured the proper position of the thermocouples by preventing any disturbance from the concrete placement.

3.6.2 Construction of Concrete Test Tracks in Phase II

Asphalt Surface Preparation and Formwork

After testing on the concrete slabs in Phase I-a was finished, the concrete slabs were removed from Lane 6, and the test sections in Phase II were placed on Lane 6. When attempts were made to remove the concrete slabs without removing the underlying asphalt layer, it was found that the concrete slabs were bonded so well to the asphalt layer that a lot of the underlying asphalt concrete was also removed at the same time. Figure 3.19 shows the condition of Lane 6

during the slab removal process. Due to this situation, a new asphalt layer was placed on Lane 6 before the concrete slabs in Phase II were placed.

Figure 3.19. Removal of Concrete Slabs from Lane 6 in Phase I-a.

Figure 3.20. Formwork for Test Slabs in Phase II.

Figure 3.20 shows the formwork for the concrete slabs in Phase II. Each test section was 18 feet long, with transition zones separating one test section from another. A tapered formwork was used at the transition from one thickness to the other to make the placement of the concrete easier.

Installation of Strain Gages and Thermocouples and Concrete Placement

The method of installation of strain gages and thermocouples was similar to that used in Phase I. Grooves were cut with a diamond saw on the surface of the asphalt surface for placement of the strain gage and thermocouple wires (Figure 3.21). Thermocouples and strain gages were installed at specified locations on the test slabs and covered by PVC pipes before placement of concrete, as described in Section 3.6.1.

Before the concrete was placed, a white pigmented curing compound was applied to the asphalt surface to act as a debonding agent between the asphalt and the concrete slab. The prepared asphalt surface is shown in Figure 3.22.

Figure 3.21. Grooves on Asphalt Surface for Placement of Strain Gages and Thermocouples Cables in Phase II.

Figure 3.22. Asphalt Surface with White Curing Compound Before Concrete Placement in Phase II.

The concrete was placed on October 11, 2005. The mix design of the concrete used is shown in Table 3.1. The same procedure used in Phase I to protect the instrumentation during concrete placement was followed in this case.

Figure 3.23 shows the finishing of the concrete test track in Phase II. The joints for the concrete slabs were sawed the following day. Each test section was sawed into six 6 ft x 6 ft panels. The concrete slabs were kept moist by sprinkling with water for at least 3 days to ensure adequate curing (Figure 3.24).

Figure 3.23. Finishing of the Concrete for the Test Track in Phase II.

Figure 3.24. Curing of Concrete by Sprinkling with Water.

CHAPTER 4
DEVELOPMENT OF A 3-D FINITE ELEMENT MODEL FOR ANALYSIS OF WHITETOPPING PAVEMENTS

4.1 Finite Element Program

The multi-purpose finite element program ADINA version 8.2 was used to build the model for the analysis of whitetopping pavements in this study. The capability of the ADINA program for 3-D finite element analysis, its versatility in modeling materials behaviors under load and temperature effects, and its capability in modeling the interface condition between two layers make this program very appropriate to model composite pavements.

The ADINA program has a very friendly user interface to build the needed models for specific applications. It has a routine to automatically create finite element meshes based on the boundary definitions and density specifications. The program also has a complete post-process routine to generate the results both numerically and graphically.

4.2 Six-Slab and Twelve-Slab 3-D Finite Element Models

Figures 4.1 shows a 6-slab 3-D FE model developed for the analysis of the composite pavement test sections with a joint spacing of 6 feet. The 6-slab model was used to analyze the test sections in Phase I-a and Phase II. The number of slabs used in this model corresponds to the actual number of slabs in each test section in these two phases of the study.

Figure 4.2 shows a 12-slab 3-D FE model developed for analysis of the composite pavement test sections with a joint spacing of 4 feet, which were used in Phase I-b. The number of slabs used in this model also corresponds to the actual number of slabs in each test section in Phase I-b of the study.

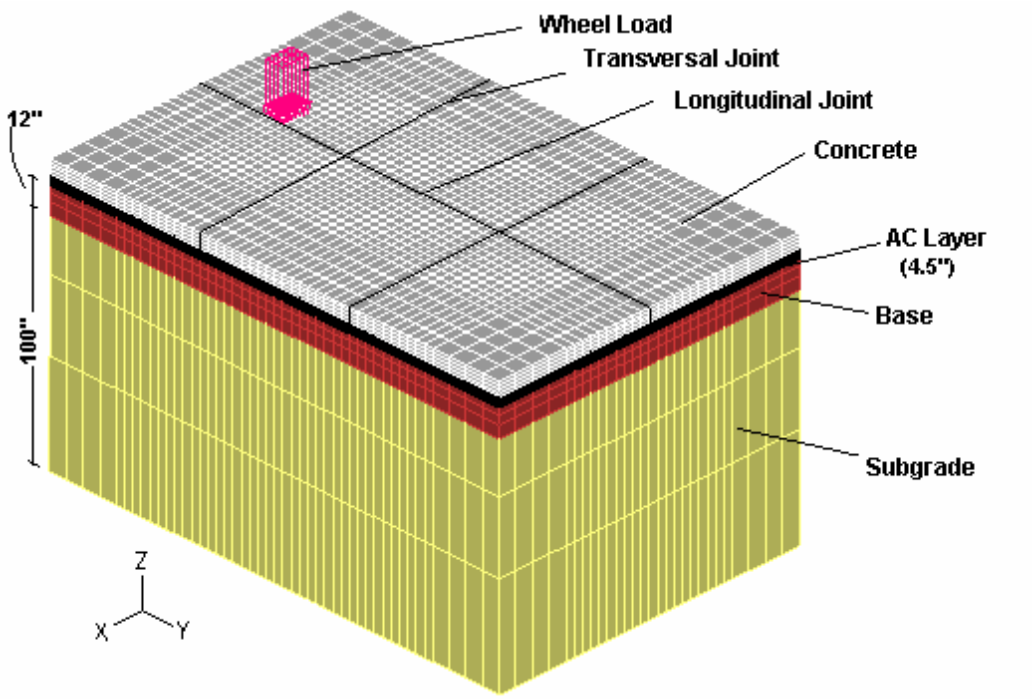

Figure 4.1. Six-Slab 3-D Finite Element Model.

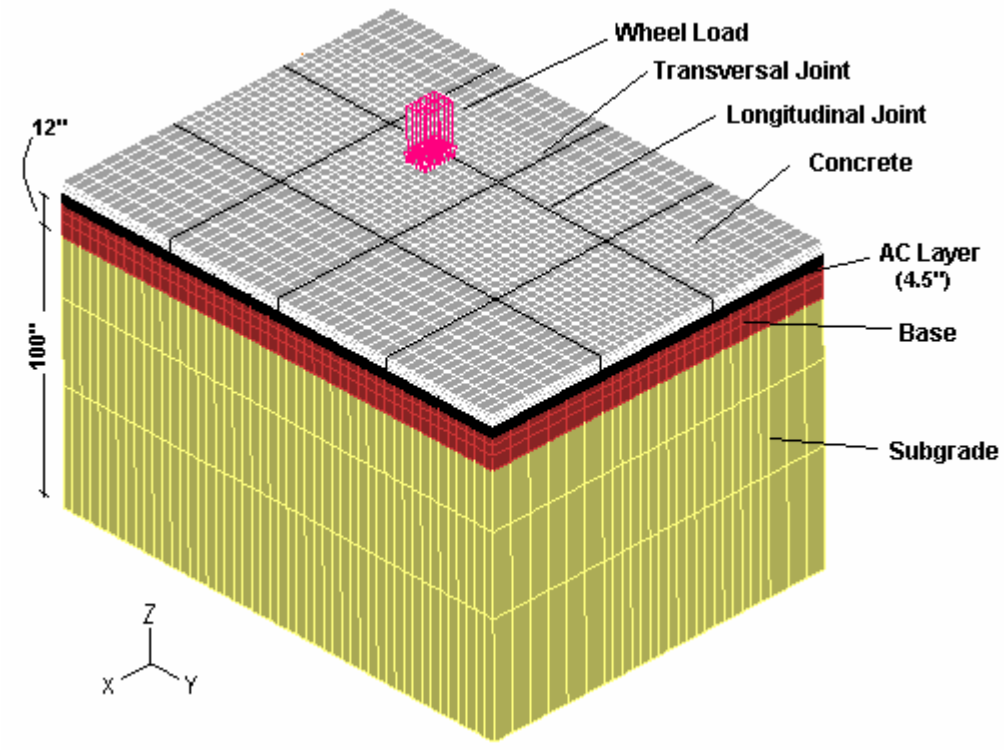

Figure 4.2. Twelve-Slab 3-D Finite Element Model.

As shown in Figures 4.1 and 4.2, the subgrade is modeled by a 100-inch thick layer at the bottom of the model. This layer is modeled as an assemblage of 3-D solid elements whose vertical dimension decreases towards the top. The bottom of this layer is modeled as fixed with no rotation or translation allowed.

On top of the subgrade layer is a 12-inch thick layer modeling the lime rock base, which is modeled as bonded to the subgrade layer. The vertical dimension of the 3-D elements in this layer also decreases towards the top.

On top of the base layer is a 4.5-inch layer modeling the AC layer, which is modeled as bonded to the base layer. The AC layer was modeled by three layers of 3-D elements, 1.5 inches thick each.

The layer at the top models the concrete slabs. The thickness of this layer is variable to represent the 4, 5, 6, 8 and 10 inches thickness of the concrete slabs used in the test sections in this study. This layer is modeled by four equal layers of 3-D element. The thicknesses of the finite elements in this layer are 1, 1.25, 1.5, 2 and 2.5 inches for the 4-, 5-, 6-, 8- and 10- inch concrete slabs, respectively.

The mesh pattern in the XY plane is the same for all four layers. Figures 4.3 and 4.4 show the mesh patterns in the XY plane used for the 6-slab model and the 12-slab model, respectively. Finer meshes are used in the areas of maximum anticipated stresses in the test sections where the strain gages were placed, in order to obtain more accurate computed strains in these areas for verification with the measured strains.

4.3 Solid 20-Node Finite Element

All 3-D solid elements were modeled as 20-node elements. Figure 4.5 shows the 3-D solid element, along with the node configuration. The 20-node element has a hexahedral shape,

with one node at each of its 8 vertices and one node at the middle of each of its 12 edges. Each node has six degrees of freedom (three translations and three rotations). This type of node configuration has been shown to give a high level of accuracy in combination with an acceptable computing time demand. Considering the mesh patterns as shown in Figures 4.3 and 4.4 and the node configuration in the 3-D solid elements as shown in Figure 4.5, the model response in terms of strains and stresses can be obtained at locations as close as 2" horizontally and 1.25" vertically from one another.

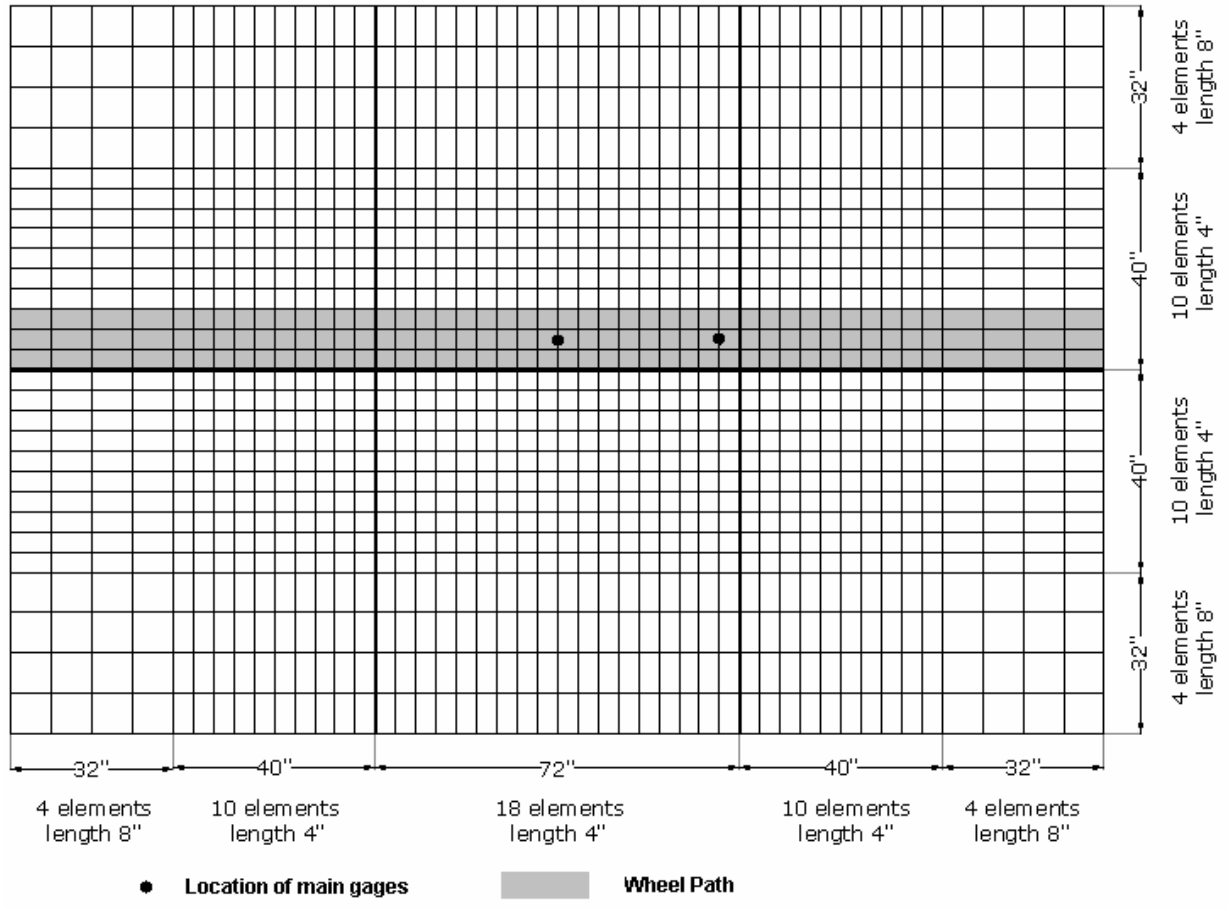

Figure 4.3. Mesh Pattern in the XY Plane for the 6-Slab Model.

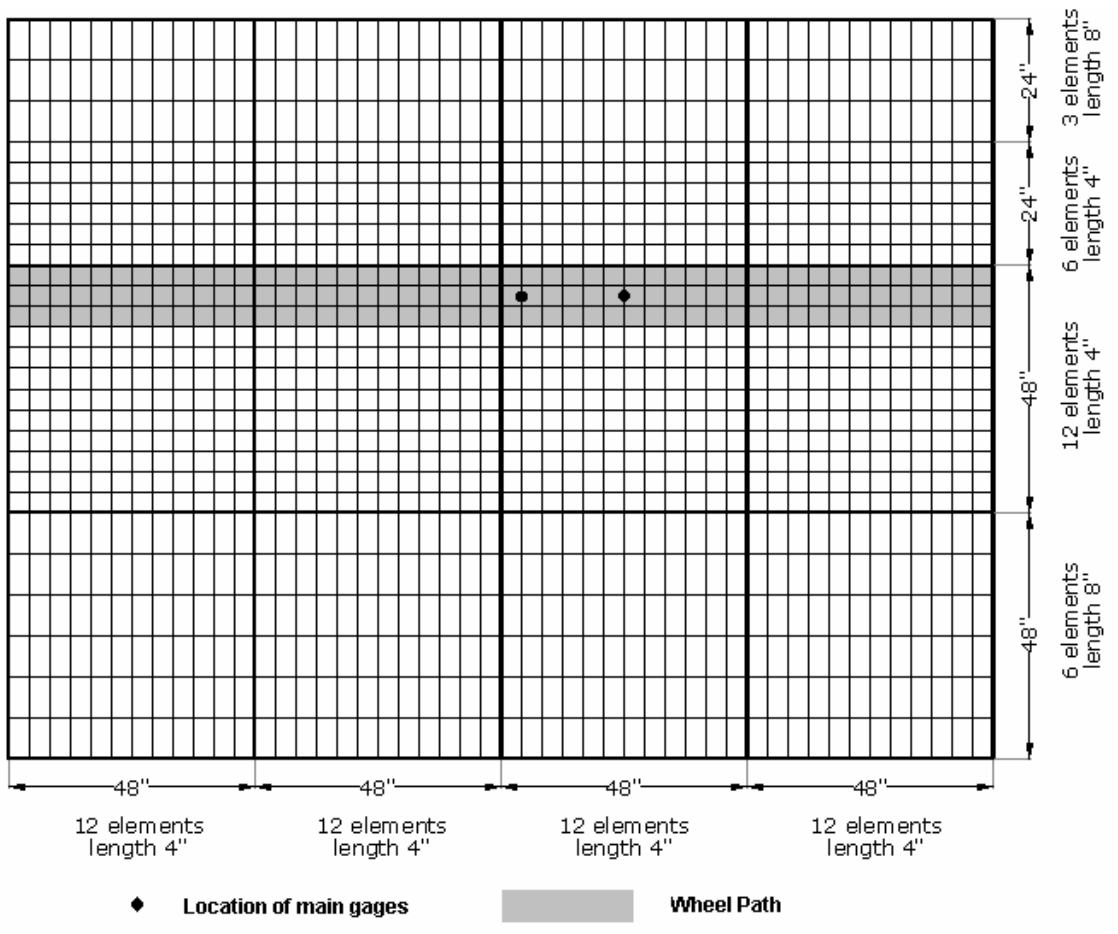

Figure 4.4. Mesh Pattern in the XY Plane for the 12-Slab Model.

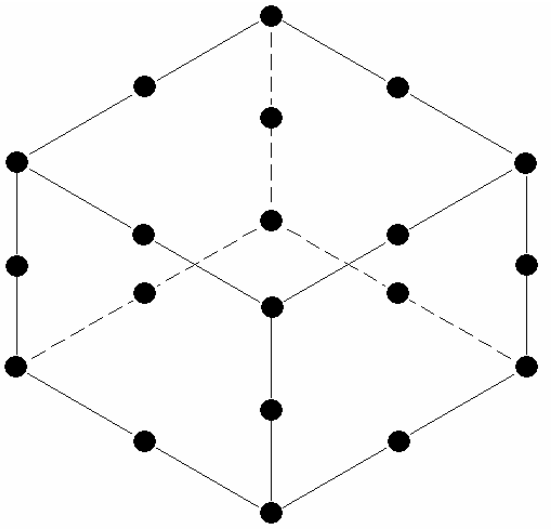

Figure 4.5. Twenty-Node 3D Solid Element Used in the Analytical Model.

4.4 Modeling of Concrete Slab Joints

Load transfer across the joints between two adjoining concrete slabs is modeled by translational springs connecting the slabs at the nodes of the finite elements along the joint. Three values of spring constants are used to represent the stiffnesses along three different directions. Figure 4.6 shows the load transfer elements used in the model. K_t, K_s and K_n are stiffness components in the Z, Y and X direction respectively, as shown in Figure 4.6.

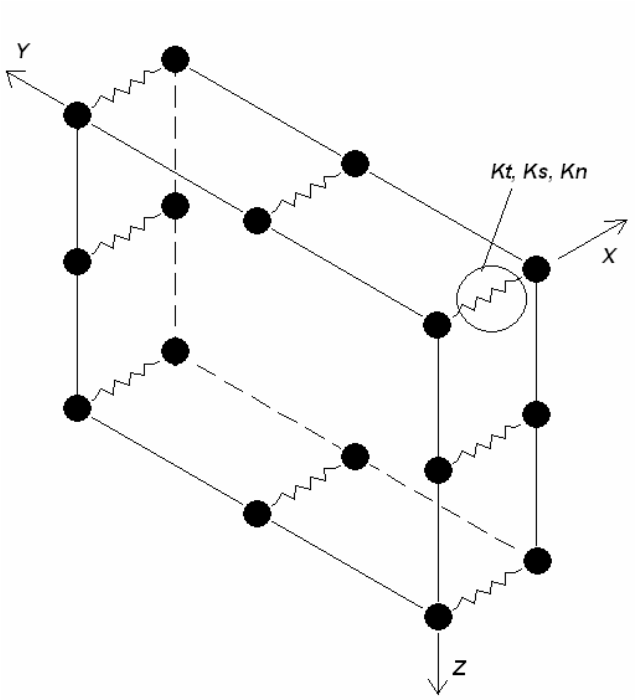

Figure 4.6. Springs to Model Load Transfer at Concrete Slab Joints.

4. 5 Modeling of Materials

The concrete, AC, base and subgrade materials are modeled as isotropic and linearly elastic, and are characterized by their elastic modulus and Poisson's ratio. The AC material is also modeled as a temperature dependent material with an elastic modulus which varies with temperature. The contraction and expansion of the concrete due to temperature effects is also

considered in the analysis and characterized by the coefficient of thermal expansion of the concrete.

4.6 Modeling of Concrete-Asphalt Interface

The concrete-asphalt interface in the composite pavement can be modeled as fully bonded, partially bonded or un-bonded.

By default, the ADINA program treats adjacent nodes as rigidly connected to one another, so that the fully bonded condition would be implicitly considered in the model with no special treatment of the interface between the concrete slab and the AC layer. The composite pavement test sections in Phase I-a and Phase I-b, which were constructed to have bonded interface between the concrete and the AC, were modeled to have a fully bonded interface in this fashion.

To model the partial bond condition in the interface, translational spring elements were used to connect the bottom of the concrete layer with the top of the AC layer at the nodes, with zero distance between the two layers. Each spring was modeled with three spring constants to represent stiffness along the three different directions. Figure 4.7 shows the configuration of the springs used at the interface. K_t and K_s represent the stiffness in the interface plane (X and Y directions), while K_n represents stiffness perpendicular to that plane (Z direction).

When the concrete-asphalt interface is fully un-bonded, there can not be any tensile load transfer across the interface, but there can still be transfer of compressive load across the interface. This is modeled by a special non-linear spring connecting the concrete and the asphalt layer at the interface. This special spring has an infinite stiffness value when the spring is in compression; however when the spring is in tension, the stiffness value is zero.

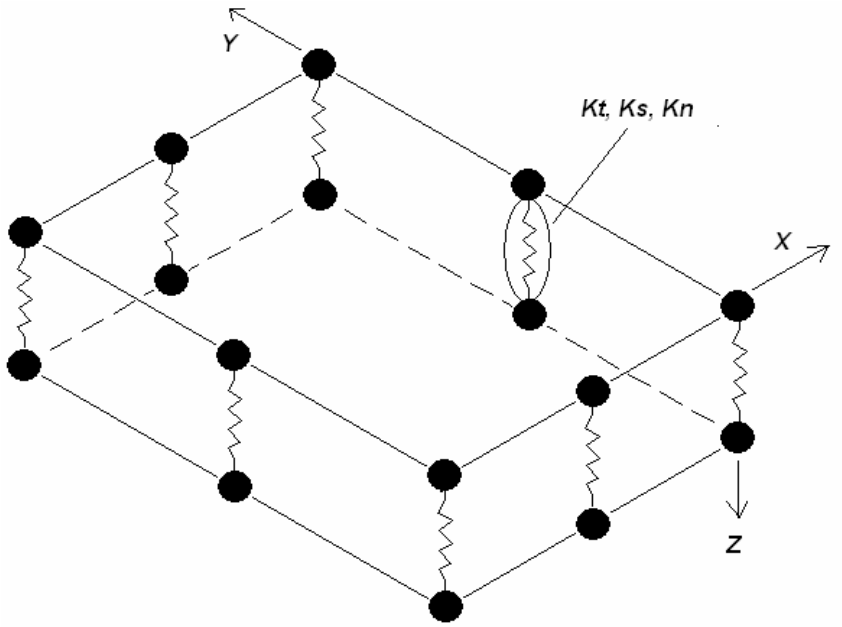

Figure 4.7. Springs in the Concrete-Asphalt Interface to Model the Partial Bond Condition.

Cores taken from the test sections in Phase II indicated that, though the concrete-asphalt interface was intended to be unbonded, there was partial bonding between the concrete and asphalt layers in these test sections. Analysis of the results of FWD tests on these test sections also indicated that the computed FWD deflections matched better with the measured deflections when the concrete-asphalt interface was modeled as partially unbonded rather than fully unbonded. Similarly, the strains calculated using the fully unbonded model resulted in strain values 25% higher than the measured strains. Thus, the model for the fully unbonded condition was not used in the analysis of the data in this study.

4.7 Modeling of Loads and Temperature Effects

To model a moving HVS wheel load on a test section in this study, computations were done for the responses of the pavement subjected to static loads placed at different consecutive

locations along the wheel path. The calculated response, such as strain at a particular location, could then be plotted versus time, as the wheel passed over the various locations at the various times. This computed strain versus time plot could then be compared to the measured strain versus time plot as obtained from the strain gage measurements during HVS loading.

The applied HVS wheel load was modeled as a uniformly distributed load over a square area. The contact area was taken to be the wheel load divided by the contact tire pressure. For example, for a 12-kip wheel load with a tire pressure of 120 psi, the contact area would be 100 in^2.

The concrete is modeled as a material which contracts or expands according to its temperature change and coefficient of thermal expansion. An initial temperature is first specified for the entire concrete layer. The effects of the change in temperature from the initial temperature were then duly considered in the analysis when the information on the temperature distribution in the concrete layer was provided in the input. The temperature at the bottom of the concrete slab is set to be unchanged from the initial temperature. The temperature in the concrete layer was assumed to vary linearly from the top to the bottom of the slab. From the temperature at the top and the bottom of the concrete slabs, the temperature of the concrete at all the nodes of the finite element mesh for the concrete slabs were computed and entered as inputs to the model.

CHAPTER 5
MATERIALS AND PAVEMENT CHARACTERIZATION

5.1. Materials Characterization

Tests were performed to characterize the pavement materials used in the test sections in this study. The properties measured include the concrete-asphalt interface bond strength, compressive strength, splitting tensile strength and elastic modulus of the concrete, resilient modulus and indirect tensile strength of the asphalt concrete, and the penetration and absolute viscosity of the recovered asphalt from the asphalt cores.

5.1.1. Interface Bond Strength

Results from Test Sections in Phase I-a

Iowa shear tests were performed on both the 4-inch and the 6-inch diameter core samples extracted from the 4-inch slabs in Phase I-a before loading started (at 28 days or later). The average shear strength for two 6-inch diameter core samples was 207.5 psi, while the shear strength for one 4-inch diameter sample was 165 psi.

Six 6-inch diameter cores of the concrete/asphalt composite layer were extracted from each of the test sections at the end of the HVS testing in Phase I-a. The locations of the cores were selected so that the bond strength for different conditions could be evaluated. For each test section, two cores were obtained from the wheel path (loaded area) - one from the corner and one from the mid edge of the slab. Four cores were obtained outside the wheel path - one from the center of an unloaded slab, one from the center of the loaded slab, one from the mid edge of the longitudinal joint, and one from the mid edge of the transverse joint. Figure 5.1 shows the core samples from the 6-inch slabs. Figure 5.2 shows the locations of the cores with the measured bond strengths displayed next to them. Table 5.1 shows the results of the Iowa tests on the cores extracted from the test lane in Phase I-a (Lane 6) after HVS loading.

Figure 5.1. Cores Samples from Lane 6 in Phase I-a After HVS Loading.

An examination of the data shows that the measured bond strength was not affected by their locations on the pavement. No loss of bonding due to repeated loading was observed. The loaded area had equally high bond strength as the unloaded area. The average bond strength was about 220 psi.

Results from Test Sections in Phase I-b

For the test sections in Phase I-b, a total of 7 cores of the concrete/asphalt composite layer were extracted from each test section. Six of these samples were tested for interface bond condition after loading. Table 5.2 summarizes the results of the Iowa Shear Test run in these samples. It can be observed that the average shear strength was 195 psi. Similar to the case for Phase I-a, no significant difference in the shear strength was observed among the cores taken from the corner, mid edge and center of the slabs both in and out the wheel path. This means that

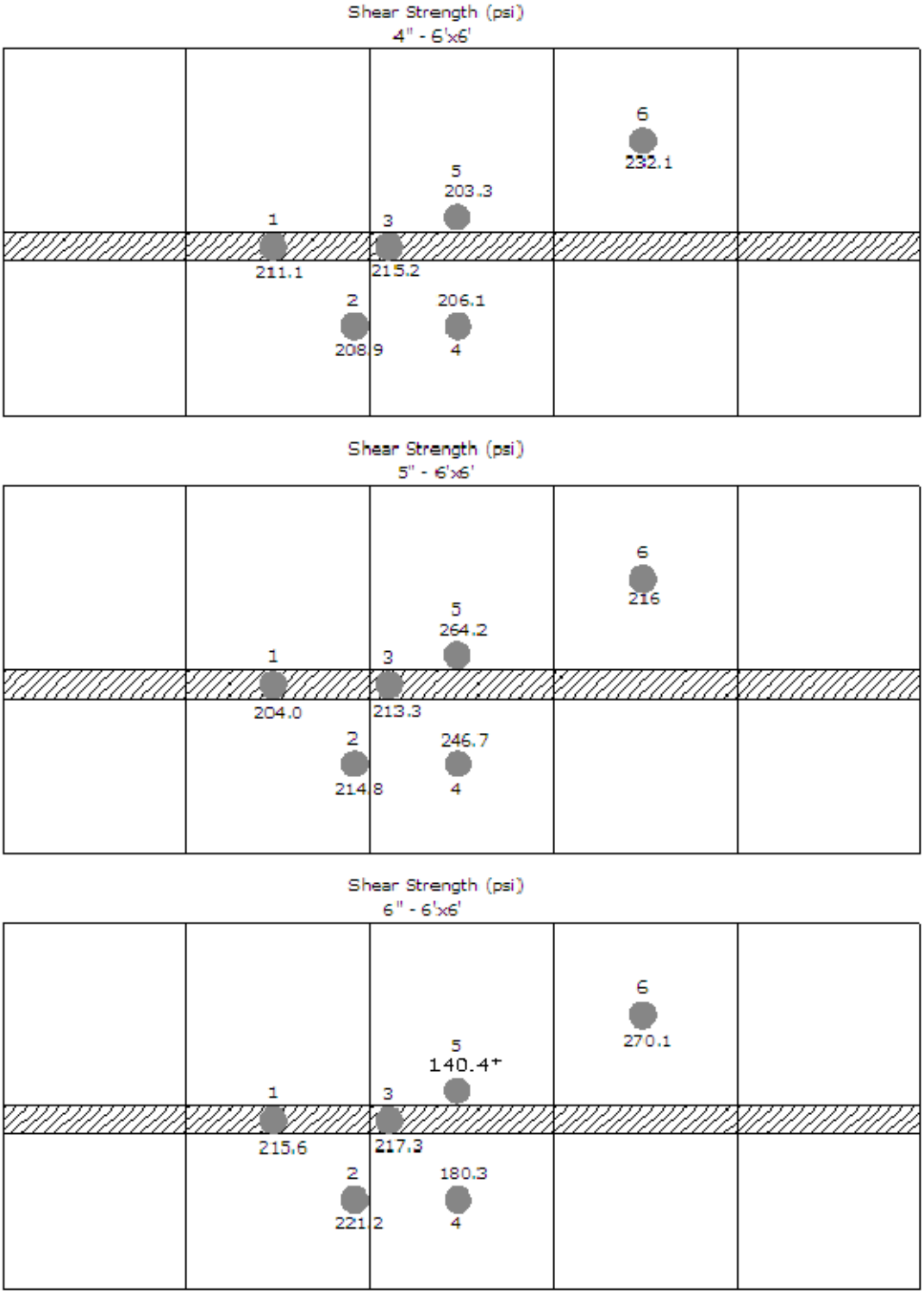

*Values of interface shear strength in psi are written next to the core locations.

Figure 5.2. Location of the Cores Taken After Loading in Phase I-a.

Table 5.1. Results of the Iowa Shear Tests on the Cored Samples from Test Sections in Phase I-a After HVS Loading.

Testing Date	Sample #	Diameter (mm)	Diameter (in)	Area (in2)	Load (lbs.)	Shear Strength (psi)
6/28/2005	1-4”	151.02	5.946	27.76	5860	211.1
6/28/2005	2-4”	151.02	5.946	27.76	5800	208.9
6/28/2005	3-4”	151.33	5.958	27.88	6000	215.2
6/28/2005	4-4”	151.00	5.945	27.76	5720	206.1
6/28/2005	5-4”	151.24	5.954	27.85	5660	203.3
6/28/2005	6-4”	150.98	5.944	27.75	6440	232.1
6/28/2005	1-5”	151.24	5.954	27.85	5680	204.0
6/28/2005	2-5”	151.21	5.953	27.83	5980	214.8
6/30/2005	3-5”	151.26	5.955	27.85	5940	213.3
6/28/2005	4-5”	151.14	5.950	27.81	6860	246.7
6/30/2005	5-5”	151.27	5.955	27.86	7360	264.2
6/30/2005	6-5”	150.95	5.943	27.74	5992	216.0
6/30/2005	1-6”	151.19	5.952	27.83	6000	215.6
6/30/2005	2-6”	150.99	5.944	27.75	6140	221.2
6/30/2005	3-6”	151.12	5.950	27.80	6040	217.3
6/30/2005	4-6”	151.23	5.954	27.84	5020	180.3
6/30/2005	**5-6”**	151.05	5.947	27.78	3900	**140.4***
6/30/2005	6-6”	151.22	5.954	27.84	7520	270.1
				Average	5995	215.6
				St. Dev.	799	28.7
				Average without specimen 5-6”	6118	220.0
				St. Dev. without specimen 5-6”	622	22.3

* Outlier, excluded in the computation of average and standard deviation.

the area of the slab interface loaded for a short period of time did not experience more deterioration than that out of the wheel path. Figure 5.3 shows the locations of the cores taken after HVS loading for each test section in Phase I-b.

Results from Test Sections in Phase II

Four cores were taken from the 10-inch slabs in Phase II before the HVS loading was started, and Iowa shear tests were run on these cores to determine the interface shear strength.

Table 5.2. Results of Iowa Shear Tests on the Cored Samples from Test Sections in Phase I-b After HVS Loading.

Core ID	Diameter (in.)	Cross Sectional Area (in2)	Load (lb.)	Shear Stress (psi)
L7-1A	5.99	28.18	5340	189.5
L7-2A	5.98	28.09	5230	186.2
L7-3A	5.98	28.09	5450	194.0
L7-4A	5.98	28.09	5030	179.1
L7-5A	5.97	27.99	5500	196.5
L7-6A	5.95	27.81	7040	251.5
L7-1B	5.97	27.99	7040	251.5
L7-2B	5.98	28.09	5590	199.0
L7-3B	5.97	27.99	5650	201.8
L7-4B	5.97	27.99	6270	224.0
L7-5B	5.97	27.99	4520	161.5
L7-6B	5.97	27.99	5050	180.4
L7-1C	5.96	27.90	7080	253.8
L7-2C	5.97	27.99	5770	206.1
L7-3C	5.99	28.18	5680	201.6
L7-4C	5.98	28.09	4500	160.2
L7-5C	5.97	27.99	5130	183.3
L7-6C	5.97	27.99	4780	170.8
			Average:	194.9
			Standard Deviation:	26.6
			Minimum:	160.2
			Maximum:	253.8

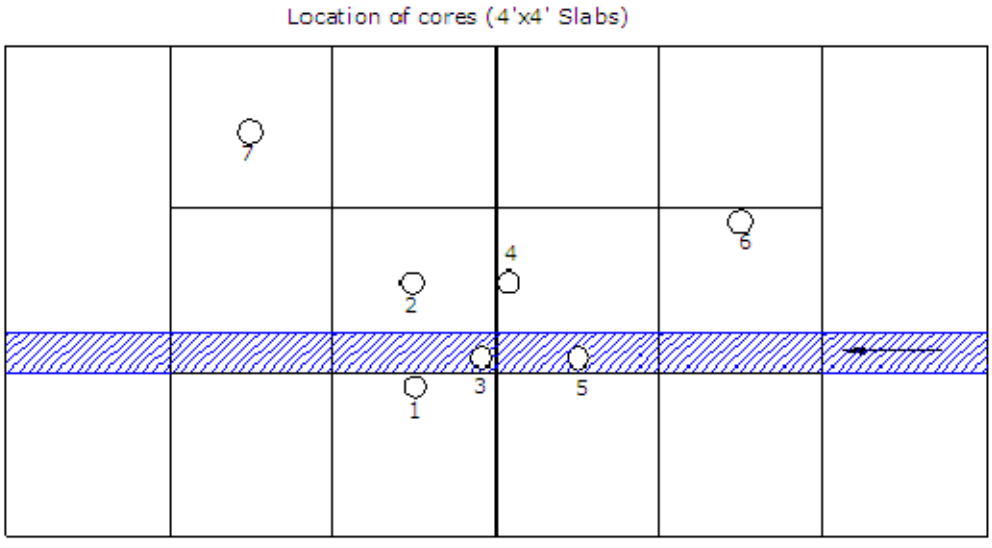

Figure 5.3. Location of the Cores Taken After Loading for Each Test Section in Phase I-b.

Though the concrete-asphalt interface was intended to be unbonded, the cores indicated that the concrete was partially bonded to the asphalt layer. The average interface shear strength from the four cores was 118.6 psi.

After HVS loading, six cores were taken from each test slab, and Iowa shear tests were run on these cores for comparison purpose. The locations of the cores in the 6' x 6' slabs were the same as the one used for the Phase I-a, which is shown in Figure 5.2. Table 5.3 displays the results of the Iowa shear tests on these cores. The average shear strength for these cores was 135 psi.

Table 5.3. Results of Iowa Shear Tests on Cores from Test Sections in Phase II After HVS Loading.

Core ID	Diameter (in.)	Cross Sectional Area (in2)	Load (lb.)	Shear Stress (psi)
L6-1A	5.94	27.71	4720	170.3
L6-2A	6.00	28.27	3980	140.8
L6-3A	5.97	27.99	4140	147.9
L6-4A	5.98	28.09	n/a	n/a
L6-5A	5.97	27.99	3800	135.8
L6-6A	5.97	27.99	4250	151.8
L6-1B	5.99	28.18	4300	152.6
L6-2B	5.95	27.81	n/a	n/a
L6-3B	5.91	27.43	2140	78.0
L6-4B	5.94	27.71	3550	128.1
L6-5B	5.94	27.71	3190	115.1
L6-6B	5.96	27.90	4200	150.5
L6-1C	5.95	27.81	4990	179.5
L6-2C	5.94	27.71	4280	154.4
L6-3C	5.94	27.71	1730	62.4
L6-4C	5.94	27.71	4270	154.1
L6-5C	5.95	27.81	2640	94.9
L6-6C	5.95	27.81	n/a	n/a
			Average:	134.4
			Standard Deviation:	33.3
			Minimum:	62.4
			Maximum:	179.5

Comparison Before and After HVS Loading

Table 5.4 summarizes the measured interface bond strength before and after HVS loading for both Phase I and Phase II. It can be noted that for the test sections in Phases I-a and I-b, where a bonded condition was intended, there was a small increase in bond strength after HVS loading. For the test sections in Phase II, where an unbonded condition was originally intended, there was a larger gain in bond strength after HVS loading.

Table 5.4. Summary of the Interface Bond Strength Before and After HVS Loading.

Intended Bond Condition	Slab Size	Shear Strength Before Loading (psi)	Shear Strength After Loading (psi)
Bonded (Phase I-a)	6' × 6'	207.5	220
Bonded (Phase I-b)	4' × 4'	-	194.5
Un-bonded (Phase II)	6' × 6'	118.6	134.4

5.1.2. Concrete Properties

Properties of Concrete Sampled from Concrete Trucks

Samples of concrete were taken from a selected truck during the placement of the test slabs. The slump, air content and temperature of the fresh concrete were measured. Samples were fabricated for compressive strength and elastic modulus, and flexural strength tests. The properties of fresh concrete used in the construction of the test sections in Phases I-a, I-b and II are shown in Table 5.5.

Additional concrete samples from Phase II were prepared to evaluate its coefficient of thermal expansion. The average value of this parameter was determined to be 6.5 X 10^{-6} 1/ºF.

Table 5.5. Properties of Fresh Concrete Used.

Properties	Phase I-a	Phase I-b	Phase II
Slump, inch	3.5	5.75	3.0
Air, %	2.50	2.00	2.4
Unit Weight, pcf	145.8	142.9	143.2
Temperature, °F	93	92	78

Tables 5.6 and 5.7 show the compressive strength, elastic modulus and flexural strength at various curing times of the concrete sampled from the truck in Phase I-a and Phase II, respectively. All these tests were performed by FDOT personnel at the FDOT facility.

Table 5.6. Properties of Hardened Concrete Sampled from Truck in Phase I-a.

Curing Time, days	Compressive Strength, psi	Elastic Modulus, psi	Flexural Strength, psi
1	1690	-	-
3	2940	-	-
7	3930	3440	-
14	4750	3737	732
28	5980	3940	772
56	6750	4380	847

Table 5.7. Properties of the Hardened Concrete Sampled from Truck in Phase II.

Age, days	Compressive Strength, (psi)	Elastic Modulus, (ksi)	Flexural Strength, (psi)
1	1,933	-	-
3	3,608	-	-
7	4,651	3,307	-
14	-	3,875	808
28	6,083	4,004	855
56	6,612	4,272	-

Properties of Concrete from Core Samples

Splitting tensile strength test was run on the concrete portion of the core samples after the Iowa bond strength test. From the core samples obtained from the test sections in Phase I-a before the start of the HVS loading, the average indirect tensile strength of concrete from three samples was 610 psi. As described earlier, 18 core samples (6 from each test section) were taken from the test sections in Phase I-a after the HVS loading. Table 5.8 displays the results of the indirect tensile strength test on the concrete portion of these 18 core samples. The average indirect tensile strength ranged from 473 psi for the 4-inch concrete slabs to 509 psi for the 5-inch slabs.

Table 5.8. Results of Indirect Tensile Strength Test on the Concrete Samples Taken From the Test Sections in Phase I-a After HVS Loading.

Sample	Diam	L1	L2	L3	L4	L	Load	Strength
	in	in	in	in	in	in	lb	psi
4”-1	6	3.81	3.86	3.66	3.78	3.78	14610	410.4
4”-2	6	3.94	4.04	3.92	4.20	4.03	14900	392.8
4”-3	6	4.11	4.18	4.14	4.04	4.12	17199	440.6
4”-4	6	4.02	4.09	4.10	4.14	4.09	24220	628.7
4”-5	6	4.43	4.26	4.30	4.32	4.33	2510*	
4”-6	6	4.44	4.49	4.55	4.52	4.50	20880	492.3
							Average	**473.0**
5”-1	6	5.40	5.25	5.38	5.34	5.34	19121	379.7
5”-2	6	5.29	5.18	5.36	5.18	5.25	22270	449.9
5”-3	6	5.29	5.31	5.23	5.23	5.27	34690	699.1
5”-4	6	5.40	5.46	5.45	5.49	5.45	30050	585.0
5”-5	6	5.45	5.47	5.47	5.52	5.48	25720	498.2
5”-6	6	5.67	5.44	5.89	5.47	5.62	23320	440.5
							Average	**508.7**
6”-1	6	6.31	6.23	6.25	6.25	6.26	25440	431.2
6”-2	6	6.18	6.20	6.15	6.16	6.17	26840	461.4
6”-3	6	6.12	6.18	6.00	6.00	6.08	27340	477.5
6”-4	6	6.13	6.20	6.10	6.11	6.14	31150	538.7
6”-5	6	6.00	6.00	6.01	6.03	6.01	30640	540.9
6”-6	6	5.94	5.91	5.94	6.00	5.95	27570	491.8
							Average	**490.3**

* Outlier

5.1.3 Asphalt Concrete Properties

Resilient modulus test was performed on the asphalt portion of a core that was obtained from a 4-inch slab in Phase I-a before HVS loading. This test was run by FDOT personnel at the FDOT facility. The resilient modulus at 10 °C was determined to be 1,263 ksi.

Resilient modulus and indirect tensile strength tests were run on the asphalt portion of the cores which were taken from the test sections in Phase I-a at the end of the HVS loading period. Theses tests were performed in the Asphalt Lab of the Department of Civil and Coastal Engineering at UF. The result of these tests are summarized in Table 5.9.

Table 5.9. Results of Resilient Modulus and Indirect Tensile Strength Tests on the Asphalt Concrete Samples Obtained from Test Sections in Phase I-a After HVS Loading.

Resilient Modulus (psi)						
Temp.	**5° C**			**15° C**		
Slab Thickness	**4”**	**5”**	**6”**	**4”**	**5”**	**6”**
1st cycle	1.86E+06	1.68E+06	1.84E+06	1.23E+06	1.17E+06	1.12E+06
2nd cycle	1.84E+06	1.68E+06	1.84E+06	1.23E+06	1.16E+06	1.11E+06
3rd cycle	1.85E+06	1.65E+06	1.85E+06	1.22E+06	1.16E+06	1.12E+06
Average	1.85E+06	1.67E+06	1.84E+06	1.23E+06	1.16E+06	1.12E+06
Indirect Tensile Strength (psi)						
				292	263	263

Additional resilient modulus tests performed at 25 ºC on three samples of AC gave an average resilient modulus of 0.75 E+06 psi.

The asphalt binders were extracted and recovered from these asphalt concrete samples. Penetration tests at 25 ºC and the absolute viscosity test at 60 ºC were run on the recovered asphalt binders. These tests were performed by FDOT personnel at the FDOT facility. The test results are shown in Table 5.10. The recovered asphalt binders were shown to be fairly

Table 5.10. Results of Penetration and Absolute Viscosity Tests on the Recovered Asphalt Binders from Cores from Phase I-a After HVS Loading.

Sample	Needle ID	Pen (@ 25 °C)	Avg. Pen	Tube	Bulb	Constant	Seconds	Viscosity (Poises) (@ 60 °C)
	A-498	20						
Core 4”	B-171	21	21.00	400/R164	D	810.00	90.30	73,143
	B-464	22						
	A-498	23						
Core 5”	B-171	23	23.00	400/E171	D	684.00	96.30	65,869
	B-464	22						
	A-498	23						
Core 6”	B-171	25	25.00	400R/E357	D	872.00	69.60	60,691
	B-464	26						

consistent in properties with the penetration ranging from 20 to 26, and the viscosity at 60 ºC varying from 61,000 to 73,000 Poises. The viscosity at 60 ºC of a recovered asphalt binder from a new pavement in Florida is generally in the range of 6,000 to 10,000 Poises. Thus, the recovered asphalt represented an asphalt binder which had been substantially aged.

5.2. Measurement of Joint Movement

Two pairs of Whitmore plugs were placed at the joints of each test slab to monitor joint movement. Each pair of Whitmore plugs were placed at a distance of 6 inches apart from one another, and one on each side of the joint. These plugs were fixed to concrete before the fresh concrete stiffened during placement. Figure 5.4 shows the Whitmore plugs fixed at a joint. The Whitmore gage with the standard Invar bar is shown in Figure 5.5. The invar bar is a reference bar which was used to calibrate the Whitmore gage. The distance between the gage points was measured in early morning before 7 AM and in mid afternoon around 3 PM, which represent the two extreme temperature conditions in a day. In addition, joint movements were measured every two hours from 6 AM to 5 PM on some selected days to monitor the slab movement throughout

Figure 5.4. A Pair of Whitmore Plugs Fixed at a Joint.

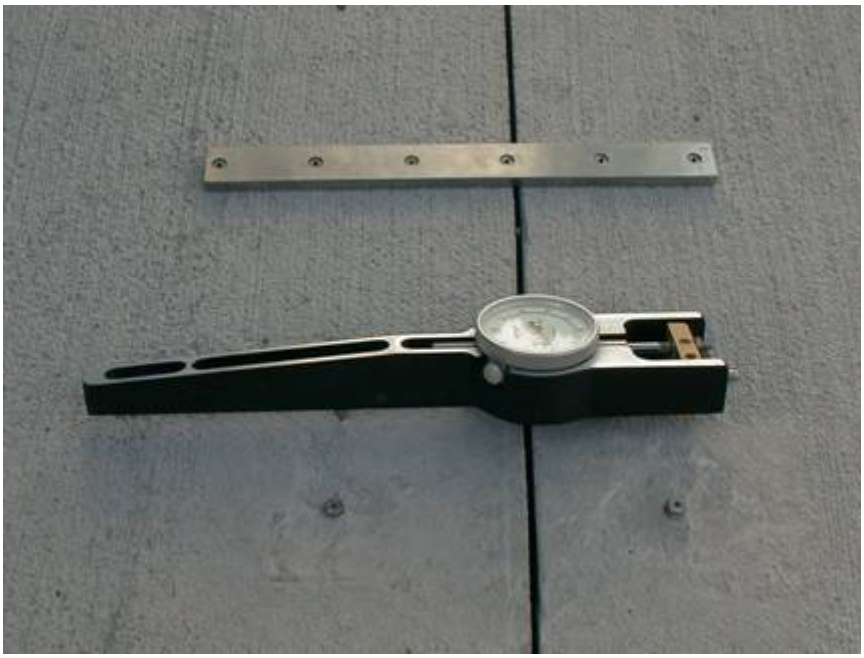

Figure 5.5. The Whitmore Gage with Invar Bar.

the day. Figures 5.6 through 5.8 show the measured Whitmore plug spacing from a 4-inch, 5-inch and 6-inch slab in Lane 6 (with 6 ft by 6 ft joint spacing) at 7 AM and 3 PM in some

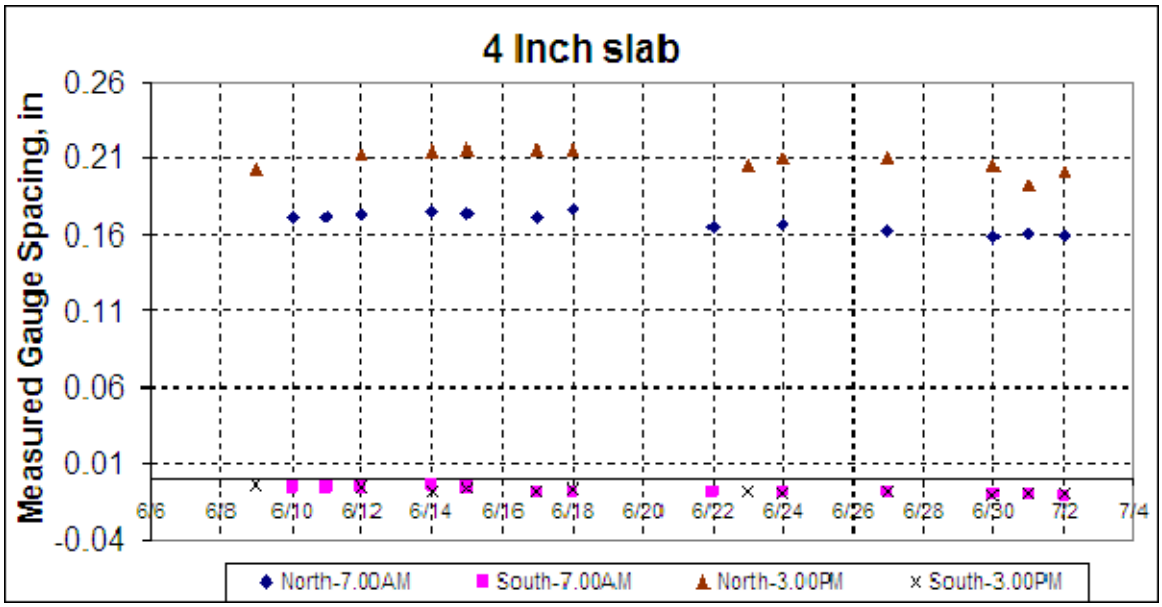

Figure 5.6. Measured Gage Spacing from a 4-inch Slab in Lane 6.

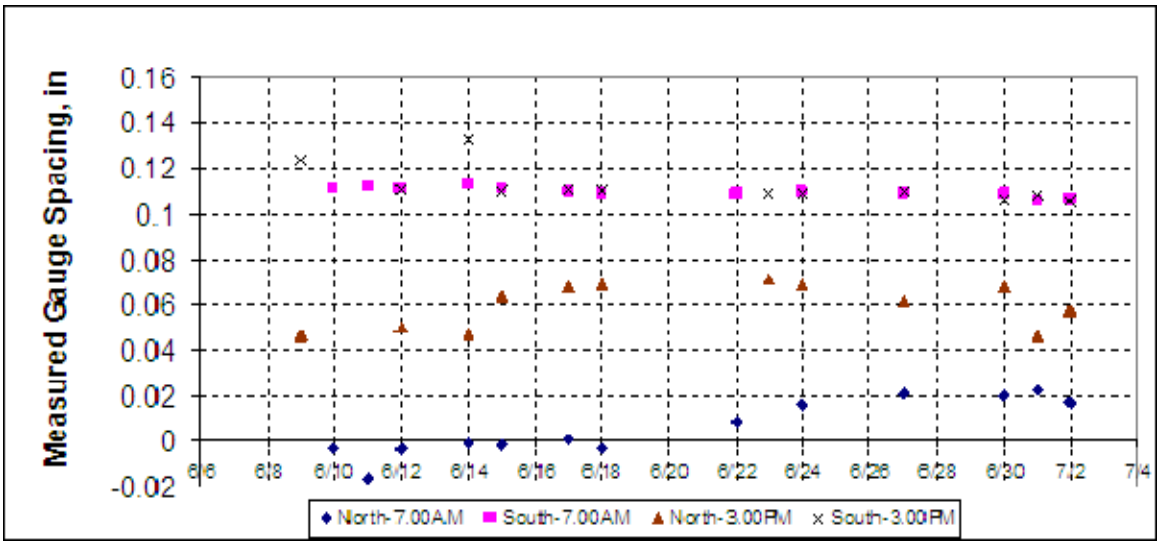

Figure 5.7. Measured Gage Spacing from a 5-inch Slab in Lane 6.

selected days. Significant joint movement was observed at the joints with extended cracks. The joint movement was minimal until the extended cracks were formed at the joints. Figure 5.9 shows the change of gage spacing for all three slabs on a selected day. Here, the gage spacing is shifted to an original gage length of 10 inches for comparison purpose. Thus, only the changes in gage spacing, rather than the absolute gage spacing, are to be read from this plot.

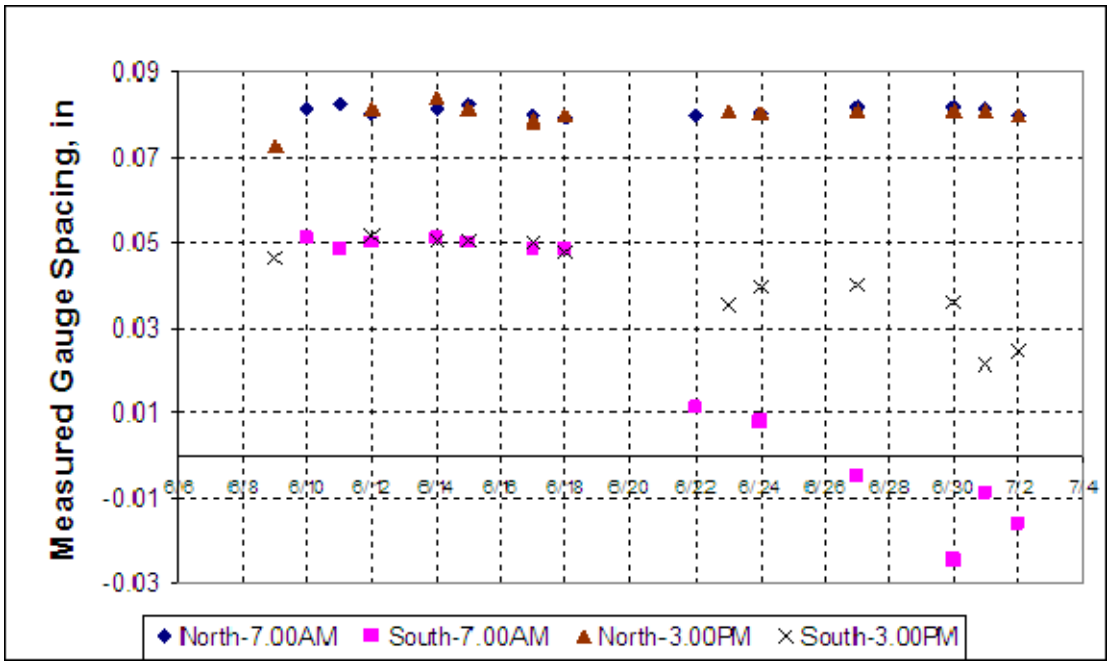

Figure 5.8. Measured Gage Spacing from a 6-inch Slab in Lane 6.

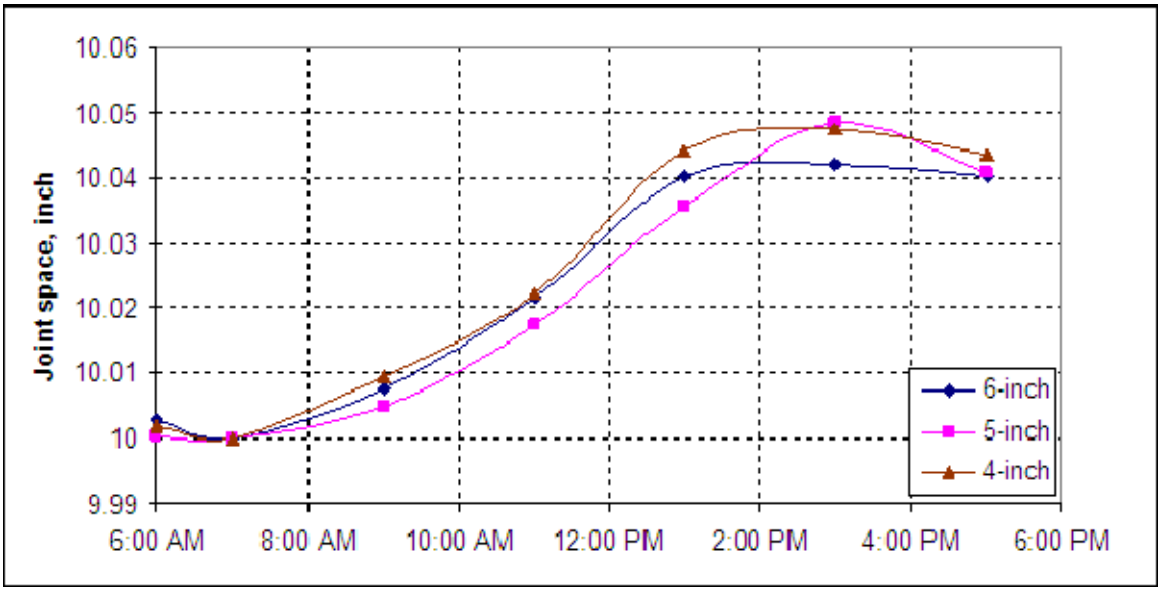

Figure 5.9. Changes of Joint Spacing on a Selected Day.

5.3. Measurement of Slab Profile Using a Dipstick

A grid was drawn on four test slabs with grid points spaced 12 inches apart. A Dipstick profiler was used to measure the elevation of the grid points with respect to a reference point

established close to the test slab. Figure 5.10 shows the grid that covers four slabs. The coordinates (1, 0) represent the reference point. Figure 5.11 shows the dipstick profiler with one leg of it placed on the reference point and the other on a point in concrete slab. The elevation collected at 7 AM and 3 PM were plotted as shown in Figure 5.12. It can be observed that this 4-slab unit curled up at the middle of the slab in the afternoon and curled up at the edges in the morning. The curling of these 4 slabs together agrees with the typical rigid pavement behavior at positive and negative temperature differentials. This observation indicates that the 4 slabs act as one continuous slab before cracking occurred at the joints.

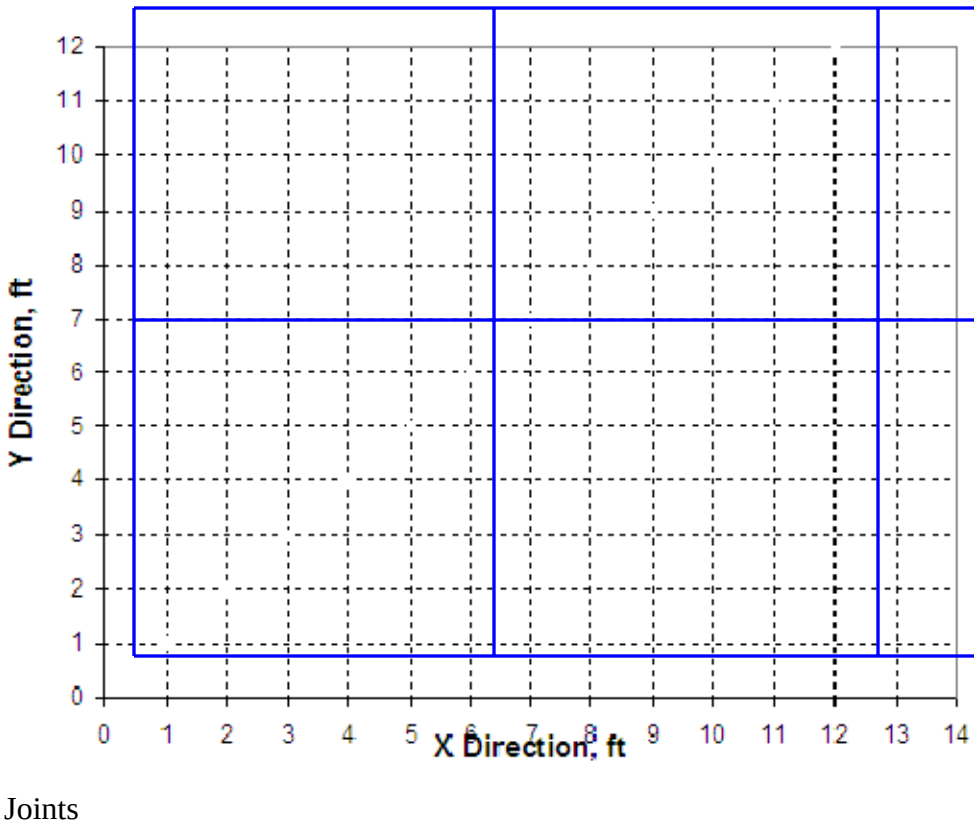

Figure 5.10. Grid Marked on Slabs for the Dipstick Measurement.

Figure 5.11. The Dipstick Instrument.

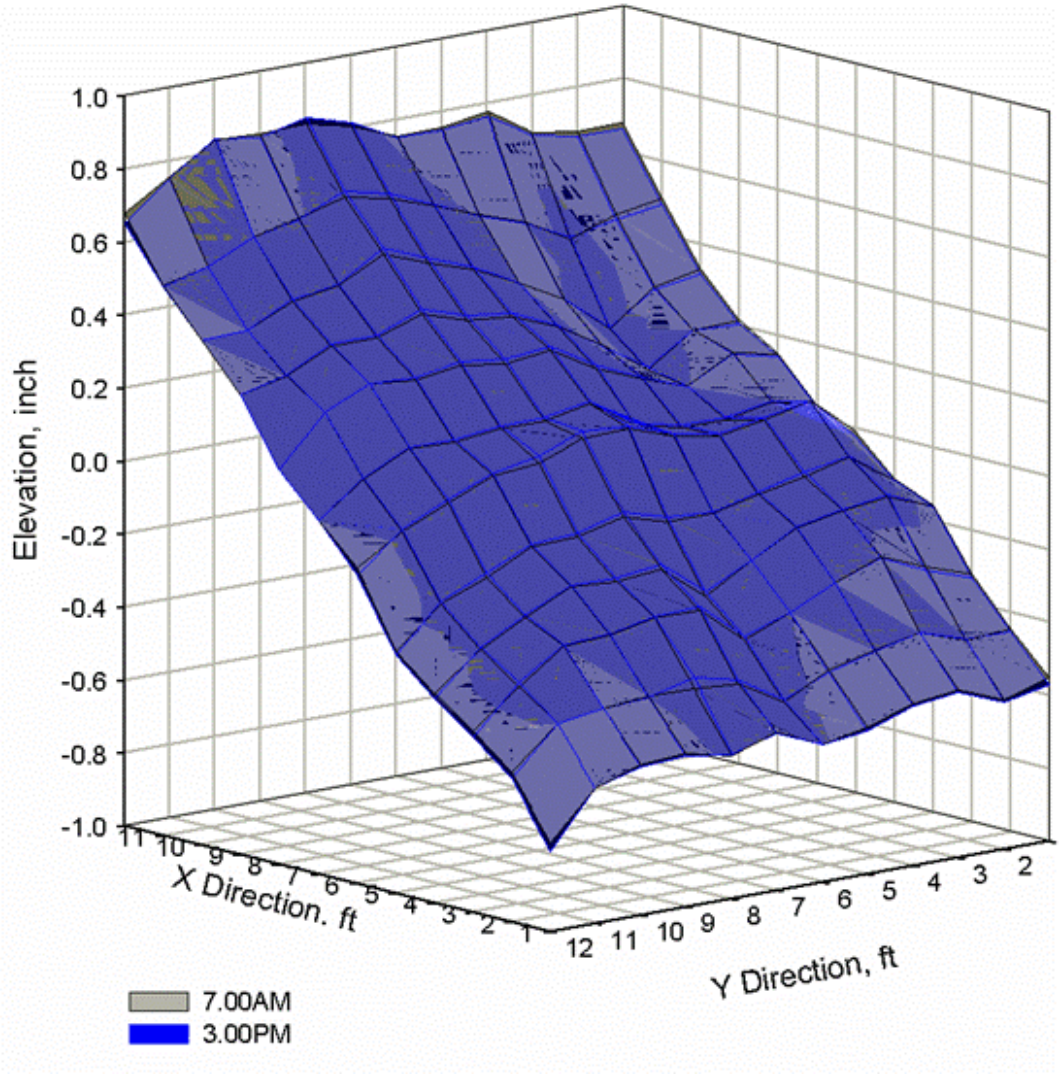

Figure 5.12. Dipstick Measurements at Two Critical Temperatures.

5.4. FWD Tests

Falling Weight Deflectometer (FWD) tests were performed on the composite pavement test sections in all phases of the study. The measured FWD deflection basins were used to estimate the elastic modulus of the pavement materials and the stiffness of the springs used to model the load transfer at the joints and concrete-asphalt interface through a back-calculation process. This back-calculation process also allowed for the verification of the elastic modulus of the concrete and the asphalt layer, previously evaluated from laboratory testing.

FWD tests were run at midday between 1:30 PM and 3:30 PM and at early morning between 7 AM and 8 AM. At mid day, the temperature differential tends to be positive and slab tends to curl down at the edges and joints. This is the best time to run the FWD test for evaluation of joints because the slab is more likely to be in full contact with the layer underneath at both the edges and joints. From midnight to early morning, the temperature differential tends to be negative and the slab tends to curl down at the center of the slab. This is an ideal time to run the FWD test at the center of the slab for evaluation of the condition of the concrete slab and the layer underneath. In order to reduce the effects of the joints, the FWD test run in the morning was performed on a transition slab with the same slab thickness but with a larger panel size.

5.4.1. FWD Tests in Phase I-a

FWD tests were run on the 4" slab of the test section in Phase I-a. Figures 5.13 and 5.14 show the schemes of the morning and afternoon tests, respectively. The morning test was run at 7AM with an average pavement temperature of 65 ºF. The afternoon test was run between 2 PM and 4 PM with an average pavement temperature of 99 ºF. In the case of the afternoon test, a load of 12 kips was applied to both the corner and at the mid-edge of the slab. In all cases the distance between sensors was 12 inches.

5.4.2. FWD Tests in Phase I-b

FWD tests were run on the test sections in Phase I-b. Three sets of reading were taken for three different loads (at around 9, 12, and 15 kips). A replicate test was run right after each test was completed to check for consistency.

Figures 5.15 and 5.16 show the FWD load and sensor positions used for the FWD test at the slab corner and slab edge, respectively. These schemes correspond to those applied in the 4' x 4' slabs (in Phase I-b). The average pavement temperatures were 56 and 75 ºF for the morning and afternoon tests, respectively. Figure 5.17 shows the FWD load and sensor positions used for

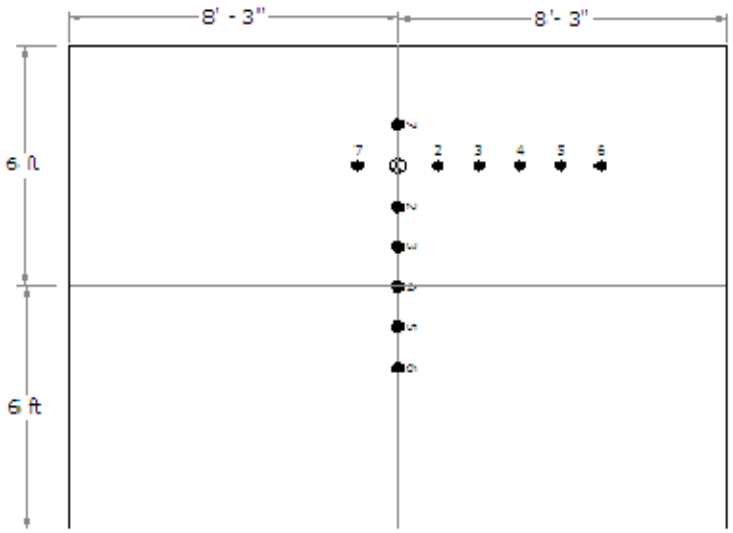

Figure 5.13. FWD Load and Sensor Locations for FWD Test at Slab Center in Phase I-a.

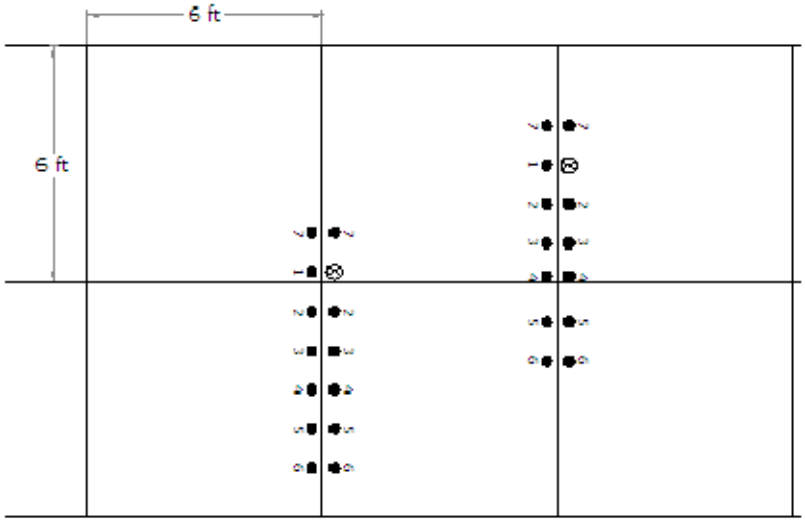

Figure 5.14. FWD Load and Sensor Locations for FWD Test at Slab Corner in Phase I-a.

the FWD test at the slab center. Figures 5.18 through 5.20 show pictures of the FWD tests run at the slab corner, slab edge and slab center, respectively.

5.4.3 FWD Tests Phase II

Figures 5.21 and 5.22 show the FWD testing plan for the test sections in Phase II. This plan is very similar to the one used for Phase I-a since both used 6' x 6' slabs. Morning and afternoon tests were performed to evaluate the elastic modulus of the layers and load transfer

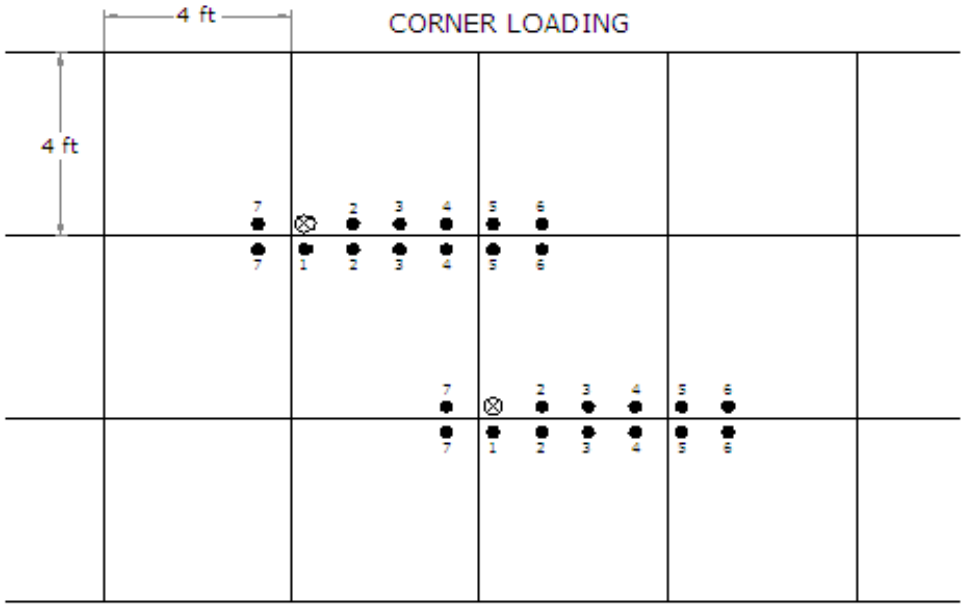

Figure 5.15. FWD Load and Sensor Locations for FWD Test at the Slab Corner in Phase I-b.

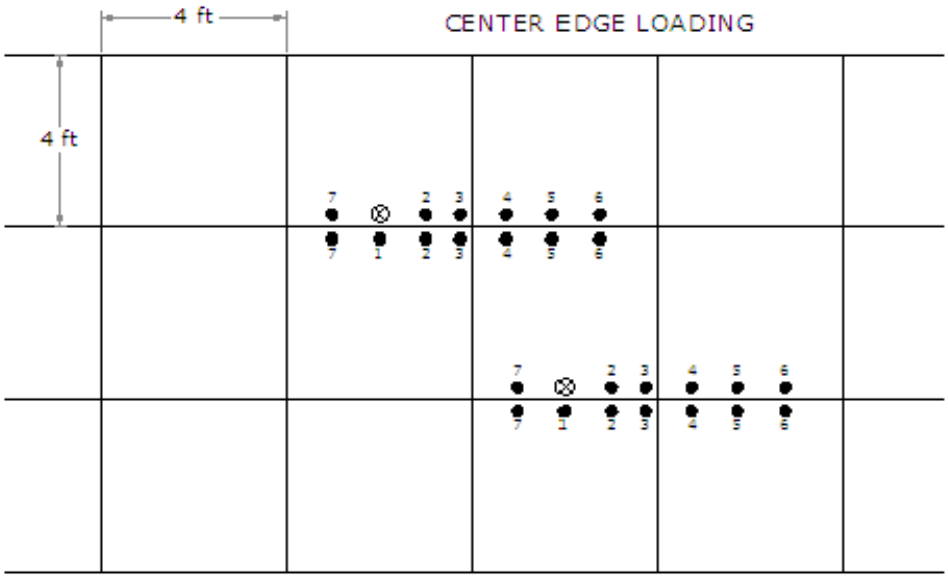

Figure 5.16. FWD Load and Sensor Locations for FWD Test at the Slab Edge in Phase I-b.

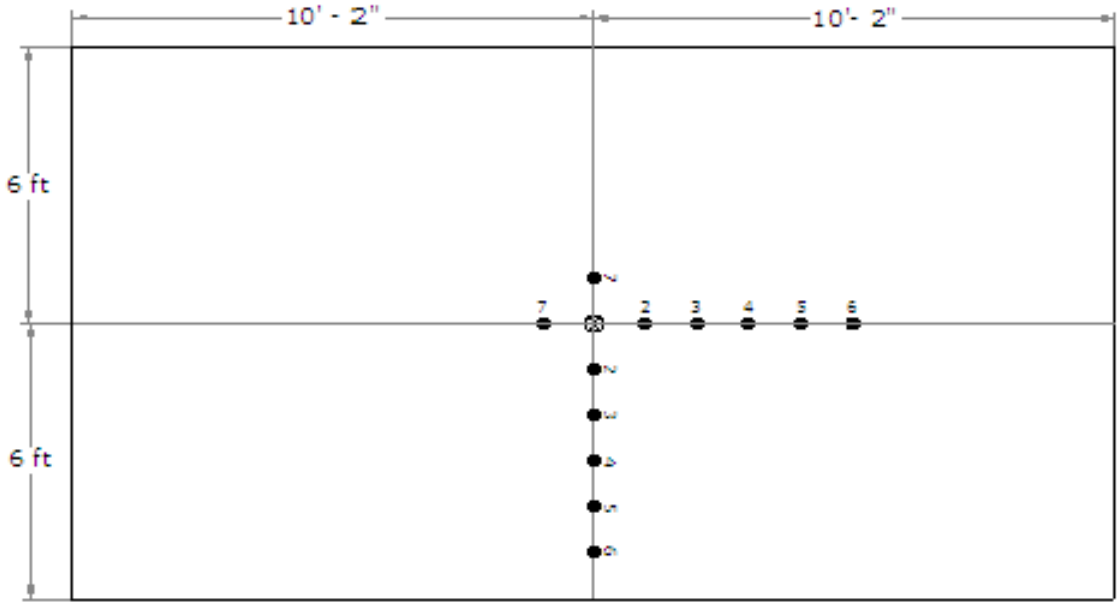

Figure 5.17. FWD Load and Sensor Locations for FWD Test at the Slab Center in Phase I-b.

Figure 5.18. FWD Test at the Slab Corner and Measuring Deflections on the Opposite Slab.

Figure 5.19. FWD Test at the Mid-Edge and Measuring Deflections in the Loaded Slab.

Figure 5.20. FWD Test at the Center and Measuring Deflections Along the Transverse Center-Line.

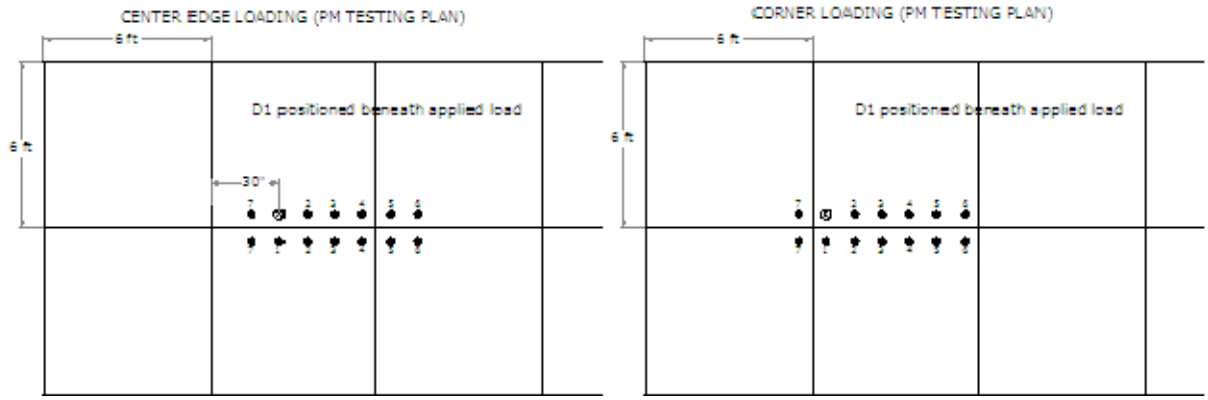

Figure 5.21. FWD Testing Plan for the Mid-Edge and Corner Load in Phase II.

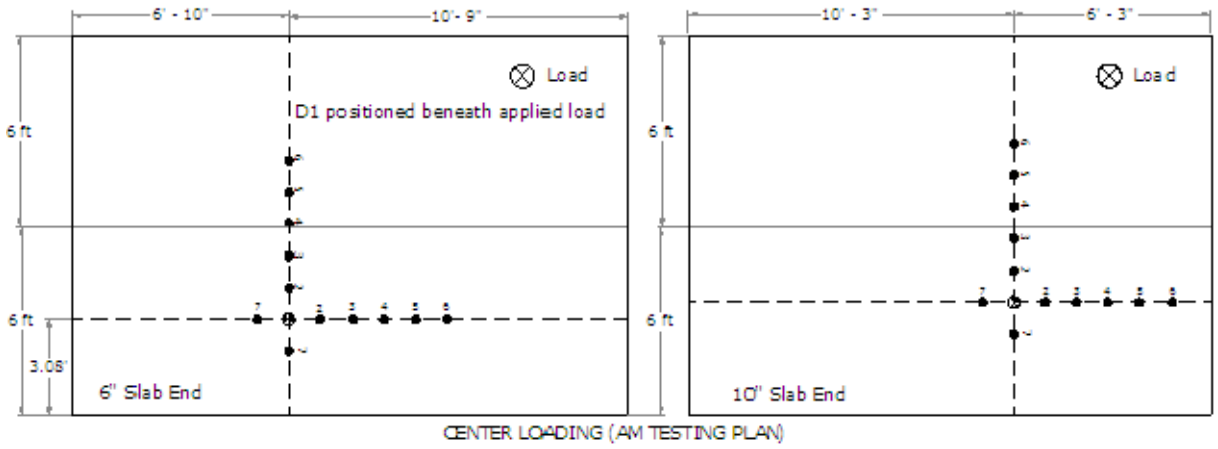

Figure 5.22. FWD Testing Plan for the Center Load at the Two Ends of the Test Track in Phase II.

characteristics at the joints, respectively. Three sets of reading were taken for three different loads (at around 9, 12, and 15 kips). The average pavement temperatures were 78 and 108 ºF during the morning and afternoon tests, respectively.

CHAPTER 6
TESTING OF TEST SECTIONS

6.1 HVS Loading of Test Sections

6.1.1 HVS Loading of Test Sections in Phase I-a

The three test sections on Lane 6 (in Phase I-a), with a panel size of 6 ft x 6 ft and concrete slab thickness of 4, 5 and 6 inches, were loaded by the HVS according to the plan as described in Section 3.4.

HVS loading of the test section with 4-inch slabs was started on July 11, 2004. This test section performed well with no observed cracking after 3 days of loading at 9 kips with a total of 36,407 passes, followed by 12 days of loading at 12 kips with a total of 146,748 passes. Then the load was increased to 15 kips for 3 days with 35,918 passes and then to 18 kips for two days with 21,727 passes. Finally, the load was increased to 21 kips, and corner cracks developed after 12,187 passes, as shown in Figure 6.1. It is to be noted that the HVS loading had to be suspended for two times during this entire test duration due to mechanical problems with the HVS.

HVS loading of the test section with 5-inch slabs was done from November 1, 2004 through January 14, 2005. This test section was loaded with 79,014 passes of 9-kip, 130,186 passes of 12-kip, 25,638 passes of 15-kip and finally 128,817 passes of 18-kip HVS wheel load. No load-induced cracks were observed during and at the end of this testing period. Only a few small shrinkage cracks were observed on the surface of the concrete.

HVS testing of the test section with 6-inch slabs was done from May 23, 2005 through May 26, 2005. This test section was loaded for three days with a total 41,239 passes of 12-kip wheel load. No load-induced cracks were observed, and only a few small shrinkage cracks were observed on the surface of the concrete.

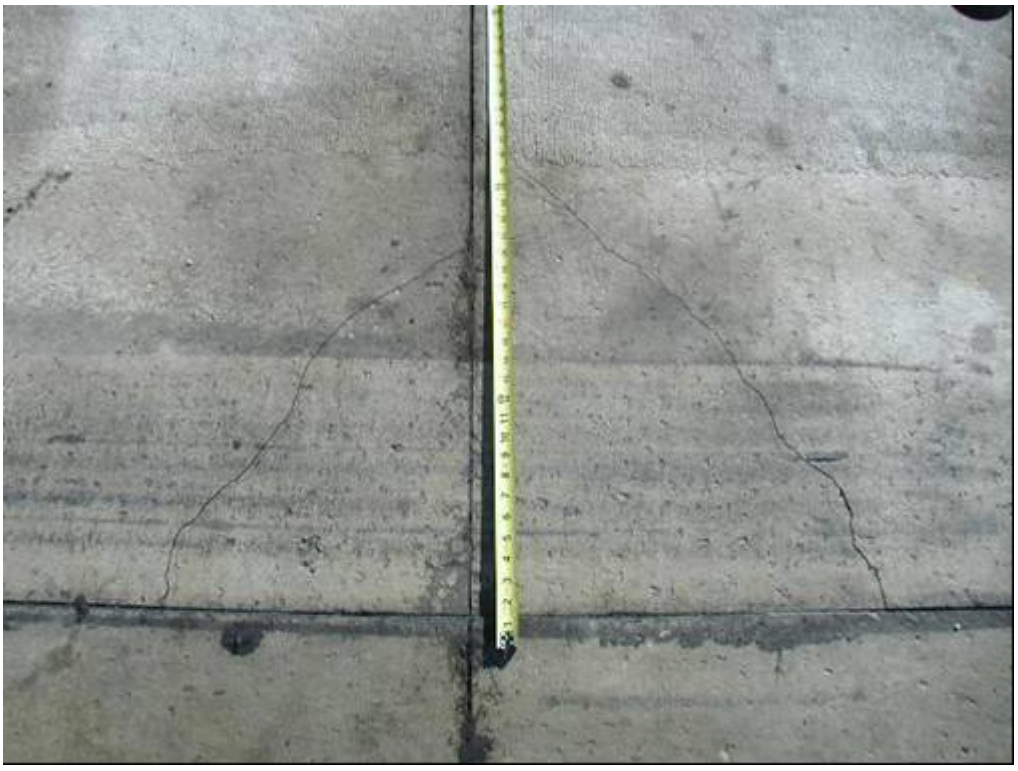

Figure 6.1. Corner Cracks on 4-inch Slabs in Phase I-a after 21-kip Wheel Loads.

Shrinkage cracks were observed in most of the slabs in Phase I-a before the loading period. Shrinkage cracks on the test slabs of the 4, 5 and 6-inch test sections are shown in Figures 6.2 to 6.4, respectively. In addition, a lot of shrinkage cracks in the transverse direction were observed in the transition zones where the thickness changes from 4 inches to 5 inches and from 5 inches to 6 inches.

6.1.2 HVS Loading of Test Sections in Phase I-b

The three test sections on Lane 7 (in Phase I-b), with a panel size of 4 ft x 4 ft and concrete slab thickness of 4, 5 and 6 inches, were loaded with 12-kip HVS wheel loads at 120 psi tire pressure. Table 6.1 shows the dates of the test and the number of wheel passes applied for each of the three test sections. No load-induced or shrinkage crack was observed in any of the three test sections at the end of each loading period.

Figure 6.2. Shrinkage Cracks on a 4-inch Test Slab in Phase I-a.

Figure 6.3. Shrinkage Cracks on a 5-inch Test Slab in Phase I-a.

Figure 6.4. Shrinkage Cracks on a 6-inch Concrete Slab in Phase I-a.

Table 6.1. HVS Loading Period and Number of 12-kip Wheel Passes on the Test Sections in Phase I-b.

Slab Thickness	Starting Date	Ending Date	# of 12-kip Wheel Passes
4”	June 9, 2005	June 12, 2005	40,650
5”	June 14, 2005	June 17, 2005	38,800
6”	June 20, 2005	June 22, 2005	26,040

6.1.3 HVS Loading of Test Sections in Phase II

The test sections in Phase II with a panel size of 6 ft x 6 ft, concrete slab thickness of 6, 8 and 10 inches, and un-bonded concrete-asphalt interface were loaded by three levels of HVS wheel loads. Table 6.2 summarizes the HVS loads, numbers of wheel passes and loading periods for the test sections in Phase II. No load-induced or shrinkage cracks were observed in any of the slabs at the end of the tests.

Table 6.2. Summary of HVS Loading on Test Sections in Phase II.

Slab	Load	Starting Date	Ending Date	# of Passes
10”	12 kips	November 14, 2005	December 4, 2005	87,508
	15 kips	December 4, 2005	December 11, 2005	86,954
	18 kips	December 11, 2005	December 16, 2005	72,554
8”	12 kips	January 9, 2006	January 15, 2006	73,662
	15 kips	January 15, 2006	January 21, 2006	60,923
	18 kips	January 21, 2006	January 28, 2006	67,015
6”	12 kips	January 30, 2006	February 5, 2006	73,108
	15 kips	February 5, 2006	February 10, 2006	67,015
	18 kips	February 10, 2006	February 15, 2006	65,908

6.2. Analysis of Temperature Data

6.2.1. Analysis of Temperature Data in Phase I-a

In Phase I-a, two sets of thermocouple wires were used to monitor the temperature in the slabs. Thermocouples were installed at various depths, at one-inch increments, in the test sections to monitor the temperature distribution. One set of thermocouples was installed at the slab corner at the side that would be loaded by the HVS wheel and the other set of thermocouples was installed at the slab center. Temperature differentials between the top and the bottom of the slab were computed and plotted against time for the 4-inch, 5-inch, and 6-inch slabs in Figures 6.5, 6.6 and 6.7, respectively.

It was observed that for the 4-inch slab, the temperature differential at the slab corner was relatively low compared with that at the slab center. In all the cases, the slab corner was under the shade of the HVS during the day time, and thus did not get as much heating from the sun as the slab center did. This explains why the slab corner had lower positive temperature differentials than the slab center, as the slab corner was less heated by direct sunlight in the day time. However, the temperature differentials computed for the 5-inch slab did not show a significant

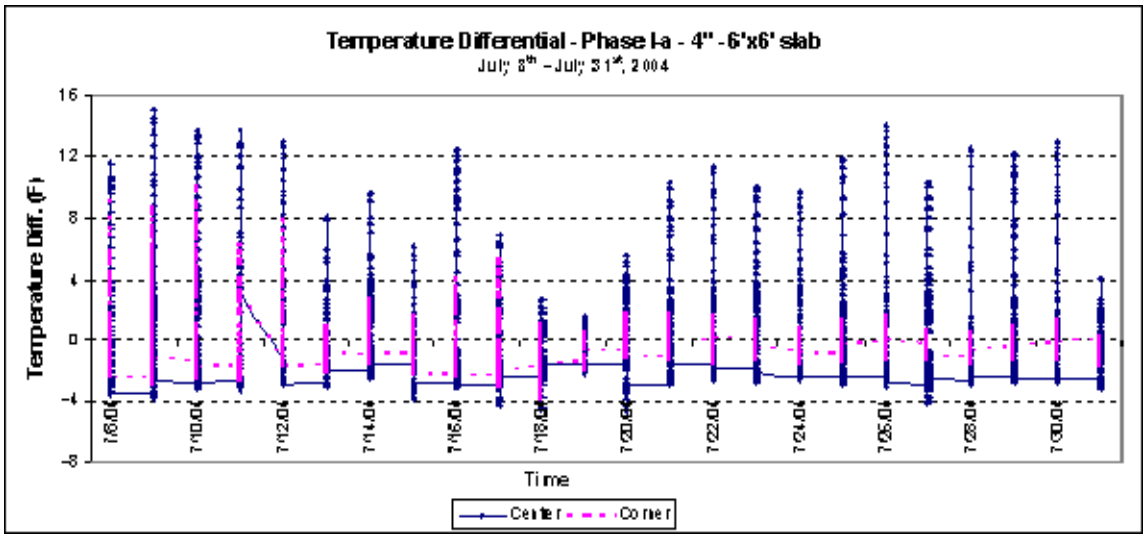

Figure 6.5. Temperature Differential Variation in the 4-inch Slab in Phase I-a.

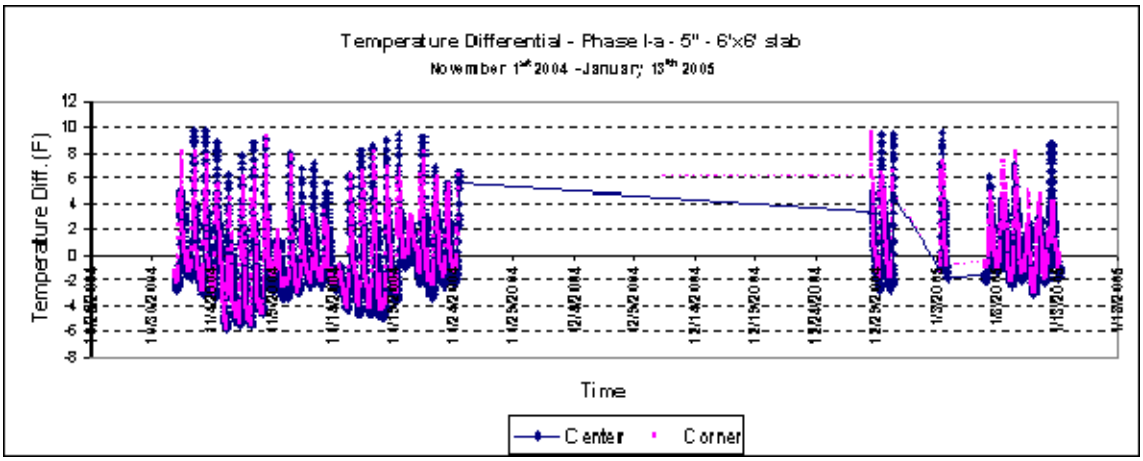

Figure 6.6. Temperature Differential Variation in the 5-inch Slab in Phase I-a.

difference between slab center and slab corner. It is to be noted that the temperature readings from the 5-inch slab were taken during the winter, while those from the 4-inch slab were taken in the summer. For the 6-inch concrete slabs, temperature was recorded between May 20 and May 25, 2005. In this case, temperature data were recorded at one minute intervals for the first three days and at 5-minute intervals for the other days.

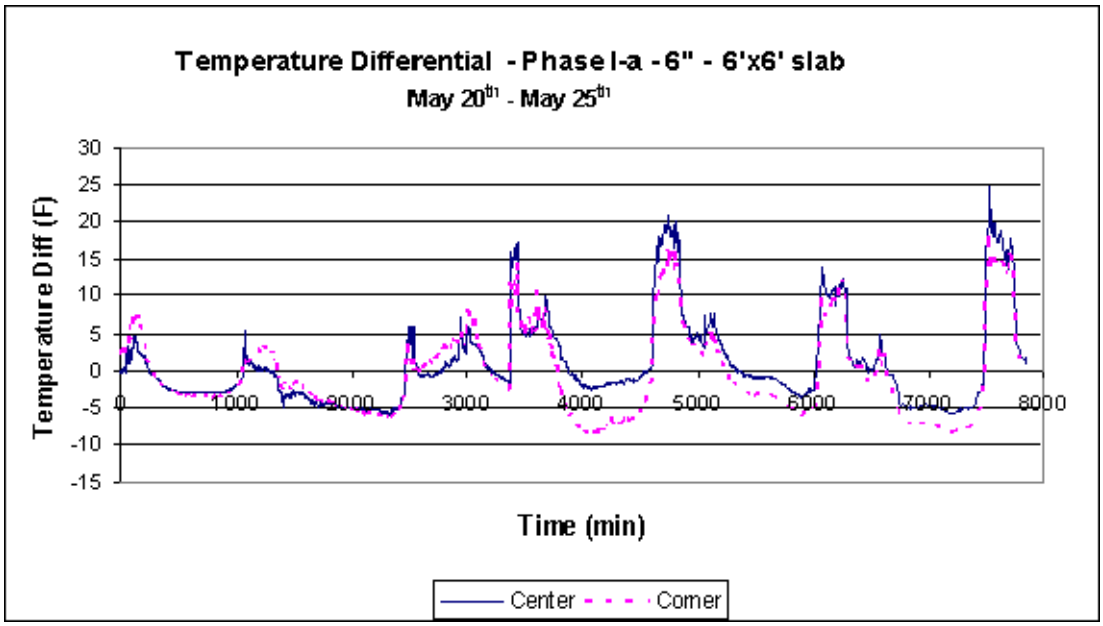

Figure 6.7. Temperature Differential Variation in the 6-inch Slab in Phase I-a.

For the 6-inch slabs, the maximum positive temperature differential at the slab corner was +18.5 ºF (+10.28 ºC), while the maximum negative at the slab corner was -8.6 ºF (-4.8 ºC) during HVS loading of these slabs. For the slab center, the maximum positive and negative values were +25 ºF (13.9 ºC) and -5.2 ºF (-2.9 ºC), respectively

The temperature differentials for the 4-inch and 5-inch slabs during the testing period were analyzed. Statistical analyses were performed to determine the number of hours in a day when the temperature differential was in a certain range. Table 6.3 shows the results of statistical analysis for the 4-inch slab in different months during the testing period. The 4-inch slab was tested during the summer of 2004. Table 6.4 shows the results of the statistical analysis for the 5-inch slab. The 5-inch slab was tested during the winter of 2004.

Figures 6.8 through 6.10 show the variation of the temperature in the surface of the asphalt concrete layer. This is an important variable to be considered in the analysis since the elastic modulus of the asphalt layer varies substantially with the changes in temperature, affecting the behavior of the composite pavement.

Table 6.3. Number of Hours in a Day When the Temperature Differential was in Certain Ranges for the 4-inch Slab in Phase I-a.

Month	T<-5°F			-5°F<T<0°F			0°F>T<+5°F			5°F>T<10°F			10°F>T<15°F		
	Ave	Max	Min	Ave	Max	Min	Ave	Max	Min	Ave	Max	Min	Ave	Max	Min
July	0.0	0.0	0.0	15.2	21.2	11.8	6.8	10.0	2.7	1.3	2.5	0.0	0.6	2	0.0
Aug.	0.4	1.2	0.0	14.7	16.7	12.8	7.5	9.8	3.8	1.1	2.3	0.0	0.3	1.2	0.0
Sep.	0.0	0.0	0.0	15.1	16.8	13.0	6.8	7.8	4.8	1.3	2.3	0.7	0.8	1.7	0.0
Oct.	0.1	0.7	0.0	15.3	17.7	13.2	6.0	8.2	3.7	1.4	2.3	0.8	1.1	1.8	0.0
Season	0.1	1.2	0.0	15.1	21.2	11.8	6.7	10.0	2.7	1.3	2.5	0.0	0.7	2.0	0.0

Time in hours

Table 6.4. Number of Hours in a Day When the Temperature Differential was in Certain Ranges for the 5-inch Slab in Phase I-a.

Month	T<-5°F			-5°F<T<0°F			0°F>T<+5°F			5°F>T<10°F			10°F>T<15°F		
	Ave	Max	Min	Ave	Max	Min	Ave	Max	Min	Ave	Max	Min	Ave	Max	Min
Nov.	0.8	7.7	0.0	15.3	24.0	8.3	7.0	11.8	0.0	0.9	1.7	0.0	0.0	0.0	0.0
Jan.	0.0	0.0	0.0	13.8	15.8	12.0	9.7	11.0	8.2	0.5	1.3	0.0	0.0	0.0	0.0
Season	0.6	7.7	0.0	14.9	24.0	8.3	7.7	11.8	0.0	0.9	2.0	0.0	0.0	0.0	0.0

Time in hours

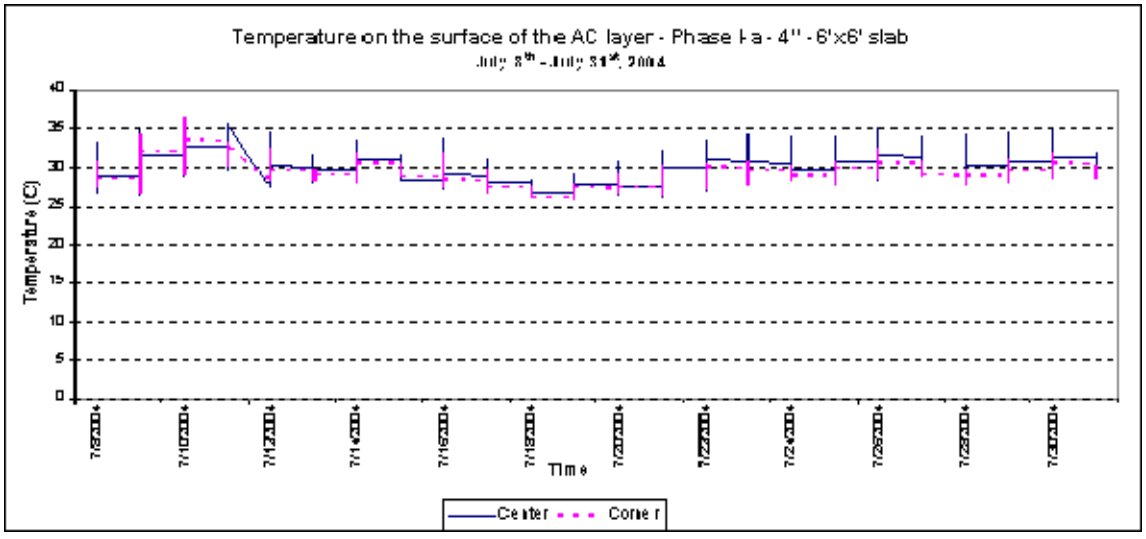

Figure 6.8. Temperature Variation on the Surface of the Asphalt Layer for the 4" Slab in Phase I-a.

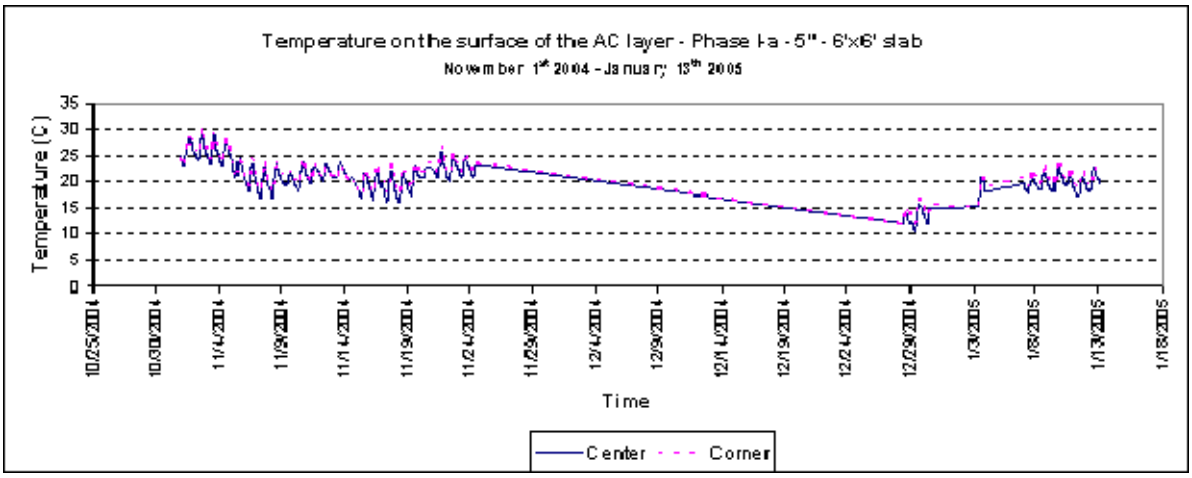

Figure 6.9. Temperature Variation on the Surface of the Asphalt Layer for the 5" Slab in Phase I-a.

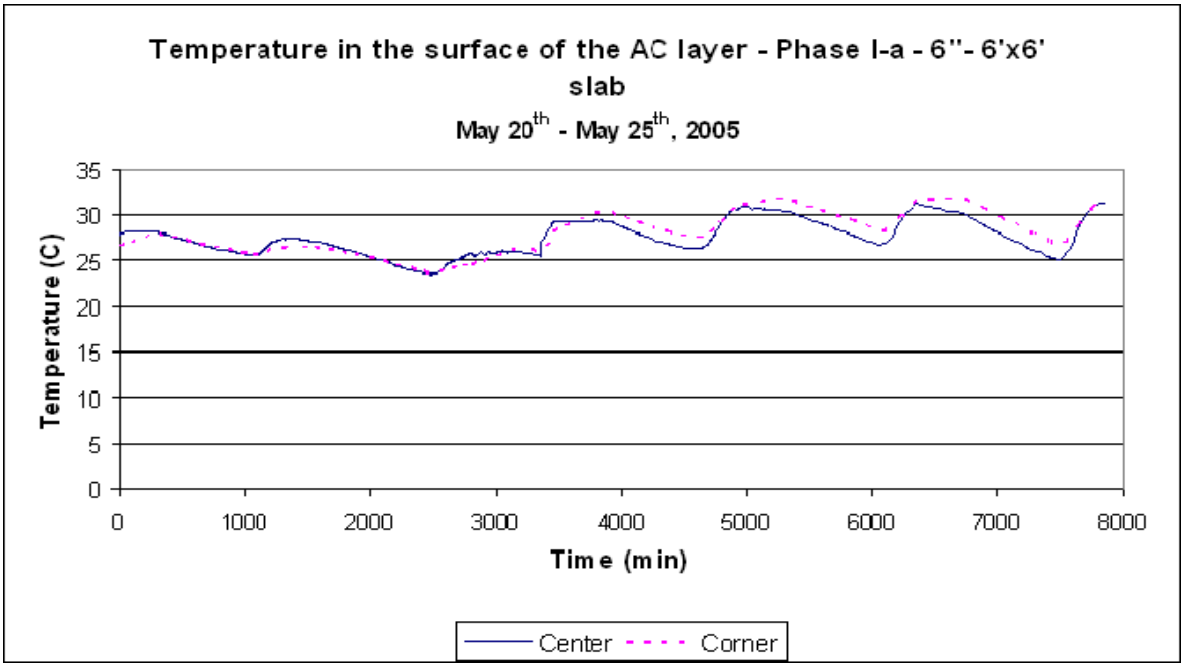

Figure 6.10. Temperature Variation on the Surface of the Asphalt Layer for the 6" Slab in Phase I-a.

6.2.2. Analysis of Temperature Data in Phase I-b

Similar to the case in Phase I-a, temperature in the 4'x 4' concrete slabs in Phase I-b was measured by means of thermocouples installed in the slabs. They were placed at one inch apart vertically in the slab at two different locations, namely at the center and at the corner of the slab. The temperature data were collected (1) between June 17 and June 22, 2005 for the 6-inch slabs, (2) between June 13 to June 17, 2005 for the 5-inch slabs, and (3) between June 9 and June 12, 2005 for the 4-inch slabs.

Figures 6.11 through 6.13 show the plots of temperature differentials versus time, as measured at the slab edge and at the slab center of the 6-, 5- and 4-inch slabs, respectively. The maximum positive and negative temperature differentials were (1) +28.8 ºF (+16 °C) and -6.3 °F (-3.5 °C) for the 6-inch slabs, (2) +27 °F (+15 °C) and -5.4 °F (-3 °C) for the 5-inch slabs, and (3) +18 °F (+10 °C) and -2.7 °F (-1.5 °C) for the 4-inch slabs during their respective test periods.

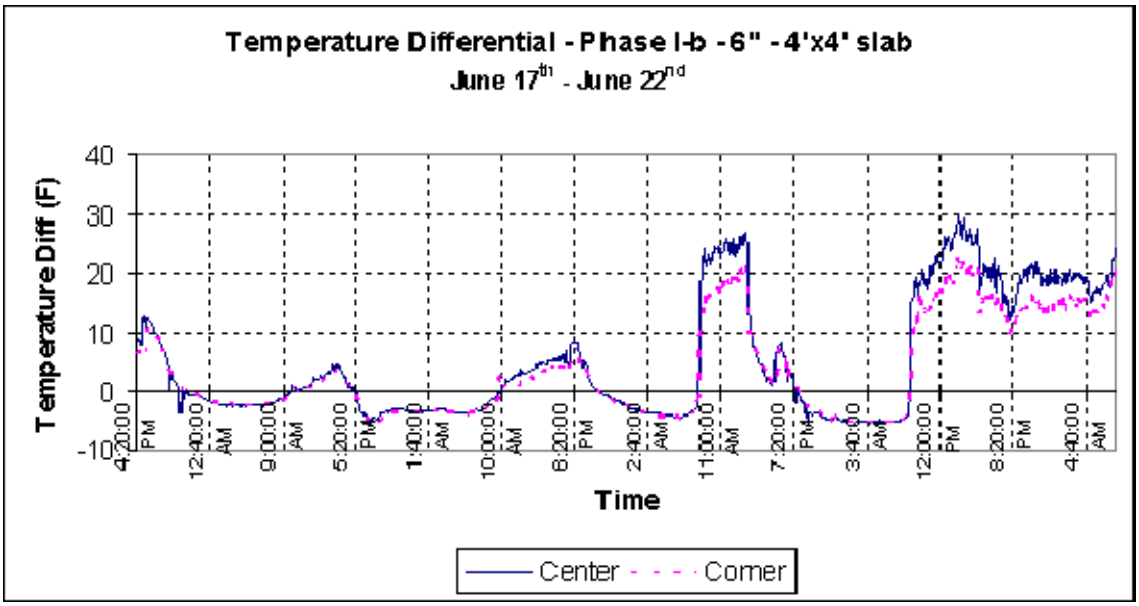

Figure 6.11. Temperature Differential Variation in the 6-inch Slabs in Phase I-b.

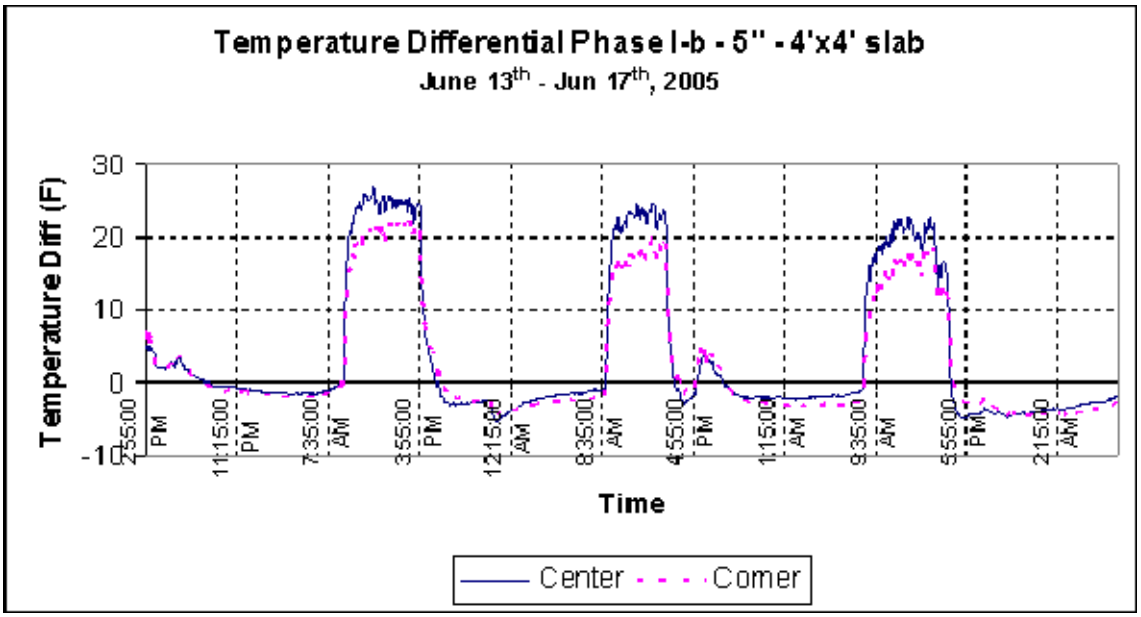

Figure 6.12. Temperature Differential Variation in the 5-inch Slabs in Phase I-b.

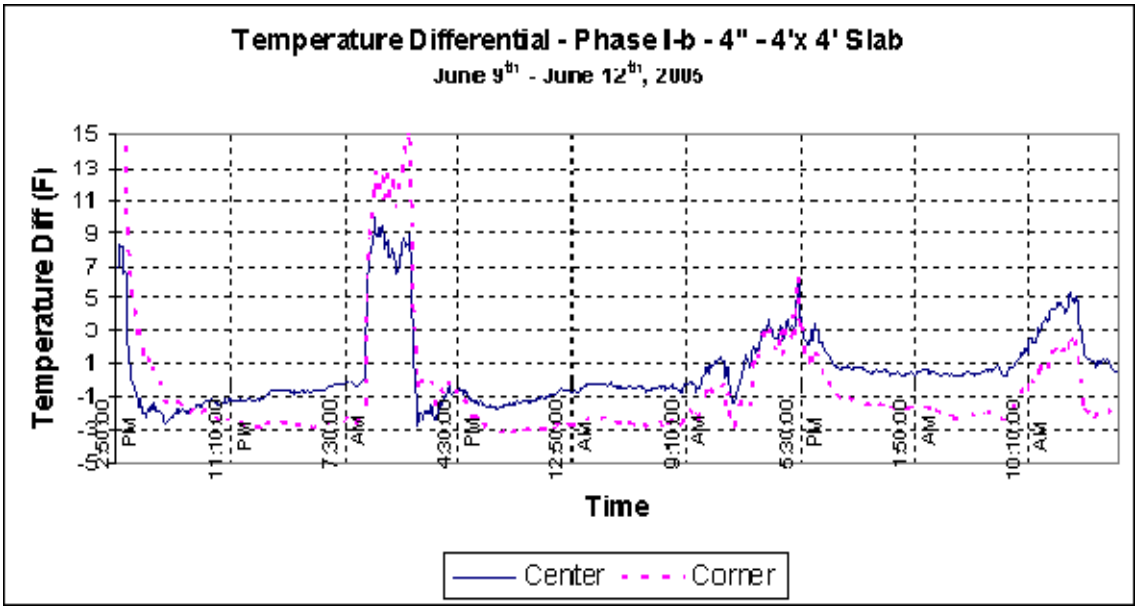

Figure 6.13. Temperature Differential Variation in the 4-inch Slabs in Phase I-b.

Figures 6.14 through 6.16 show the temperature on the surface of the asphalt layer. All these temperatures were measured during the very hot summer of 2005, and temperatures in the range of 78-106 °F (25 – 41 °C) were observed.

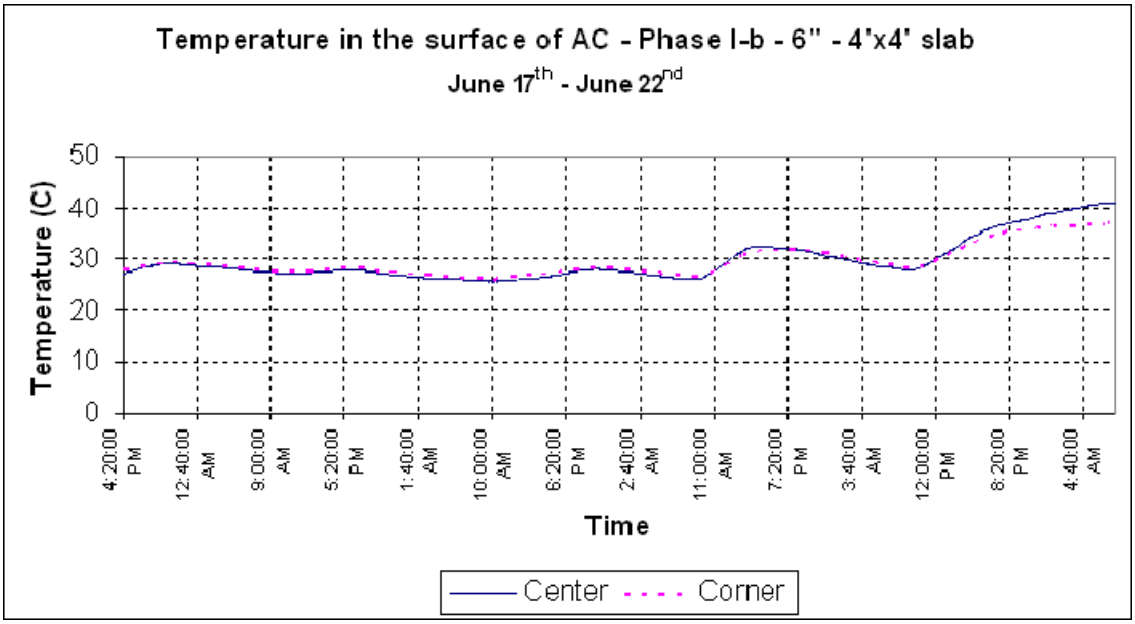

Figure 6.14. Temperature on the Surface of the AC Layer for the 6-inch Slab in Phase I-b.

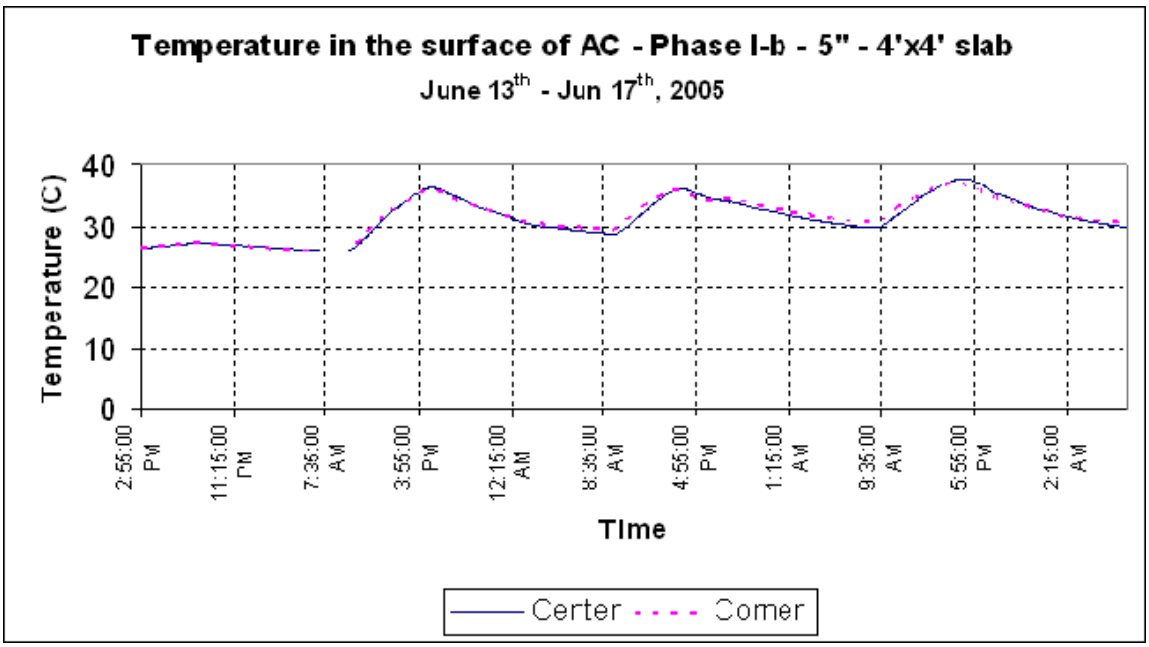

Figure 6.15. Temperature on the Surface of the AC Layer for the 5" Slab in Phase I-b.

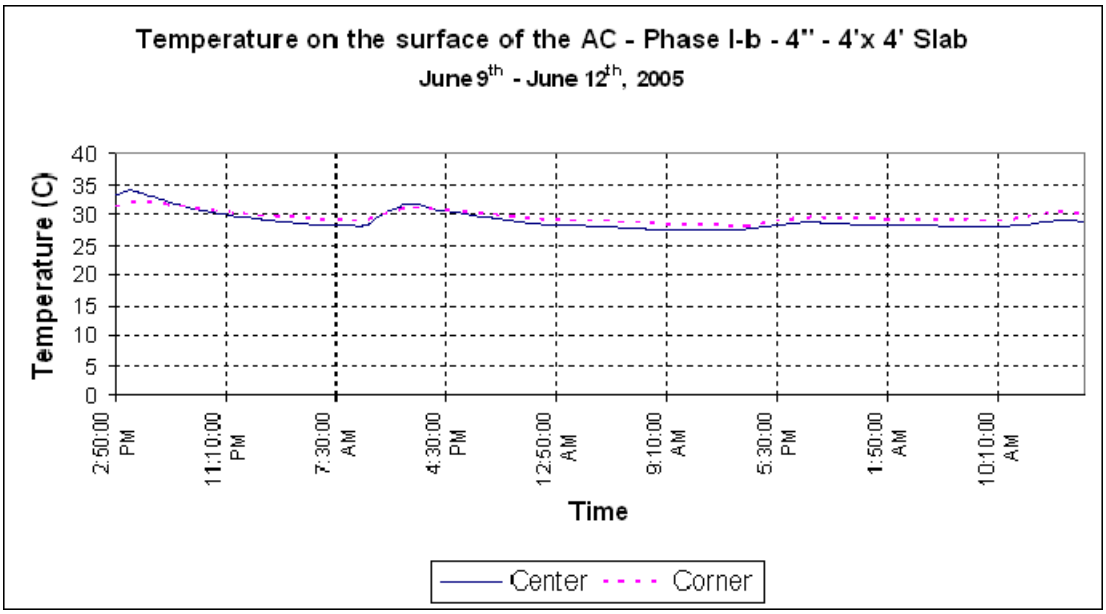

Figure 6.16. Temperature on the Surface of the AC Layer for the 4" Slab in Phase I-b.

6.2.3 Analysis of Temperature Data in Phase II

Similar to the previous phases, data for temperature were collected every 5 minutes during the loading period. Thermocouples were installed in three different locations in the slab. At each location, thermocouples were installed at 1 inch from the top of the slabs and then at 2-inch increments along the thickness of the slab. One thermocouple was installed in the interface between the concrete slab and the asphalt surface. Figures 6.17 through 6.19 show the temperature differential for the 10-, 8- and 6-inch slabs, respectively. The slabs in Phase II were loaded during winter time, and for this reason the maximum positive temperature differential was less than 15 °F. The maximum negative temperature differential reached -10 °F in the 10-inch slab. The actual temperature differential should be slightly higher since the thermocouple used to estimate the temperature at the top was located at 1 inch below the surface of the slab.

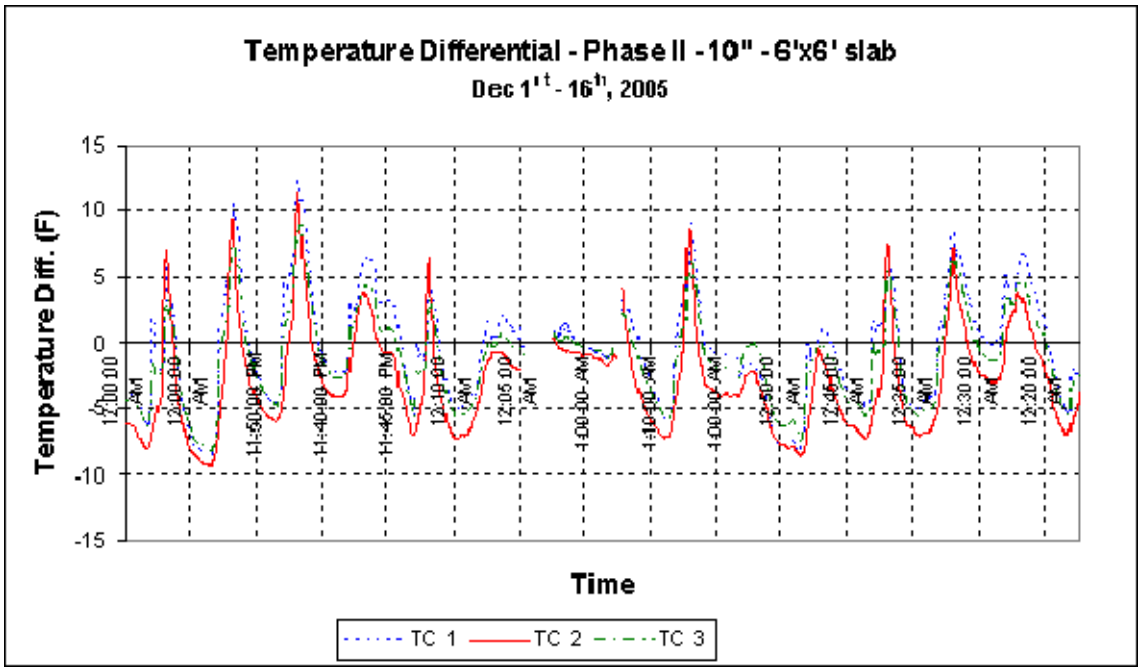

Figure 6.17. Temperature Differential Variation in the 10-inch Slab in Phase II.

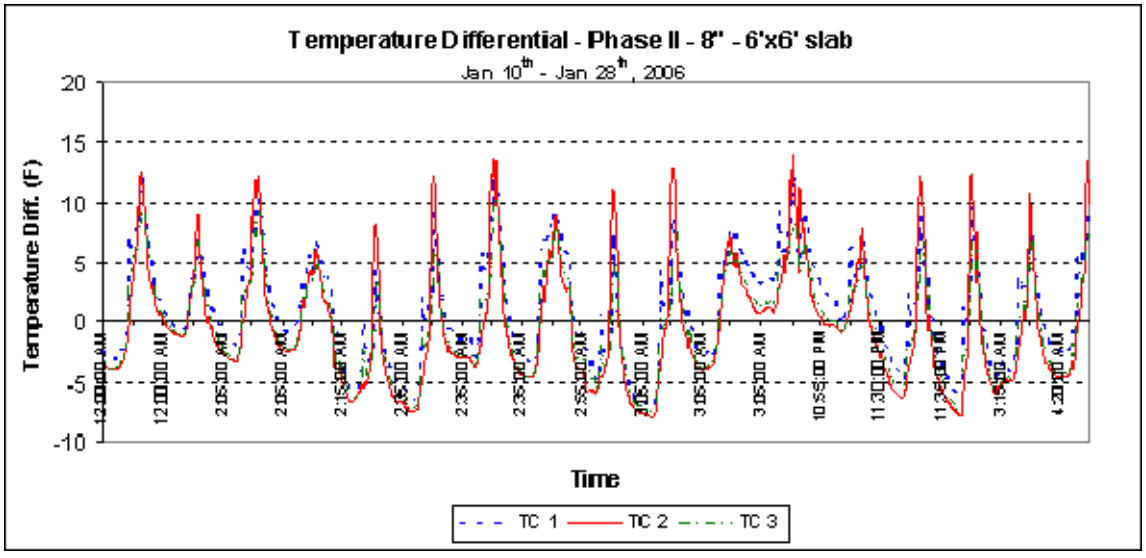

Figure 6.18. Temperature Differential Variation in the 8-inch Slab in Phase II

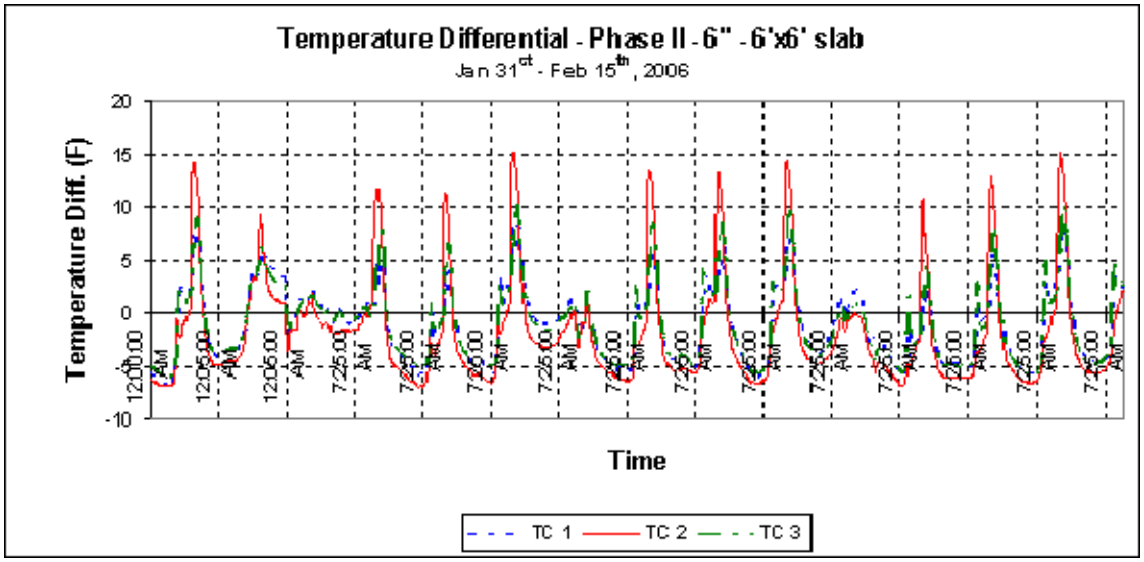

Figure 6.19. Temperature Differential Variation in the 6-inch Slab in Phase II.

Figures 6.20 to 6.22 show the temperature in the AC layer. As indicated previously, the variation of the temperature in the AC layer is an important parameter affecting the elastic modulus of the AC and therefore the strain at the bottom of the concrete slab. Since the loading period was during the winter time, the temperature in the asphalt layer was in the range of 50 to 73 ºF (10 to 23 °C).

Table 6.5 shows a summary with the extreme values for temperature differential and the absolute temperature on the AC layer for all the slabs in the different phases. It can be noticed that a maximum temperature of 106 ºF (41 ºC) and a minimum of 48 ºF (8.9 ºC) were reached on the surface of the asphalt concrete layer depending on the season.

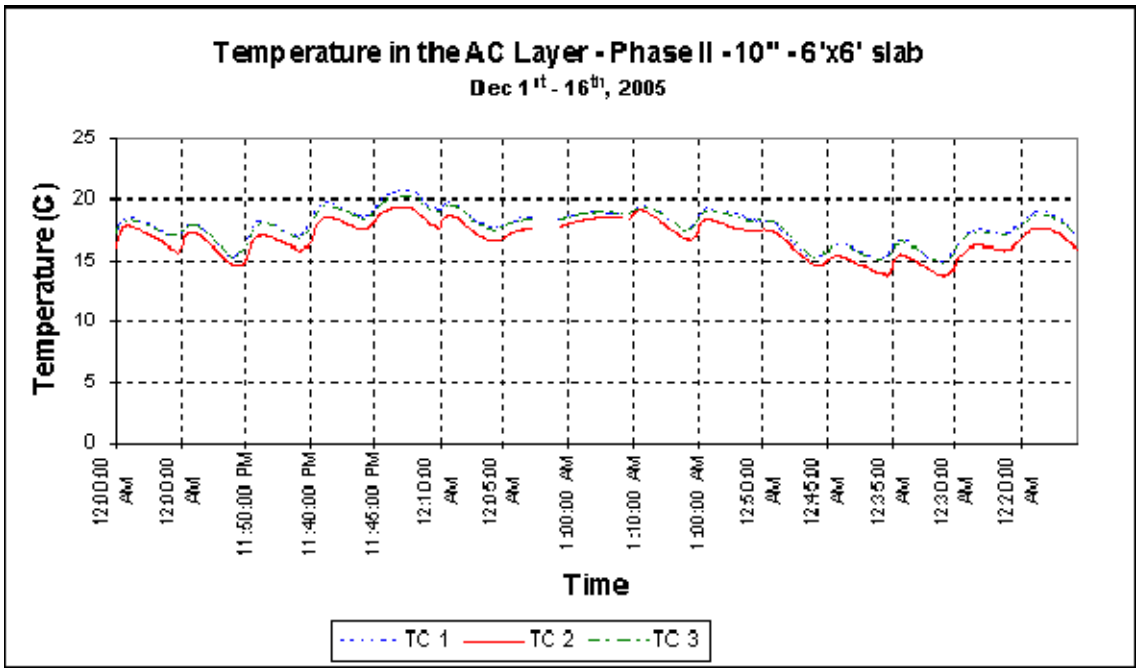

Figure 6.20. Temperature on the Surface of the AC Layer in the 10-inch Slab in Phase II.

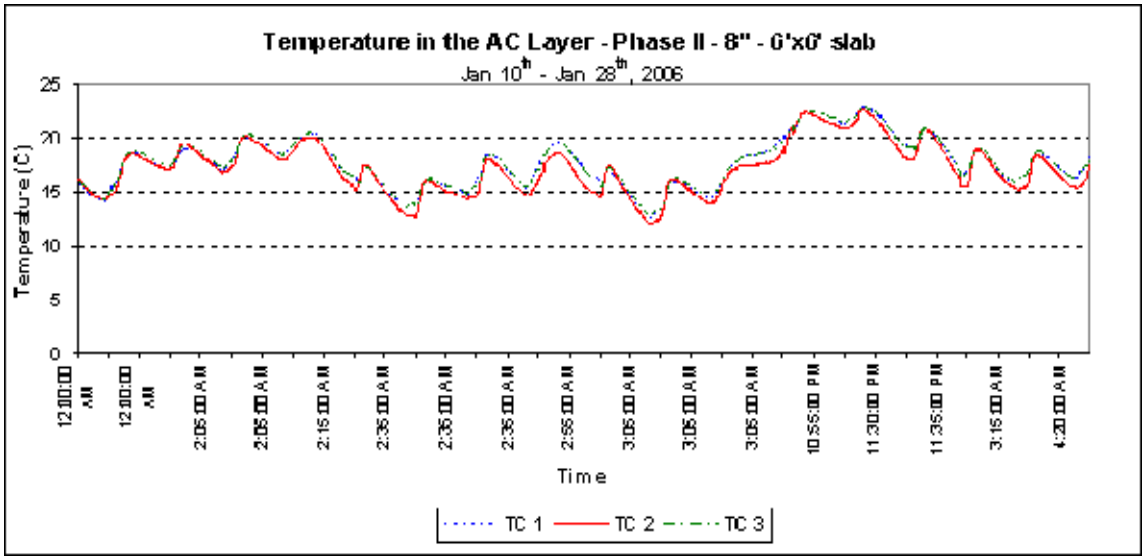

Figure 6.21. Temperature on the Surface of the AC Layer in the 8-inch Slab in Phase II.

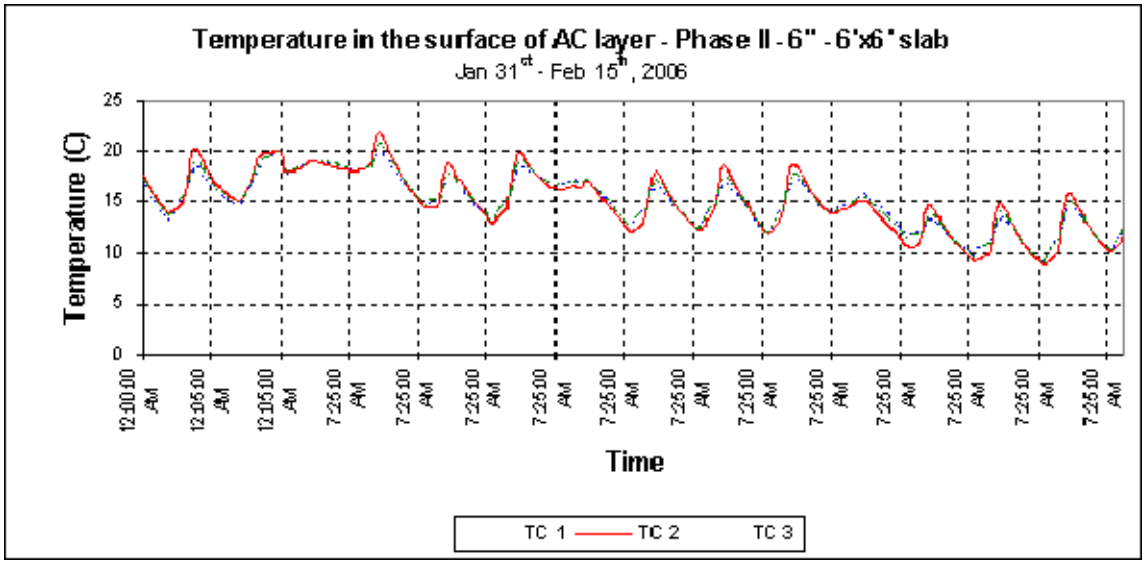

Figure 6.22. Temperature on the Surface of the AC Layer in the 6-inch Slab in Phase II.

Table 6.5. Extreme Values for Temperature Differential and Temperature in the AC Layer.

Phase	Slab	Temperature Differential °F (°C)		Temperature in AC Layer °F (°C)	
		Min	Max	Min	Max
I-a	4”	-4.6 (-2.5)	15.1 (8.4)	78.1 (25.6)	97.7 (36.5)
	5”	-5.7 (-3.2)	9.7 (5.4)	50.7 (10.37)	86.2 (30.1)
	6”	-8.4 (-4.7)	24.7 (13.7)	78.5 (23.6)	89.2 (31.8)
I-b	4”	-3.1 (-1.7)	15.5 (8.6)	81.1 (27.3)	93.0 (33.9)
	5”	-5.6 (-3.1)	26.8 (14.9)	78.8 (26.0)	99.9 (37.7)
	6”	-5.2 (-2.9)	29.9 (16.6)	78.3 (25.7)	105.6 (40.9)
II	6”	-6.9 (-3.8)	15.0 (8.3)	48 (8.9)	71.6 (22.0)
	8”	-7.8 (-4.3)	14.0 (7.8)	53.6 (12.0)	72.9 (22.7)
	10”	-9.3 (-5.2)	12.2 (6.8)	56.7 (13.7)	69.3 (20.7)

6.3 Analysis of Strain Data

6.3.1 Dynamic Strain versus Static Strain

A comparison was made between the maximum strains (compression or tension) measured when the slab loaded by a moving HVS wheel load with the corresponding maximum strains when the same HVS load was applied statically. Table 6.6 shows the maximum static and dynamic strains as measured by Gages 1, 2 and 5 of the 4-inch slab in Phase I-a, when the wheel load of various magnitudes was applied at the mid-edge or corner of the slab. Comparison of measured strains caused by dynamic loads and static loads indicated that they were very close to one another for Gage 1, which was in compression. However, the difference between static strain and dynamic strain increased with time due possibly to the micro cracks induced in the concrete. Figure 6.23 shows the comparison of static and dynamic strain at Gage1. There were significant differences between the strains measured for dynamic and static loads at Gages 2 and 5, which were in tension. It appears that the effects of micro cracks were more significant when the concrete was in tension than when it was in compression. Figure 6.24 shows the comparison of static and dynamic strains for Gages 2 and 5.

Comparisons were also made for the static and dynamic strains for the strain gages in the 5-inch slab in Phase I-a. Dynamic strains caused by slow moving HVS loads at 1 mph were also measured to detect any positioning errors and to determine the strains measured at a slow speed. Table 6.7 shows the static and dynamic strains for Gages 2 and 4 caused by 9 and 12 kip loads. Dynamic strain measurement at slow speed was made at the end of the testing. Table 6.8 shows the strains data obtained with slow-speed loads at 1 mph, along with the strains obtained with static loads and loads at 8 mph, caused by 15 and 18 kip loads . The plots of dynamic and static strains for Gage 2 and 4 are shown in Figures 6.25 and 6.26, respectively.

Table 6.6. Measured Static and Dynamic Strains for Gages 1, 2 and 5 in the 4-inch Slab in Phase I-a Caused by 9 and 12-kip Loads.

Date	Load	Measured Strain, 10-6 in/in					
		Gage 1		Gage 2		Gage 5	
		Static	Dynamic	Static	Dynamic	Static	Dynamic
7/8/2004	9	22	24	30	25	21	14
7/9/2004	9	22	22	20	22	18	15
7/10/2004	9	23	28	35	27	25	15
7/12/2004	12	30	36	30	29	24	16
8/4/2004	12	39	32	50	35	22	16
9/23/2004	12	35	32	47	31	24	15
9/24/2004	12	36	37	47	34	29	18
10/1/2004	12	43	38	53	37	31	18
10/2/2004	12			57	38	34	17
10/4/2004	12			50	34	28	19
10/5/2004	15			53	42	32	24
10/6/2004	15			54	41	34	23
10/7/2004	15			63	47	35	28

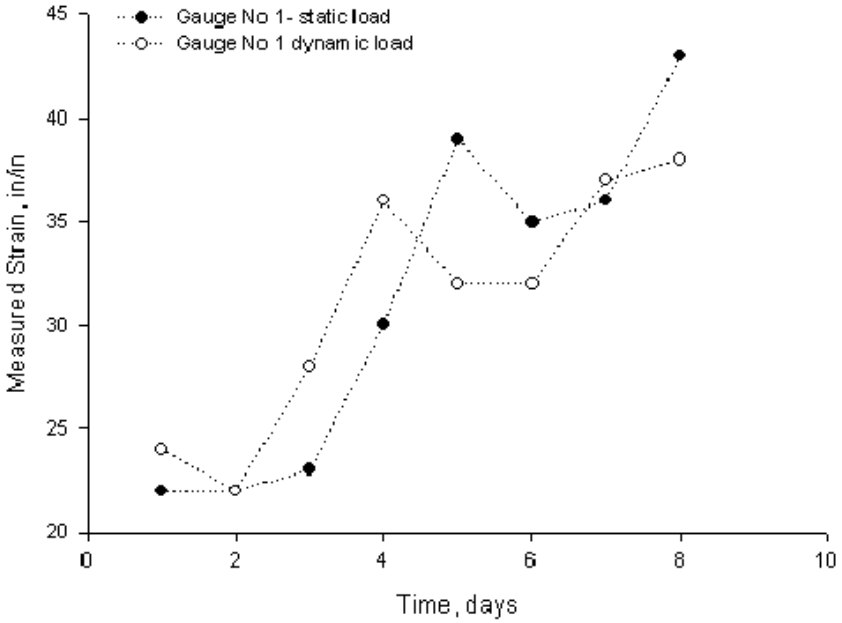

Figure 6.23. Comparison of Dynamic and Static Strain for Gage 1 in the 4-inch Slab in Phase I-a.

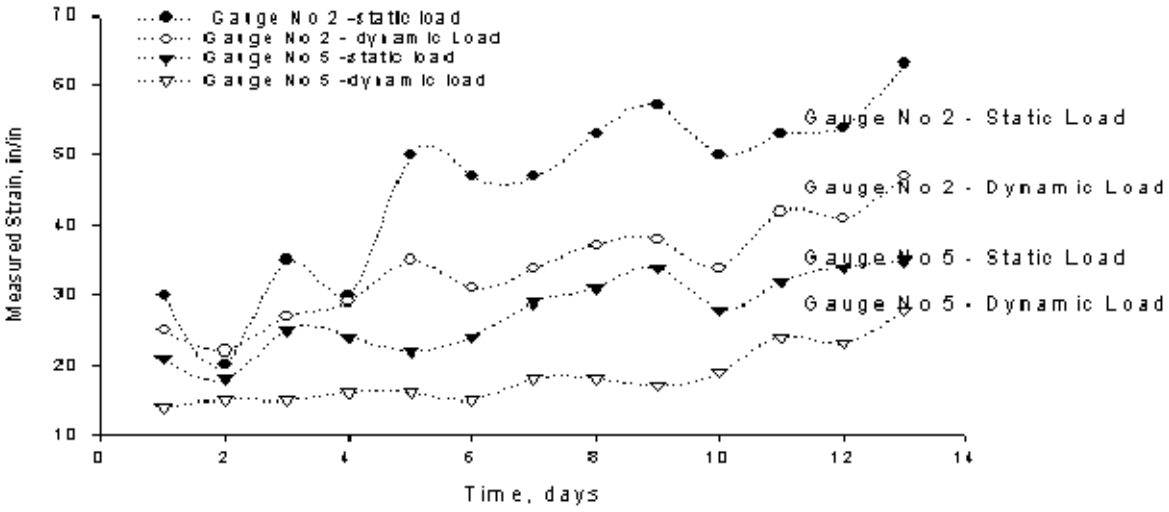

Figure 6.24. Comparison Between Static and Dynamic Strain for Gages 2 and 5 in the 4-inch Slab in Phase I-a.

Table 6.7. Measured Static and Dynamic Strains for Gages 2 and 4 in the 5-inch Slab in Phase I-a Caused by 9 and 12-kip Loads.

Date	Load	Dynamic			Static	
		Gage No 2		Gage No 4	Gage No 2	Gage No 4
11/1/2004	9	21	-6	-4	21	
11/2/2004	9	21	-5	-3	20	
11/3/2004	9	21	-5	-4	17	
11/4/2004	9	20	-6	-4	25	
11/6/2004	9	17	-5	-4		
11/7/2004	9	18	-7	-4.5	30	
11/8/2004	12	21	-6	-4	27	3
11/9/2004	12	20	-8	-5	22	
11/10/2004	12	20	-7	-7	35	2
11/15/2004	12	20	-6	-7	33	2
11/16/2004	12	18	-5	-6	23.5	3
11/17/2004	12	20	-7	-7	31	2
11/18/2004	12	20	-7	-7	30	
11/19/2004	12	21	-7	-6	32	
11/22/2004	12	21	-8	-6	34	
11/23/2004	12	23	-8	-7	31	

Table 6.8. Measured Static and Dynamic Strains for Gages 2 and 4 in the 5-inch Slab in Phase I-a Caused by 15 and 18-kip Loads

Date	Load	Dynamic — 8 mph			Static		Dynamic-1 mph		
		Gage No 2		Gage No 4	Gage No 2	Gage No 4	Gage No 2		Gage No 4
12/28/2004	15	18	-4	-5	26		23	-4	-5
12/29/2004	15	19	-6	-6	37		25	-7	-7
12/30/2004	15	20	-7	-6	36		28	-8	-8
1/3/2005	18	25	-9	-7	29	-2	32	-11	-9
1/4/2005	18	25	-10	-9	43		33	-13	-11
1/5/2005	18	27	-13	-9	39	-4	35	-13	-11
1/6/2005	18	27	-11	-9	40	-4	36	-14	-11
1/7/2005	18	28	-9	-9	46	-4	37	-14	-12
1/9/2005	18	33	-12	-11	45	-7	40	-14	-9
1/10/2005	18	30	-11	-9	38	-3	38	-16	-10
1/11/2005	18	30	-11	-10	41	-4	39	-15	-11
1/13/2005	18	31	-11	-9	50	-6	40	-14	-13
1/14/2005	18	32	-10	-9	51	-6	39	-13	-12

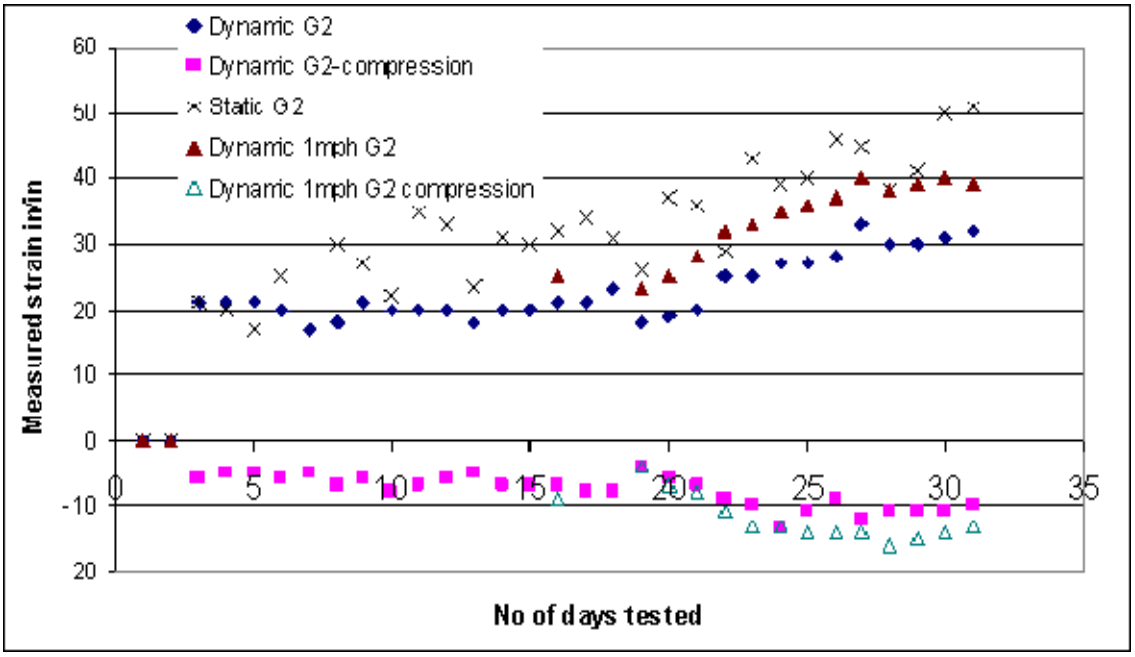

Figure 6.25. Measured Dynamic and Static Strains at Gage 2 in the 5-inch Slab in Phase I-a

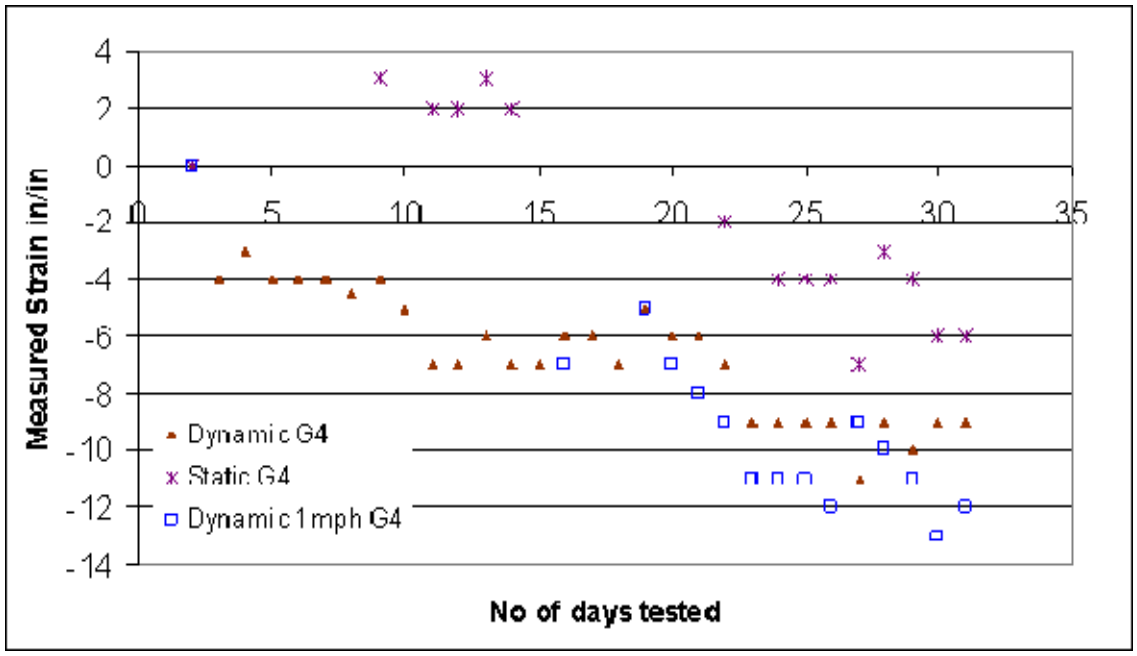

Figure 6.26. Measured Dynamic and Static Strains at Gage 4 in the 5-inch Slab in Phase I-a

6.3.2 Analysis of Strain Data in Phase I-a

Dynamic strain data were collected at each hour for 30 seconds during the loading period. Figure 6.27 shows a plot of typical strain data for two gages at Location 1 at the mid edge of the 6-inch slab. One gage was located at a depth of 1 inch from the top of the slab, and the other gage was located at a depth of 5.5 inches. The positions of the strain gages in Phase I-a have been shown previously in Figures 3.5 and 3.6.

Figure 6.27 clearly depicts the strain reversal that was observed during the passing of a wheel load. For the gage located at the top of the slab in the mid edge, as the wheel approached the gage location, tensile strain was measured by the gage. When the wheel was directly above the gage location, the strain reversed to a high value of compressive strain, and when the wheel moved away from the gage location, the strain again reversed to a tensile strain. Strains of opposite sign can be observed for the strain gage located at the bottom of the slab.

Gage at depth of 1 inch from the top of slab

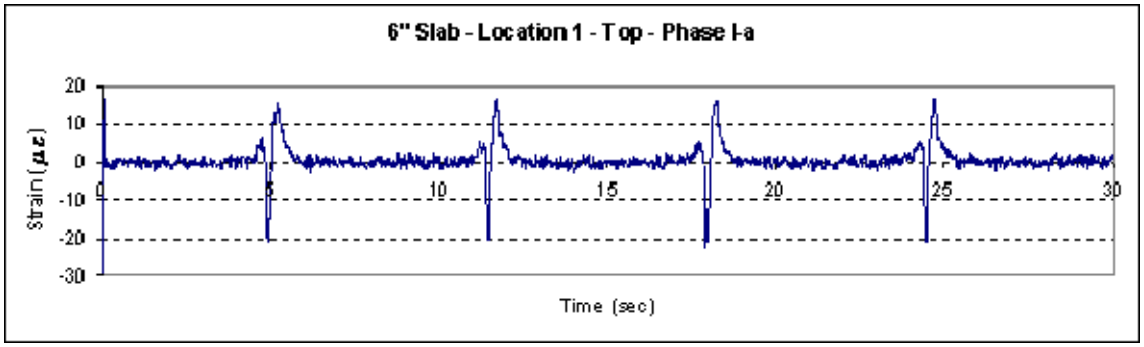

Gage at depth of 5.5 inches form the top of slab

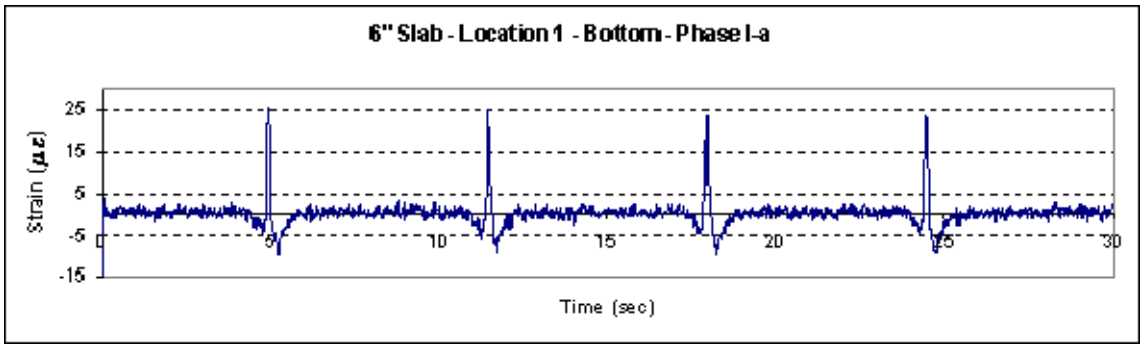

Figure 6.27. Measured Strains at Different Depths at the Mid Edge of the 6-inch Slab in Phase I-a.

The peak load-induced strain in compression (at the top gage) and tension (at the bottom gage) were extracted from each 30-sec data file. Peak load-induced strain here refers to the highest value of strain observed in the 30-sec strain data as shown in Figure 6.27, which happened when the wheel load passed directly above the strain gage location.

Figure 6.28 shows a plot of the peak load-induced strains measured at different gage locations as a function of the number of passes of the wheel load for the 6-inch slabs. Gages 1 and 2 were located at the mid edge (Location 1) at the top and bottom of the slab, respectively. Gage 3 was located at the top of the concrete slab in Location 2. Gage 4 was located at the bottom of Location 3, in the corner of the slab. Similarly, Figure 6.29 shows a plot of the

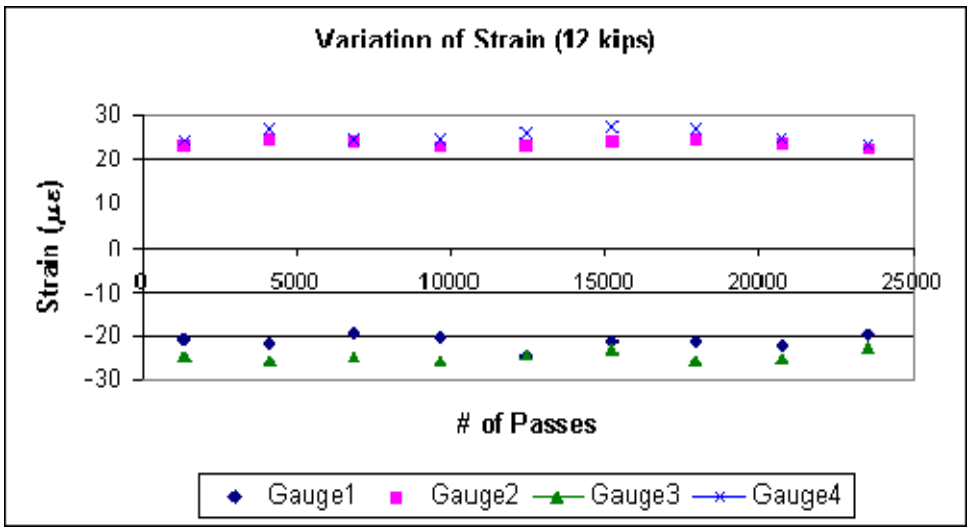

Figure 6.28. Variation of Peak Strains During the HVS Test in the 6-inch Slab in Phase I-a.

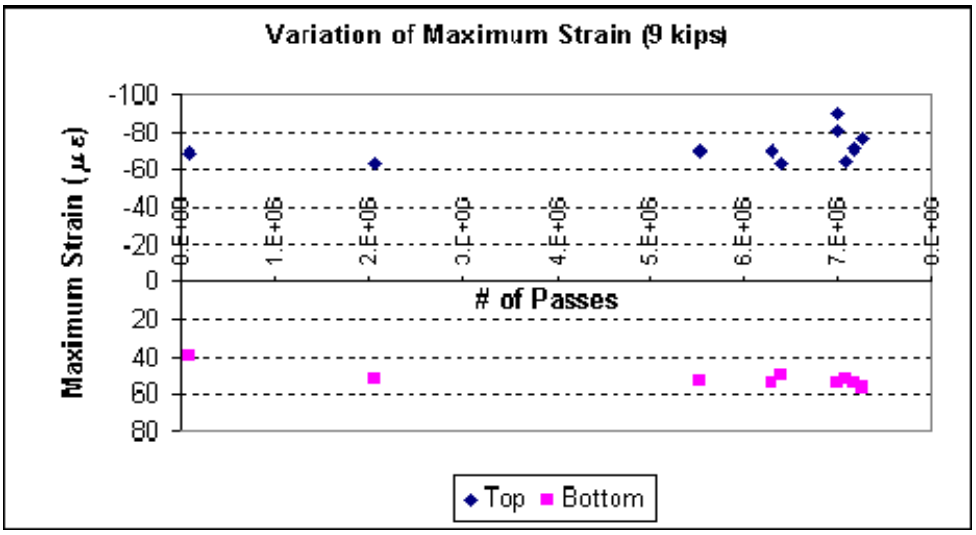

Figure 6.29. Variation of Maximum Strains During the HVS Test in the 4-inch Slab in Phase I-a.

maximum strains at Location 1 for the 4-inch slab in Phase I-a. Maximum strains here refer to both the strain at the top surface and at the bottom surface of the concrete slab. They were calculated by assuming a linear variation of the strain along the depth of the slab. For the 5-inch slabs, the strain gage at the top of the slab at Location 1 (gage 1) was out of order from the

beginning of the test, and thus a comparison between the maximum strains at the top and bottom of the slab was not possible. It can be observed from Figures 6.28 and 6.29 that no appreciable change in the load-induced strains occurred over the testing period. This may indicate that no crack had occurred near the locations of the strain gauges during the testing period for the specific load shown in the plot.

6.3.3 Analysis of Strain Data in Phase I-b

Similar to the procedure used in Phase I-a, strain data were collected every hour during HVS loading of each test section, at the rate of 100 measurements per second for 30 seconds. In addition to the calculation of the peak strain at the top and at the bottom of the concrete slab as indicated in Phase I-a, the strains in the AC surface were also extracted from each strain record.

Figure 6.30 depicts the maximum load-induced strains at the top and at the bottom of the concrete at Location 1 in the 6-inch slabs as a function of the number of HVS wheel passes. This figure also shows the strains at the surface of the asphalt layer. Theoretically, due to the bonding between the concrete and the asphalt layer, the maximum load-induced tensile strains at the bottom of the concrete layer should be lower than the maximum strains at the top of the concrete layer. However, the maximum tensile strains were fairly close to the maximum compressive strains. This might be caused by either (1) the loss of bonding between the concrete and the asphalt layer, or (2) inappropriate placement or functioning of the strain gages.

Figure 6.31 shows the similar plots of load-induced strains versus number of HVS wheel passes for the 5-inch concrete slabs. In this case, the maximum compressive strains at the top of the concrete were substantially higher than the maximum tensile strains at the bottom of the concrete. This observation agrees with the predicted behavior. This indicates good bonding between the concrete and the asphalt layer, which resulted in the reduction of tensile strains at the bottom of the concrete layer.

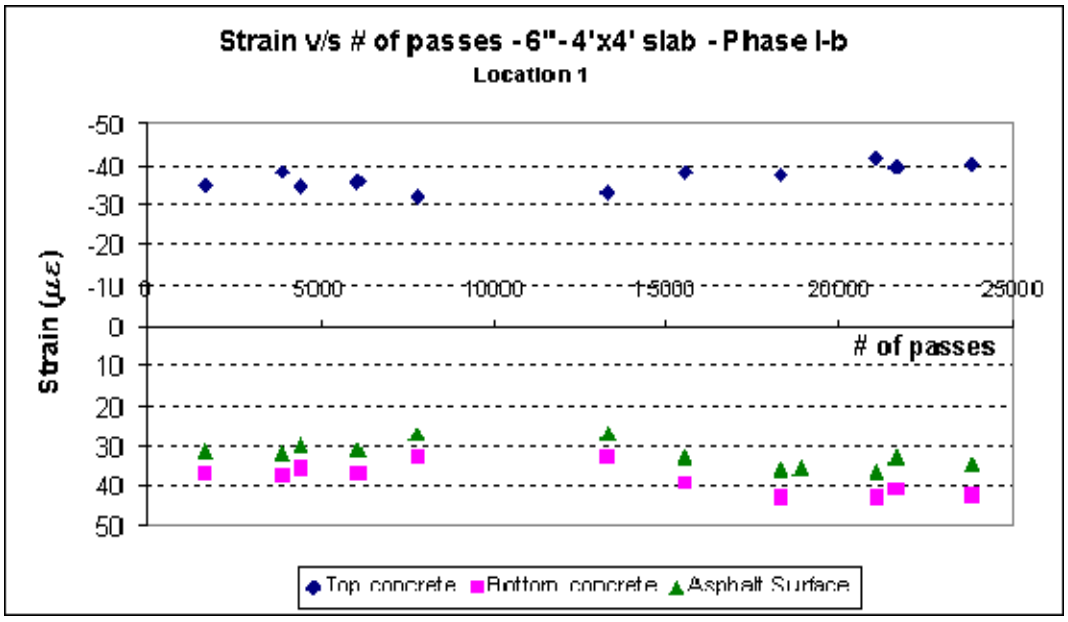

Figure 6.30. Variation of Peak Strains in the 6-inch Concrete Slab and on the Surface of the Asphalt Layer at Location 1 (mid edge of the slab) During HVS Test in Phase I-b.

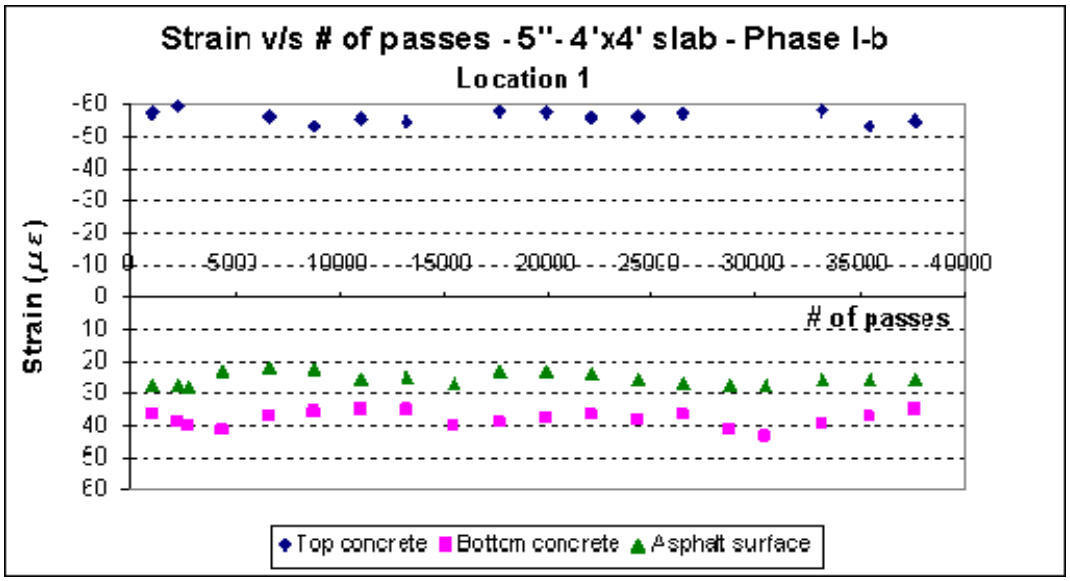

Figure 6.31. Variation of Maximum Strains in the 5-inch Concrete Slab and on the Surface of the Asphalt Layer at Location 1 (mid-edge of the slab) During HVS Test in Phase I-b.

Figure 6.32 shows the peaks strain at the bottom of the concrete slab and on the surface of the AC layer for the 4” slab. In this case, the analysis of maximum strain was not possible to perform due to the failure of the gage located at the top of the slab. The values showed in this figure cannot be used to check the bonded condition in the interface, since the strains plotted here were measured by gages close to the interface but at different depths.

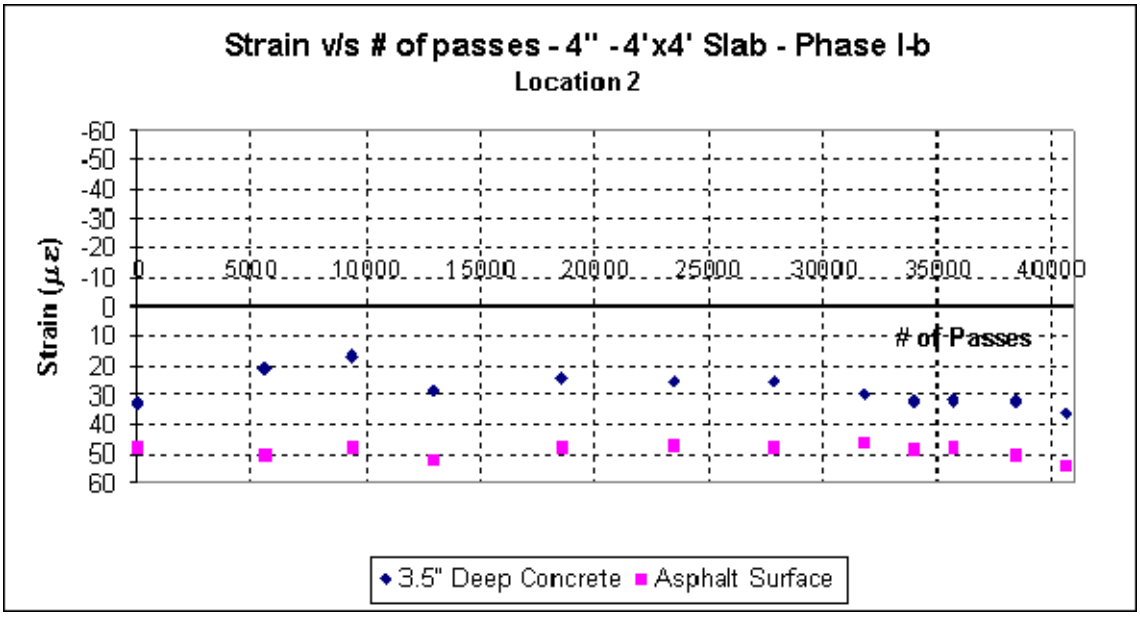

Figure 6.32. Variation of Peak Strains in the 4-inch Concrete Slab and on the Surface of the Asphalt Layer at Location 2 (corner of the slab) During HVS Test in Phase I-b.

6.3.4 Analysis of Strain Data in Phase II

In Phase II, a total of 15 strain gages were installed in the slabs to record the strain at different locations. Figures 6.33 through 6.38 show the maximum measured HVS load-induced strains in Location 1 (at mid-edge) and Location 5 (at slab corner) as a function of the number of passes of the 12-kip wheel load. The measured strains shown include (1) the strain near the top of the concrete layer, (2) the strain near the bottom of the concrete layer, and (3) the strain on top of the asphalt layer.

Using the measured strain near the top of the concrete layer and that near the bottom of the concrete layer, the strain at the bottom of the concrete layer was computed by linear extrapolation. The computed strains at the bottom of the concrete layer were also plotted in Figures 6.33 through 6.38. The strains at the bottom of the concrete layer can be compared with the strains at the surface of the asphalt layer to indicate how well the concrete is bonded to the asphalt layer. If these two layers were perfectly bonded, the strains at the bottom of the concrete layer should be the same as the strains on the surface of the asphalt layer.

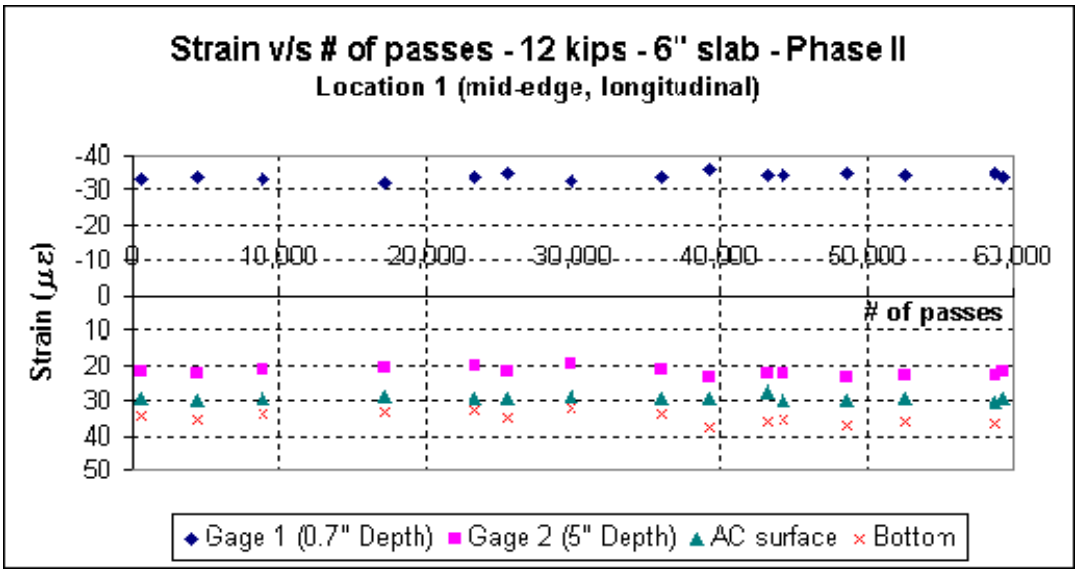

Figure 6.33. Variation of Peak Strains in the 6-inch Slab at Location 1 During HVS Test in Phase II.

From the comparison of the computed strains at the bottom of the concrete layer with the measured strains at the top of the asphalt layer as shown in Figures 6.33 through 6.38, a difference of more than 15 micro-strains can be observed between the two layers at the interface in the 10-inch slab, while the difference was much lower for the 8- and 6-inch slabs. This means that the 10-inch slab had a relatively poorer bond at the interface as compared with the 8- and 6-inch

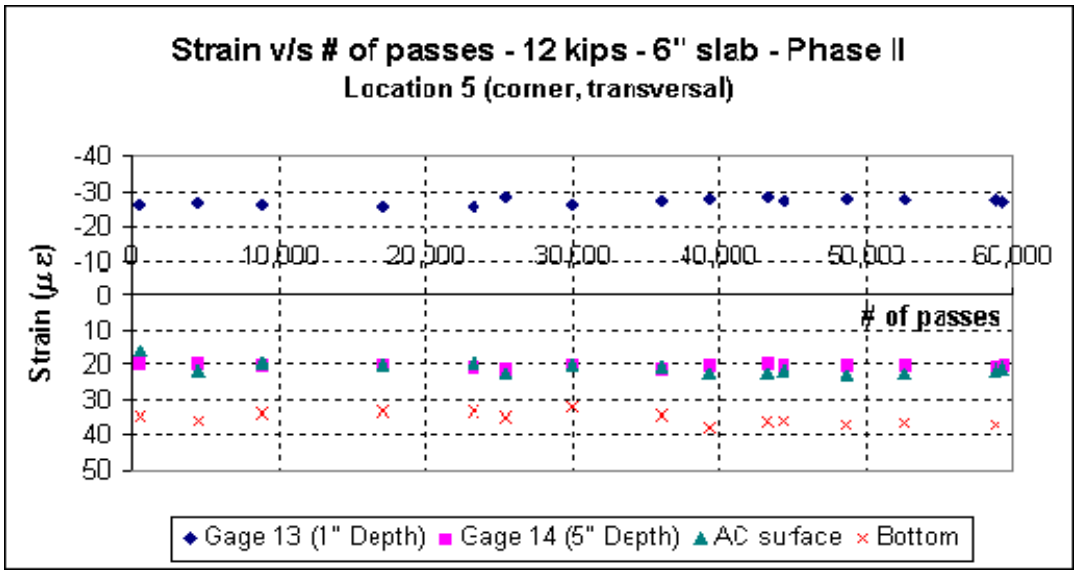

Figure 6.34. Variation of Peak Strains in the 6" Slab at Location 5 During HVS Test in Phase II.

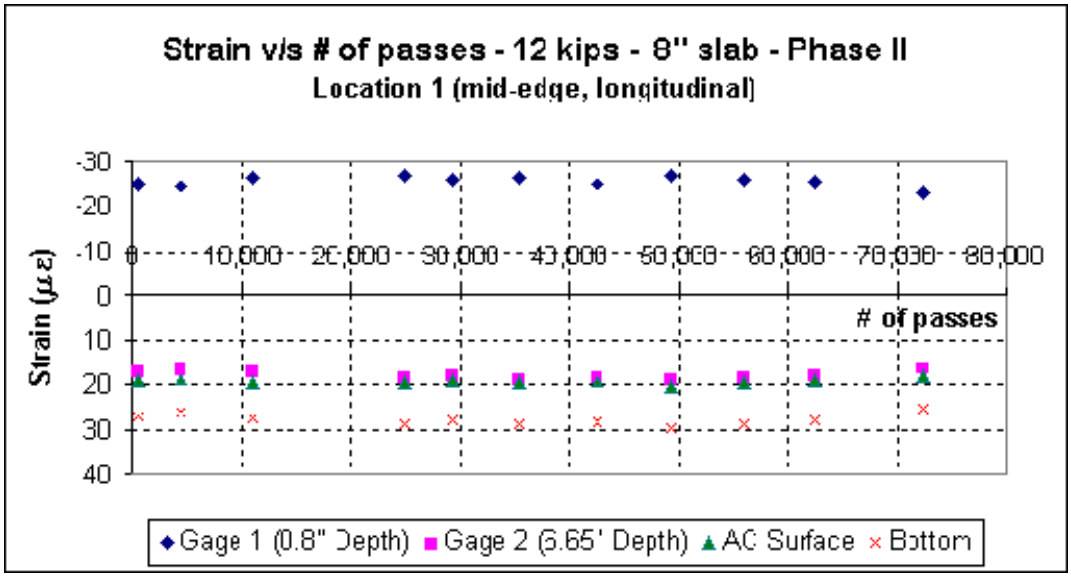

Figure 6.35. Variation of Peak Strains in the 8-inch Slab at Location 1 During HVS Test in Phase II.

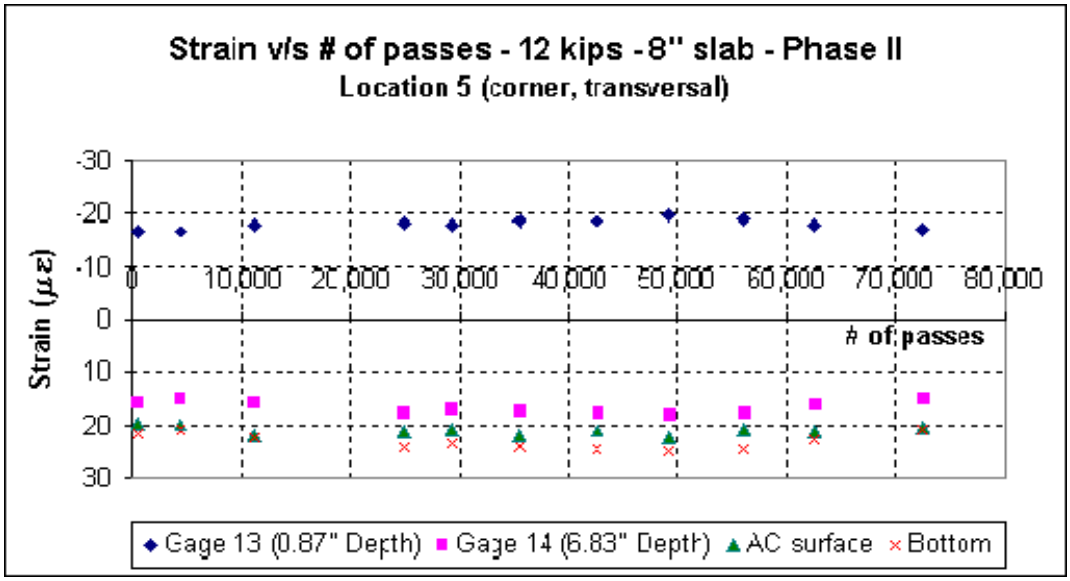

Figure 6.36. Variation in Peak Strains in the 8-inch Slab at Location 5 During HVS Test in Phase II.

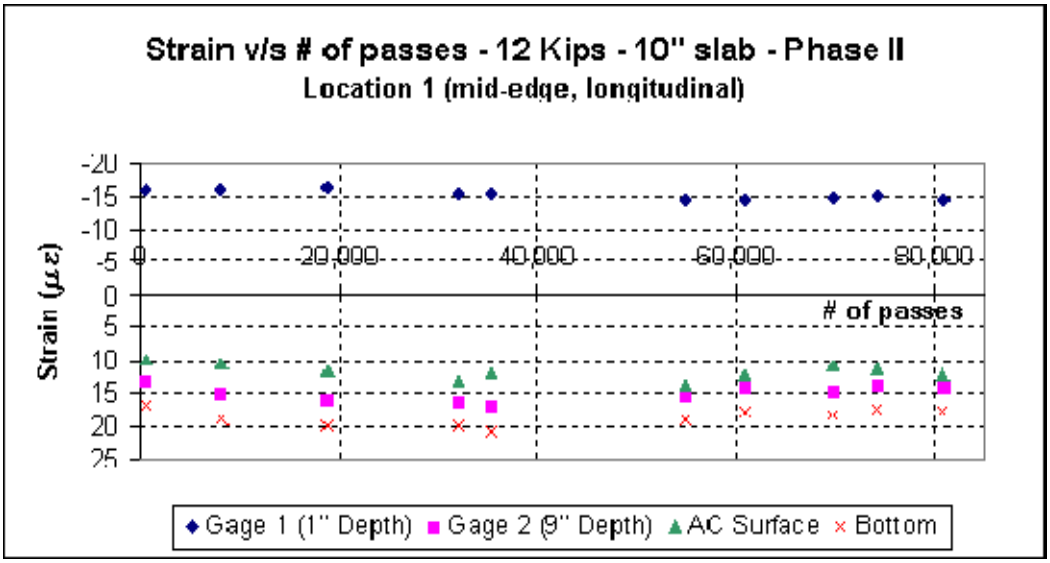

Figure 6.37. Variation of Peak Strains in the 10-inch Slab at Location 1 during HVS test in Phase II.

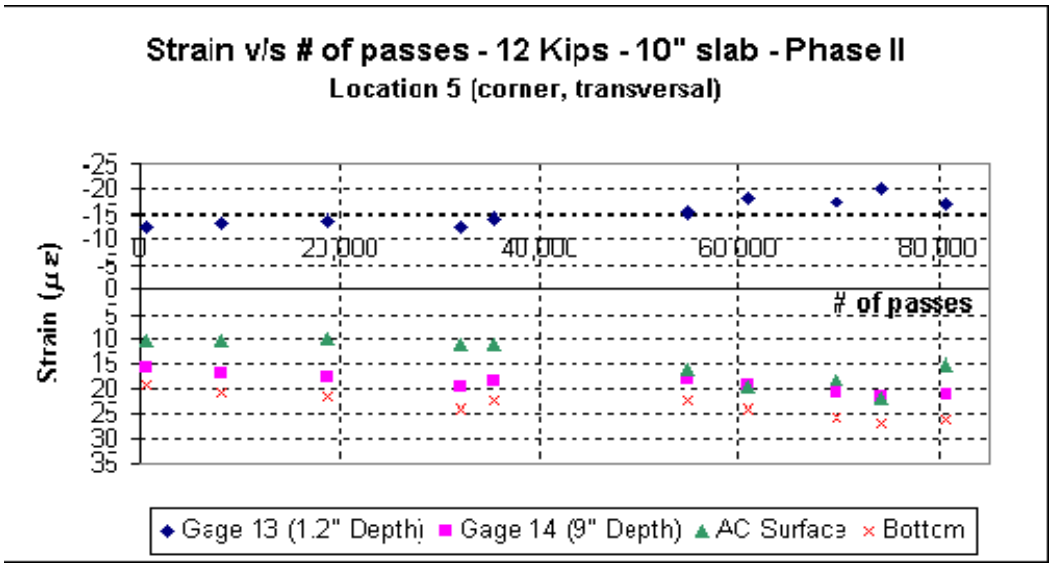

Figure 6.38. Variation of Peak Strains in the 10-inch Slab at Location 2 During HVS Test in Phase II.

slabs. This may be explained by the fact that the 10-inch slab was the first slab being loaded, at 28 days after the concrete was placed. It has been reported in other studies that the bond in the interface tends to increase with time due to mainly the effect of the slab weight. The 8-inch and the 6-inch slabs were loaded at 2 and 3 months after concrete placement. In these two cases, the bond at the interface might have gained somewhat during this time.

Similar to the results from Phase I-1 and Phase I-b, no significant variation in the strain was observed as a function of the number of passes for the 8- and 6-inch slabs. However for the 10-inch slab, an increase in the strain was observed at the end of the 12-kips loading period.

CHAPTER 7
MODEL CALIBRATION AND VERIFICATION

7.1 Overview of Model Calibration

In order for the 3-D analytical model to accurately analyze the behavior of whitetopping pavements, it needs to have the correct properties of the pavement materials and the correct values of spring stiffness for modeling the behavior of joints and concrete-asphalt interface. The elastic moduli of the concrete and asphalt materials were initially estimated from the results of laboratory tests on these materials, as described in Chapter 5. The results of the FWD tests on the composite pavement test sections were used to estimate the elastic moduli of the other pavement materials and the joint and interface spring stiffnesses, and also to adjust the values of elastic moduli of the concrete and asphalt materials by back-calculation method (of matching the analytically computed deflections with the measured FWD deflections). This process is referred to as "deflection-based calibration" of the model in this study.

The estimation of the pavement materials properties and parameters was further refined by matching the analytically computed strains with the measured strains in the test sections caused by HVS wheel loads. This process is referred to as "strain-based calibration" in this study.

7.2 Deflection-Based Calibration of Model Parameters

7.2.1 Phases I-a and I-b

As mentioned in Chapter 5, FWD tests were run on the test sections to estimate the values of the elastic moduli for the pavement layers and the stiffness of the springs used to model the load transfer at the joints and concrete-asphalt interface (for the partially-bonded condition).

To better estimate the elastic moduli of the pavement layers independently of the effects of joints, FWD tests were run on large slabs which were located at both ends of the test track, and had a size of 12 ft X 18 ft. Pavement surface deflection basins caused by a 12-kip FWD load were used to estimate the elastic moduli of the pavement layers by the back-calculation method. Figures 7.1 through 7.5 show examples of the matched deflection basins from the back-calculation process in which the elastic moduli of the concrete, asphalt, limerock base and subgrade materials were estimated. The estimated elastic modulus had a range of 130,000 - 160,000 psi and 28,000 - 30,000 psi for the lime rock base and the subgrade, respectively. The value of the elastic modulus of the AC layer was seen to vary significantly with temperature. From the results of laboratory tests on the AC samples (as presented in Chapter 5), the resilient modulus of the AC varied from 0.75×10^6 psi at 25 °C (representing summer condition) to 1.7×10^6 psi at 5 °C (representing winter condition). FWD tests for Phase I-a and Phase II were run in the summer time, while FWD test for Phase I-b were run in the Fall (at the end of October of 2005). The elastic modulus of the AC layer, estimated from the back-calculation method using the FWD data from Phase I-a, was very close to that obtained in the laboratory (0.7×10^6 psi). By using the data from the FWD tests run in a colder condition, the back-calculation process gave a value of 1.1×10^6 psi for the elastic modulus of the AC. The elastic modulus of the concrete was estimated as 4.35×10^6 psi, which compares very well with the one obtained by laboratory testing.

After the elastic moduli of the pavement layers had been estimated, the joint spring stiffnesses, which were used to model the load transfer at the joints, were estimated by matching the analytical with the measured deflection basins caused by a FWD load applied at the corner and the mid-edge of the test slab (as described in Chapter 5). Deflection basins were recorded along the edge of the slab on both the loaded and the un-loaded slab, as described in Chapter 5.

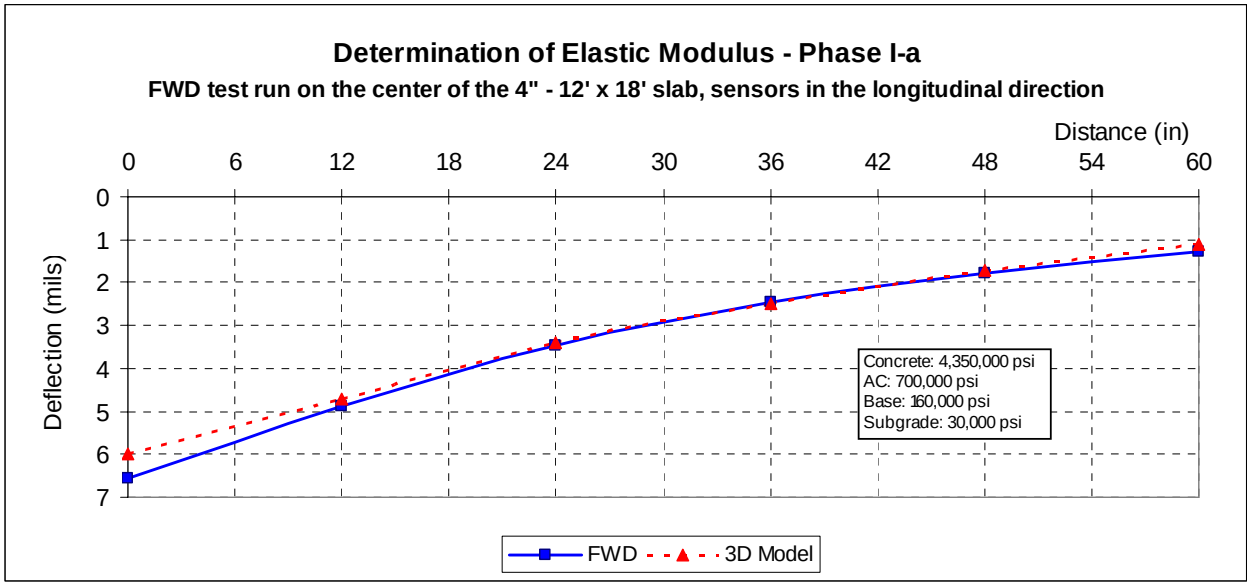

Figure 7.1. Matching of Deflection Basin in the Longitudinal Direction Caused by a 12-kip FWD Load Applied to the Center of a 4" Slab in Phase I-a.

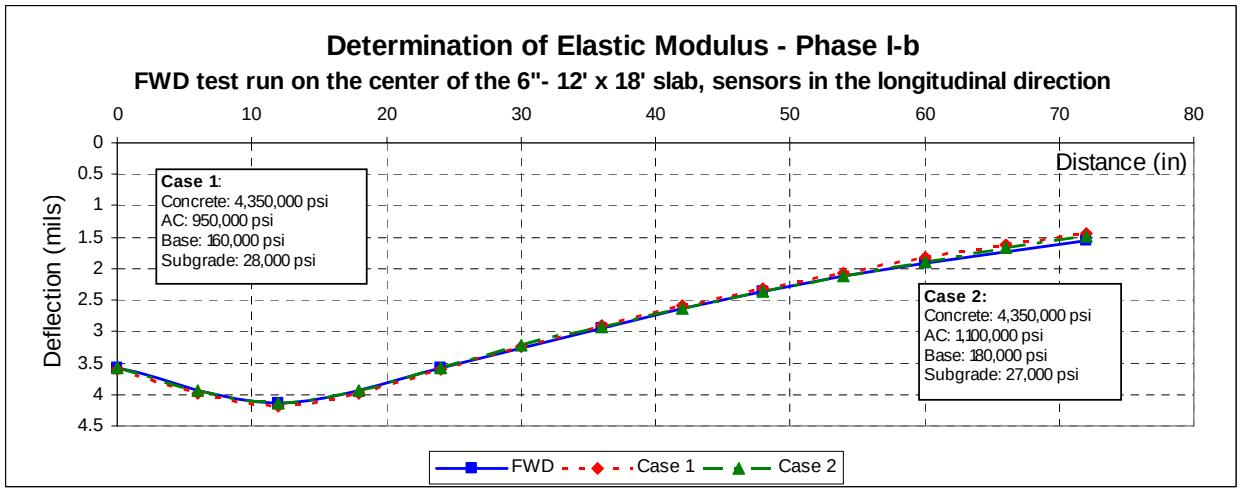

Figure 7.2. Matching of Deflection Basin in the Longitudinal Direction Caused by a 12-kip FWD Load Applied to the Center of a 6" Slab in Phase I-b.

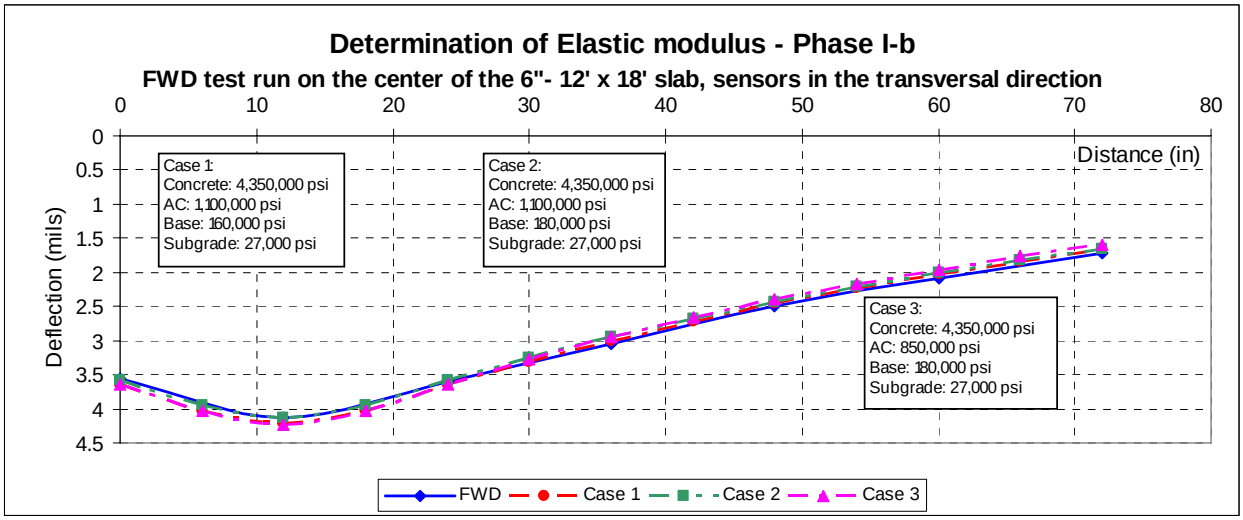

Figure 7.3. Matching of Deflection Basin in the Transverse Direction Caused by a 12-kip FWD Load Applied to the Center of a 6" Slab in Phase I-b.

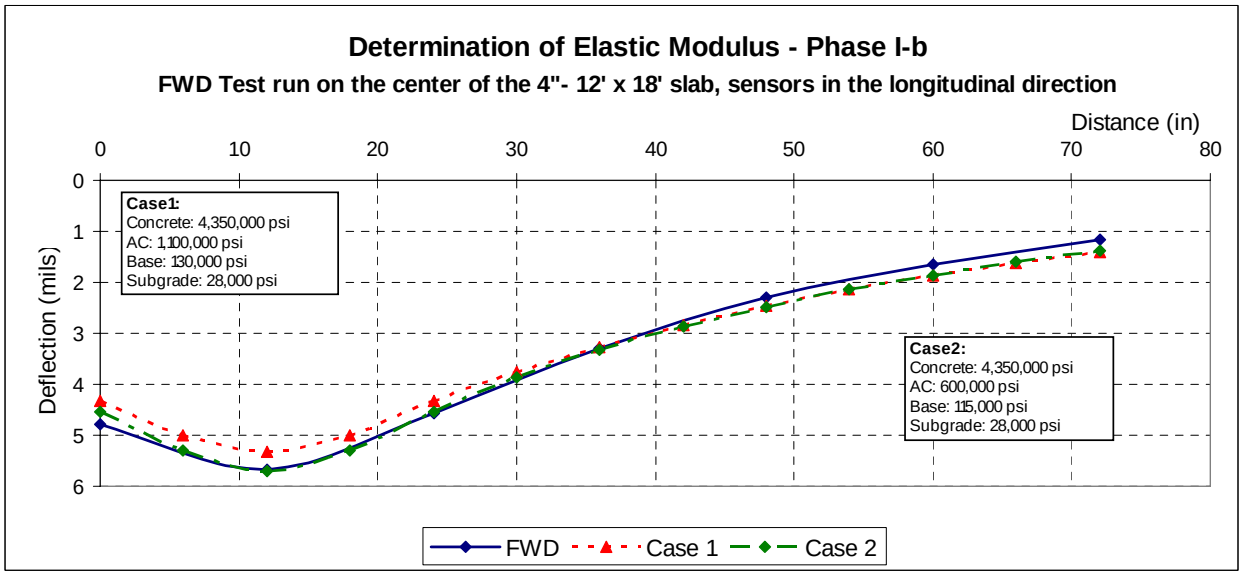

Figure 7.4. Matching of Deflection Basin in the Longitudinal Direction Caused by a 12-kip FWD Load Applied to the Center of a 4" Slab in Phase I-b.

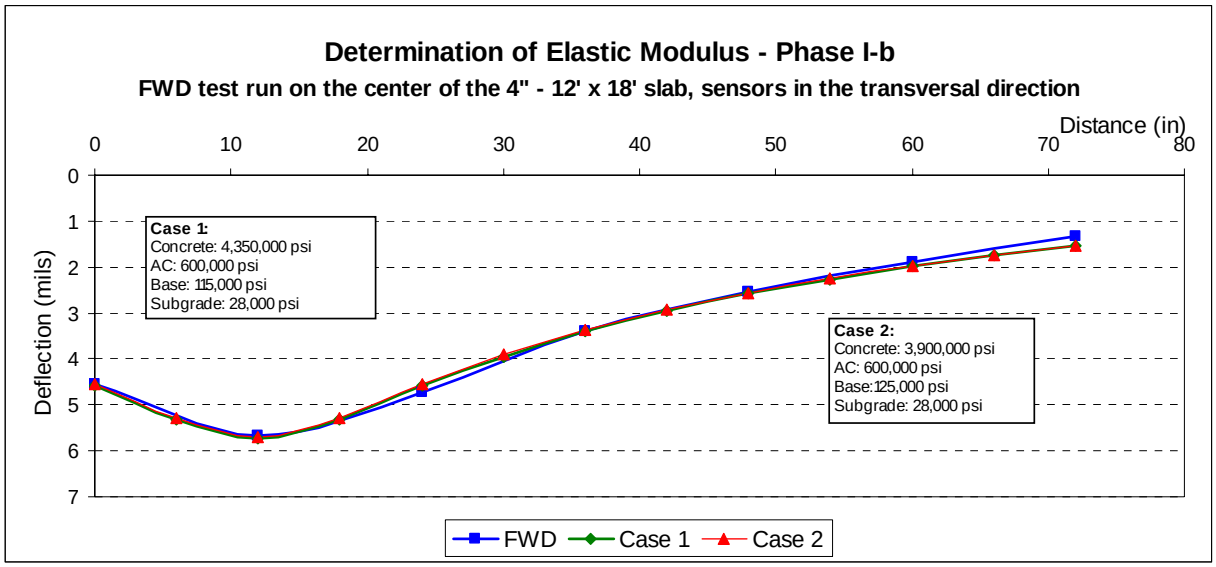

Figure 7.5. Matching of Deflection Basin in the Transverse Direction Caused by a 12-kip FWD Load Applied to the Center of a 4" Slab in Phase I-b.

Figures 7.6 through 7.9 show examples of the matched deflection basins from the back-calculation process for the estimation of the joint spring stiffnesses. From the results of FWD tests run on a 4-inch slab on Lane 6 (Phase I-a) as seen from Figures 7.6 and 7.7, an appropriate match between the measured and the calculated deflection basin was achieved with a single vertical stiffness in the order of 100,000 lb/in, and with stiffnesses of zero in the other directions.

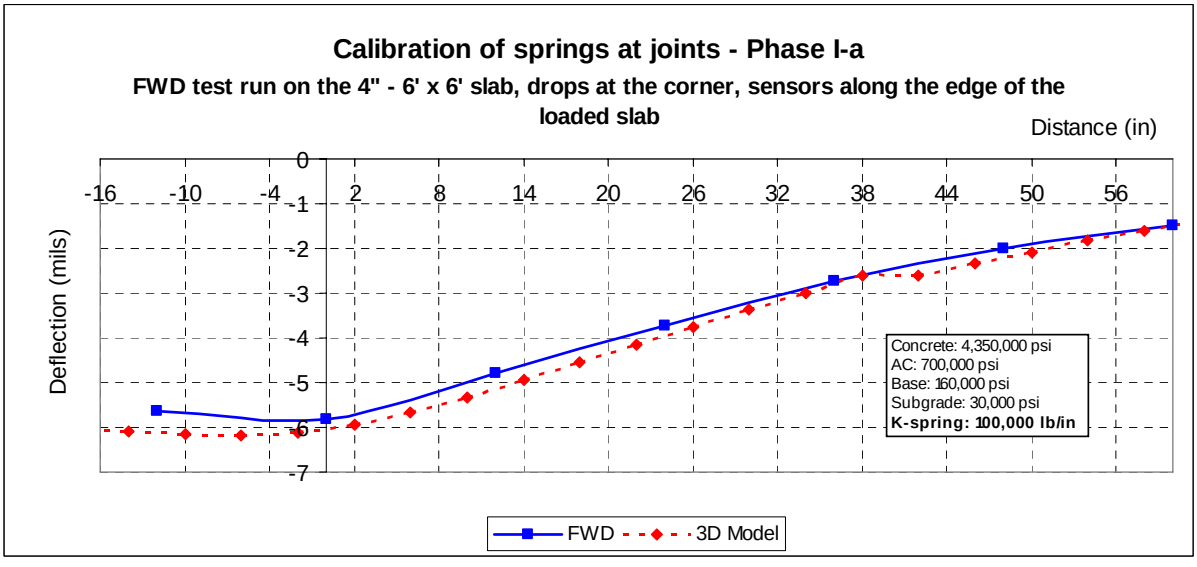

Figure 7.6. Matching of Deflection Basin Along the Edge of Loaded Slab Caused by a 12-kip FWD Load Applied to the Corner of a 4" Slab in Phase I-a.

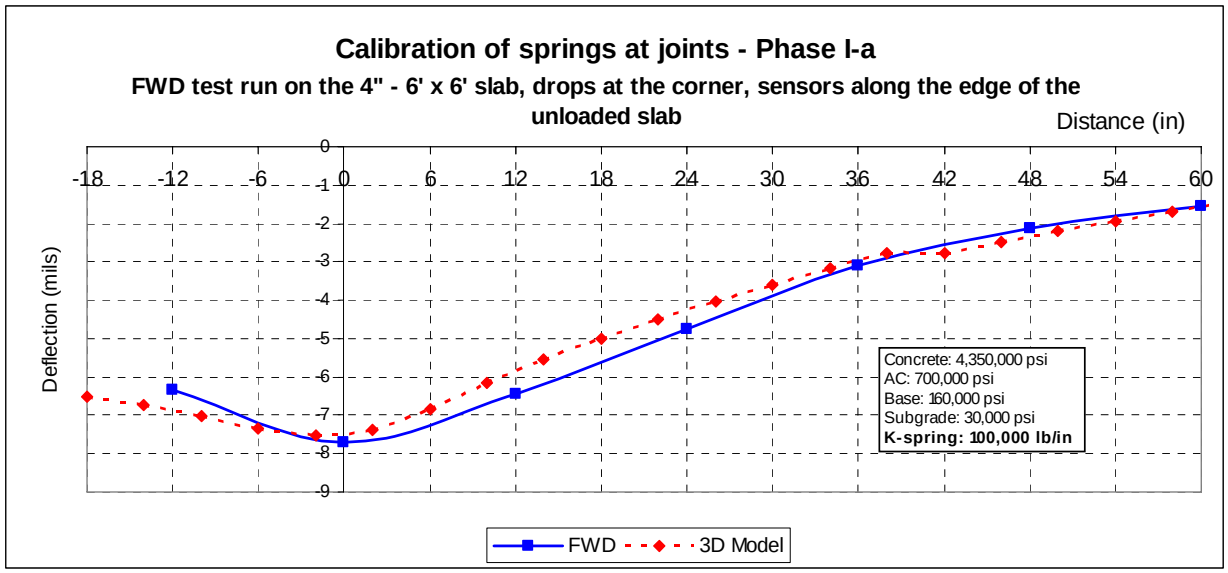

Figure 7.7. Matching of Deflection Basin Along the Edge of Unloaded Slab Caused by a 12-kip FWD Load Applied to the Corner of a 4" Slab in Phase I-a.

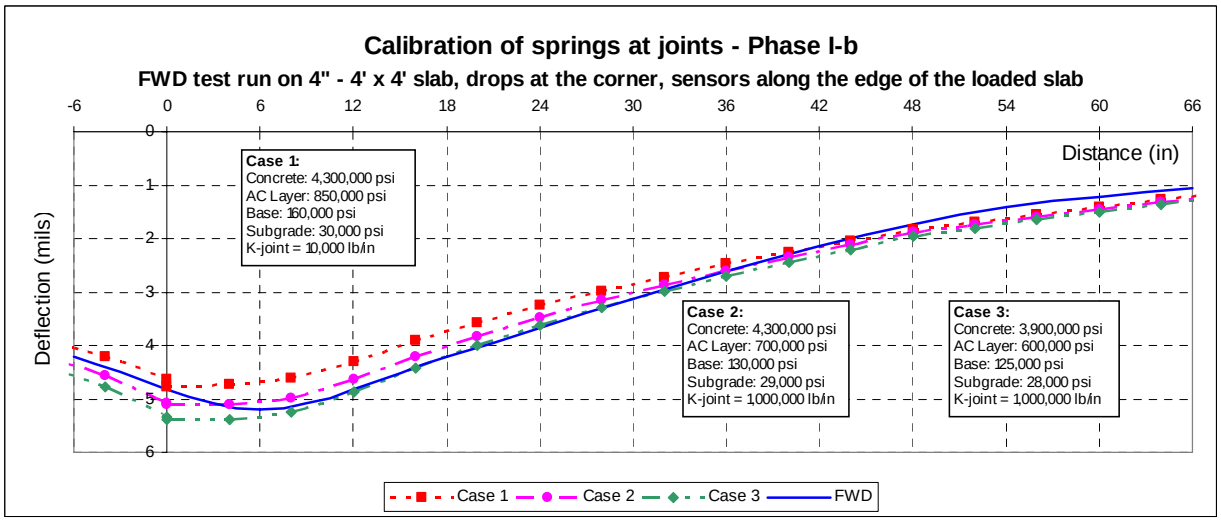

Figure 7.8. Matching of Deflection Basin Along the Edge of Loaded Slab Caused by a 12-kip FWD Load Applied to the Corner of a 4" Slab in Phase I-b.

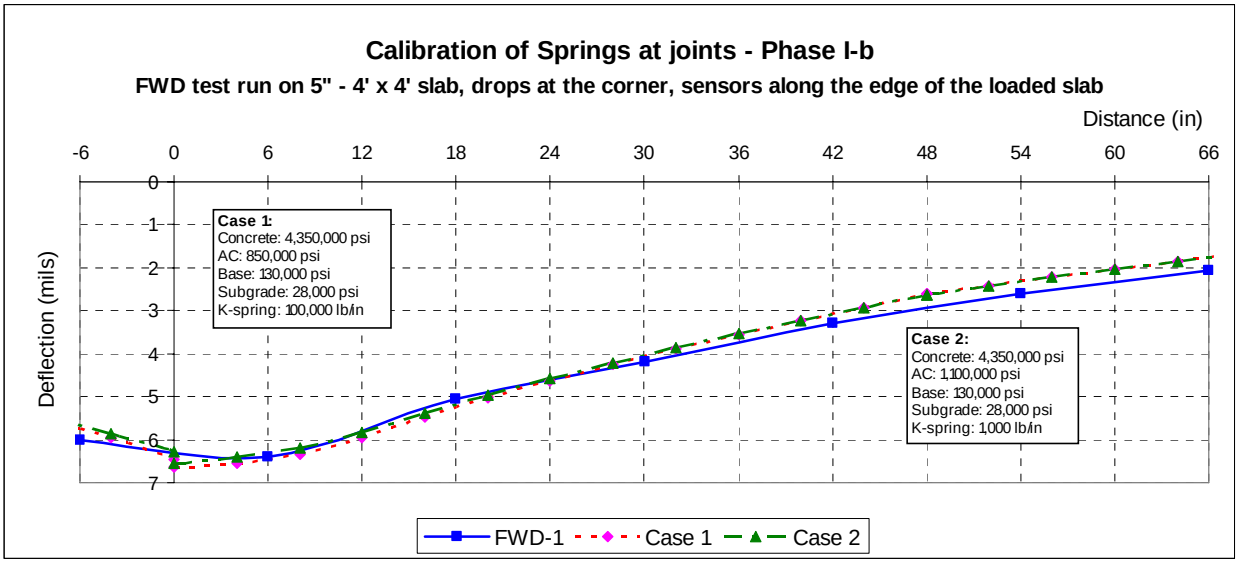

Figure 7.9. Matching of Deflection Basin Along the Edge of Loaded Slab Caused by a 12-kip FWD Load Applied to the Corner of a 5" Slab in Phase I-b.

Back-calculations performed using FWD data from the tests run in Phase I-b (using 4' x 4' slabs) showed that the effect of the load transfer can be properly modeled with a spring constant in the range of 100,000 to 1,000,000 lb/in for the vertical spring, and that it is not necessary to use the springs in the other two directions, similar to what happened in Phase I-a.

7.2.2 Phase II

The elastic moduli of the pavement layers for the test sections in Phase II were assumed to be similar to those in Phase I-a and Phase I-b, due to the fact that the same pavement materials were used.

The deflection basins along the edge of the slabs caused by a 12-kip FWD load applied to the corner and the mid-edge of the slabs were used to estimate the joint spring stiffnesses, and the interface spring stiffnesses by back-calculation method. In this phase, many spring constants had to be calibrated since three springs were used to model the load transfer at the joints and three springs were used to model the interaction between the concrete slab and the AC layer in

the interface. Also, the springs used in both the transverse and longitudinal joints were considered separately (as they might have different stiffness values), which gave more flexibility when matching the FWD deflection basins first and the measured HVS load-induced strains later.

Figures 7.10 through 7.19 show examples of the matched deflection basins from the back-calculation process for the estimation of the joint spring stiffnesses and interface spring stiffnesses for the test sections in Phase II. The analytical deflections matched well with the measured deflections in all the cases shown in these figures.

During the deflection-based calibration process, it was found that the parameter that had the greatest effect on the FWD deflection of the composite pavement was the stiffness of the vertical springs modeling the vertical load transfers at the concrete-asphalt interface. Using a vertical spring stiffness ranging between 10^{18} and 10^{19} lb/in appeared to produce calculated deflections that matched well with the measured FWD deflections.

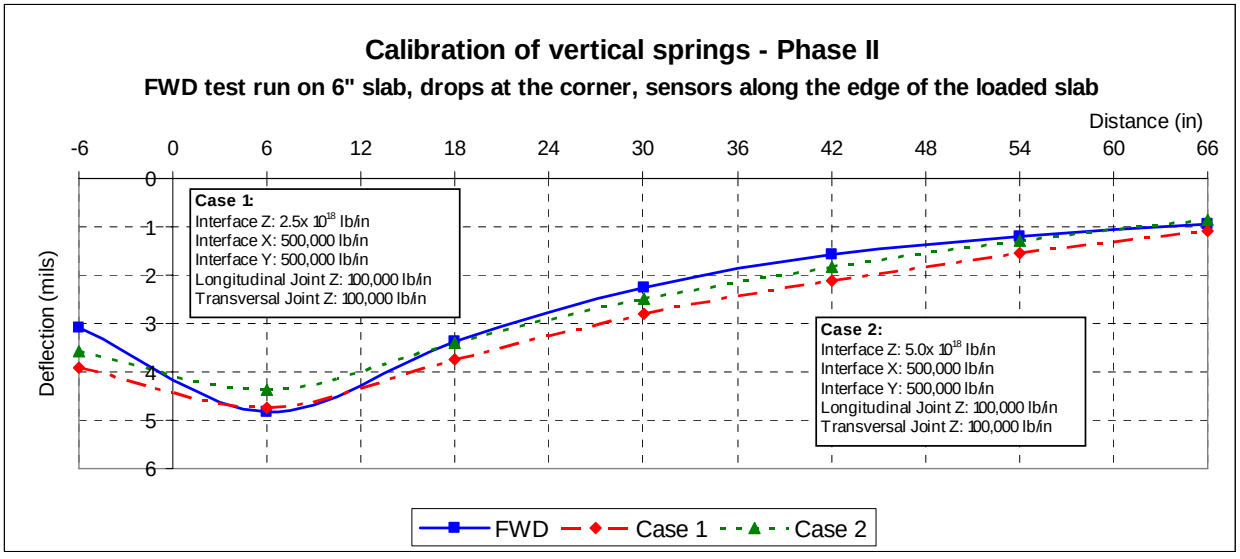

Figure 7.10. Matching of Deflection Basin Along the Edge of Loaded Slab Caused by a 12-kip FWD Load Applied to the Corner of a 6" Slab in Phase II.

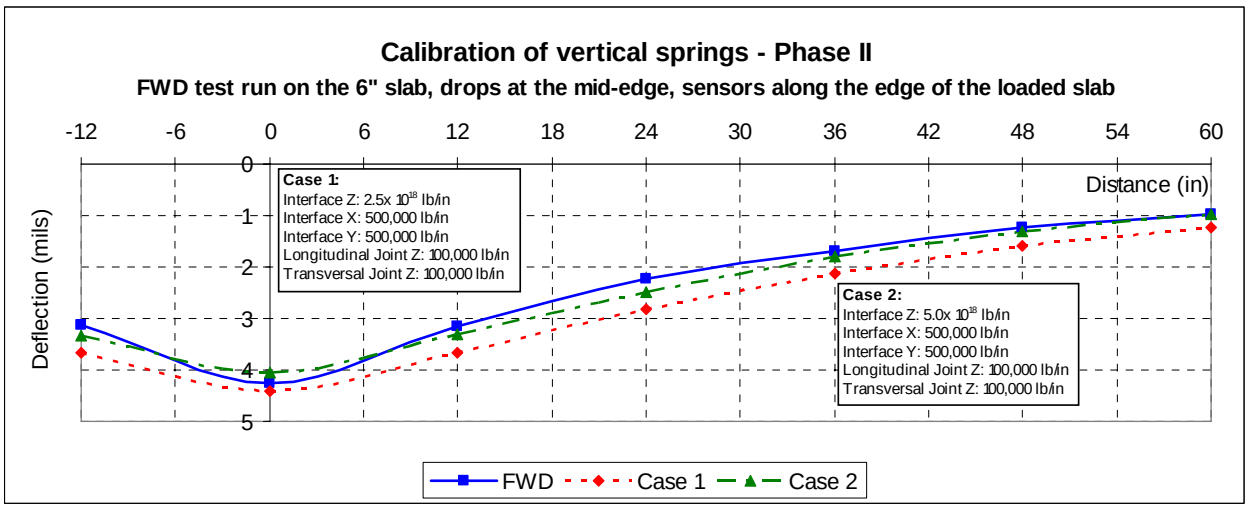

Figure 7.11. Matching of Deflection Basin Along the Edge of Loaded Slab Caused by a 12-kip FWD Load Applied to the Mid-Edge of a 6” Slab in Phase II.

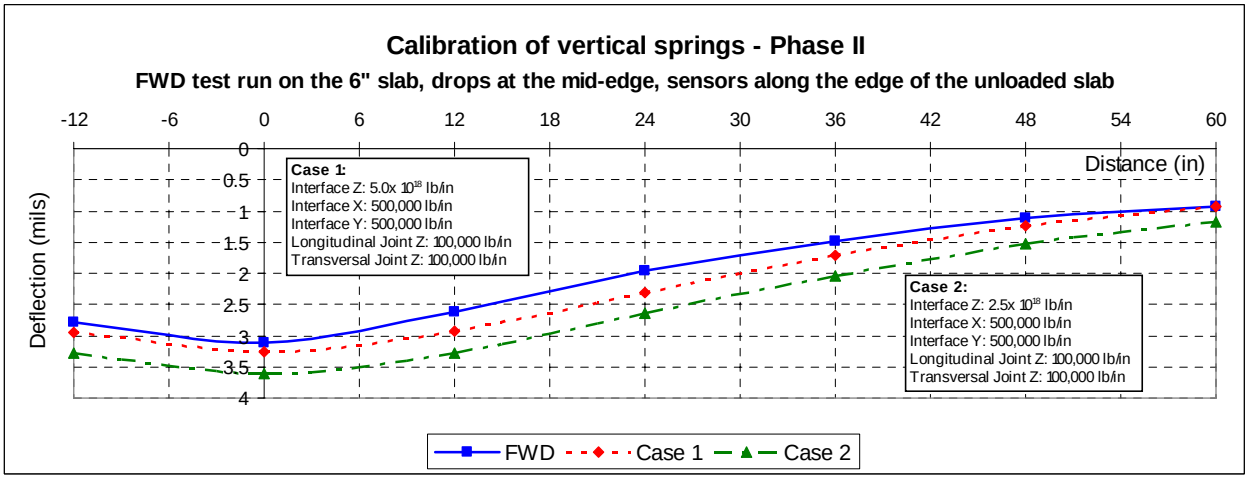

Figure 7.12. Matching of Deflection Basin Along the Edge of Unloaded Slab Caused by a 12-kip FWD Load Applied to the Mid-Edge of a 6” Slab in Phase II.

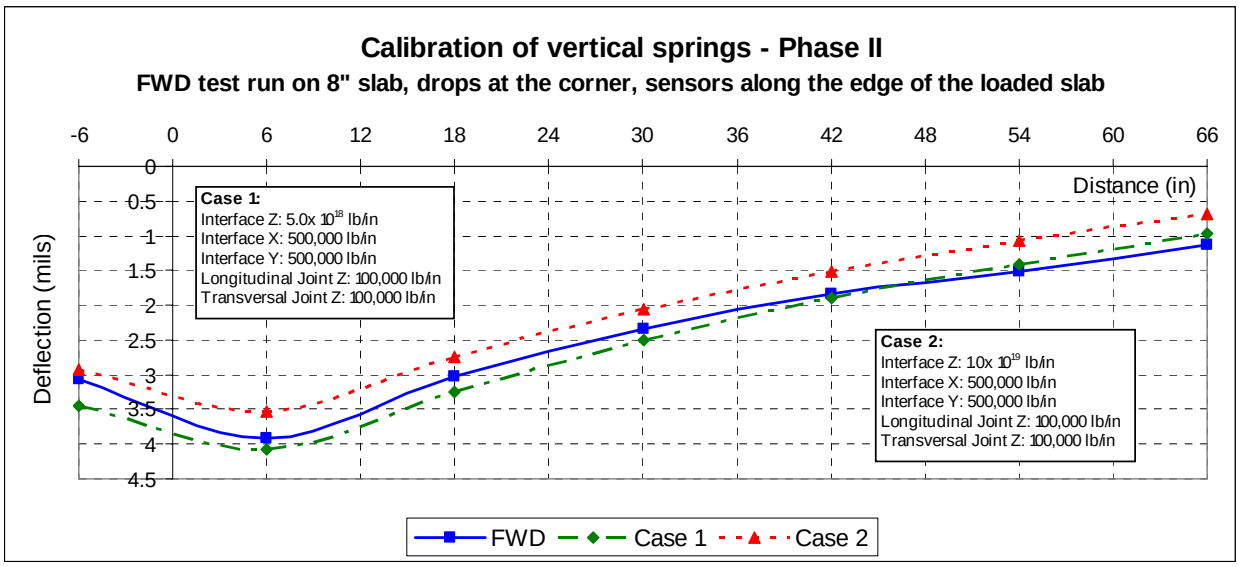

Figure 7.13. Matching of Deflection Basin Along the Edge of Loaded Slab Caused by a 12-kip FWD Load Applied to the Corner of an 8” Slab in Phase II.

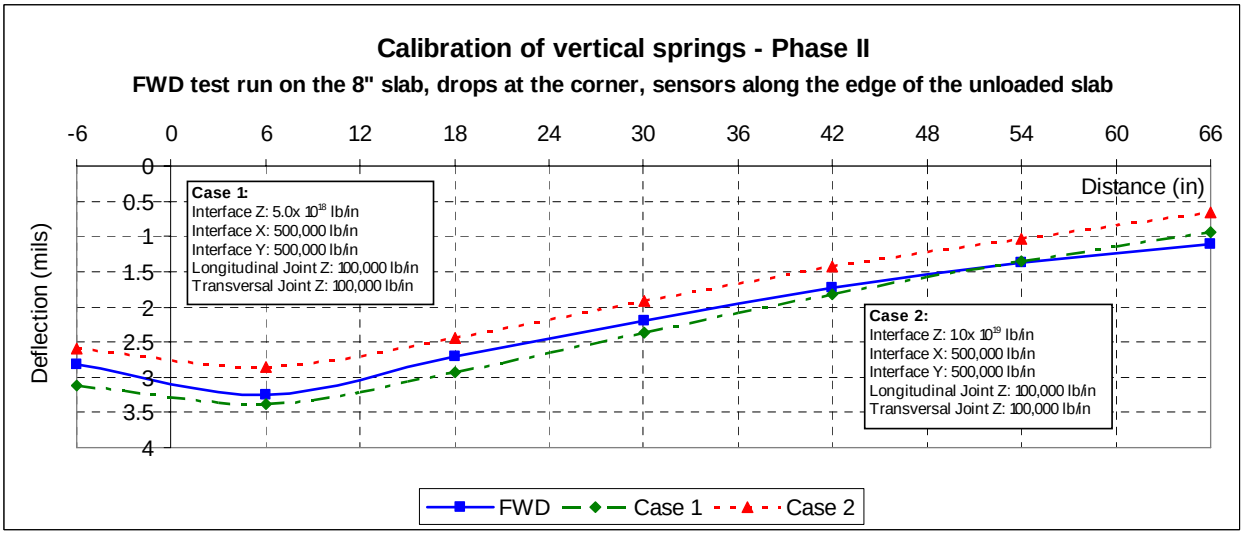

Figure 7.14. Matching of Deflection Basin Along the Edge of Unloaded Slab Caused by a 12-kip FWD Load Applied to the Corner of an 8” Slab in Phase II.

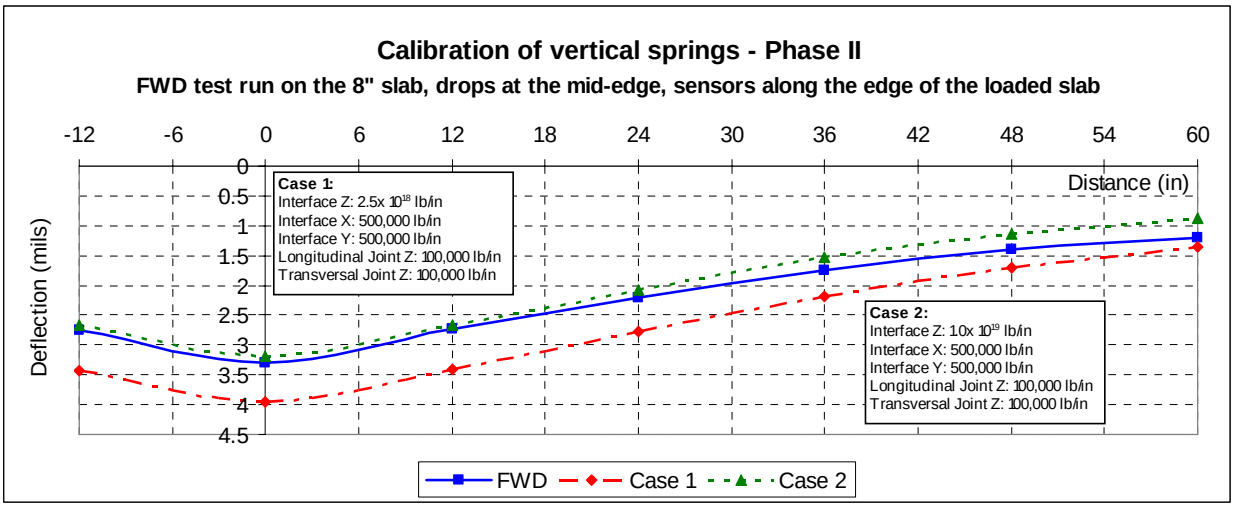

Figure 7.15. Matching of Deflection Basin Along the Edge of Loaded Slab Caused by a 12-kip FWD Load Applied to the Mid-Edge of an 8" Slab in Phase II.

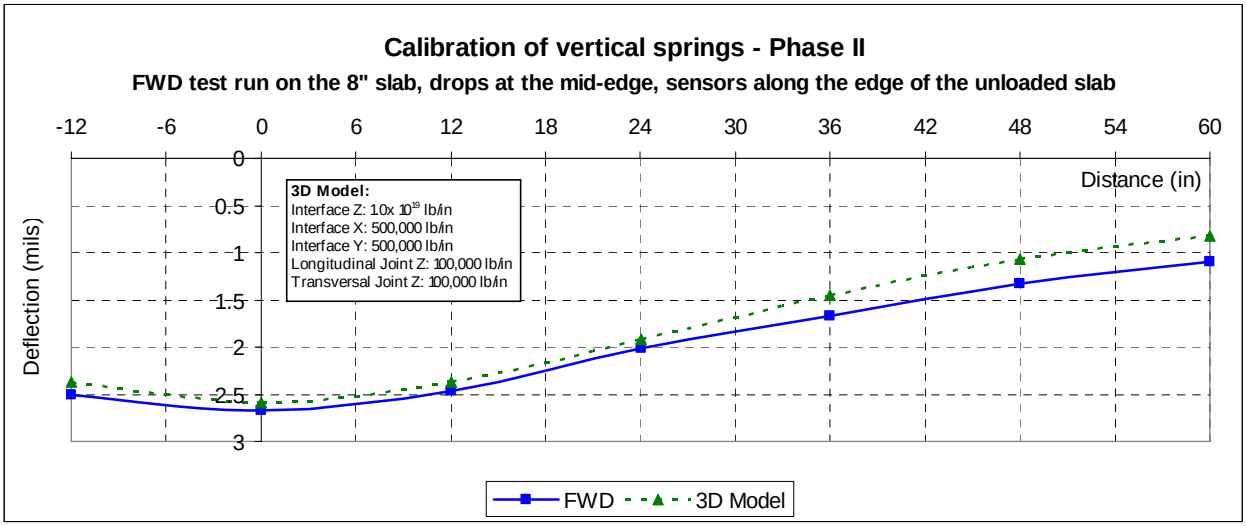

Figure 7.16. Matching of Deflection Basin Along the Edge of Unloaded Slab Caused by a 12-kip FWD Load Applied to the Mid-Edge of an 8" Slab in Phase II.

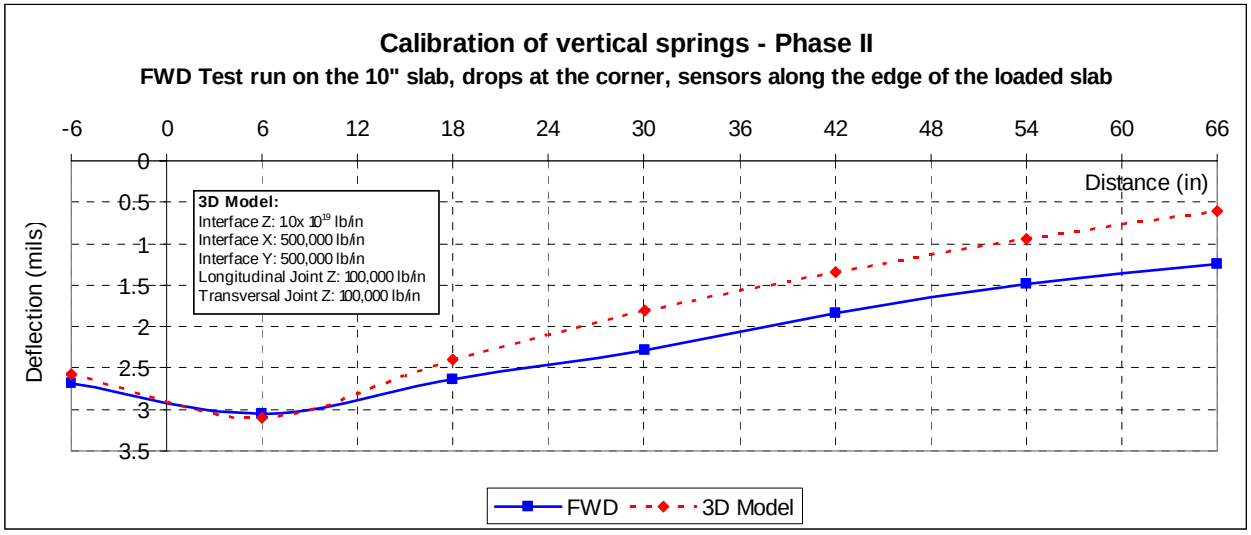

Figure 7.17. Matching of Deflection Basin Along the Edge of Loaded Slab Caused by a 12-kip FWD Load Applied to the Corner of a 10” Slab in Phase II.

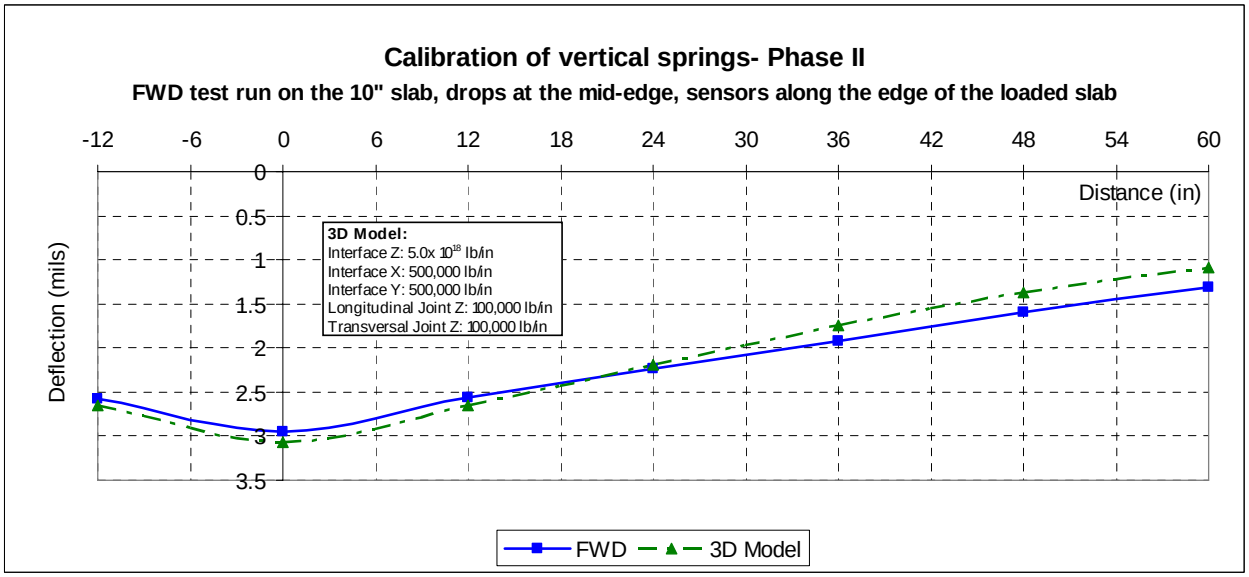

Figure 7.18. Matching of Deflection Basin Along the Edge of Loaded Slab Caused by a 12-kip FWD Load Applied to the Mid-Edge of a 10” Slab in Phase II.

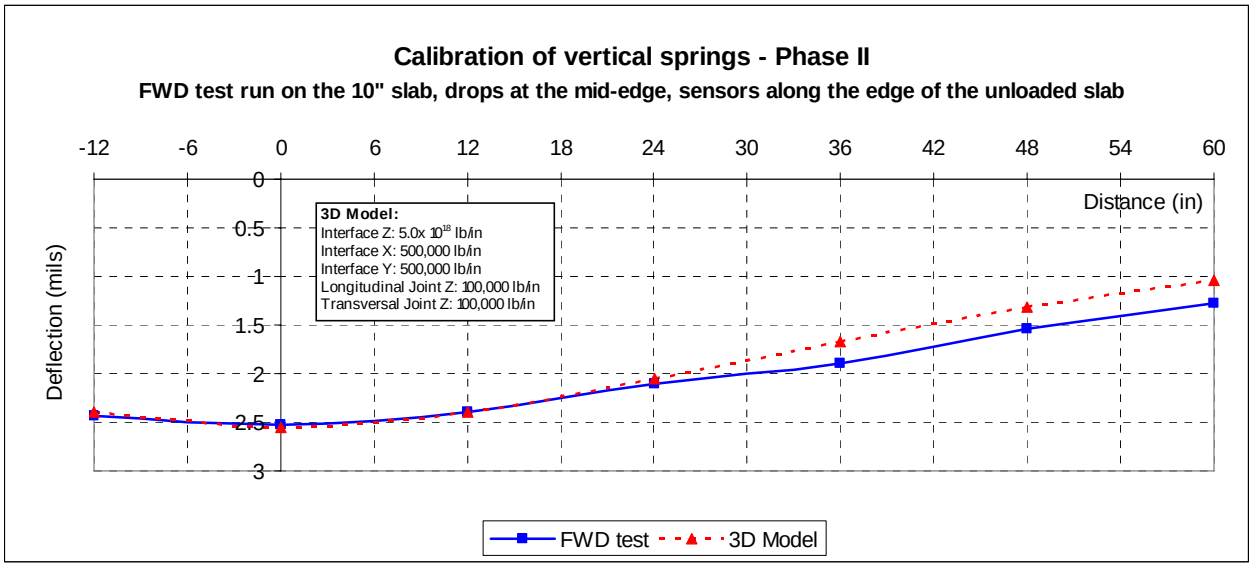

Figure 7.19. Matching of Deflection Basin Along the Edge of Unloaded Slab Caused by a 12-kip FWD Load Applied to the Mid-Edge of a 10" Slab in Phase II.

The horizontal springs (in the X and Y directions) modeling the horizontal load transfers at the interface were found to have no effect on the calculated deflections. It is to be noted that a value of 500,000 lb/in was used for the interface horizontal springs in the calculation of the FWD deflection basins, which are presented in Figures 7.10 through 7.19. If a different value of horizontal spring stiffness were used, the calculated FWD deflections would essentially be the same. However, it is to be pointed out that in the strain-based calibration process, which is presented in the next section, the horizontal springs at the interface were found to have significant effects on the load-induced strains, and thus need to be properly calibrated.

Similar to the cases in Phases I-a and I-b, a vertical spring stiffness of 100,000 lb/in appeared to work well in modeling the joint behavior of the composite pavement test sections in Phase II.

7.3 Strain-Based Calibration of Model Parameters

7.3.1 General Approach

The pavement parameters and spring stiffness values of the 3-D models for analysis of the composite pavement test sections were further calibrated by matching the computed strains caused by the HVS wheel loads to the strains measured by the strain gages. In the HVS experiment, the wheel load traveled at a speed of 8 mph (140 in/sec). In the analysis for the load-induced strains in the test sections, a static load was positioned in different locations along the wheel path to represent a moving load. The distances between the load positions were converted to time using this speed. The computed strains at a strain gage location under different load positions were then plotted on a time scale, and compared with the measured strain versus time plot.

Table 7.1 presents the elastic moduli and Poisson's ratios of the pavement materials of the test sections as determined from the deflection-based calibration procedure as presented in the previous section. A range of values was given for the elastic modulus of the AC since it varied with temperature. The lower and the upper values correspond to the elastic modulus of the AC at 25 and 5 °C, respectively.

Table 7.1. Elastic Modulus and Poisson's Ratio of the Pavement Materials Used in the 3-D Finite Element Model.

Material	Modulus of Elasticity (psi)	Poisson's Ratio
Subgrade	30,000	0.35
Base	160,000	0.35
Asphalt	300,000 – 1,400,000	0.35
Concrete	4,350,000	0.20

The elastic moduli of the concrete, base and subgrade materials as given in Table 7.1 were used in the 3-D models in computing the load-induced strains, while the elastic modulus of the AC was varied to match the analytical strains to the measured strains. The stiffness of the joint vertical spring modeling the load transfer at the joint was fixed at a value of 100,000 lb/in in the analysis.

7.3.2 Phase I-a

Table 7.2 shows the HVS loading periods for the 4-, 5- and 6-inch slabs when they were loaded with 12 kips in Phase I-a. While the 4- and 6-inch slabs were loaded mainly during the summer time, the 5-inch slabs were loaded in the winter time.

Table 7.2. HVS Loading Periods for Phase I-a.

Thickness	Joint Spacing	From	To
4”	6’ × 6’	07/11/04	10/03/04
5”	6’ × 6’	11/01/04	11/24/04
6”	6’ × 6’	05/23/05	05/26/05

Figures 7.20 through 7.26 show the comparison of the computed strains with the measured strains for various test sections and gage locations. The values of the pavement parameters used in the analyses are also given in these figures. It can be seen that the elastic modulus of the AC varied from 300,000 psi for the 4-inch slab (which was tested in the summer time) to 1,100,000 psi for the 5-inch slab (which was tested in the winter time).

It is to be pointed out that the intended vertical positions of the strain gages were used in the analysis. In Phase I-b and Phase II, when cores were taken to check the vertical positions of the strain gages, it was found that most of the strain gages had shifted a little bit during concrete

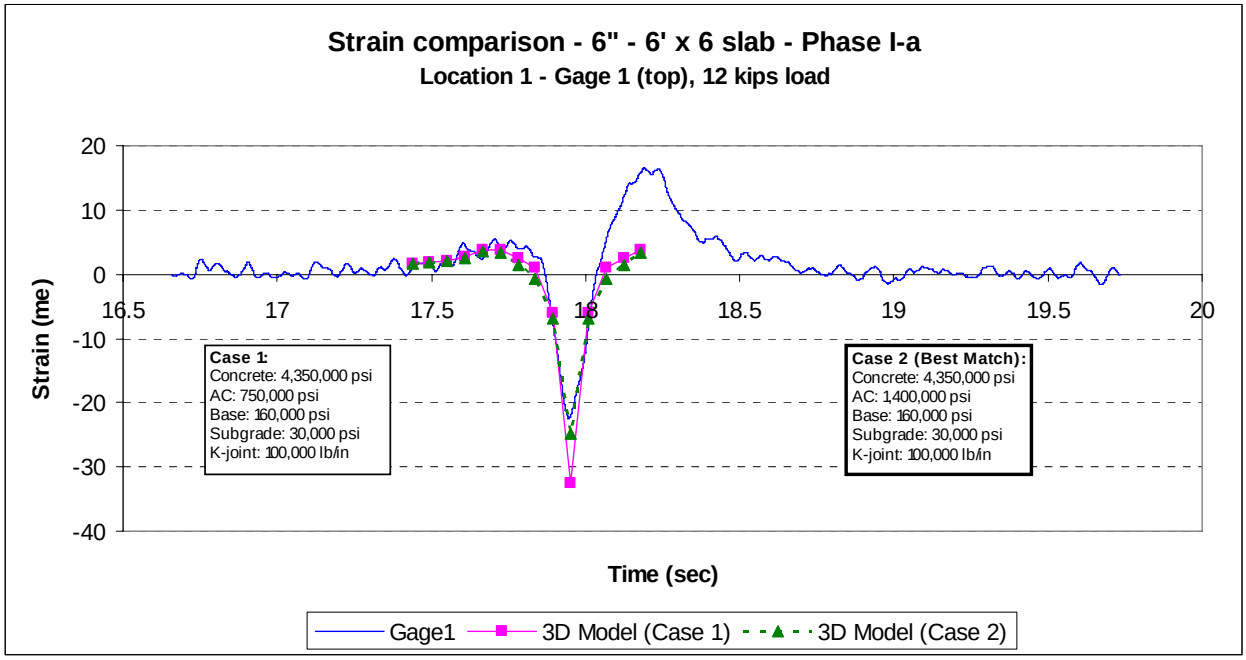

Figure 7.20. Strain Comparison at Gage 1 in the 6" Slab in Phase I-a.

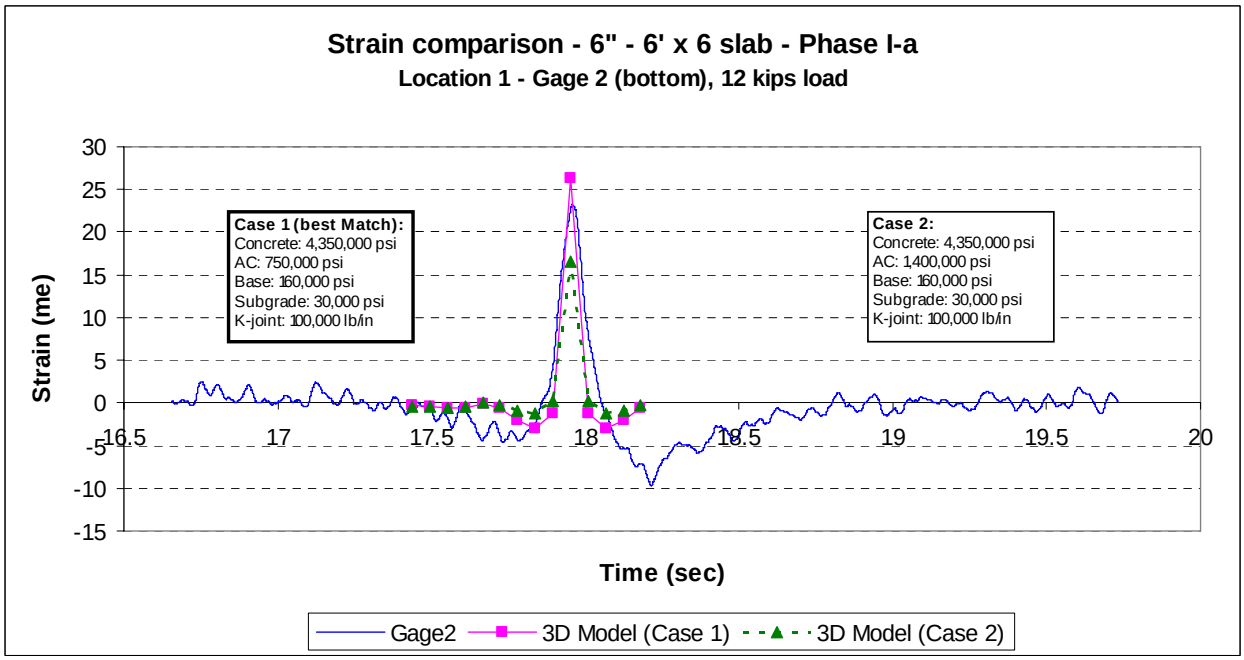

Figure 7.21. Strain Comparison at Gage 2 in the 6" Slab in Phase I-a.

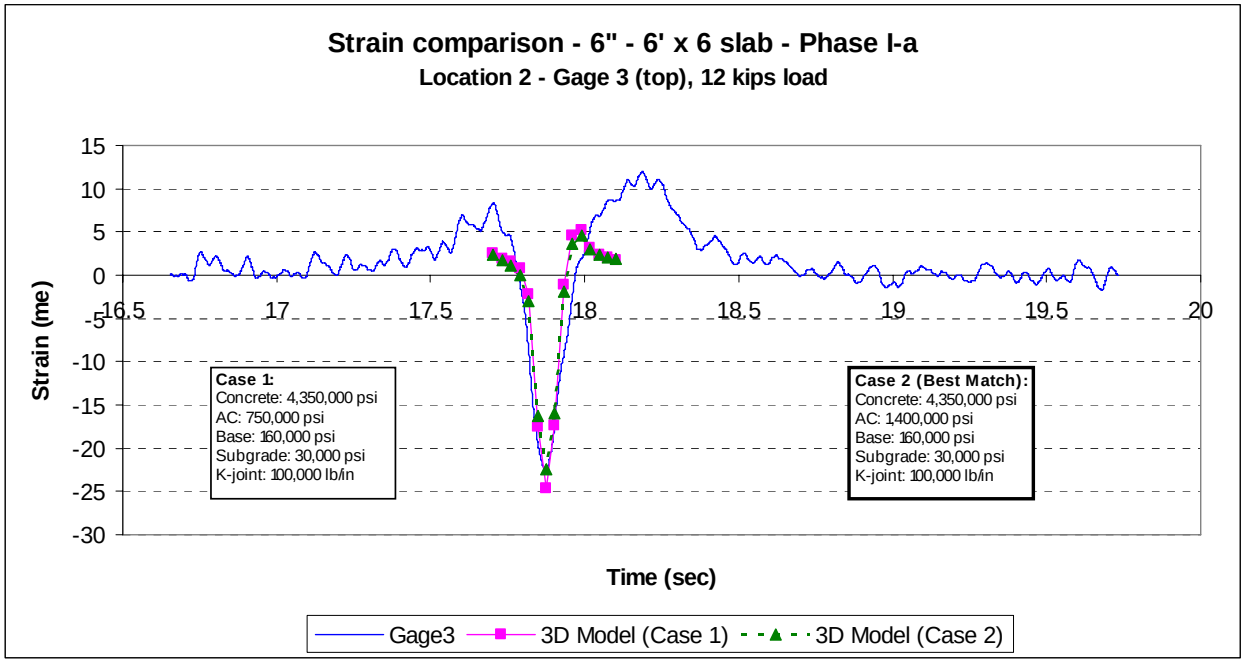

Figure 7.22. Strain Comparison at Gage 3 in the 6" Slab in Phase I-a.

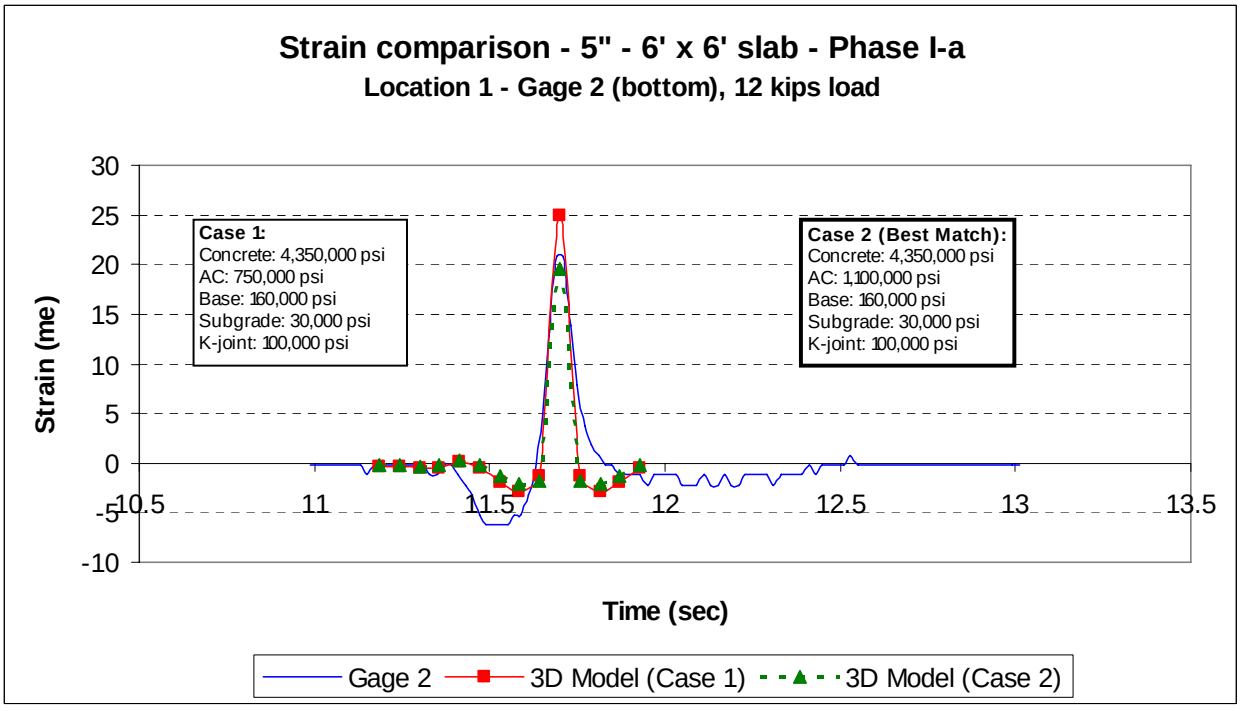

Figure 7.23. Strain Comparison at Gage 2 in the 5" Slab in Phase I-a.

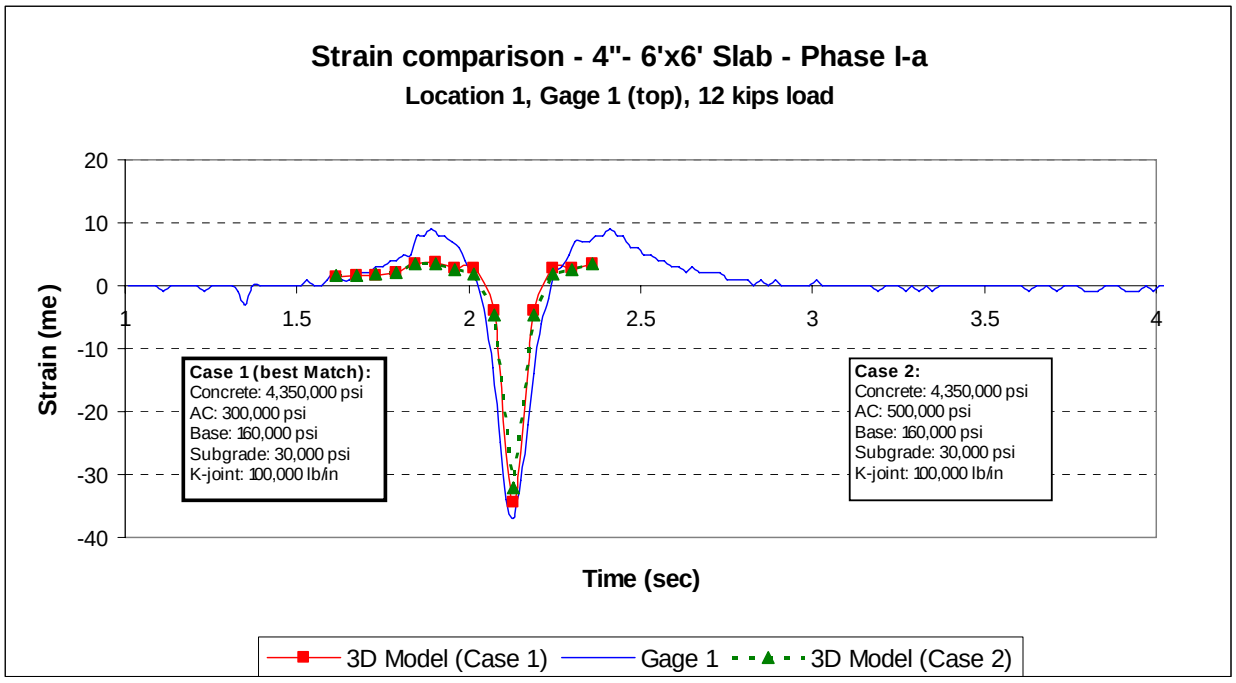

Figure 7.24. Strain Comparison at Gage 1 in the 4" Slab in Phase I-a.

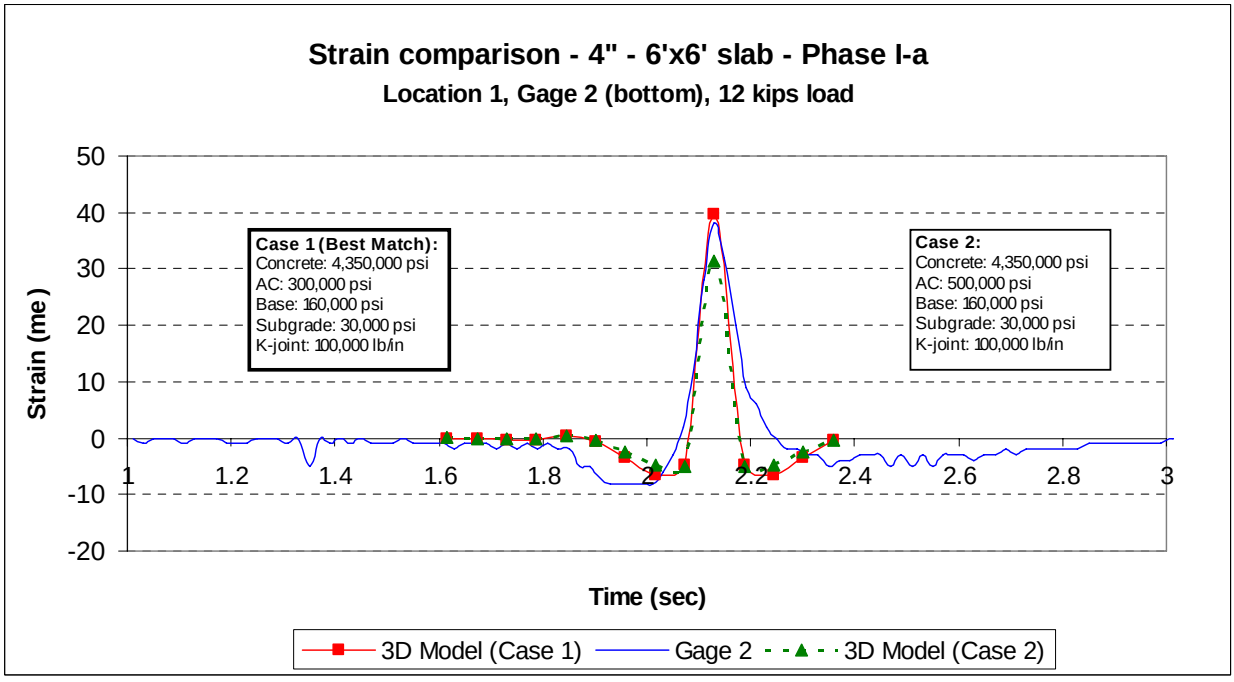

Figure 7.25. Strain Comparison at Gage 2 in the 4" Slab in Phase I-a.

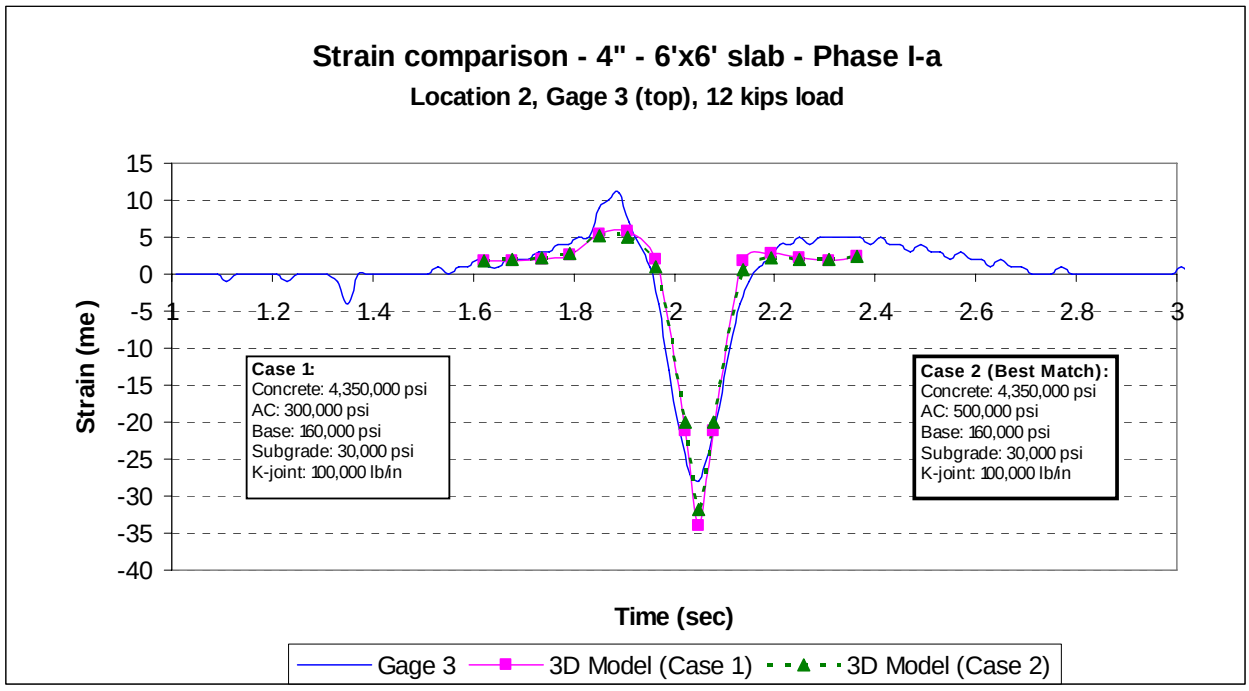

Figure 7.26. Strain Comparison at Gage 3 in the 4" Slab in Phase I-a.

placement. Unfortunately, cores were not able to be taken to check the positions of the strain gages in the test slabs in Phase I-a. The possible shifting of the positions of the strain gages could explain why some of the computed strains did not match too well with the measured strains. The differences were more substantial for thinner slabs, as a small variation in vertical position in the slab could result in large percentage change in strain.

Even though the model could replicate the measured peak strain, the strain reversal phenomenon was not completely replicated by the model. It seems that the magnitude of the strain reversal is affected also by the dynamic behavior of the slab under the passing of the wheel load. The analytical model computes the strains due to static loads applied at different locations, and does not analyze the possible dynamic effects. The analytical strain versus time plots were all symmetrical around the point of maximum strain, while the measured strains plots were not entirely symmetrical. The measured strains were observed to have higher reversal strains when

the wheel load moved away from the gage location as compared with the strains when the wheel approached the location.

7.3.3 Phase I-b

The strain-based calibration of the model parameters in Phase I-b was undertaken in the same way as in Phase I-a, except that in this case, some vertical positions of the gages were verified through cores taken at the locations of the strain gages after HVS testing. A total of 7 gage positions were verified in this phase. When the exact vertical position of a strain gage is known, then more attempts to exactly match the strains can be done, since the uncertainties in this variable are now excluded. In the case where the exact vertical position of a gage was known, the gage position was corrected in the analytical model and the strain in the right place was calculated. In the cases where the positions of the gages were not verified, the original intended positions of the gages were used in the analysis.

Table 7.3 shows the verified vertical position of the gages for this phase. In this table, the distances from the top of the concrete slab are given.

Table 7.3. Verified Depths of Strain Gages in Phase I-b.

	Intended Position	**Location 1 (mid-edge)**			**Location 2 (corner)**		
		6”	**5”**	**4”**	**6”**	**5”**	**4”**
Gage Top	1” from top	1.25	-	0.75”	N/A	N/A	N/A
Gage Bottom	0.5” from bottom	5.5”	-	3.2”	5.3”	4.3”	3.3”

HVS loading for all the test sections in Phase I-b were run at the beginning of the summer of 2005 as shown in Table 7.4. Thus, the values of the elastic modulus of the AC layer were expected to be lower than those for the winter time.

Table 7.4. HVS Loading Periods for Phase I-b.

Thickness	Joint Spacing	From	To
4”	4’ × 4’	06/09/05	06/12/05
5”	4’ × 4’	06/14/05	06/17/05
6”	4’ × 4’	06/20/05	06/22/05

Figures 7.27 to 7.32 show the comparison of the computed strains with the measured strains for various test sections and gage locations, for the cases where the exact gage locations are known. The exact vertical positions of the gages and the values of the pavement parameters used in the analyses are also given in these figures. It can be seen that the analytical strains match well with the measured strain at their maximum values. The range of elastic modulus of the AC was from 300,000 to 700,000 psi.

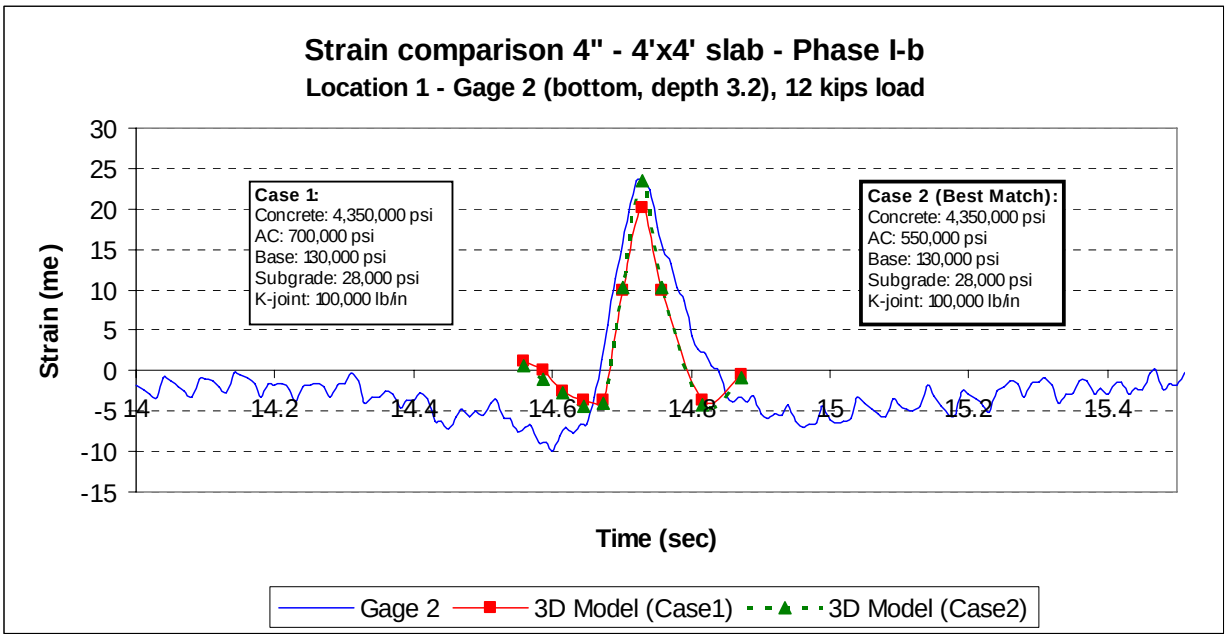

Figure 7.27. Strain Comparison at Gage 2 in the 4-inch Slab in Phase I-b.

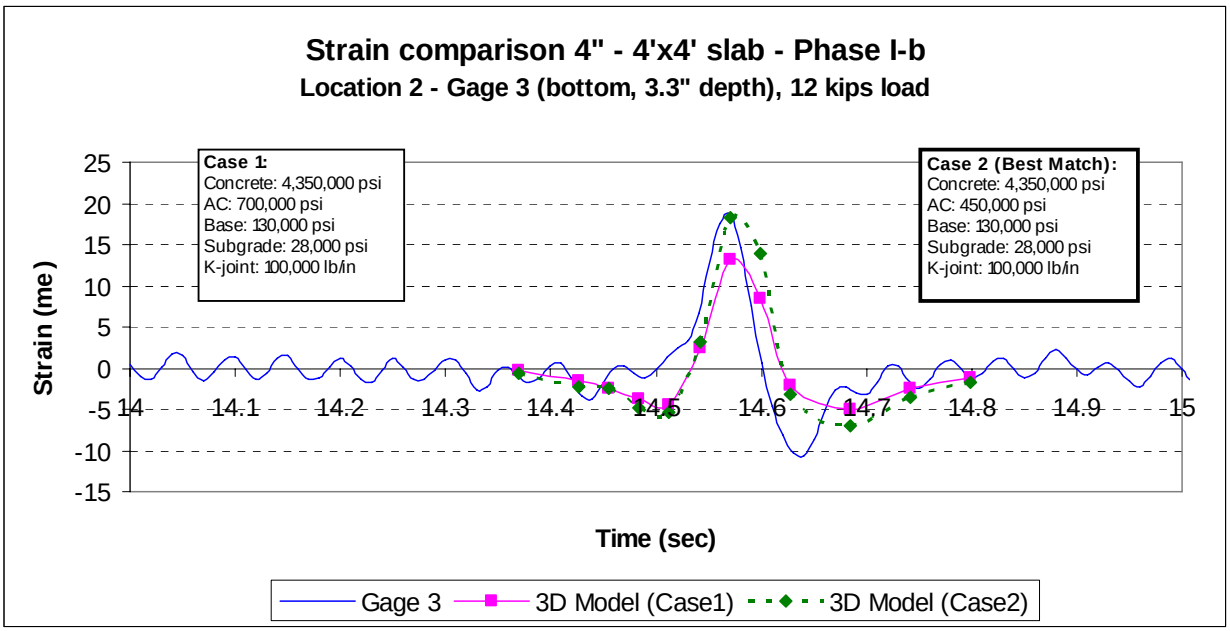

Figure 7.28. Strain Comparison at Gage 3 in the 4-inch Slab in Phase I-b.

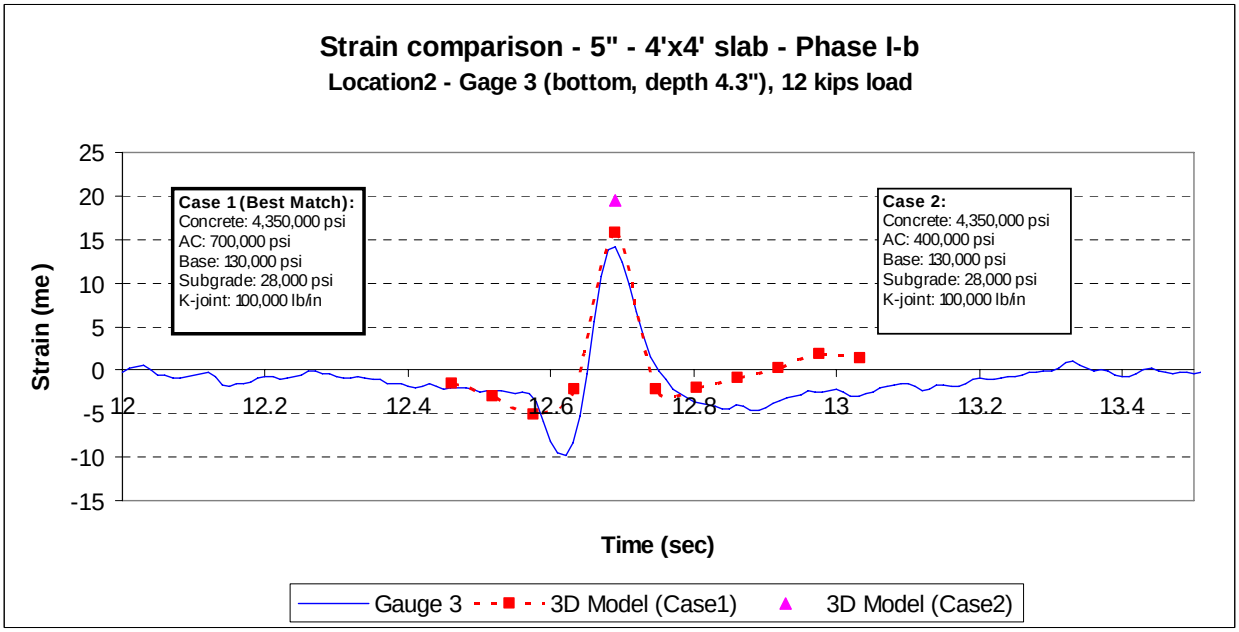

Figure 7.29. Strain Comparison at Gage 3 in the 5-inch Slab in Phase I-b.

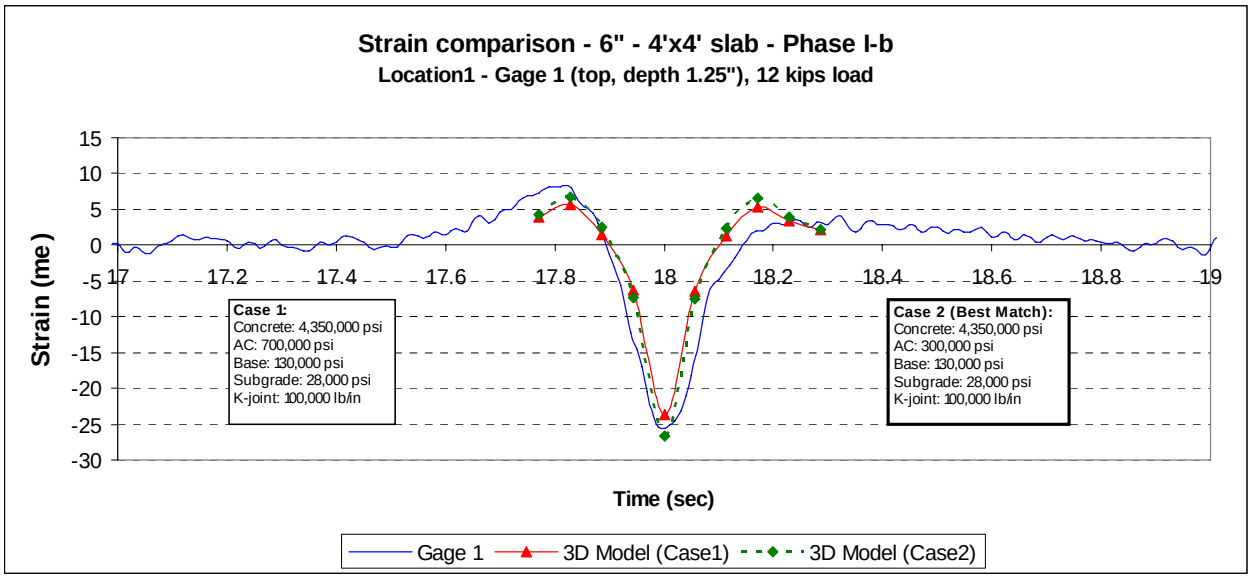

Figure 7.30. Strain Comparison at Gage 1 in the 6-inch Slab in Phase I-b.

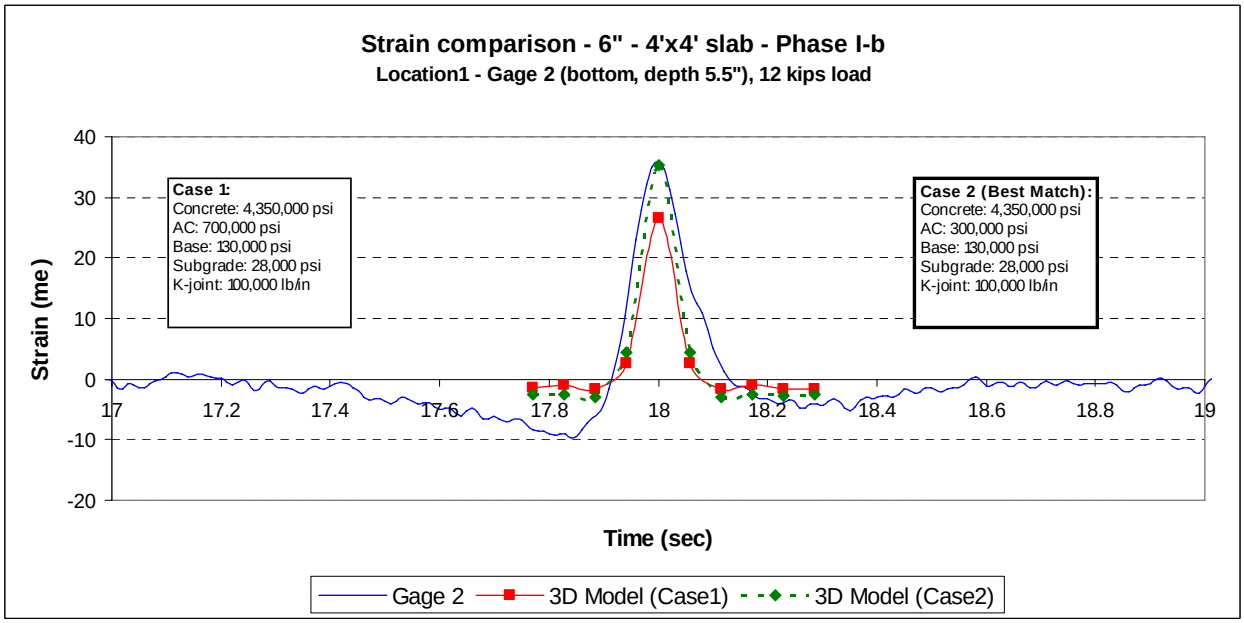

Figure 7.31. Strain Comparison at Gage 2 in the 6-inch Slab in Phase I-b.

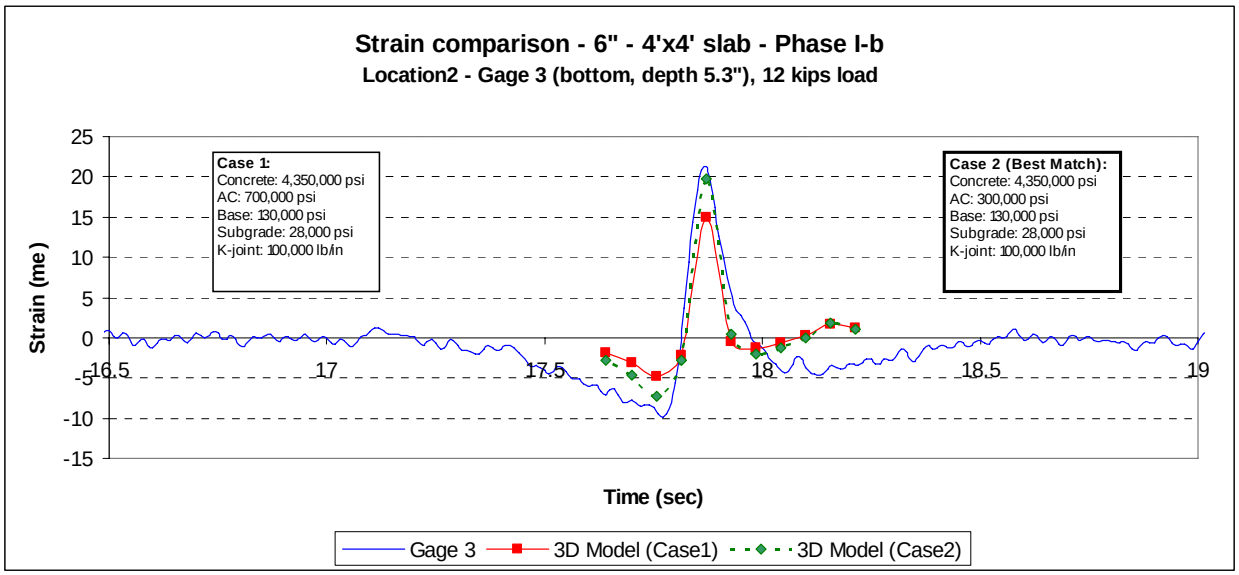

Figure 7.32. Strain Comparison at Gage 3 in the 6-inch Slab in Phase I-b.

Figures 7.33 and 7.34 show the comparison of the computed strains with the measured strains for two gages where the exact gage locations were not known. These two gages were located at the same horizontal location in the same slab, with one gage at the top and the other at the bottom. Because the exact positions of the gages were not known, the figures also include the cases if the gages had been displaced up by 0.2". These figures show examples of the effects of the vertical position of the gage on the load-induced strains at the gage. For the case of the gage at the top (as shown in Figure 7.33), the best match was achieved with an elastic modulus of the AC layer of 400,000 psi, whereas for the case of the gage at the bottom (as shown in Figure 7.34), the best match was achieved with a value of 700,000 psi. When a different vertical position of the gage at the top was used, an exact match in maximum strain was obtained, as shown in Figure 7.33. However, the consideration of a different vertical position of the gage at the bottom made the match worse, as shown in Figure 7.34. That means that the gage at the bottom was probably displaced down rather than up.

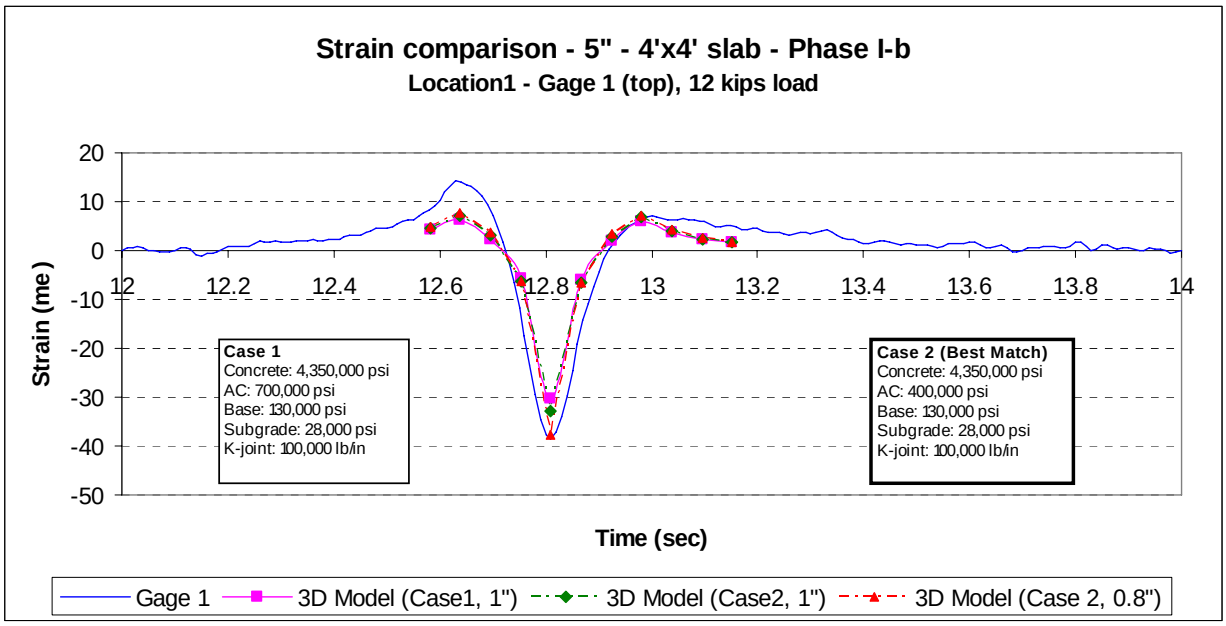

Figure 7.33. Strain Comparison at Gage 1 in the 5-inch Slab in Phase I-b.

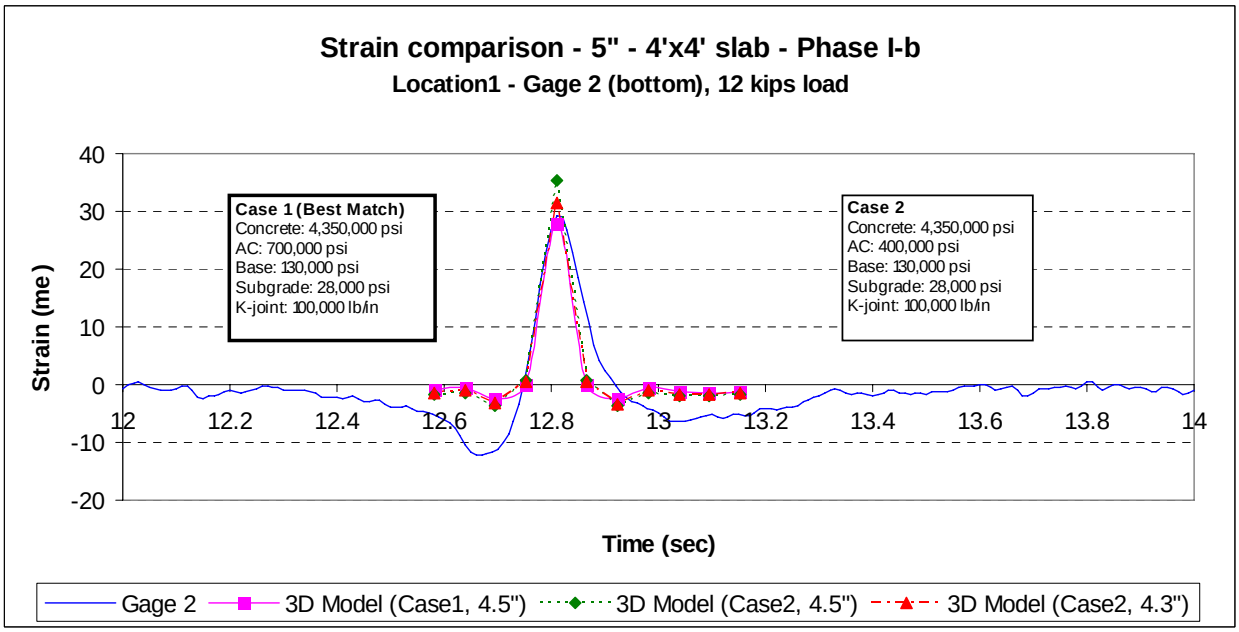

Figure 7.34. Strain Comparison at Gage 2 in the 5-inch Slab in Phase I-b.

7.3.4 Phase II

The strain-based calibration of the model parameters in Phase II was performed in a similar manner as in Phases I-a and I-b, except that in this case the springs modeling the partial bonding condition of the concrete-asphalt interface had also to be calibrated. Similar to the case in Phase I-b, the vertical positions of a few strain gages were verified through cores taken at the locations of the strain gages after HVS testing. In the case where the exact vertical position of a gage was known, the verified gage position was used in the analytical model to calculate the strain at the gage location. In the cases where the positions of the gages were not verified, the original intended positions of the gages were used in the analysis.

Table 7.5 shows the verified vertical positions of the gages for Phase II. In this table, the distances from the top of the concrete slab are given.

Table 7.5. Verified Depths of Strain Gages in Phase II.

	Intended Position	Location 1 (mid-edge)			Location 2 (corner)		
		6”	8”	10”	6”	8”	10”
Gage Top	1” (from top)	0.7”	0.8”	1.0”	-	0.87”	1.2”
Gage Bottom	1” (from bottom)	5.0”	6.65”	-	-	7.0”	9.0”

HVS loading for all the slabs were run during the winter of 2005-2006, as shown in Table 7.6. Thus, the elastic modulus of the AC layer were expected to be higher than that in the summer time.

Table 7.6. HVS Loading Periods for Phase II.

Thickness	Joint Spacing	From	To
6”	6’ × 6’	01/30/06	02/15/06
8”	6’ × 6’	01/09/06	01/28/06
10”	6’ × 6’	11/14/05	12/16/05

Figures 7.35 through 7.52 show the comparison of the computed strains with the measured strains for various test sections and gage locations. For the cases where the gage positions have been verified, the vertical positions of the gages are also shown on the figures. It can be seen that in general, the analytical strains match well with the measured strain at their maximum values. The calibrated model parameters for the three test sections in Phase II are presented in the next section, along with those for the test sections in Phases I-a and I-b.

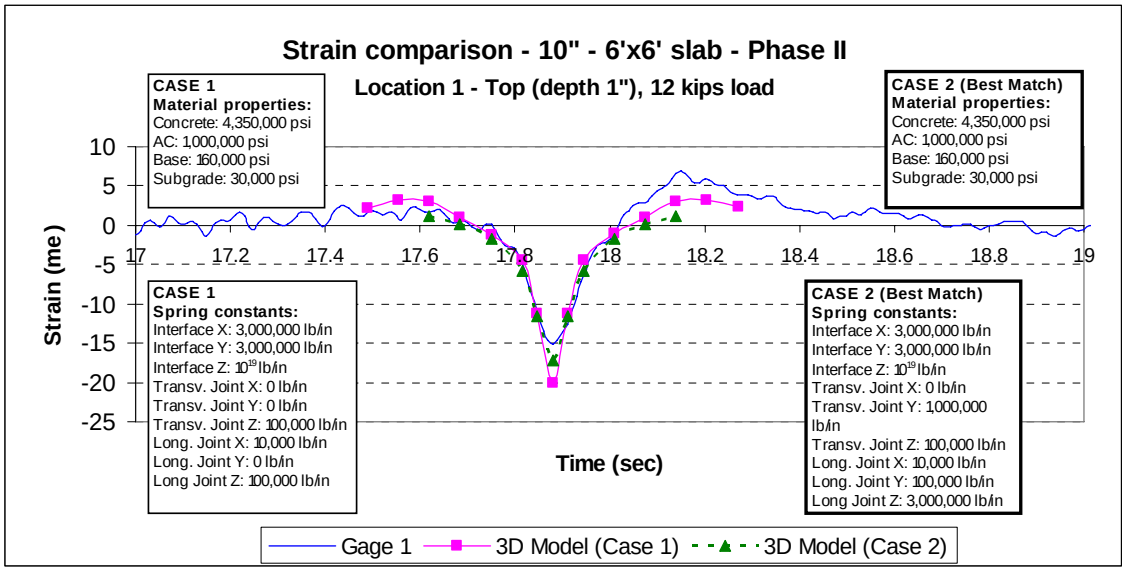

Figure 7.35. Strain Comparison at Top of Location 1 (mid edge) of the 10-inch Slab in Phase II.

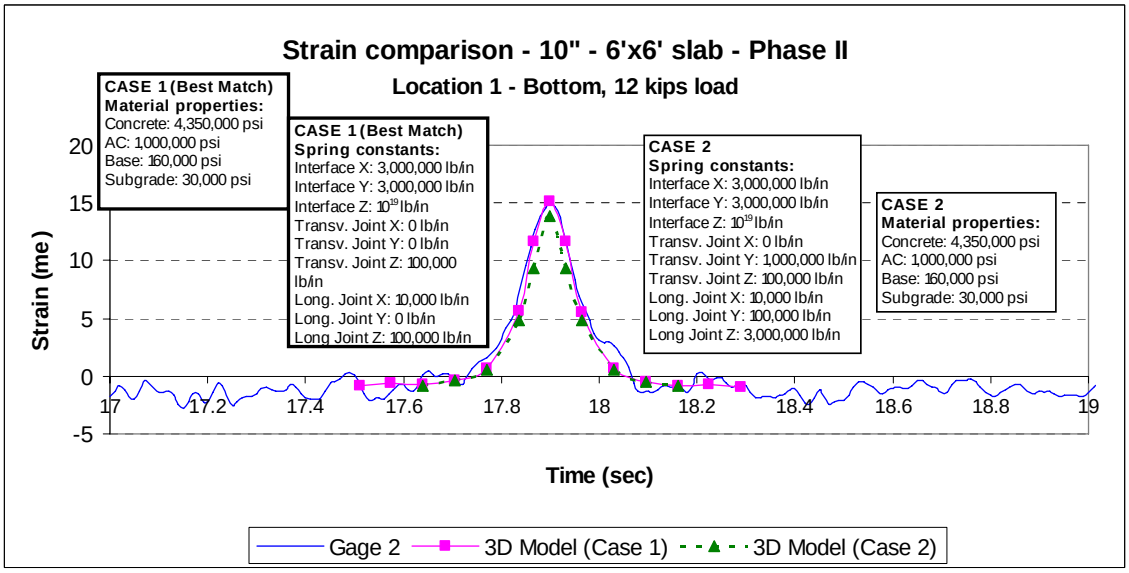

Figure 7.36. Strain Comparison at Bottom of Location 1 (mid edge) of the 10-inch Slab in Phase II.

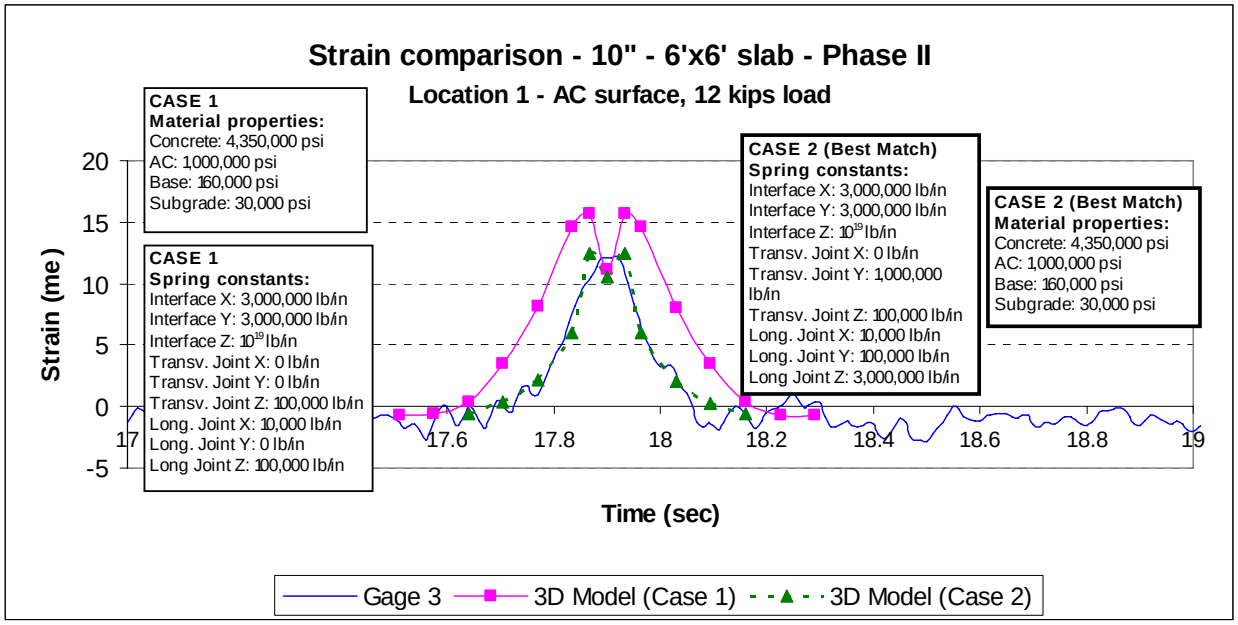

Figure 7.37. Strain Comparison on the Surface of the AC Layer at Location 1 (mid edge) of the 10-inch Slab in Phase II.

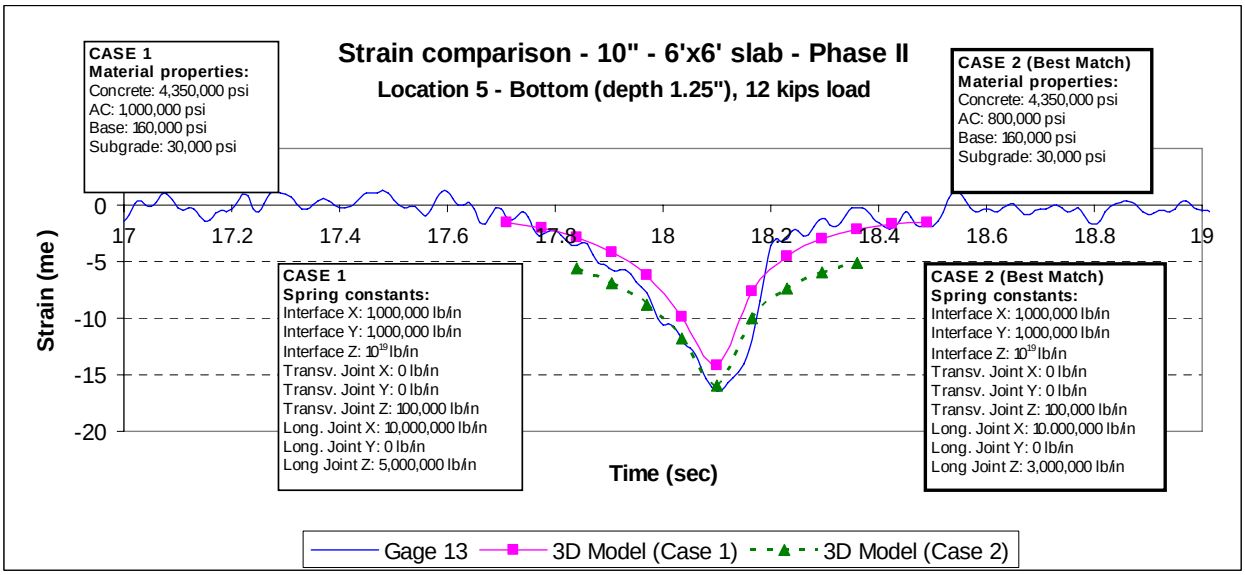

Figure 7.38. Strain Comparison at Top of Location 5 (slab corner) of the 10-inch Slab in Phase II.

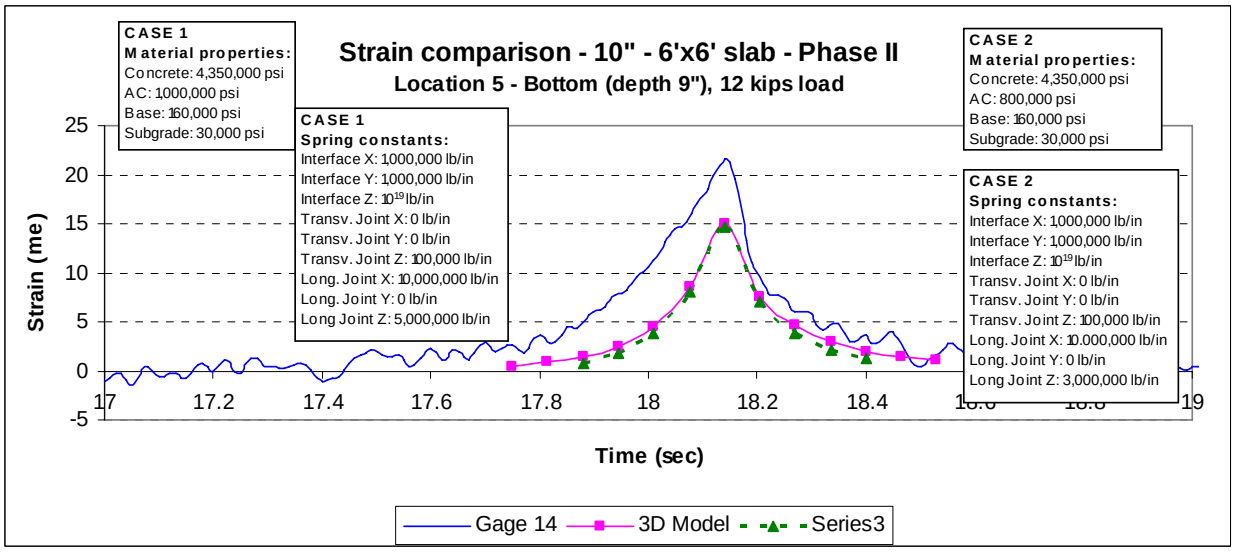

Figure 7.39. Strain Comparison at Bottom of Location 5 (slab corner) of the 10-inch Slab in Phase II.

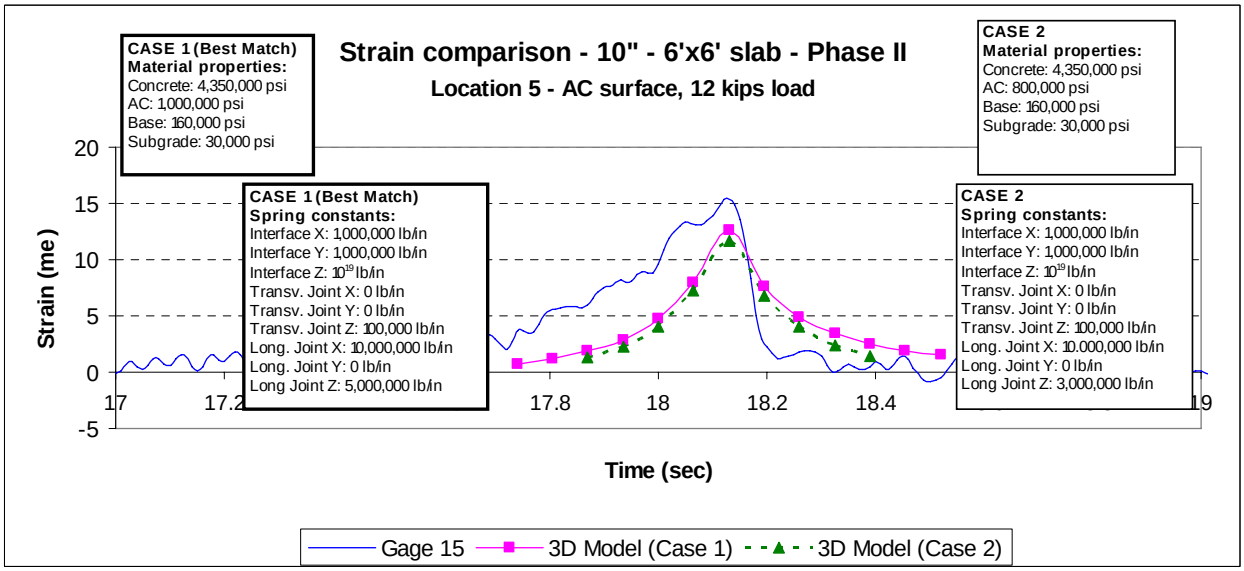

Figure 7.40. Strain Comparison on the Surface of the AC Layer at Location 5 (slab corner) of the 10-inch Slab in Phase II.

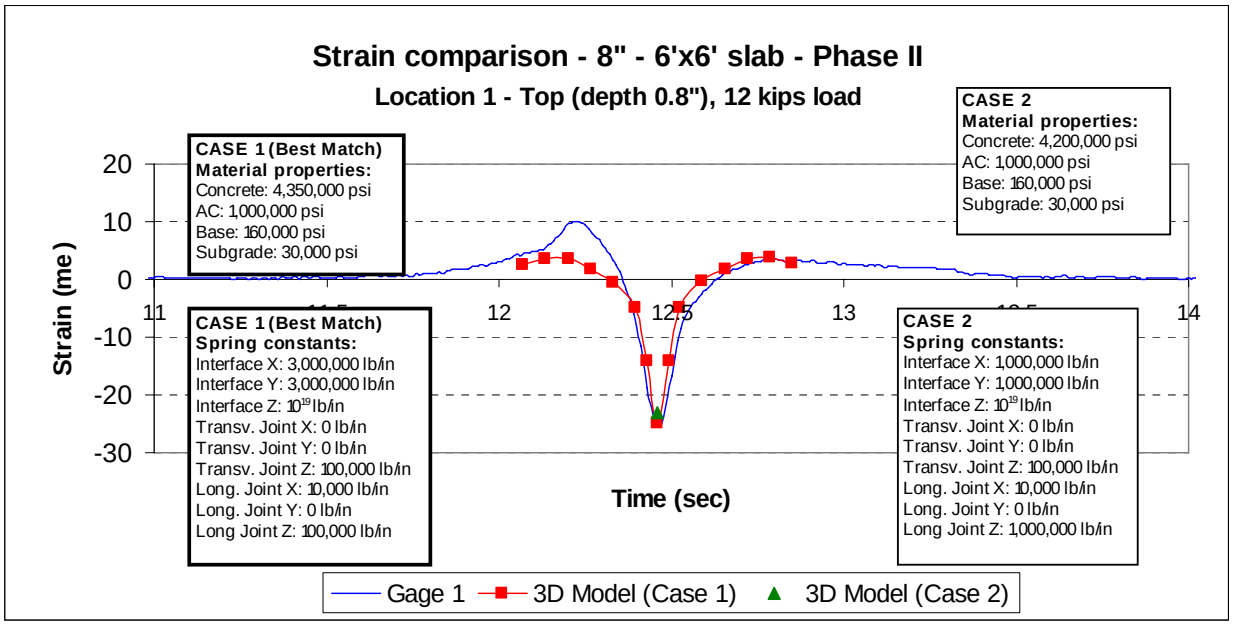

Figure 7.41. Strain Comparison at Top of Location 1 (mid edge) of the 8-inch Slab in Phase II.

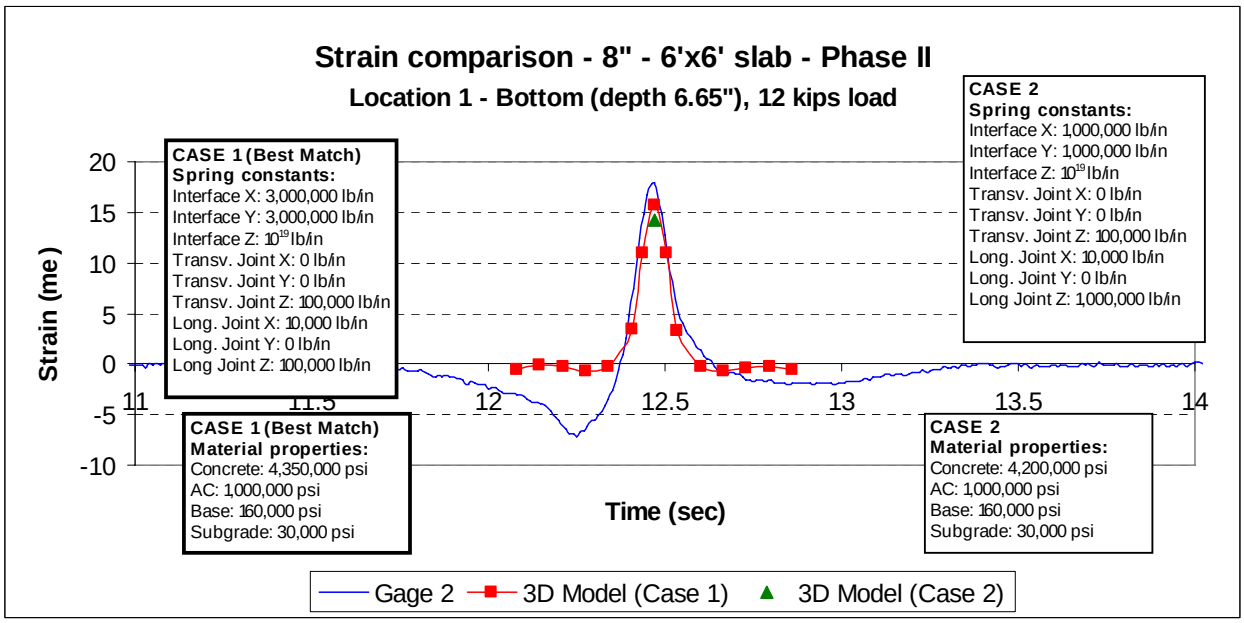

Figure 7.42. Strain Comparison at Bottom of Location 1 (mid edge) of the 8-inch Slab in Phase II.

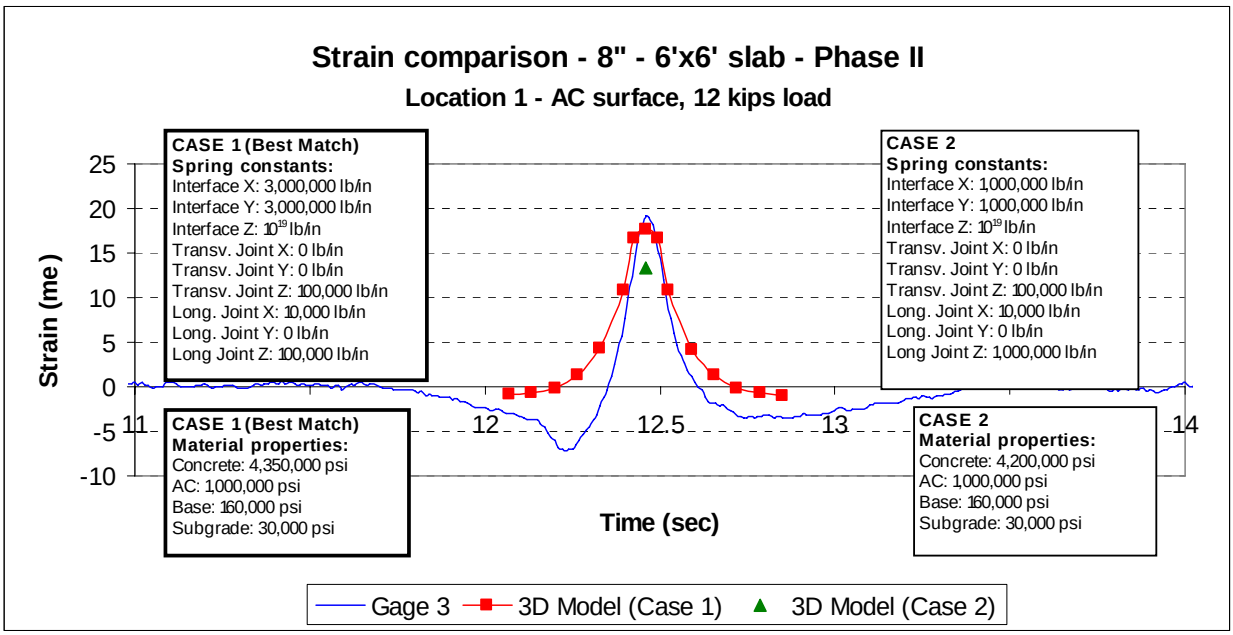

Figure 7.43. Strain Comparison on the Surface of the AC Layer at Location 1 (mid edge) of the 8-inch Slab in Phase II.

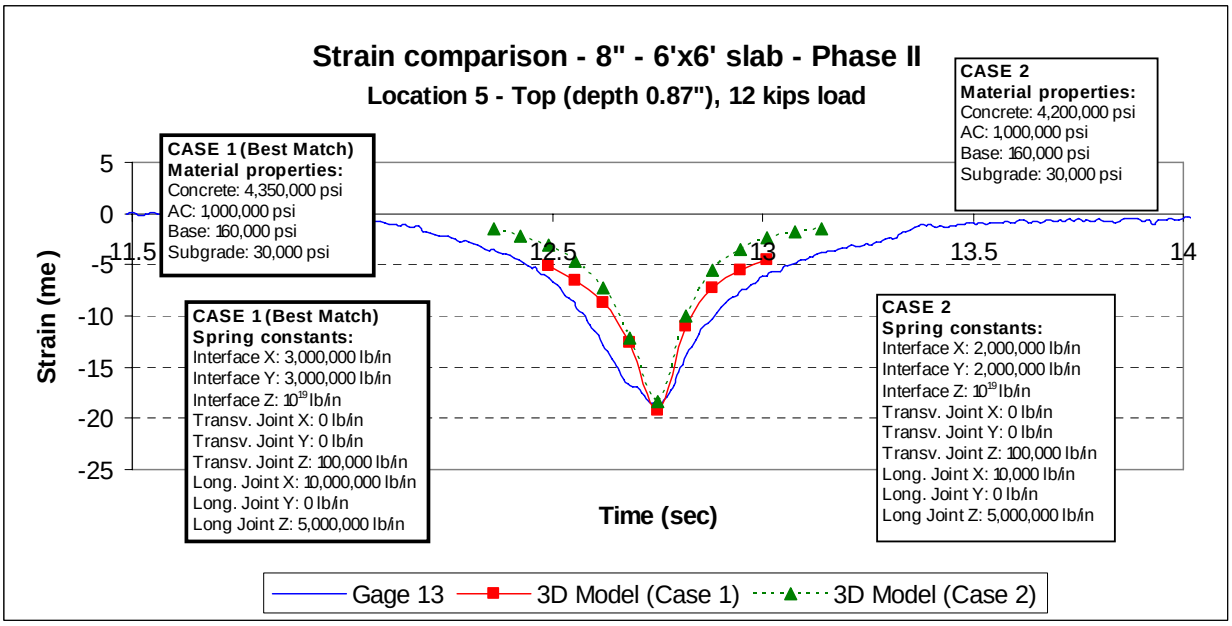

Figure 7.44. Strain Comparison at Top of Location 5 (slab corner) of the 8-inch Slab in Phase II.

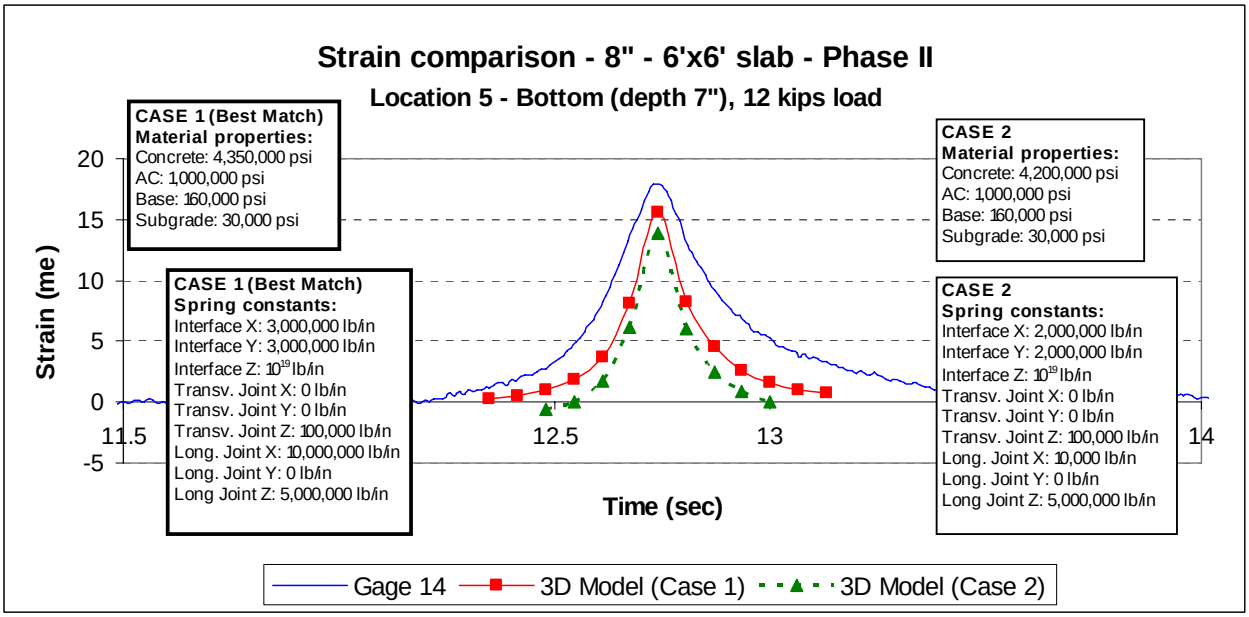

Figure 7.45. Strain Comparison at Bottom of Location 5 (slab corner) of the 8-inch Slab in Phase II.

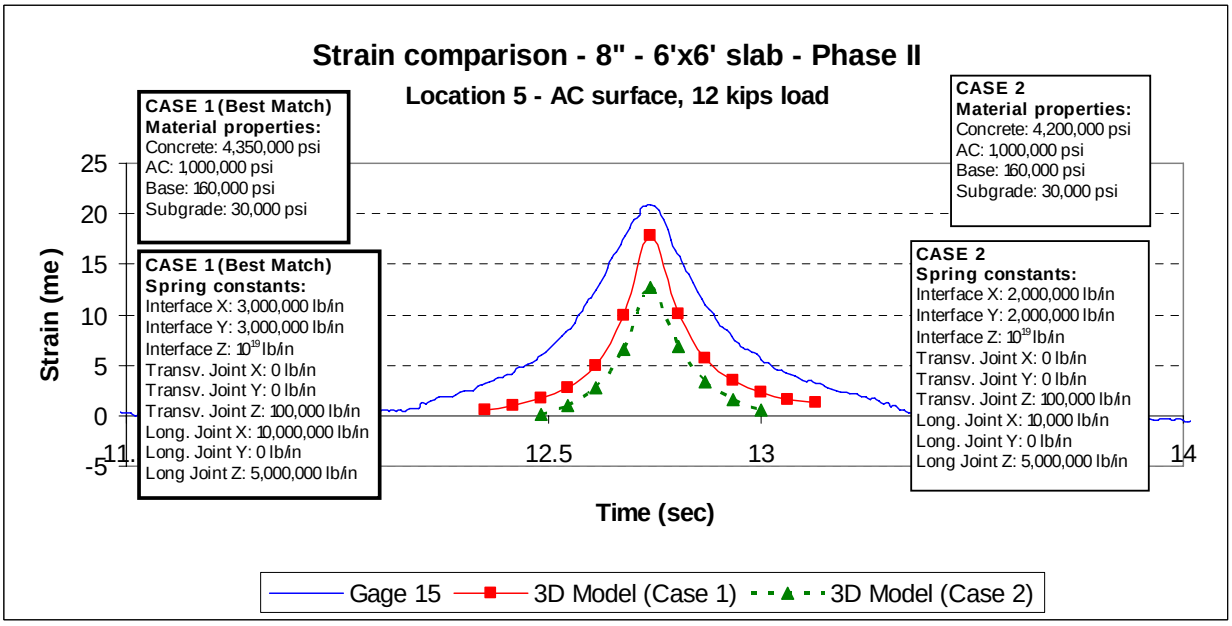

Figure 7.46. Strain Comparison on the Surface of the AC Layer at Location 5 (slab corner) of the 8-inch Slab in Phase II.

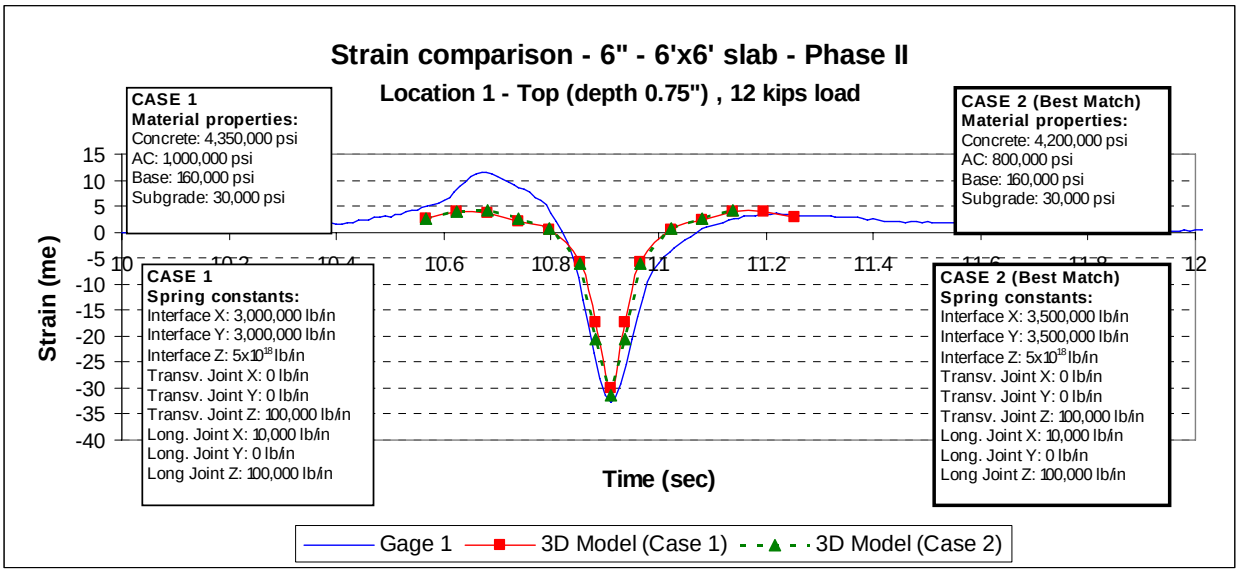

Figure 7.47. Strain Comparison at Top of Location 1 (mid edge) of the 6-inch Slab in Phase II.

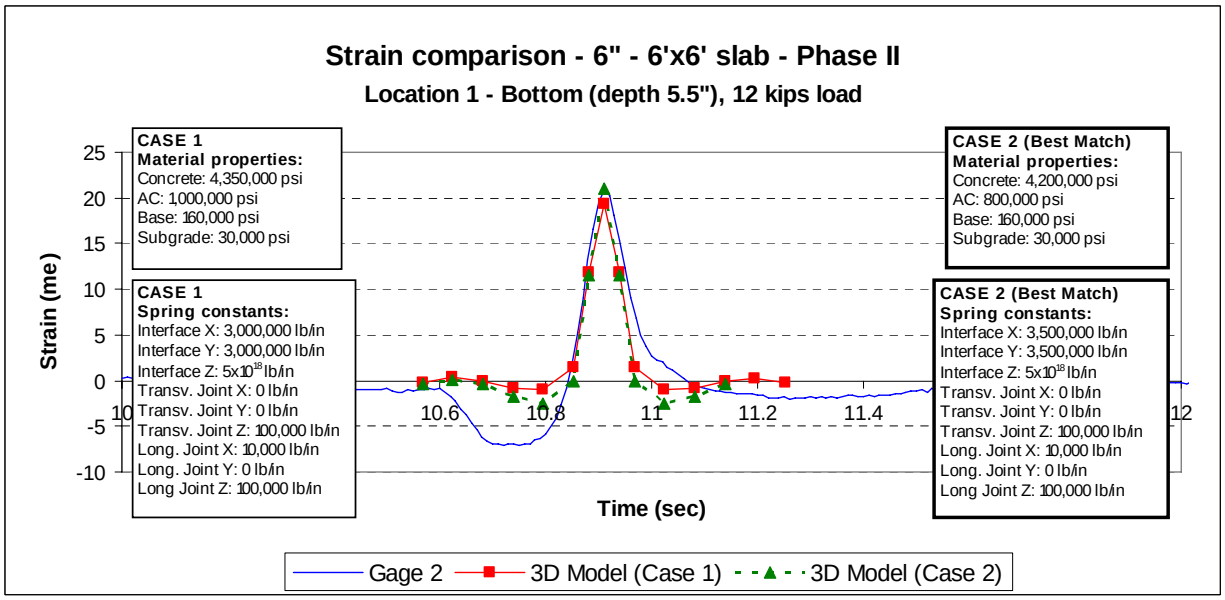

Figure 7.48. Strain Comparison at Bottom of Location 1 (mid edge) of the 6-inch Slab in Phase II.

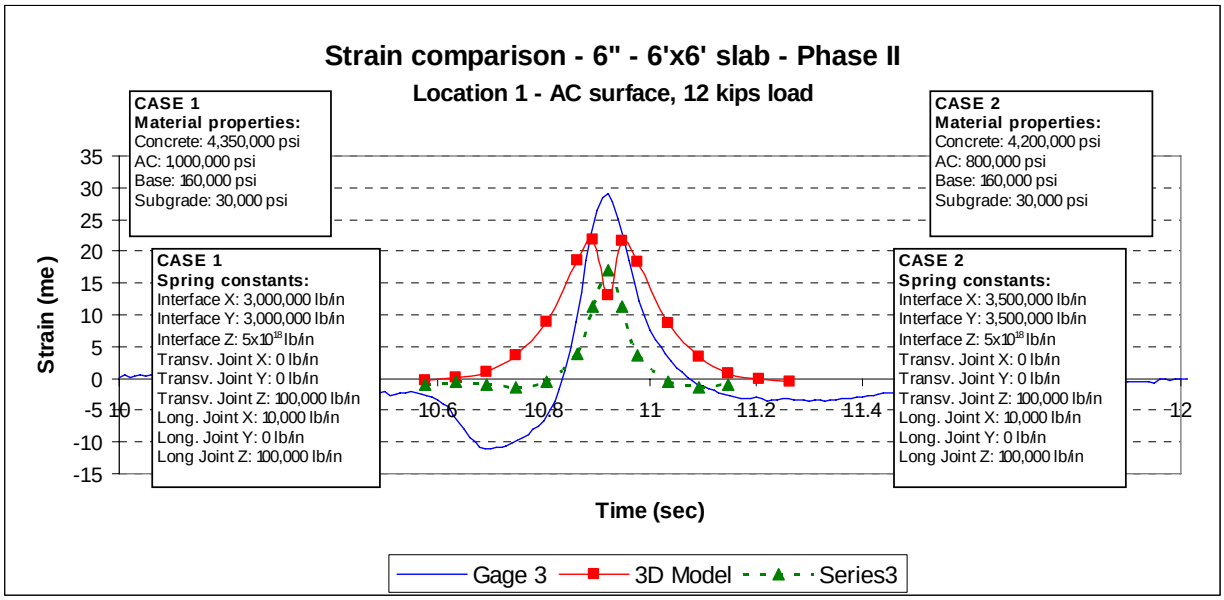

Figure 7.49. Strain Comparison on the Surface of the AC Layer at Location 1 (mid edge) of the 6-inch Slab in Phase II.

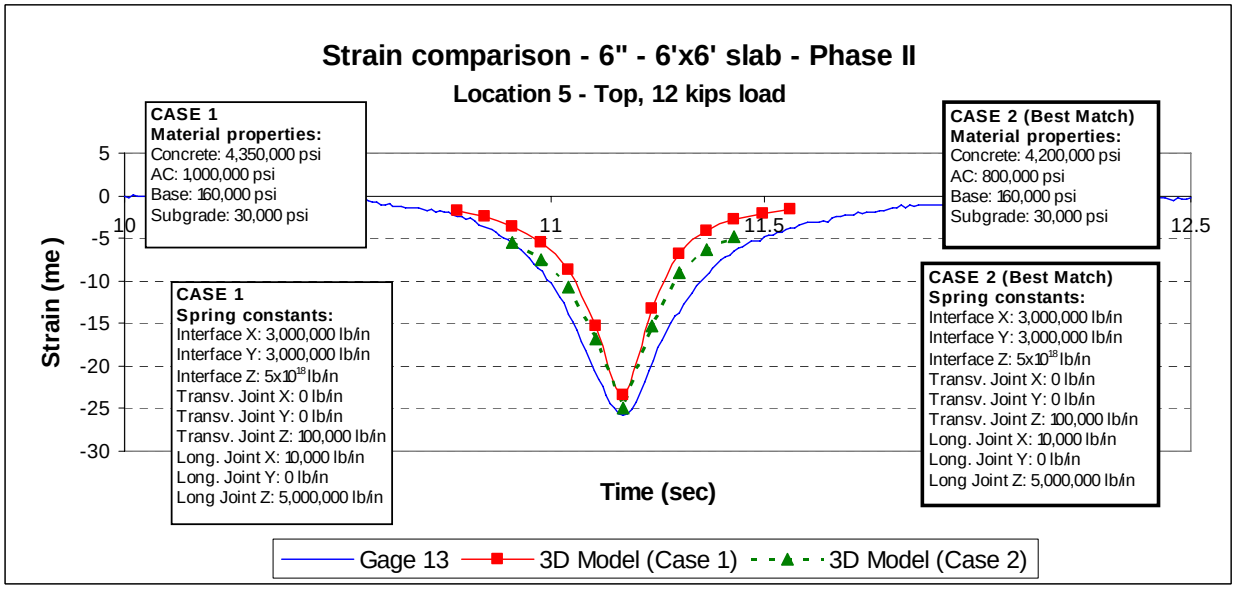

Figure 7.50. Strain Comparison at Top of Location 5 (slab corner) of the 6-inch Slab in Phase II.

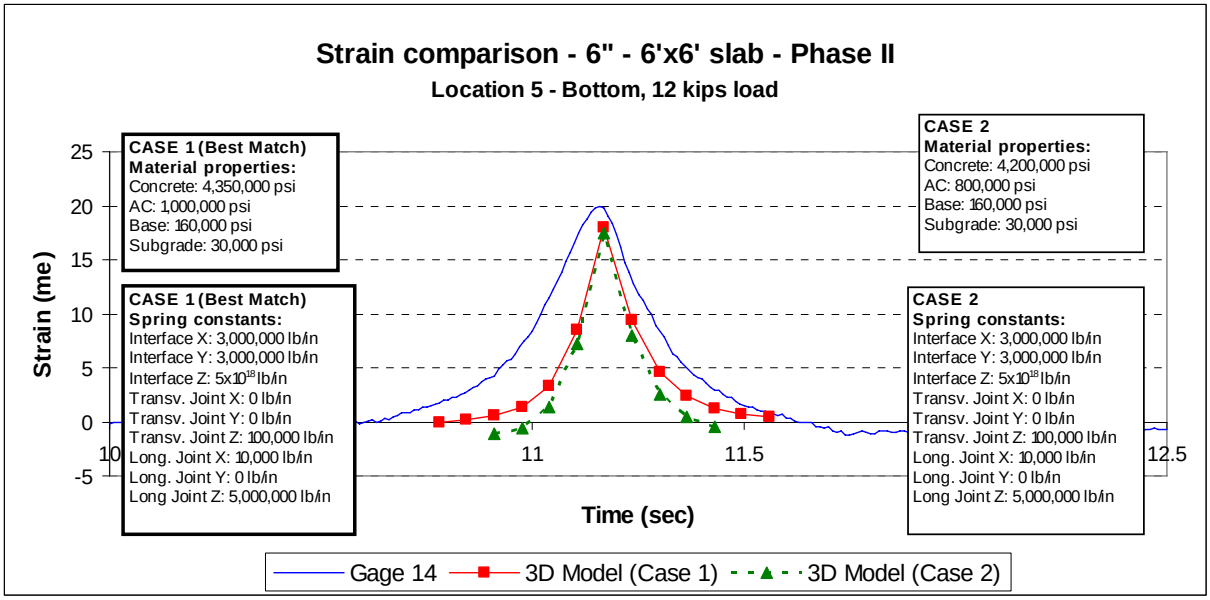

Figure 7.51. Strain Comparison at Bottom of Location 5 (slab corner) of the 6-inch Slab in Phase II.

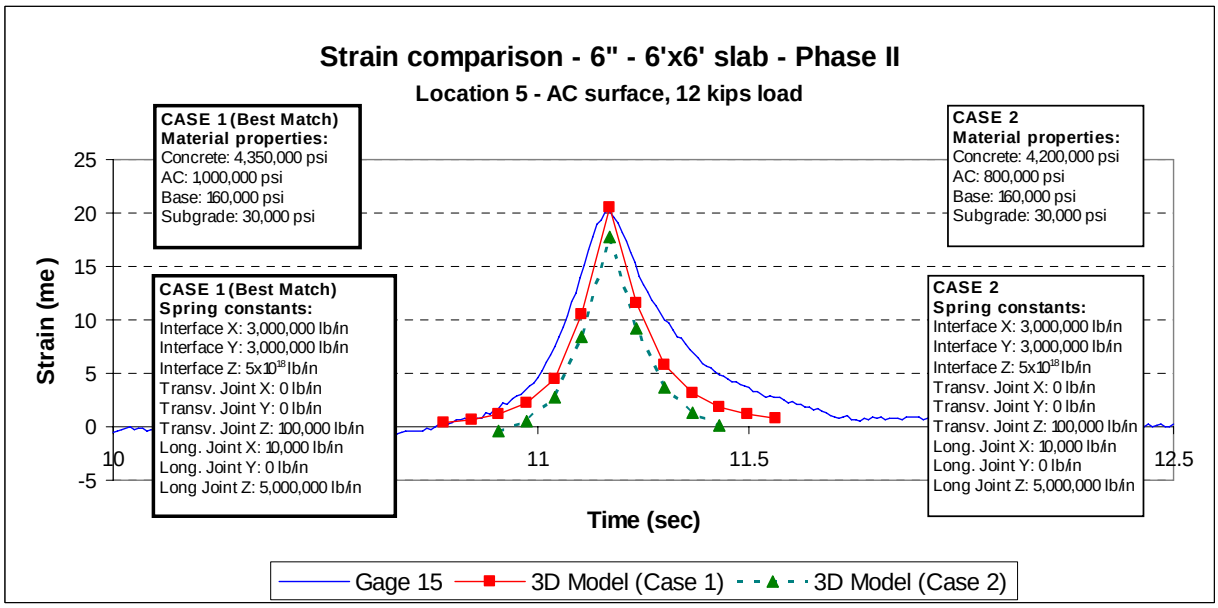

Figure 7.52. Strain Comparison on the Surface of the AC Layer at Location 5 (slab corner) of the 6-inch Slab in Phase II.

From the results of the calibration process, it can be observed that the values of the interface horizontal springs modeling the concrete-asphalt interface were consistently higher at the mid-edge than at the slab corners. This indicates that there was less interface bond at the slab

corner than at the slab edge. The values of these springs also varied from one test slab to another, indicating the non-uniformity of the partial bond condition.

7.4 Summary of Calibration Results

The best estimated model parameters of the 3-D model for all the test sections in this study, based on the results of the deflection-based and strain-based calibration, are summarized in Table 7.7. It is to be pointed out that these model parameters are only applicable to the conditions at the time of the HVS loading when the strain data were taken. The variation in the elastic modulus of the AC layer from one test section to another, or within the same test section was due to the different temperatures at the time of the tests. For the test sections in Phase II, the stiffness values of the horizontal springs modeling the interface can be observed to decrease as the slab thickness increases from 6 inches to 10 inches. For each test section, the range of stiffness values for the joint and interface horizontal springs are given. For the joint horizontal springs, the higher values generally represent the condition at the slab corners, while the lower values represent the condition at the edge of the joints. Conversely, for the interface horizontal springs, the higher values generally represent the condition at the edge of the joints, while the lower values represent the condition at the slab corners.

Table 7.7. Summary of the Best Estimated Parameters of the 3-D Model for All Test Sections in This Study.

		Phase I-a			Phase I-b			Phase II		
		4”	5”	6”	4”	5”	6”	6”	8”	10”
Material Elastic Moduli (ksi)	Concrete	4,350	4,350	4,350	4,350	4,350	4,350	4,200-4,350	4,350	4,350
	AC Layer	300-500	750-1,000	750-1,400	550-700	400-700	300-700	800-1,000	1,000	800-1,000
	Base	160	160	160	130	130	130	160	160	160
	Subgrade	30	30	30	28	28	28	30	30	30
Spring Constants (lb/in 106)	Interface X							3-3.5	2-3	1-3
	Interface Y							3-3.5	2-3	1-3
	Interface Z							5x1012	1013	1013
	Trans. Joint X	-	-	-	-	-	-	-	-	-
	Trans. Joint Y	-	-	-	-	-	-	0-0.1	0	1-0
	Trans. Joint Z	0.1	0.1	0.1	0.1	0.1	0.1	0.1	0.1-1	0.1
	Long. Joint X	-	-	-	-	-	-	0.01-1	0.01-10	0.01-1
	Long. Joint Y	-	-	-	-	-	-	0	0	0-0.1
	Long. Joint Z	0.1	0.1	0.1	0.1	0.1	0.1	0.1	0.1-5	3

CHAPTER 8
EVALUATION OF POTENTIAL PERFORMANCE OF THE WHITETOPPING DESIGNS USED IN THIS STUDY

8.1. Overview

This chapter presents the evaluation of the potential performance of WT pavements with the same designs as those used in the test sections in this study.

The 3-D finite element model with the model parameters for each test section, as determined from the deflection-based and strain-based calibration (as presented in Chapter 7), was used to perform a stress analysis to determine the maximum stresses in each WT pavement under typical critical temperature-load conditions in Florida. The potential performance of each WT pavement was assessed based on (1) the maximum tensile stress in the concrete, (2) the maximum shear stress at the concrete-asphalt interface, and (3) the maximum tensile stress in the AC.

8.2. Method of Analysis

8.2.1 Critical Loading Conditions

A 24-kip single axle load, which is slightly higher than the maximum legal single axle load of 22 kips in Florida, was used as the applied load in the analysis. The two critical loading positions used in the analysis were (1) the mid-edge and (2) the corner of the slab. Figures 8.1 and 8.2 show the positions of the axle load used for the slabs with joint spacings of 4 ft and 6 ft, respectively. These figures also show the comparison between a typical load position with the critical load position.

The minimum and maximum temperature differential in the concrete slab as observed during the HVS loading were around -10 ºF and +20 ºF, respectively. These two extreme temperature differentials were used in the critical stress analysis.

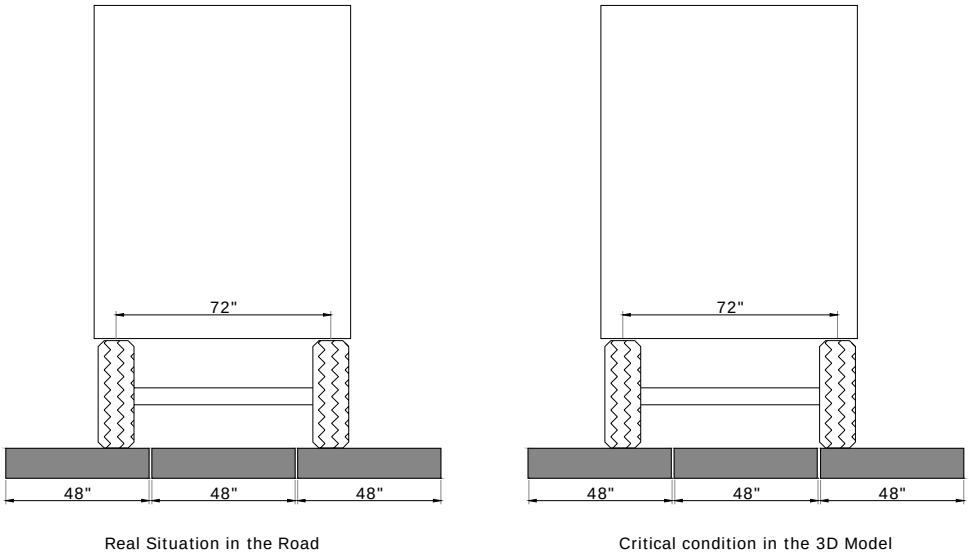

Figure 8.1. Axle Load Positioned on Slabs with 4-ft Joint Spacing.

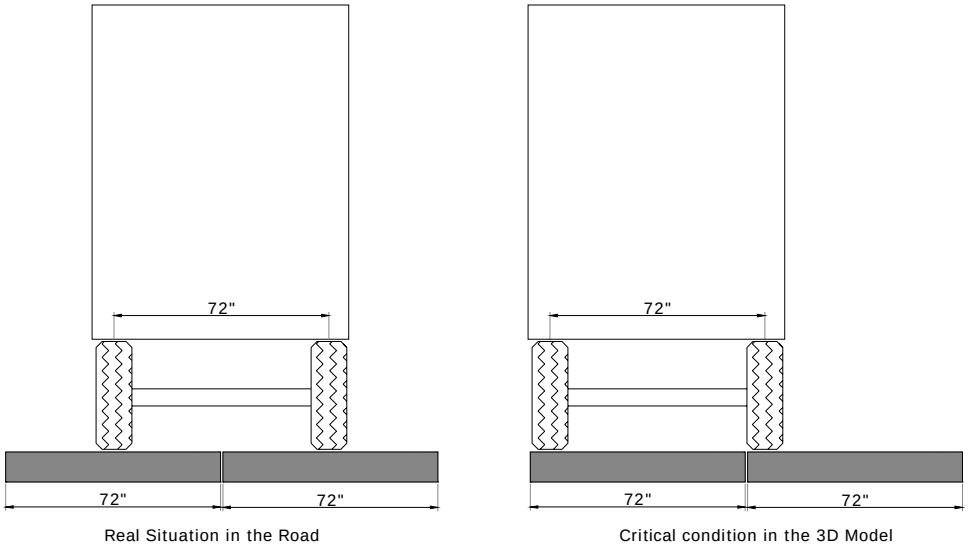

Figure 8.2. Axle Load Positioned on Slabs with 6-ft Joint Spacing.

8.2.2. Model Parameters

The model parameters of the 3-D model for each test section used in the critical stress analysis are displayed in Table 8.1. It is to be noted that all the model parameters, except for the joint spring stiffnesses, are from the results of deflection-based and strain-based calibration as presented in Chapter 7. All the joint spring stiffnesses are set to be zero in this analysis, based

on the expectation that all the joints will eventually crack all the way through, and there will eventually be less load transfer across the joints as compared with their initial conditions.

To represent different temperature conditions, which affect the elastic modulus of the AC layer, all the test sections were analyzed using three different values of the AC elastic modulus, namely 300,000 psi, 700,000 psi and 1,100,000 psi.

For the interface horizontal springs, two spring stiffness values are given. The higher values were used for the condition at the edge of the joints, while the lower values were used for the condition at the slab corners.

Table 8.1. Model Parameters of the 3-D Model for Each Test Section Used in the Analysis.

		Phase I-a			**Phase I-b**			**Phase II**		
		4”	**5”**	**6”**	**4”**	**5”**	**6”**	**6”**	**8”**	**10”**
Material Elastic Moduli (ksi)	Concrete	4,350	4,350	4,350	4,350	4,350	4,350	4,200	4,350	4,350
	AC Layer	3-11 × 10^5	3-11 × 10^5	3-11 × 10^5	3-11 × 10^5	3-11 × 10^5	3-11 × 10^5	3-11 × 10^5	3-11 × 10^5	3-11 × 10^5
	Base	160	160	160	130	130	130	160	160	160
	Subgrade	30	30	30	28	28	28	30	30	30
Spring Constants (lb/in 10^6)	Interface X							3-3.5	2-3	1-3
	Interface Y							3-3.5	2-3	1-3
	Interface Z							5×10^{12}	10^{13}	10^{13}
	Trans. Joint X	0	0	0	0	0	0	0	0	0
	Trans. Joint Y	0	0	0	0	0	0	0	0	0
	Trans. Joint Z	0	0	0	0	0	0	0	0	0
	Long. Joint X	0	0	0	0	0	0	0	0	0
	Long. Joint Y	0	0	0	0	0	0	0	0	0
	Long. Joint Z	0	0	0	0	0	0	0	0	0

8.3. Results of Critical Stress Analysis

8.3.1. Maximum Stresses in the Concrete Slabs

The maximum computed tensile stresses in the various bonded concrete slabs (in Phases I-a and I-b) and partially bonded concrete slabs (in Phase II) caused by a 24-kip single axle load placed at two different critical positions (mid-edge or corner), and for three different temperature

differentials in the concrete slab (-10, 0 or +20 °F) are shown in Table 8.2. Three different AC moduli, namely 300,000 psi, 700,000 psi or 1,100,000 psi, which represent the condition of the AC at different temperatures, were used in the analysis.

Table 8.2. Maximum Tensile Stresses in the Concrete Slabs Caused by a 24-kip Single Axle Load at Various Critical Loading Conditions.

			AC Elastic Modulus (psi)					
Tensile Stress (psi)			Mid-Edge			Corner		
Phase	Slab	Temp	300,000	700,000	1,100,000	300,000	700,000	1,100,000
I-a (bonded) (6' × 6')	4"	-10	246.48	307.7	379.6	259.55	347.5	418.53
		0	333.76	221.15	158.66	204.3	134.2	95.91
		20	568.3	441.66	366.71	325.78	290.96	268.03
	5"	-10	223.72	285.4	360.9	251.5	333.08	409.2
		0	293.51	208.2	157.87	170.95	119.6	89.81
		20	531.43	433.27	371.6	290.91	267.8	249.9
	6"	-10	202.03	260.5	336.6	248.3	315.6	391.5
		0	256.64	190.7	149.9	145.99	104	80.5
		20	488.6	412.06	361.42	279.2	260.86	245.9
I-b (bonded) (4' × 4')	4"	-10	323.6	298.9	304.3	331	303.6	341.3
		0	286.3	186.7	131.07	206.53	152.71	125.23
		20	555.06	435.9	364.8	411.7	340	295.9
	5"	-10	315.23	295.8	289.8	340.9	315.47	328.7
		0	243.3	170.85	127.7	200.84	160.75	135.45
		20	486.94	405.44	352	366.5	316.7	283.6
	6"	-10	296.8	281.6	277.07	340.42	315.86	308.9
		0	209.66	154.23	119.7	196.31	161.32	138.8
		20	416.15	362.9	324.18	318.74	284.5	260.2
II (partially bonded) 6' × 6'	6"	-10	227.8			217.6		
		0	253.6			182.94		
		20	476	398.2	361.4	272.4		
	8"	-10	186.04					
		0	200.13					
		20	400.42	353.07	323.9			
	10"	-10	165.33					
		0	158.6					
		20	318.4	290.25	273.9			
Hypothetical case (bonded) 6' × 6'	8"	-10	172.73					
		0	197.5					
		20	398.8					
	10"	-10	148.6					
		0	156.1					
		20	316.75					

Effects of elastic modulus of AC layer

Figure 8.3 shows the effects of the elastic modulus of the AC layer on the maximum stresses in the concrete caused by a 24-kip axle load applied at mid edge for 4-inch bonded concrete slabs with 6 ft joint spacing. It can be seen that at the condition of temperature differential of +20 °F, an increase of 55% in tensile stress (from 367 to 568 psi) in the concrete was obtained when the elastic modulus of the AC layer dropped from 1,100,000 psi to 300,000 psi. However, at the condition of temperature differential of -10 °F, a decrease of 35% in tensile stress (from 380 to 246 psi) in the concrete was obtained when the elastic modulus of the AC layer changed from 1,100,000 psi to 300,000 psi.

Figure 8.4 shows similar plots for 5-inch bonded concrete slabs with 4 ft joint spacing. In this case, a decrease in the elastic modulus of the AC caused an increase in the tensile stress in the concrete for all temperature conditions.

Effects of temperature differential

Figures 8.5 and 8.6 show the effects of temperature differentials on the maximum stresses in the bonded slabs with 6 ft joint spacing (test slabs in Phase I-a), caused by a 24-kip single axle load placed at mid-edge, and corner of the slab, respectively. An AC elastic modulus of 300,000 psi was used in these analyses. Figures 8.7 and 8.8 show similar plots for the bonded slabs with 4 ft joint spacing (test slabs in Phase I-b). It can be seen from these figures that higher stresses in the concrete were obtained at a temperature differential of +20 °F than at a temperature differential of -10 °F. For the condition of temperature differential of +20 °F, loads at slab mid-edge produced higher stresses than those produced by loads at slab corner.

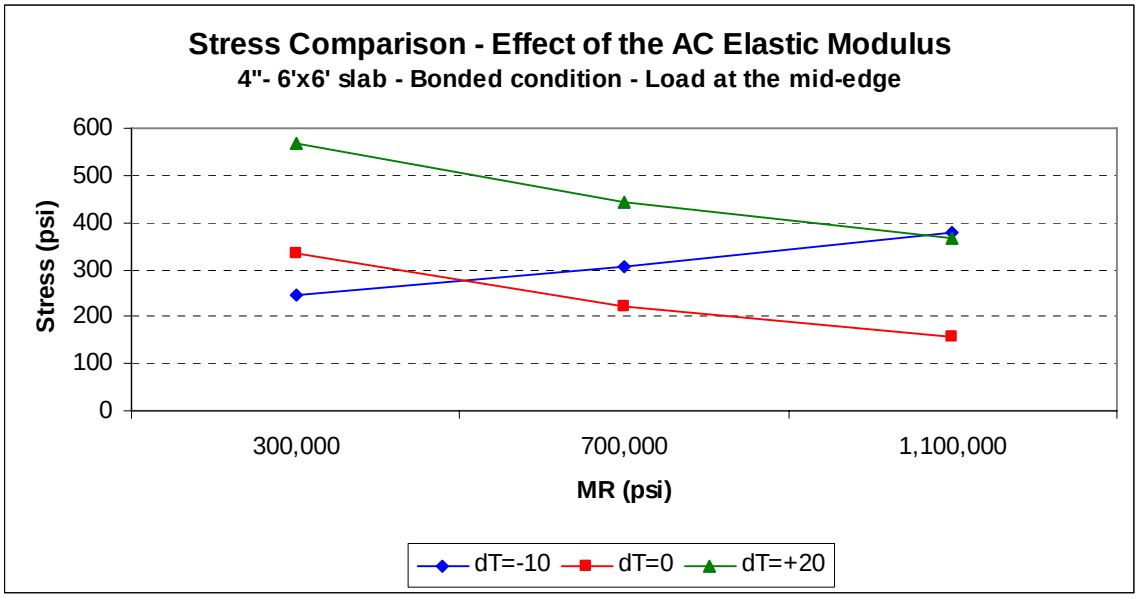

Figure 8.3. Effects of AC Modulus on Maximum Tensile Stress in Concrete Caused by a 24-kip Axle Load at Mid-Edge of 4-inch Bonded Concrete Slabs With 6 ft Joint Spacing.

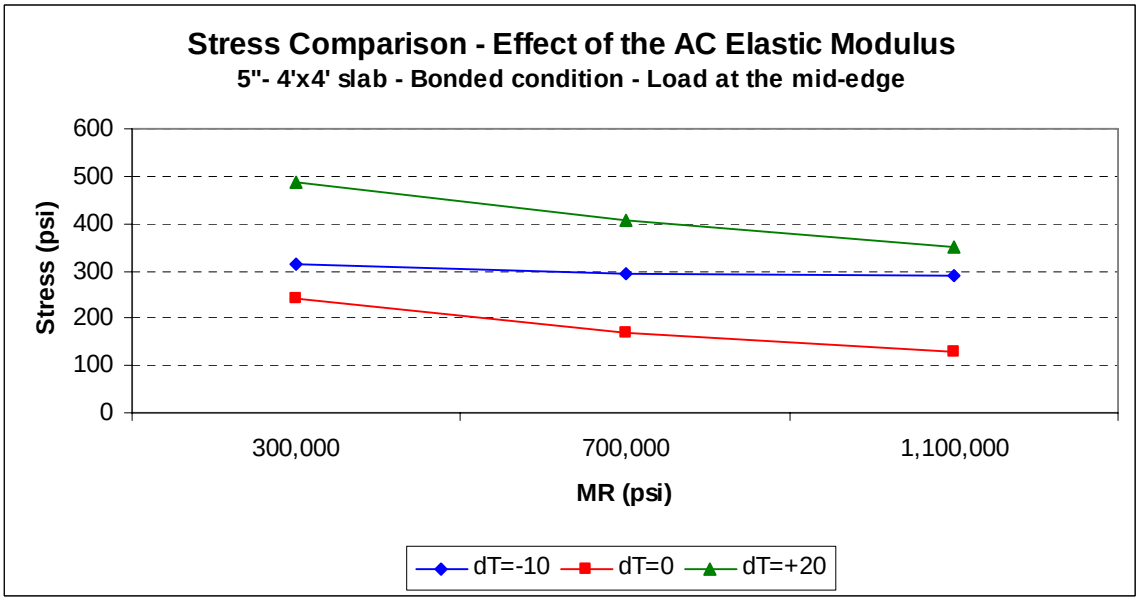

Figure 8.4. Effects of AC Modulus on Maximum Tensile Stress in Concrete Caused by a 24-kip Axle Load at Mid-Edge of 5-inch Bonded Concrete Slabs With 4 ft Joint Spacing.

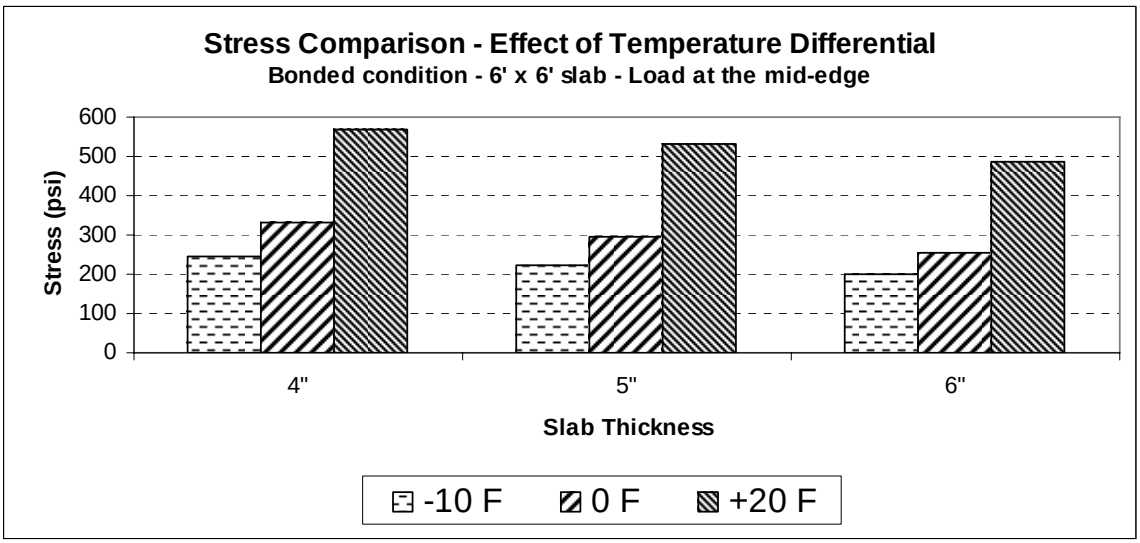

Figure 8.5. Effects of Temperature Differential on Maximum Tensile Stresses in Concrete Caused by a 24-kip Single Axle Load at Mid-Edge of Bonded Slabs With 6 ft Joint Spacing.

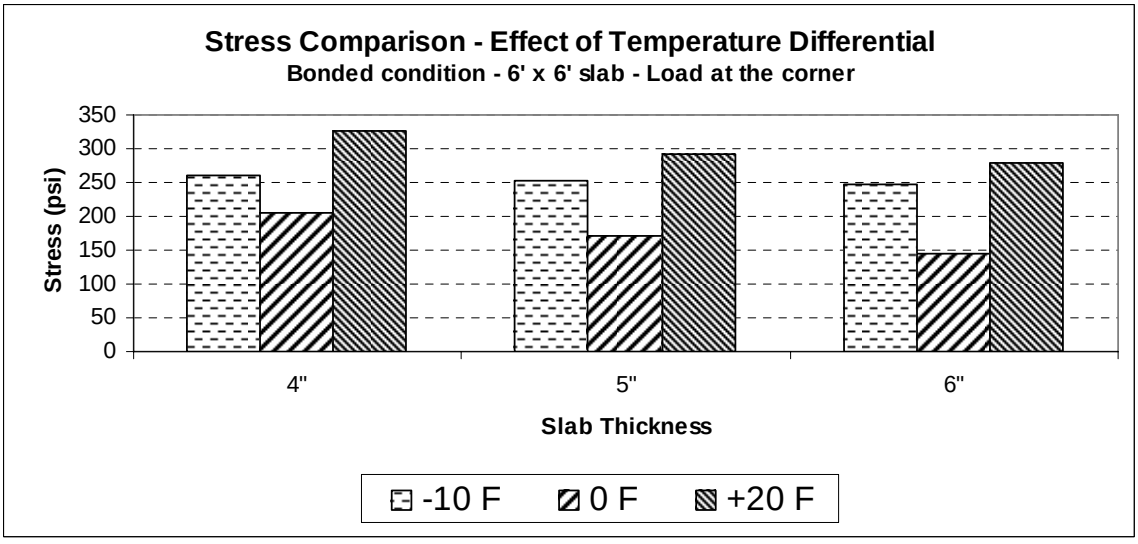

Figure 8.6. Effects of Temperature Differential on Maximum Tensile Stresses in Concrete Caused by a 24-kip Single Axle Load at Corner of Bonded Slabs With 6 ft Joint Spacing.

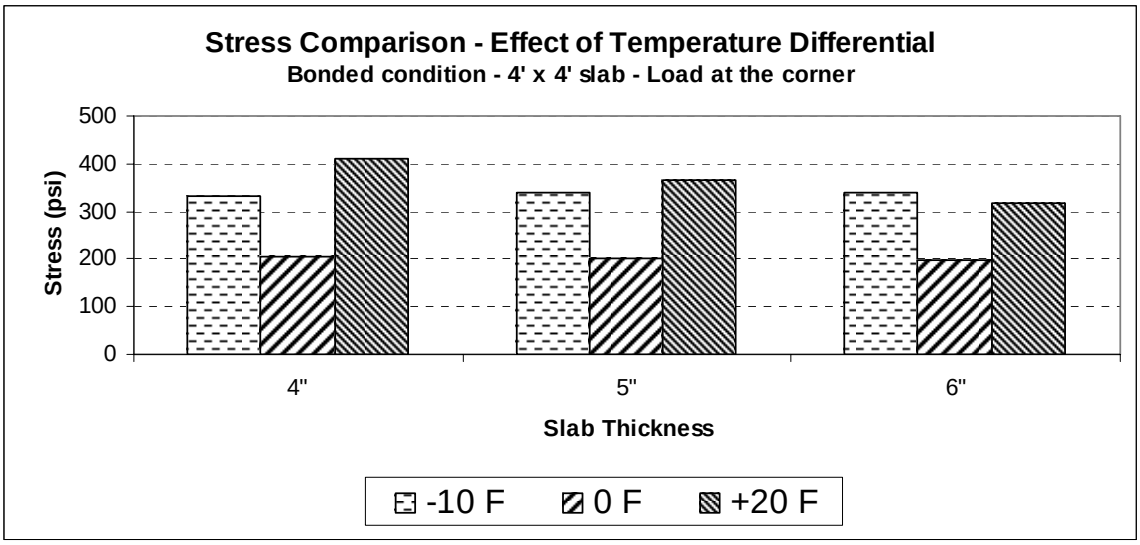

Figure 8.7. Effects of Temperature Differential on Maximum Tensile Stresses in Concrete Caused by a 24-kip Single Axle Load at Mid-Edge of Bonded Slabs With 4 ft Joint Spacing.

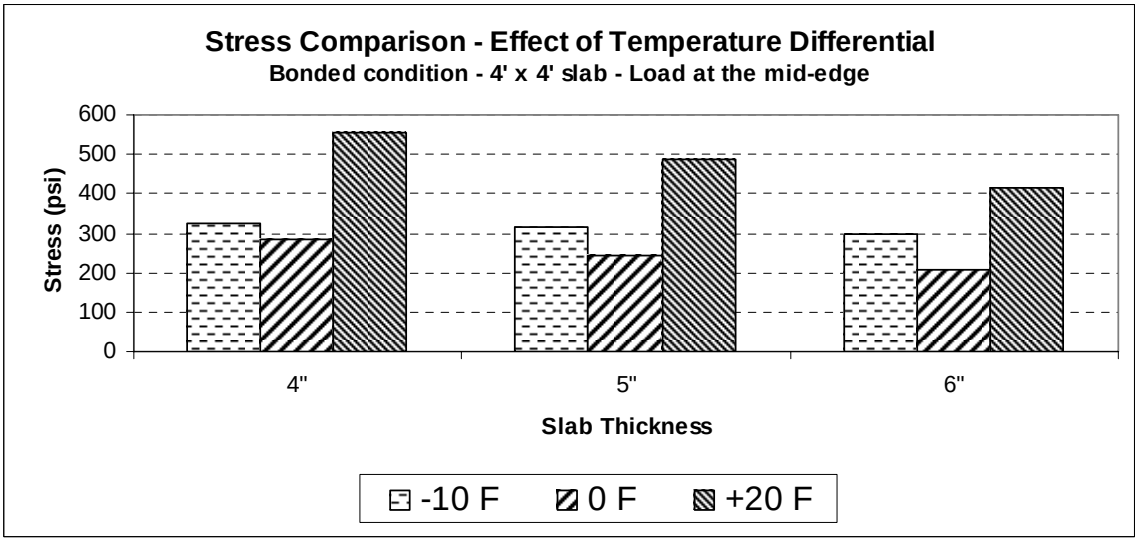

Figure 8.8. Effects of Temperature Differential on Maximum Tensile Stresses in Concrete Caused by a 24-kip Single Axle Load at Corner of Bonded Slabs With 4 ft Joint Spacing.

Similar observation about the effects of temperature differential and loading positions can be made for the partially bonded slabs in Phase II. Figure 8.9 shows the effects of temperature

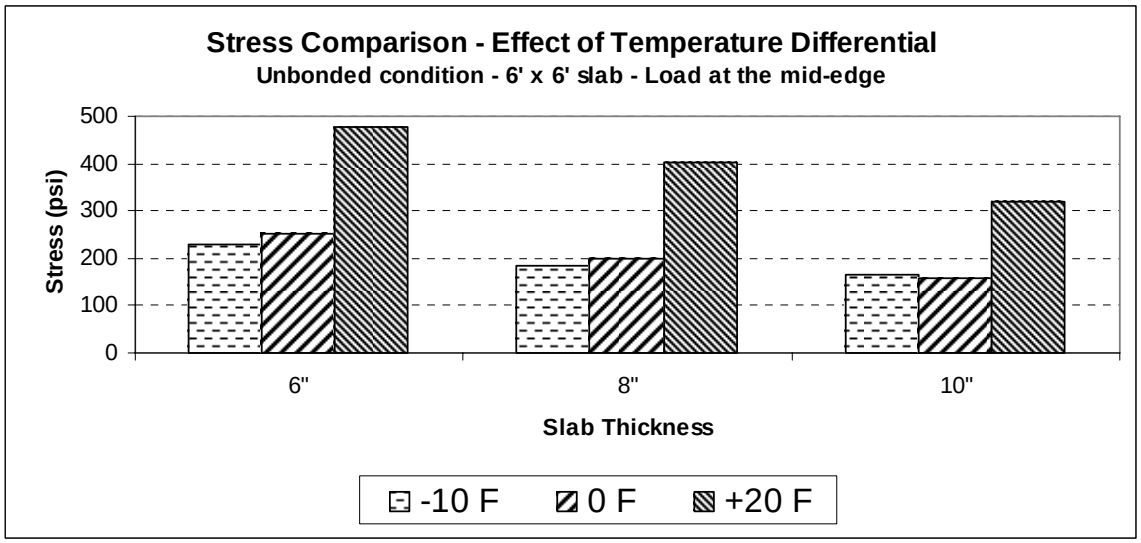

Figure 8.9. Effects of Temperature Differential on Maximum Tensile Stresses in Concrete Caused by a 24-kip Single Axle Load at Mid-Edge of Partially Bonded Slabs With 6 ft Joint Spacing.

differentials on the maximum stresses in the partially bonded slabs with 6 ft joint spacing (test slabs in Phase II), caused by a 24-kip single axle load placed at mid-edge of the slab. It can be seen that the condition of temperature differential of +20 °F produced much higher stresses than a temperature differential of -10 °F.

Effects of panel size

Figures 8.10 and 8.11 show the effects of panel size on the maximum stresses in the bonded concrete slabs caused by a 24-kip single axle load at mid-edge and corner of the slabs, respectively. An AC elastic modulus of 300,000 psi was used in these analyses. It can be seen that at the most critical temperature and load condition (when the temperature differential was +20 °F and the load was applied at mid-edge of slab), the 4 ft X 4 ft panels had slightly lower stresses than the 6 ft X 6 ft panels. The reduction in stress ranges from 2% for the 4-inch slabs to 15% for the 6-inch slabs.

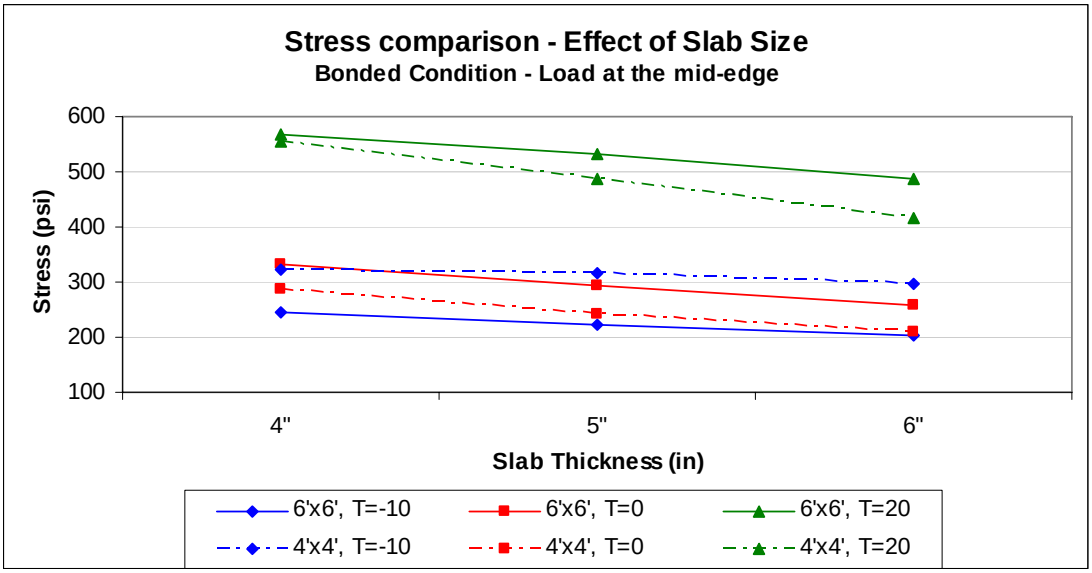

Figure 8.10. Effects of Slab Size on the Maximum Tensile Stresses in Concrete Caused by a 24-kip Single Axle Load at Mid-Edge of Bonded Slabs.

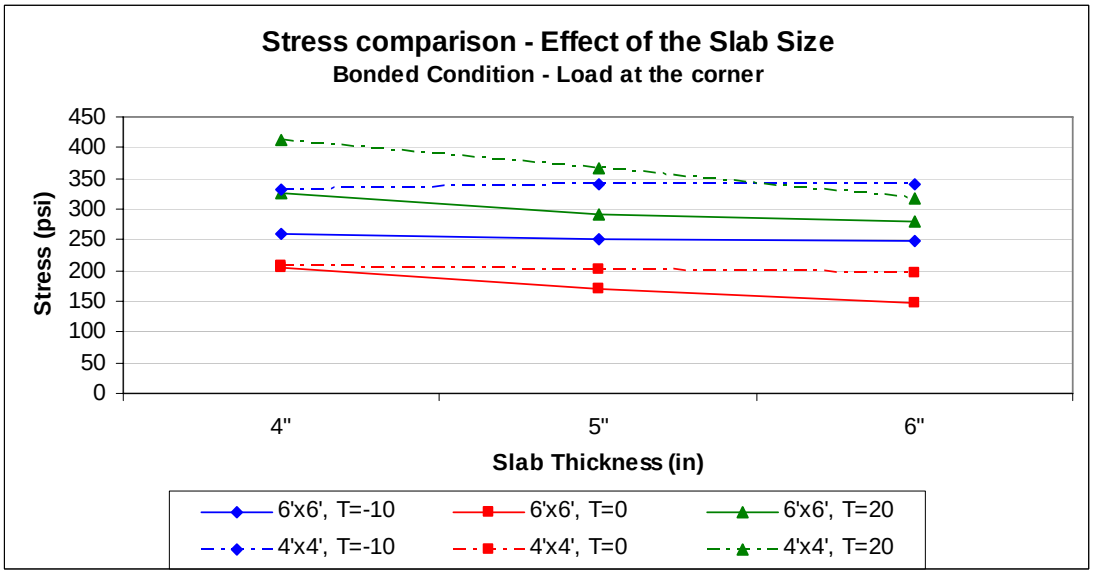

Figure 8.11. Effects of Slab Size on the Maximum Tensile Stresses in Concrete Caused by a 24-kip Single Axle Load at Corner of Bonded Slabs.

When the load was applied to the slab corner, the 4 ft X 4 ft panels had significantly higher stresses than the 6 ft X 6 ft panels. For example, when the temperature differential was +20 °F and the load was applied at the slab corner, the 4 ft X 4 ft panels had higher stresses than the 6 ft X 6 ft panels by 26% for the 5-inch slabs.

Effects of bonded versus partially bonded interface

A direct comparison of the effects of a bonded concrete-asphalt interface versus a partially bonded interface can be made by comparing the computed maximum tensile stresses in the 6-inch bonded slabs in Phase I-a with those in the 6-inch partially bonded slabs in Phase II. Figures 8.12 and 8.13 show the comparison of maximum computed tensile stresses in concrete for these two test slabs under a 24-kip single axle load applied at the mid-edge and corner of the slabs, respectively. An AC elastic modulus of 300,000 psi was used in these analyses.

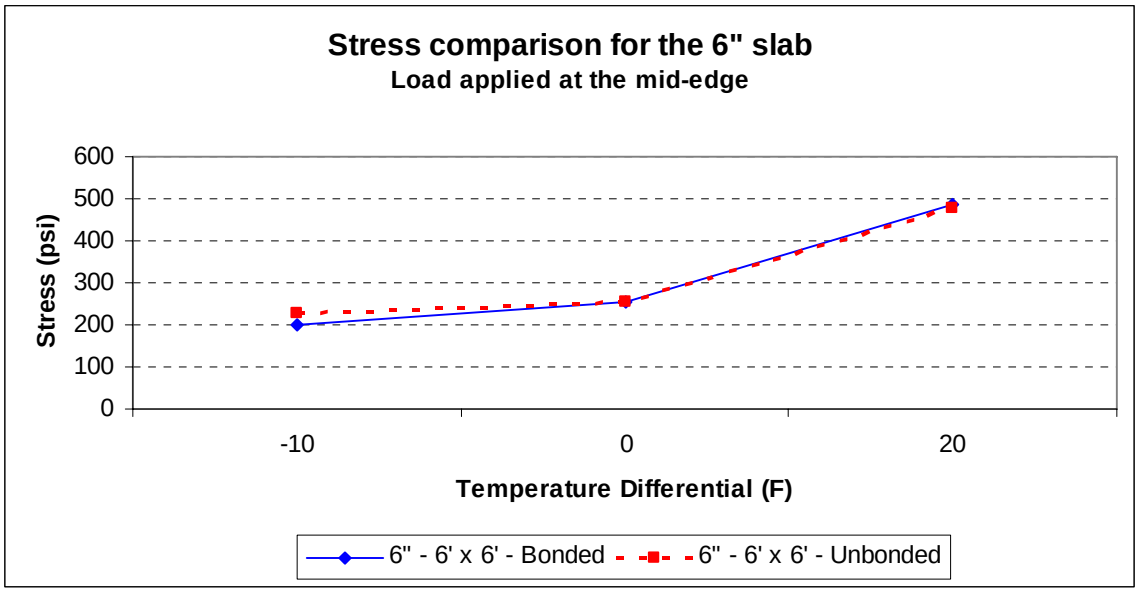

Figure 8.12. Effects of Interface Condition on Maximum Tensile Stresses in Concrete Caused by a 24-kip Single Axle Load at Mid-Edge of 6-inch Slabs with 6 ft Joint Spacing.

From these two figures, it can be seen that, for the most critical condition of a temperature differential of +20 °F, the bonded slabs have about the same maximum tensile stresses as those in the partially bonded slabs. However, for the condition of a temperature differential of -10 °F, the bonded slabs have slightly lower maximum tensile stresses than the partially bonded slabs.

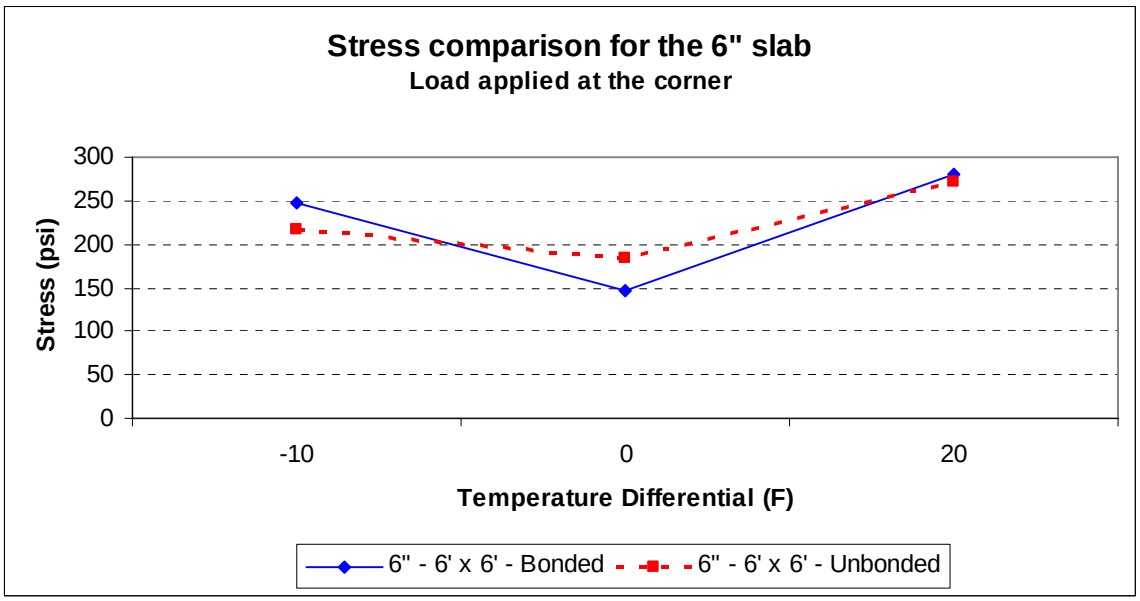

Figure 8.13. Effects of Interface Condition on Maximum Tensile Stresses in Concrete Caused by a 24-kip Single Axle Load at Corner of 6-inch Slabs With 6 ft Joint Spacing.

Analyses were also performed to determine the maximum stresses in concrete under critical loading conditions for the hypothetical cases if the test slabs in Phase II were constructed as fully bonded to the asphalt layer. These computed stresses are also shown in Table 8.2. Figure 8.14 shows the comparison of the maximum stresses in concrete caused by a 24-kip single axle load at mid-edge of slab for the test sections in Phase II with those for the hypothetical cases if the same slabs were constructed bonded to the asphalt layer. Similar trends can be observed here. For the condition of a temperature differential of +20 °F, the bonded slabs have about the same maximum tensile stresses as those in the partially bonded slabs. However, for the condition of a temperature differential of -10 °F, the bonded slabs have slightly lower maximum tensile stresses than the partially bonded slabs.

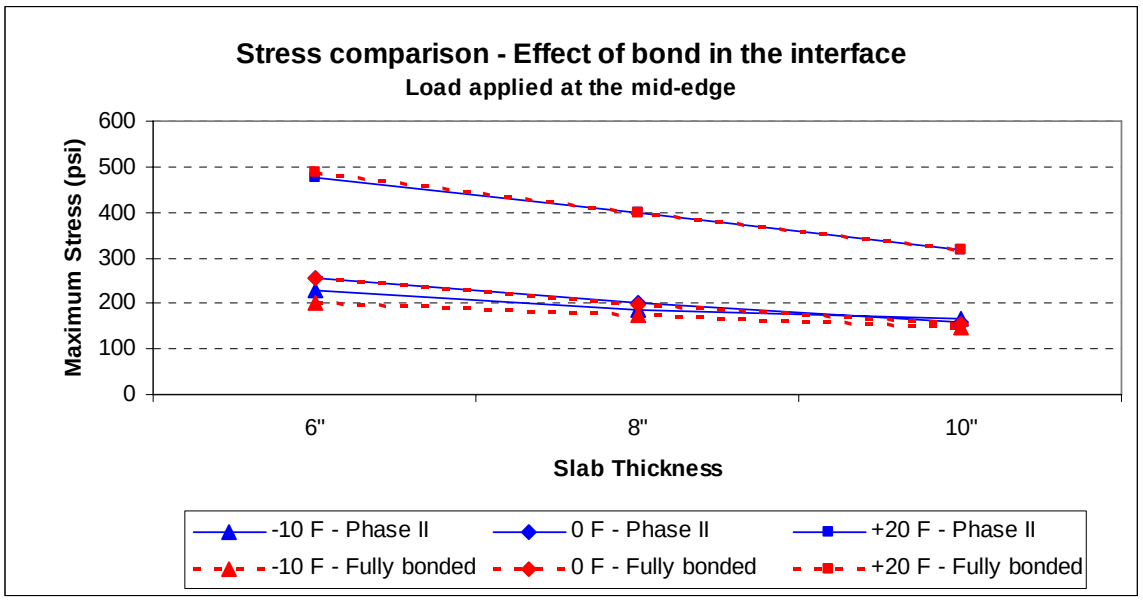

Figure 8.14. Effects of Interface Condition on Maximum Stresses in Concrete Caused by a 24-kip Single Axle Load at Mid-Edge of Slab for the Test Sections in Phase II.

8.3.2. Maximum Shear Stresses at the Interface

The 3-D finite element model was also used to calculate the shear stresses at the concrete-asphalt interface under critical loading conditions. Table 8.3 displays the maximum shear stresses at the interface caused by a 24-kip single axle load at a temperature differential of +20 °F for the bonded slabs in Phases I-a and I-b. Figures 8.15 and 8.16 show the plots of these maximum shear stresses at the interface for the bonded slabs with 6 ft joint spacing and 4 ft joint spacing, respectively. Three AC elastic moduli, namely 300,000, 700,000 and 1,100,000 psi, were used in the analyses.

From these two figures, it can be observed that for both load locations (mid-edge and corner), the shear stress is higher when the AC layer is stiffer. It can also be observed that the smaller 4 ft X 4 ft slabs (Phase I-b) had lower maximum shear stresses.

Table 8.3. Maximum Shear Stress at the Concrete-Asphalt Interface Caused by a 24-kip Single Axle Load at a Temperature Differential of +20 °F for the Bonded Slabs.

Shear Stress in the Interface (psi)		AC Elastic Modulus (psi × 103)					
		Load at the Mid-Edge			Load at the Corner		
Phase	Slab	300	700	1100	300	700	1100
I-a	4”	36.0	47.0	53.0	59.3	71.7	78.8
	5”	34.7	44.2	49.6	63.0	75.5	82.7
	6”	33.6	41.8	46.6	65.5	77.7	84.8
I-b	4”	35.8	46.7	52.3	45.1	56.9	62.8
	5”	34.3	43.5	48.5	46.0	56.8	62.4
	6”	33.1	40.9	45.3	46.8	56.5	61.7

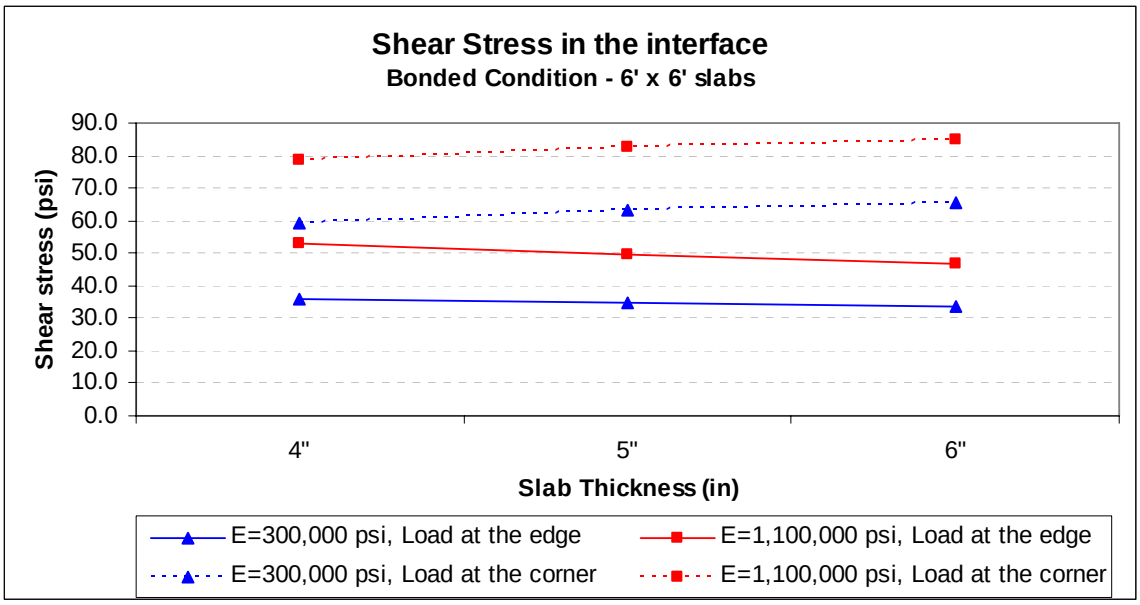

Figure 8.15. Maximum Shear Stresses at the Interface Caused by a 24-kip Single Load at a Temperature Differential of +20 °F for the Bonded Slabs With 6 ft Joint Spacing.

In all cases, the maximum computed shear stress at the interface are very low compared with the shear strength measured from the core samples from the test sections using the Iowa Shear test. From Table 5.4 in Chapter 5, it can be seen that the average shear strength for the 4 ft × 4 ft slabs was 194.5 psi, and the average shear strength for the 6 ft X 6 ft slabs was 220 psi.

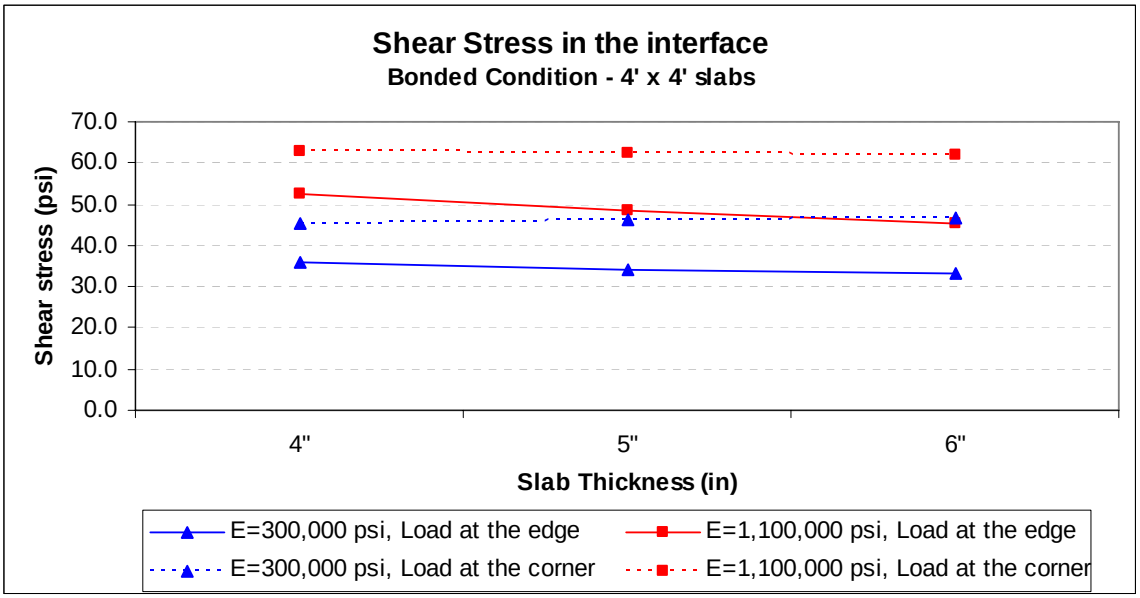

Figure 8.16. Maximum Shear Stresses at the Interface Caused by a 24-kip Single Load at a Temperature Differential of +20 °F for the Bonded Slabs With 4 ft Joint Spacing.

The maximum shear stress among all cases was only 84.8 psi. The fact that the shear stress developed at the interface is much lower than the shear strength indicates that the fully bonded condition at the interface may remain in place for a long time during the life time of the composite pavement.

8.3.3. Maximum Stresses in the AC Layer

The 3-D analytical model was also used to determine the tensile stresses in the AC layer under critical loading conditions. Table 8.4 displays the maximum tensile stresses in the asphalt concrete layer caused by a 24-kip single axle load at various critical loading conditions. Figures 8.17 and 8.18 show the maximum tensile stresses in the AC layer caused by a 24-kip single axle load at a temperature differential of +20 °F for the bonded slabs with 6 ft joint spacing and 4 ft joint spacing, respectively. Two AC elastic moduli, namely 300,000 psi and 1,100,000 psi, were used in the analyses.

Table 8.4. Maximum Tensile Stresses in the Asphalt Concrete Layer Caused by a 24-kip Single Axle Load at Various Critical Loading Conditions.

			AC Elastic Modulus (psi)					
Tensile Stress (psi)			Mid-Edge			Corner		
Phase	Slab	Temp Diff. °F	300,000	700,000	1,100,000	300,000	700,000	1,100,000
I-a (bonded) (6’ × 6’)	4”	-10	97.82	172.3	230.91	103.64	182.09	243.4
		0	21.84	65.6	97.75	25.29	78.96	122.3
		20	40.8	127.8	202.67	45.48	150.75	246.7
	5”	-10	100.7	179.5	242.6	107.5	191.4	258
		0	18.34	55.95	84.25	22.57	74.27	116.38
		20	40.54	129.8	208.3	44.8	156.8	260.7
	6”	-10	101.92	182.8	248	109.8	196.8	266.8
		0	15.68	48.23	73.21	19.32	66.2	104.62
		20	39.7	129.06	208.62	43.9	160	268.8
I-b (bonded) (4’ × 4’)	4”	-10	91.07	161.5	216.4	90	159.8	214.2
		0	21.3	58.7	85.6	23.95	68.2	101.4
		20	48.4	135.3	206.81	57.8	169.4	266.7
	5”	-10	92.6	165.4	222.9	91.6	163.5	220.3
		0	17.27	48.8	72.12	21.53	63.26	95.55
		20	46.92	133.5	206.12	55.9	173.2	276.4
	6”	-10	91.9	165.9	222.9	90.9	163	220
		0	14.38	41.18	61.52	19.53	58.82	90
		20	44.64	128.7	206.82	63.4	173.02	278.5
II (partially bonded) 6’ × 6’	6”	-10	107.6			86.7		
		0	15.74			18.6		
		20	36.95	121.1	197.9	42.9		
	8”	-10	110.3					
		0	14.1					
		20	33.74	114	193.8			
	10”	-10	104.3					
		0	16.2					
		20	29.82	105.9	188.9			
Hypothetical Bonded 6’ × 6’	8”	-10	100.4					
		0	11.84					
		20	37					
	10”	-10	95					
		0	9.16					
		20	33.7					

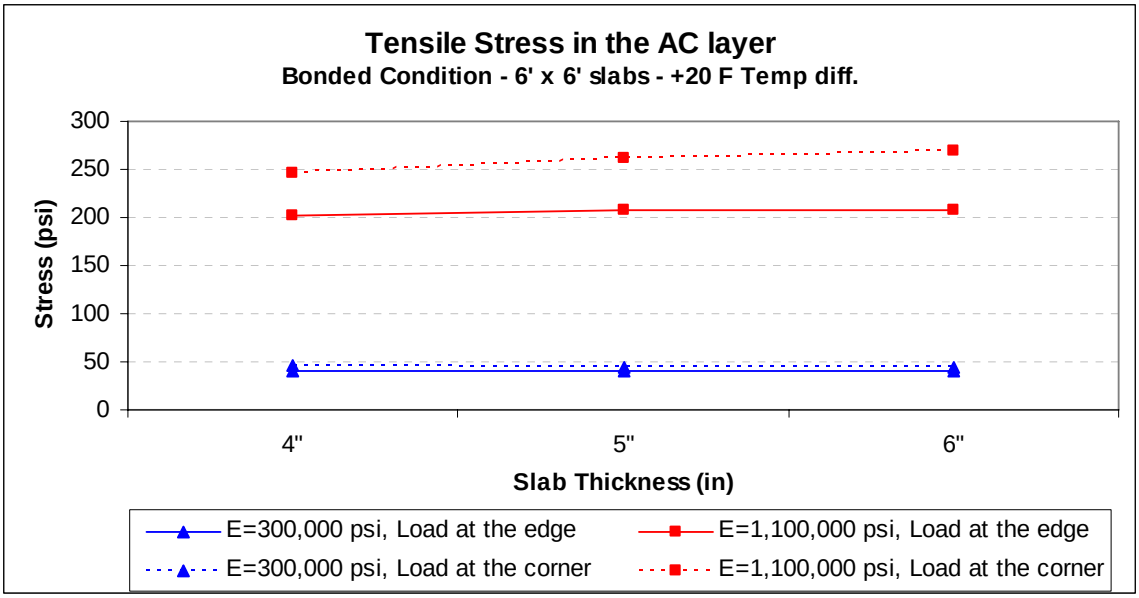

Figure 8.17. Maximum Tensile Stresses in the AC Layer Caused by a 24-kip Single Axle Load at a Temperature Differential of +20 °F for the Bonded Slabs With 6 ft Joint Spacing.

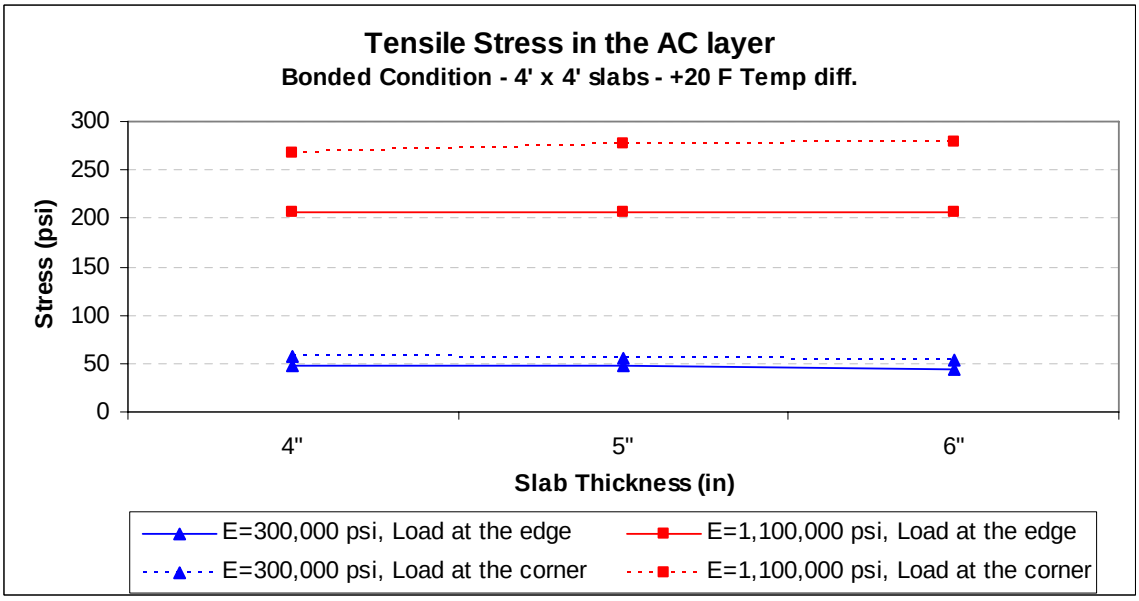

Figure 8.18. Maximum Tensile Stresses in the AC Layer Caused by a 24-kip Single Axle Load at a Temperature Differential of +20 °F for the Bonded Slabs With 4 ft Joint Spacing.

From these two figures, it can be observed that the tensile stress in the AC layer increases as the elastic modulus of the AC increases and that the size of the slab concrete has little effect on the tensile stresses in the AC layer.

The maximum calculated tensile stresses in the AC layer are lower than the tensile strength of the AC measured in the IDT test at 15 ºC. The highest tensile stresses in the AC layer were obtained when a high value of the AC elastic modulus was used. Since high values of the AC elastic modulus occur at low temperatures when the tensile strength of the AC layer is high, this creates a favorable condition where the AC is less likely to crack. Thus, stresses in the AC layer should not be a controlling factor in the performance of these WT pavements.

8.4. Assessment of Potential Performance of the Test Sections

The maximum computed stresses in the concrete slab caused by the critical loading condition (of a 24-kip single axle load, placed at the mid-edge of the slab, and at a temperature differential of +20 °F in the concrete slab) were used to assess the potential performance of the WT pavement test sections evaluated in this study. The fatigue curve given by the PCA, which relates the stress/strength ratios with the number of repetitions to produce fatigue failure in concrete, was used to estimate the number of load repetitions to failure. The following equations were used to calculate the maximum number of load repetitions as a function of the stress/strength ratio:

$$NLR = 10^{(96.5 - 100\,r)/8.1} \qquad \text{If} \qquad r > 0.5$$

$$NLR = \text{infinite} \qquad \text{If} \qquad r < 0.5$$

Where NLR = number of load repetitions to failure, and

r = stress/strength

The average flexural strength at 56 days of the concrete used in the test sections was 842 psi, as presented in Table 5.6 in Chapter 5. This flexural strength value was used in the computation of the stress to flexural strength ratios for the WT pavement test sections.

Table 8.5 displays the computed maximum stresses and stress to flexural strength ratios for all the WT pavement test sections evaluated in this study. The allowable number of 24-kip single axle loads under critical loading conditions were also computed and shown in this table. It is to be stressed that the results of these analyses are only applicable to the condition of the test sections, which had 4.5 inches of AC layer over 12 inches of limerock base.

Table 8.5. Computed Stress Ratio in the Concrete and Allowable Number of 24-kip Single Axle Loads Under Critical Loading Conditions for the Test Sections Evaluated in This Study.

Phase	Slab Thickness	Stress (psi)	Stress-strength Ratio	# of Repetitions of 24-kip Axle Loads to Failure
I-a	4”	568.3	0.675	3,810
	5”	531.43	0.631	13,231
	6”	488.6	0.580	56,178
I-b	4”	555.06	0.659	5,958
	5”	486.94	0.578	59,416
	6”	416.15	0.494	no limit
II	6”	476	0.565	85,963
	8”	400.42	0.476	no limit
	10”	318.4	0.378	no limit

It can be seen that the maximum computed stresses were all below the flexural strength of the concrete for all the test sections. This means that all the WT pavement test sections with a concrete slab thickness of 4 inches or higher can withstand certain number of repetitions of the 24-kip single axle load under the critical loading condition without cracking. The allowable number of repetitions of this critical load increases with slab thickness. The allowable number of load repetitions also increases with smaller joint spacing.

In order to be able to withstand the critical load without fear of fatigue failure (for an infinite number of critical load repetitions), a minimum slab thickness of 6 inches would be needed for a joint spacing of 4 ft, and a minimum slab thickness of 8 inches would be needed for a joint spacing of 6 ft.

CHAPTER 9
FINDINGS AND RECOMMENDATIONS

9.1. Summary of Findings

A full scale experiment was performed at the APT facility located at the FDOT Material Research Park to evaluate the feasibility of using whitetopping (WT) pavements in Florida. A total of nine instrumented WT test sections were constructed and tested using a Heavy Vehicle Simulator (HVS). A 3-D finite element model was developed to analyze the behavior of the WT pavement test sections. The model was verified and calibrated using the measured FWD deflections and HVS load-induced strains from the test sections. The model was then used to evaluate the potential performance of these test sections under a typical critical temperature-load condition in Florida. A summary of the findings from this study is presented in the following section.

Bond Strength at the Concrete-Asphalt Interface

In the construction of the test sections with a bonded concrete-asphalt interface (in Phases I-a and I-b), the asphalt surface was milled, cleaned and sprayed with water before the placement of concrete. This method was found to produce excellent bonding at the interface. The average shear strength from the Iowa shear test on the cores from these test sections was 220 psi for Phase I-a, and 195 psi for Phase I-b. The maximum computed shear stress at the interface under the critical temperature-load condition for all cases is only 85 psi.

In the construction of the test sections with an unbonded concrete-asphalt interface (in Phase II), a white-pigmented curing compound was sprayed on the surface of the asphalt to act as a debonding agent before the placement of concrete. Results of Iowa shear test on the cores from these test sections indicated an average shear strength of 119 psi before the HVS loading

and 135 psi after the HVS loading. This indicates that partial bonding existed at the interface though an unbonded condition was intended, and that the bonding improved with additional loading on the pavement.

Development of the 3-D Finite Element Model

A 3-D finite element model, as described in Chapter 4 of this report, was developed for the analysis of WT pavements. The model was verified and calibrated with the measured FWD deflections and HVS load-induced strains. It was founded that the bonded interface (as existed in the test sections in Phases I-a and I-b) could be modeled well by modeling the concrete as perfectly bonded to the asphalt. The partially-bonded interface (as existed in the test sections in Phase II) could be modeled well by vertical and horizontal springs connecting the concrete layer with the asphalt layer.

For the conditions at the time of the HVS loading on the test sections, it was found that joints could be modeled well by springs connecting the slabs at the joint. It is postulated that load transfer at the joints will eventually decrease with time. In the analysis for long-term performance of the test sections under the critical condition, the worst joint condition was assumed and thus springs of zero stiffness were used to model the joint behavior in this analysis.

Effects of Elastic Modulus of AC

The elastic modulus of the AC layer was found to have great influence on the maximum tensile stresses in the concrete slab. Thus, for the analysis for the most critical loading condition, the lowest possible elastic modulus of the AC (at the highest temperature) was used.

Effects of Concrete Panel Size

Maximum stresses in the concrete were found to decrease as the joint spacing decreases. At the most critical loading condition, the concrete slabs with 4 ft joint spacing had lower maximum stresses than those with 6 ft joint spacing.

Effects of Bonded versus Partially Bonded Interface

At the condition of negative temperature differentials in the concrete slab, the concrete slabs with a partially bond interface were found to have higher maximum stresses than those with a fully bonded interface. However, at the condition of zero or positive temperature differential in the slab, the maximum stresses in the partially bonded slabs are about the same as those in the fully bonded slabs.

Potential Performance of the Test Sections

The verified and calibrated 3-D finite element model was used to evaluate the potential performance of the nine test sections under a critical temperature-load condition. Maximum tensile stresses in the pavement were computed for the critical condition when a 24-kip single axle load (which is higher than the legal limit of 22 kips in Florida) was placed at the mid-edge of the slab (which is the most critical loading position) and when the temperature differential in the concrete slab was +20 °F (which is a typical severe temperature condition in the summer time in Florida.)

The maximum computed stresses in the concrete slabs were all below the flexural strength of the concrete for all the 9 test sections. Based on the computed maximum stresses in the concrete, the expected numbers of repetitions of the 24-kip single axle loads at the critical thermal condition were computed for the nine test sections. The results show that the 4-inch slabs can be used for heavy (24-kip single axle) load but only for low-volume traffic condition. The allowable traffic volume increases as the concrete slab thickness increases. In order to be able to withstand the critical load without fear of fatigue failure (for an infinite number of critical load repetitions), a minimum slab thickness of 6 inches would be needed for a joint spacing of 4 ft, and a minimum slab thickness of 8 inches would be needed for a joint spacing of 6 ft.

9.2. Recommendations

The developed 3-D finite element model is recommended for use for analysis of WT pavements subjected to load and temperature effects. The model parameters needed in the analysis include the elastic moduli of the concrete, AC, base and effective subgrade layers. For analysis of long-term behavior, the joint stiffness can be assumed to be zero. For partially bonded interface condition, the stiffness values of the springs for modeling the interface are also needed as model parameters. The elastic moduli of concrete and AC can be determined by testing in the laboratory, while the other parameters can be determined through the back-calculation method of matching analytical deflections and strains due to an applied load with measured values.

The WT pavement test sections in this study were limited to the following conditions:

(1) When each test section was tested by the HVS, the test section was shaded by the HVS. As a result, the temperature differential in the concrete slabs was much lower than its maximum potential amount if the slabs were unshaded. The test sections could not be tested and monitored for the most critical temperature condition.

(2) Due to the high demand on the use of the HVS, it was not possible to load the test sections for an extended period of time to evaluate the long-term performance of the WT pavements and the modes of failures under actual traffic and weather conditions.

It is recommended that experimental WT pavement test sections of various designs be constructed on actual roadways in Florida to evaluate their behavior and performance under actual environmental and traffic conditions. The experimental pavement sections will be instrumented for monitoring of temperature and strains on a long-term basis. This will enable the monitoring of the behavior of the WT pavements under critical load and temperature conditions,

and the verification of the predicted response from the analytical model. It will also enable the evaluation of the long-term behavior of the WT pavements under actual traffic and weather conditions.

REFERENCES

American Association of State Highway and Transportation Officials, 1993. **"Guide for Design of Pavement Structures,"** Washington, DC.

American Concrete Pavement Association, 1998. **"Whitetopping – State of the Practice,"** ACPA Engineering Bulletin EB210P, Skokie, IL.

Armaghani, J.M. and Tu, Diep, 1999. **"Rehabilitation of Ellaville Weigh Station with Ultra-Thin Whitetopping,"** Transportation Research Record 1654, Transportation Research Board, National Research Council, Washington, DC, pp. 3-11.

Brown, D., 1995. **"Ultra-Thin Whitetopping Emerges as Rehab Technique,"** Transportation Builder, V7, No. 1, Jan. 1995, pp 37-41.

Cable, J.K., Grove, J.D., and Heyer, M., 1997. **"Ultra-thin Pavements Making the Grade,"** Proceedings, Sixth International Purdue Conference on Concrete Pavement Design and Materials for High Performance, Volume II, Indianapolis, IN, pp. 245-266.

Cable, J.K, 1998. **"Iowa Ultra-thin Whitetopping Research, A Performance Update,"** Paper Presented at 1998 Transportation Research Board Annual Meeting, Washington DC, January.

Cable, J.K. and Ciha, T., 2001. **"The Ultra-thin Whitetopping Option,"** Proceedings of the Seventh International Conference on Concrete Pavements, Vol. 2, Orlando, Florida, September, pp. 969-975.

Cole, L.W., and Mohsen, J.P., 1993. **"Ultra-Thin Concrete Overlays on Asphalt,"** Paper prepared for presentation at the 1993 TAC Annual Conference, Ottawa, Ontario, Canada.

Cole, L.W., Sherwood, J., Qi, X., 1999. **"Accelerated Pavement Testing of Ultra-Thin Whitetopping,"** Accelerated Pavement Testing International Conference, Reno.

Cown, R.M., 1993. **"Experimental Concrete Inlay on Existing Asphalt Pavement, Georgia,"** Department of Transportation, Office of Materials and Research, Concrete Branch, Forest Park, GA.

Dumitru, N. I., Hossain, M., and Wojakowski, J., 2002. **"Construction and Performance of Ultra-Thin Whitetopping in Kansas,"** Paper Presented at the 2002 Transportation Research Board Annual Meeting, Washington, DC.

Edwards, W. F. and Sargand, S. M., 1999. **"Response of an Ultra-Thin Whitetopping Pavement to Moving Wheel Loads,"** Accelerated Pavement Testing International Conference, Athens, Ohio, October 18-20.

Galal, K. A., Newbolds, S.A., Olek, J., Weiss, W. J., and Nantung, T., 2004. **"Stress and Strain Analysis of Ultra-Thin Whitetopping over Composite Pavement Section using Accelerated Pavement Testing,"** Paper Presented at 2004 Transportation Research Board Annual Meeting, Washington, DC.

Hutchinson, R.L., 1982. **"Resurfacing with Portland Cement Concrete,"** Synthesis of Highway, Practice, NCHRP 99, Transportation Research Board, Washington, DC.

Khazanovich, Lev, Gotlif, Alex, 2002. **"ISLAB2000 Simplified Friction Model."** Paper Presented at 2002 Transportation Research Board Annual Meeting, Washington, DC.

Mack, J.W., Wu, C.L., Tarr, S.M., and Refai, T., 1997. **"Model Development and Interim Design Procedure Guidelines for Ultra-thin Whitetopping Pavements,"** Proceedings, Sixth International Purdue Conference on Concrete Pavement Design and Materials for High Performance, Volume I, Indianapolis, IN, pp. 231-256.

McGhee, Kenneth, H**.,** 1994. **"Portland Cement Concrete Resurfacing,"** Synthesis of Highway Practice, NCHRP 204, Transportation Research Board, Washington, DC.

Middleton, Brent, Fall, Lynne, Day, Robert, 2005. **"Durability and mechanical Properties of High Performance Concrete for Ultra-Thin Whitetopping Pavements."** Paper Presented at 2005 Transportation Research Board Annual Meeting, Washington, DC.

Nelson, Patricia K., Rasmussen, Robert O., 2002. **"Delamination Stresses at the Interface of Bonded Concrete Overlays."** Paper Presented at 2002 Transportation Research Board Annual Meeting, Washington, DC.

Nishiyama, Taizo, Lee, Hosin, Bhatti, M. Asghar, 2005. **"Investigation of Bonding Condition in Concrete Overlay by Laboratory Testing, Finite Element Modeling and Field Evaluation,"** Paper Presented at 2005 Transportation Research Board Annual Meeting, Washington, DC.

Nishizawa, Tasuo, Murata, Yoshiki, Kokubu, Katsuro, 2003. **"Mechanical behavior of Ultra-Thin whitetopping structure under stationary and moving loads."** Paper Presented at 2003 Transportation Research Board Annual Meeting, Washington, DC.

Portland Cement Association, 1984. **"Thickness Design for Concrete Highway and Street Pavements,"** Publication No. EB109.01P, Skokie, IL .

Rajan, S., Olex, J., Robertson, T.L., Galal, K., Nantung, T., and Weis, J., 2001. **"Analysis of Performance of Ultra-Thin Whitetopping Subjected to Slow Moving Loads in an Accelerated Pavement Testing Facility,"** 7th International Conference on Concrete Pavements, Orlando, Florida, September 9-13.

Rasmussen, Robert O., Rozycki, Dan K., 2001. **"Characterization and Modeling of Axial Slab-Support Restraint,"** Paper Presented at 2001 Transportation Research Board Annual Meeting, Washington, DC.

Risser, R.J., LaHue, S.P., Voigt, G.F., and Mack, J., 1993. **"Ultra-Thin Concrete Overlays on Existing Asphalt Pavement,"** 5th International Conference on Concrete Pavement Design and Rehabilitation, Vol. 2, April, Purdue University, Lafayette, IN., pp. 247-254.

Saeed A., Hammons, M.I., and Hall, Jr., J.W., 2001. **"Design, Construction, and Performance Monitoring of Ultra-thin Whitetopping at a General Aviation Airport,"** proceedings, 2001 ASCE Airfield Pavement Specialty Conference, American Society of Civil Engineers, Chicago, Illinois.

Saeed, A. and Hall, Jr., J.W., 2001. **"Non-destructive Pavement Evaluation and Design of Ultra-thin Whitetopping at a General Aviation Airport in Tennessee,"** Proceedings Second International Conference on Maintenance and Rehabilitation of Pavements and Technical Control, Auburn University, Alabama.

Speakman, J., and Scott, III, H., 1996. **"Ultra-Thin, Fiber-Reinforced Concrete Overlays for Urban Intersections,"** Transportation Research Record 1532, Advancements in Concrete Materials Technology, TRB, National Research Council, Washington, DC, pp.15-20.

Sprinkel, M.M., and Ozyildirim C., 1999. **"Evaluation of the Installation and Initial Condition of Hydraulic Cement Concrete Overlays Placed on Three Pavements in Virginia,"** Interim Report. Report No. VTRC 99-IR3, April.

Tarr, Scott M., Sheehan, Mattew J., Ardani, Ahmad, 2000. **"Mechanistic Design of Thin Whitetopping Pavements in Colorado,"** Paper Presented at 2000 Transportation Research Board Annual Meeting, Washington, DC, January.

Tia, M., and Kumara, W., 2003. **"Evaluation of performance of Ultra-thin whitetopping by means of Heavy vehicle simulator (Analysis, Planning and Design phase)."** Final Report UF Project No: 49104504863-12. Gainesville, Florida.

Tia, M., Wu, C.L., Kumara, W., 2002. **"Forensic Investigation of the Ellaville Weigh Station UTW Pavements,"** UF Project No: 49104504831-12. Gainesville, Florida.

Tritsch, S., 1995. **"Whitetopping, Technique Revives Burgeoning Kansas Thoroughfare,"** Roads and Bridges, September, pp. 52-55.

Vandenbossche, J.M. and Fagerness, A.J., 2002. **"Performance and Repair of Ultra-Thin Whitetopping: The Minnesota Experience,"** Paper Presented at the 2002 Transportation Research Board Annual Meeting, Washington, DC.

Winkelman, Thomas J., 2005. **"The Illinois Whitetopping Experience: A Practical Approach,"** Proceeding International Conference on Best Practices for Ultra-thin and Thin Whitetopping, Denver, Colorado.

Wu, C.L., Tarr, S.M., Refai, T.M., Nagi, M.N., and Sheehan, M.J., 1997. **"Development of Ultra-Thin Whitetopping Design Procedure,"** Report prepared for Portland Cement Association (PCA), PCA Serial No. 2124, Skokie, Illinois, January.

Wu, C.L., Tayabji, S.D., Sheehan, M.J., and Sherwood, J., 2001. **"Performance and Repair of UTW Pavements,"** Proceedings of the Seventh International Conference on Concrete Pavements, Vol. 2, Orlando, Florida, September, pp. 839-856.

Wu, C.L., and Sheehan, M.J., 2002. **"Testing and Performance Evaluation of UTW Pavements at the Spirit of St. Louis Airport,"** Paper Presented at the 2002 Transportation Research Board Annual Meeting, Washington, DC.